

**DYNAMIC MODELING OF FREE FATTY ACID,
GLUCOSE, AND INSULIN DURING REST AND
EXERCISE IN INSULIN DEPENDENT DIABETES
MELLITUS PATIENTS**

by

Anirban Roy

B.S., University of Pune, India, 2001

M.S., University of Arkansas, 2004

Submitted to the Graduate Faculty of
the Swanson School of Engineering in partial fulfillment
of the requirements for the degree of

Doctor of Philosophy

University of Pittsburgh

2008

UNIVERSITY OF PITTSBURGH
THE SWANSON SCHOOL OF ENGINEERING

This dissertation was presented

by

Anirban Roy

It was defended on

July 15, 2008

and approved by

Dr. Robert S. Parker, Associate Professor, Department of Chemical and Petroleum
Engineering

Dr. Joseph J. McCarthy, Associate Professor and W. K. Whiteford Faculty Fellow,
Department of Chemical and Petroleum Engineering

Dr. Steven R. Little, Assistant Professor, Department of Chemical and Petroleum
Engineering

Dr. Gille Clermont, Associate Professor, Department of Critical Care Medicine

Dissertation Director: Dr. Robert S. Parker, Associate Professor, Department of Chemical
and Petroleum Engineering

Copyright © by Anirban Roy
2008

**DYNAMIC MODELING OF FREE FATTY ACID, GLUCOSE, AND
INSULIN DURING REST AND EXERCISE IN INSULIN DEPENDENT
DIABETES MELLITUS PATIENTS**

Anirban Roy, PhD

University of Pittsburgh, 2008

Malfunctioning of the β -cells of the pancreas leads to the metabolic disease known as diabetes mellitus (DM), which is characterized by significant glucose variation due to lack of insulin secretion, lack of insulin action, or both. DM can be broadly classified into two types: type 1 diabetes mellitus (T1DM) - which is caused mainly due to lack of insulin secretion; and type 2 diabetes mellitus (T2DM) - which is caused due to lack of insulin action. The most common intensive insulin treatment for T1DM requires administration of insulin subcutaneously 3 - 4 times daily in order to maintain normoglycemia (blood glucose concentration at 70 to 120 $\frac{mg}{dl}$). Although the effectiveness of this technique is adequate, wide glucose fluctuations persist depending upon individual daily activity, such as meal intake, exercise, *etc.* For tighter glucose control, the current focus is on the development of automated closed-loop insulin delivery systems. In a model-based control algorithm, model quality plays a vital role in controller performance.

In order to have a reliable model-based automatic insulin delivery system operating under various physiological conditions, a model must be synthesized that has glucose-predicting ability and includes all the major energy-providing substrates at rest, as well as during physical activity. Since the 1960s, mathematical models of metabolism have been proposed in the literature. The majority of these models are glucose-based and have ignored the contribution of free fatty acid (FFA) metabolism, which is an important source of energy for the body. Also, significant interactions exist among FFA, glucose, and insulin. It is

important to consider these metabolic interactions in order to characterize the endogenous energy production of a healthy or diabetic patient. In addition, physiological exercise induces fundamental metabolic changes in the body; this topic has also been largely overlooked by the diabetes modeling community.

This dissertation takes a more lipocentric (lipid-based) approach in metabolic modeling for diabetes by combining FFA dynamics with glucose and insulin dynamics in the existing glucocentric models. A minimal modeling technique was used to synthesize a FFA model, and this was coupled with the Bergman minimal model [1] to yield an extended minimal model. The model predictions of FFA, glucose, and insulin were validated with experimental data obtained from the literature. A mixed meal model was developed to capture the absorption of carbohydrates (CHO), proteins, and FFA from the gut into the circulatory system. The mixed meal model served as a disturbance to the extended minimal model. In a separate study, an exercise minimal model was developed to incorporate the effects of exercise on glucose and insulin dynamics. Here, the Bergman minimal model [1] was modified by adding equations and terms to capture the changes in glucose and insulin dynamics during and after mild-to-moderate exercise.

A single composite model for predicting FFA-glucose-insulin dynamics during rest and exercise was developed by combining the extended and exercise minimal models. To make the composite model more biologically relevant, modifications were made to the original model structures. The dynamical effects of insulin on glucose and FFA were divided into three parts: (i) insulin-mediated glucose uptake by the tissues, (ii) insulin-mediated suppression of endogenous glucose production, and (iii) anti-lipolytic effects of insulin. Labeled and unlabeled intra-venous glucose tolerance test data were used to estimate the parameters of the glucose model, which facilitated separation of insulin action on glucose utilization and production. The model successfully captured the FFA-glucose interactions at the systemic level. The model also successfully predicted mild-to-moderate exercise effects on glucose and FFA dynamics.

A detailed physiologically-based compartmental model of FFA was synthesized and integrated with the existing physiologically-based glucose-insulin model developed by Sorensen [2]. Distribution of FFA in the circulatory system was evaluated by developing mass balance

equations across the major FFA-utilizing tissues/organs. Rates of FFA production or consumption were added to each of the physiologic compartments. In order to incorporate the FFA effects on glucose, modifications were made to the existing mass balance equations in the Sorensen model. The model successfully captured the FFA-glucose-insulin interactions at the organ/tissue levels.

Finally, the loop was closed by synthesizing model predictive controllers (MPC) based on the extended minimal model and the composite model. Both linear and nonlinear MPC algorithms were formulated to maintain glucose homeostasis by rejecting disturbances from mixed meal ingestion. For comparison purposes, MPC algorithms were also synthesized based on the Bergman minimal model [1], which does not account for the FFA dynamics. The closed-loop simulation results indicated a tighter blood glucose control in the postprandial period with the MPC formulations based on the lipocentric (extended minimal and composite) models.

TABLE OF CONTENTS

PREFACE	xxiv
1.0 INTRODUCTION	1
1.1 A brief overview of the insulin-glucose-FFA system	6
1.2 Previous Literature on Mathematical Models of Metabolism	7
1.2.1 Empirical Models	10
1.2.2 Semi-Empirical Models	12
1.2.3 Physiological Models	18
1.2.4 Metabolic Models Considering FFA and Exercise Effects	20
1.3 Overview of Closed-loop Insulin Delivery Systems	22
1.4 Thesis Overview	27
2.0 AN EXTENDED “MINIMAL” MODEL OF FFA, GLUCOSE, AND INSULIN	29
2.1 Bergman minimal model	31
2.2 Extended minimal model	32
2.3 Parameter estimation and goodness of fit technique	36
2.4 Results of the extended minimal model	38
2.4.1 Antilipolytic Effect of Insulin	38
2.4.2 Lipolytic Effect of Hyperglycemia	39
2.4.3 Impairing Effect of FFA on Glucose Uptake Rate	41
2.4.4 Model Validation	42
2.4.4.1 Anti-lipolytic action of insulin:	42
2.4.4.2 Intra-venous glucose tolerance test:	43

2.4.5	Model Structure Justification	45
2.5	Mixed Meal Modeling	49
2.5.1	Mixed Meal Modeling	50
2.5.2	Mixed Meal Tolerance Test (MTT)	52
2.6	Summary	54
3.0	“MINIMAL” MODEL WITH EXERCISE EFFECTS ON GLUCOSE AND INSULIN	56
3.1	Quantitating exercise intensity	58
3.2	Exercise Minimal Model	58
3.2.1	Parameter Estimation Technique	62
3.3	Results of the exercise minimal model	62
3.3.1	Plasma Insulin Dynamics During Exercise	62
3.3.2	Plasma Glucose Dynamics During Exercise	64
3.4	Model Structure Justification	72
3.4.1	Validity of $I_e(t)$ (Equation 3.6)	72
3.4.2	Validity of $G_{up}(t)$ (Equation 3.5)	73
3.4.3	Validity of $G_{prod}(t)$ (Equation 3.4)	74
3.5	Summary	77
4.0	A LOWER-ORDER MODEL OF FFA, GLUCOSE, AND INSULIN AT REST AND DURING EXERCISE	79
4.1	Interactions between insulin, glucose, and FFA during rest and exercise	80
4.2	Composite model structure	83
4.2.1	Insulin Dynamics	83
4.2.2	FFA Dynamics	85
4.2.3	Glucose Dynamics	96
4.3	Parametric Sensitivity Analysis by Finite Difference Method	107
4.4	Validation of the lower-order composite model	111
4.4.1	Effect of Exercise on Plasma Insulin Concentration	112
4.4.2	Effect of Insulin on Plasma FFA Dynamics	113
4.4.3	Effect of Exercise on Plasma FFA Dynamics	114

4.4.4	Effect of Insulin on Plasma Glucose Dynamics	116
4.4.5	Effect of Exercise on Glucose Dynamics	116
4.4.6	Effect of FFA on Glucose Uptake Rate at Rest	117
4.5	Summary	119
5.0	A PHYSIOLOGICALLY-BASED FFA, GLUCOSE, AND INSULIN	
	MODEL	123
5.1	Glucose-Insulin Physiological Model of Sorensen	125
5.2	Physiological FFA Model Structure	135
5.3	Modified version of the Sorensen Glucose-Insulin Model	140
5.4	Metabolic Sinks and Sources of the FFA Model	144
5.4.1	Heart and Lungs FFA Uptake Rate (R_{HFU})	144
5.4.2	Gut FFA Uptake Rate (R_{GFU})	145
5.4.3	Liver FFA Uptake Rate (R_{LFU})	146
5.4.4	Kidney FFA Uptake Rate (R_{KFU})	146
5.4.5	Muscle FFA Uptake Rate (R_{MFU})	146
5.4.6	AT FFA Production Rate (R_{AFP})	148
5.4.7	AT FFA Uptake Rate (R_{AFU})	150
5.5	Inter-connecting Points Between the FFA and Glucose Model	152
5.6	The Physiologically-based FFA, Glucose, and Insulin Model	160
5.6.1	Modified-Insulin Frequently Sampled Intravenous Glucose Tolerance Test (MI-FSIGT)	160
5.6.2	Validation of the Physiologically-Based Model	160
5.6.2.1	MI-FSIGT:	160
5.6.2.2	Effect of plasma FFA on plasma glucose levels:	161
5.7	Summary	162
6.0	MODEL PREDICTIVE CONTROL OF BLOOD GLUCOSE FOR T1DM	
	PATIENTS	165
6.1	Model predictive controller	168
6.2	Closed-loop simulation of mixed meal disturbance rejection	172
6.2.1	MPC Formulation Based on the Extended Minimal Model	172

6.2.2	MPC Formulation Based on the Composite Model	174
6.3	Summary	180
7.0	SUMMARY AND FUTURE RECOMMENDATIONS	184
7.1	Summary	184
7.1.1	Semi-Empirical Metabolic Models	184
7.1.2	Physiologically-Based Metabolic Model	186
7.1.3	Model-Based Control of Blood Glucose for T1DM	187
7.2	Future Recommendations	187
7.2.1	Incorporating Exercise Effects in the Physiologically-Based Model . .	187
7.2.2	<i>A Priori</i> Structural Identifiability of the Metabolic Models	189
7.2.3	Advanced MPC for Blood Glucose Control of T1DM	190
	7.2.3.1 Asymmetric objective function:	191
	7.2.3.2 Prioritized objective function:	192
	APPENDIX. LINEARIZATION USING TAYLOR SERIES EXPANSION	195
	BIBLIOGRAPHY	197

LIST OF TABLES

1.1	Summary of glycemic recommendations for adults with diabetes (adapted from [3])	3
2.1	Parameters of the Bergman minimal model, from [1]	33
2.2	Parameters of the extended minimal model, in addition to those in Table 2.1. 95% confidence interval (CI) bounds were calculated by using the <i>nlparci.m</i> MATLAB function.	37
2.3	Calculated AIC values of the extended minimal model with and without the $Y(t)$ and $Z(t)$ sub-compartments	48
3.1	Initial condition of the equations belonging to the exercise minimal model	60
3.2	Parameters of the exercise minimal model with 95% confidence intervals (CI), in addition to those in Table 2.1	63
3.3	Calculated AIC values of the exercise minimal model with and without the $I_e(t)$, $G_{up}(t)$ and $G_{prod}(t)$ filter equations	76
4.1	Parameter values of the composite model.	108
4.2	List of states of the composite model used in the parametric sensitivity analysis	111
5.1	Parameter values of the Sorensen model, adapted from [2]	133
5.2	Nomenclature of the Sorensen model [2]	134
5.3	Nomenclature of the physiologically-based FFA model	137
5.4	Parameter values of the physiologically-based FFA model	139
5.5	Parameter values of the modified glucose model	142
5.6	Parameter values of the modified insulin model	144

5.7	Closing the FFA mass balance at R_{AFU} . Symbol † indicates mean data obtained from [4]	152
6.1	Performance of $NMPC_{E-E}$, $LMPC_{E-LE}$, $NMPC_{E-B}$, and $LMPC_{E-LB}$	175
6.2	New Parameters of the Bergman minimal model, from [5]	179
6.3	Performance of $NMPC_{PB-C}$, $LMPC_{PB-LC}$, $NMPC_{PB-B}$ and $LMPC_{PB-LB}$	180
6.4	Performance of $NMPC_{PB-PB}$	181
7.1	Discretized objectives that could be used in PO MPC, numbered in order of priority. The glucose measurement is represented as $G(k + \phi) \frac{mg}{dl}$, where ϕ is the number of steps over which the objective is not enforced (adapted from [6]).	194

LIST OF FIGURES

1.1	Schematic diagram of intensive insulin therapy: (A) blood glucose is measured by using a self-monitoring blood glucose device by finger-pricking before meal intake/bed-time; (B) estimated insulin dosage is injected subcutaneously via a syringe to achieve required glycemic goals. This procedure is repeated 3-4 times a day [3, 7]	3
1.2	Block diagram of closed-loop insulin delivery system	5
1.3	Schematic diagram of the major interactions taking place between plasma insulin, glucose, and FFA during rest and exercise. The arrows with a solid line represent transport clearance of metabolites and hormones. Dashed line arrows with + and – signs represent upregulating and downregulating effects on plasma FFA, glucose, or insulin, respectively.	8
2.1	Bergman minimal model of insulin and glucose dynamics, adapted from [1] .	32
2.2	Extended minimal model of insulin, glucose, and free fatty acid dynamics . .	34
2.3	Predicted (solid lines) and published (cross) [4] ($\mu \pm \sigma$) plasma FFA concentration in response to euglycemic hyperinsulinemic clamp. Plasma insulin concentration was maintained at $20 \frac{\mu U}{ml}$ [$R^2 = 0.77$] (top), $30 \frac{\mu U}{ml}$ [$R^2 = 0.94$] (middle), $100 \frac{\mu U}{ml}$ [$R^2 = 0.98$] (bottom)	39
2.4	Predicted values of parameter p_9 in response to increasing glucose clamps for 90 min. [$R^2 = 1$]	40
2.5	Predicted and published ($\mu \pm \sigma$) glucose uptake rate in response to no intralipid infusion - control [$R^2 = 0.9771$] (top); low intralipid infusion rate [$R^2 = 0.9528$] (middle); and high intralipid infusion rate [$R^2 = 0.9115$] (bottom) .	42

2.6	Model simulation validation versus published data ($\mu \pm \sigma$) of plasma FFA concentration in response to euglycemic hyperinsulinemic clamp ($100 \frac{\mu U}{ml}$) [$R^2 = 0.901$]	43
2.7	Model simulation validation versus published data ($\mu \pm \sigma$) of plasma insulin [$R^2 = 0.974$] (top) and glucose [$R^2 = 0.98$] (bottom) concentration dynamics in response to an intra-venous glucose tolerance test	44
2.8	Model simulation validation versus published data ($\mu \pm \sigma$) of FFA concentration dynamics in response to an intra-venous glucose tolerance test [$R^2 = 0.8756$]	45
2.9	Extended model prediction versus data (cross) [4] ($\mu \pm \sigma$) of plasma FFA concentration in response to euglycemic hyperinsulinemic clamp ($100 \frac{\mu U}{ml}$) with (solid line) and without (dashed line) the $Y(t)$ sub-compartment	46
2.10	Extended model prediction versus data (cross) [8] ($\mu \pm \sigma$) of plasma glucose uptake rate in response to low intralipid infusion rate ($0.5 \frac{ml}{min}$) with only $Z(t)$ sub-compartment (solid line), with $Z(t)$ and $Z_2(t)$ sub-compartments (dotted line), and without any filter sub-compartment ($Z(t)$ or $Z_2(t)$) (dashed line) sub-compartment	49
2.11	Published data [9] (cross) versus predicted values of parameter $p_9(G(t))$ from equation (2.7) (solid line) and equation (2.20) (dashed line) in response to increasing glucose clamps for 90 <i>min</i>	50
2.12	Model simulation of total meal gastric emptying rate (top); glucose (G) appearance, protein (P) appearance, and G plus glucose derived from protein (G(P)) appearance (middle); and FFA appearance (bottom), in response to 108 <i>g</i> mixed meal tolerance test.	53
2.13	Insulin concentration data from normal subjects [10] ($\mu \pm \sigma$) and piecewise linear approximation (top), model simulation versus published data [10] ($\mu \pm \sigma$) of plasma glucose concentration dynamics in response to mixed meal tolerance test (bottom).	54

3.1	Dependence of time at which hepatic glycogen starts to deplete, t_{gly} , on exercise intensity ($u_{Ex}(t)$). Published data (cross) from Pruett <i>et al.</i> [11] and linear fit (solid line) [$R^2 = 0.9908$]	61
3.2	Plasma insulin concentration in response to mild exercise ($PVO_2^{max} = 40$) lasting from $t_{ex} = 0$ to 60 <i>min.</i> Published data (circles) ($\mu \pm \sigma$) from Wolfe <i>et al.</i> [12], model fit (solid line), and 95% confidence interval of the model output (dotted line).	64
3.3	Plasma insulin concentration in response to mild exercise ($PVO_2^{max} = 30$) lasting from $t_{ex} = 0$ to 120 <i>min.</i> Model simulation validation (solid line) and published data (cross) ($\mu \pm \sigma$) from Ahlborg <i>et al.</i> [13]	65
3.4	Model simulation (solid lines), 95% confidence intervals of model outputs (dotted lines) and published data (circles) ($\mu \pm \sigma$) from Wolfe <i>et al.</i> [12] in response to mild exercise ($PVO_2^{max} = 40$) lasting from $t_{ex} = 0$ to 60 <i>min.</i> Top: hepatic glucose uptake rate (G_{up}), and Bottom: hepatic glucose production rate (G_{prod}). Both G_{up} and G_{prod} are plotted in deviation form.	66
3.5	Plasma glucose concentration (G) in response to mild exercise ($PVO_2^{max} = 40$) lasting from $t_{ex} = 0$ to 60 <i>min.</i> Model simulation (solid line), 95% confidence intervals of model output (dotted lines), and published data (circles) ($\mu \pm \sigma$) from Wolfe <i>et al.</i> [12].	67
3.6	Response to moderate exercise ($PVO_2^{max} = 50$) lasting from $t_{ex} = 0$ to 45 <i>min.</i> Model simulation validation (solid lines) and published data (cross) ($\mu \pm \sigma$) from Zinman <i>et al.</i> [14]. Top: glucose uptake rate (G_{up}); Middle: hepatic glucose production rate (G_{prod}); Bottom: difference [$G_{prod} - G_{up}$]. Both G_{up} and G_{prod} are shown in deviation form.	68
3.7	Plasma glucose concentration (G) in response to moderate exercise ($PVO_2^{max} = 50$) lasting from $t_{ex} = 0$ to 45 <i>min.</i> Model simulation validation (solid line) versus published data (cross) ($\mu \pm \sigma$) from Zinman <i>et al.</i> [14].	69

3.8	Model response to mild exercise ($PVO_2^{max} = 30$) lasting from $t_{ex} = 0$ to 120 <i>min</i> . Published data (circles) ($\mu \pm \sigma$) from Ahlborg <i>et al.</i> [13], model fit (solid line), and 95% confidence interval of fit (dashed line). Top: model prediction of plasma glucose (G); Middle: model prediction of hepatic glucose uptake rate (G_{up}); and Bottom: model prediction of net liver glucose production. Both G_{up} and $[G_{prod} - G_{gly}]$ are shown in deviation form.	70
3.9	Model response to moderate exercise ($PVO_2^{max} = 60$) lasting from $t_{ex} = 0$ to 210 <i>min</i> . Published data (cross) ($\mu \pm \sigma$) from Ahlborg <i>et al.</i> [15] and model prediction validation (solid line). Top: model prediction of plasma glucose (G); Middle: model prediction of hepatic glucose uptake rate (G_{up}); and Bottom: model prediction of net liver glucose production. Both G_{up} and $[G_{prod} - G_{gly}]$ are shown in deviation form.	71
3.10	Plasma insulin concentration in response to mild exercise ($PVO_2^{max} = 40$) lasting from $t_{ex} = 0$ to 60 <i>min</i> . Published data (circles) ($\mu \pm \sigma$) from Wolfe <i>et al.</i> [12], proposed model fit [AIC = -32.194] (solid line), and reduced model fit [AIC = -11.83] (dashed line).	74
3.11	Proposed model simulation (solid lines), reduced model simulation (dotted lines) and published data (circles) ($\mu \pm \sigma$) from Wolfe <i>et al.</i> [12] in response to mild exercise ($PVO_2^{max} = 40$) lasting from $t_{ex} = 0$ to 60 <i>min</i> . Top: glucose uptake rate (G_{up}), and Bottom: hepatic glucose production rate (G_{prod}). Both G_{up} and G_{prod} are plotted in deviation form.	75
4.1	Schematic diagram of the composite model. Sections I, II, III, and IV represent the insulin, glucose, FFA, and exercise sub-models, respectively. I: Insulin; G: Glucose; F: FFA; u_I : Exogenously infused insulin; u_G , u_F : Glucose or FFA absorbed from meal or infused; u_{Ex} : Exercise intensity; PVO_2^{max} : Percentage of maximum rate of oxygen uptake; x_G , x_{EGP} , x_{EFP1} : Remote insulin compartments; y_{IU} , y_{GU} , y_{GP} , y_{IFU} , y_{IFP} : 1 st -order filters capturing exercise effects.	81

4.2	Plasma insulin concentration in response to mild exercise ($PVO_2^{max} = 40\%$) lasting from time $t_{Ex} = 0$ to 60 min . Published data (circles) ($\mu \pm \sigma$) from Wolfe <i>et al.</i> [12] and model fit (solid line)	84
4.3	Model fit (solid line) versus published data ($\mu \pm \sigma$) (circle) [16] of steady state endogenous FFA production rate, FFP , as a function of normalized remote insulin concentration x_{FFP1_N} . Data-point (a) indicates the lowest FFA production rate, FFP_{lo}	87
4.4	Euglycemic hyperinsulinemic clamp study, where plasma insulin concentration was maintained at $20 \frac{\mu U}{ml}$ (top); $30 \frac{\mu U}{ml}$ (middle); and, $100 \frac{\mu U}{ml}$ (bottom). Model prediction (solid line) using only one insulin filter (x_{FFP1}) and published data ($\mu \pm \sigma$) (circle) [4] of plasma FFA concentration.	88
4.5	MI-FSIGTT study, where plasma insulin boluses were administered at $t = 0$ and 20 min . Model prediction (solid line) and published data ($\mu \pm \sigma$) (circle) [17] of plasma insulin concentration (top); model prediction (solid line) of the unobserved remote insulin concentration x_{FFP1} (middle); model prediction using only one insulin filter (x_{FFP1}) (solid line) and published data ($\mu \pm \sigma$) (circle) [17] of plasma FFA concentration (bottom)	89
4.6	Schematic diagram of the modified insulin model section (I) of the composite model with modifications	90
4.7	Euglycemic hyperinsulinemic clamp study, where plasma insulin concentration was maintained at $20 \frac{\mu U}{ml}$ (top); $30 \frac{\mu U}{ml}$ (middle); $100 \frac{\mu U}{ml}$ (bottom). Model prediction (solid line) using two insulin filters (x_{FFP1} and x_{FFP2}) and published data ($\mu \pm \sigma$) (circle) [4] of plasma FFA concentration.	91
4.8	MI-FSIGTT study, where plasma insulin boluses were administered at $t = 0$ and 20 min . Model prediction (solid line) and published data ($\mu \pm \sigma$) (circle) [17] of plasma insulin concentration (top); model predictions of the first, x_{FFP1} (solid line), and second x_{FFP2} (dashed line) remote insulin concentrations (middle); model prediction (solid line) using both the insulin filters (x_{FFP1} and x_{FFP2}) and published data ($\mu \pm \sigma$) (circle) [17] of plasma FFA concentration (bottom)	92

4.9 Plasma FFA kinetics in response to mild exercise ($PVO_2^{max} = 45\%$) lasting from $t_{ex} = 0$ to 240 <i>min</i> . The exercise model is comprised of two compartments, y_{1FU} and y_{1FP} , to capture the FFA kinetics during exercise. Model prediction (solid line) and published data ($\mu \pm \sigma$) (circle) [18] of plasma FFA uptake rate (Rd_F) (top); model prediction (solid line) and published data ($\mu \pm \sigma$) (circle) [18] of plasma FFA production rate (Ra_F) (middle); model prediction (solid line) and published data ($\mu \pm \sigma$) (circle) [18] of plasma FFA concentration (bottom)	93
4.10 Schematic diagram of the exercise section (IV) of the composite model with modifications	94
4.11 Plasma FFA kinetics in response to mild exercise ($PVO_2^{max} = 45\%$) lasting from $t_{ex} = 0$ to 240 <i>min</i> . The exercise model is comprised of four compartments, y_{1FU} , y_{2FU} , y_{1FP} and y_{2FP} , to capture the FFA kinetics during exercise. Model prediction (solid line) and published data ($\mu \pm \sigma$) (circle) [18] of plasma FFA uptake rate (Rd_F) (top); model prediction (solid line) and published data ($\mu \pm \sigma$) (circle) [18] of plasma FFA production rate (Ra_F) (middle); model prediction (solid line) and published data ($\mu \pm \sigma$) (circle) [18] of plasma FFA concentration (bottom).	95
4.12 Model fit (solid line) versus published data ($\mu \pm \sigma$) (circle) [19, 20] of endogenous glucose production rate, EGP , as a function of normalized insulin concentration x_{EGPN}	98
4.13 Model fit (solid line) versus published data ($\mu \pm \sigma$) (circle) [8, 21] of normalized glucose uptake rate, f_{FG} , as a function of normalized FFA concentration F_N	99
4.14 Model prediction (solid line) versus published data ($\mu \pm \sigma$) (circle) [22] of plasma insulin concentration in response to a labeled-IVGTT (top); normalized insulin action with respect to their basal values on glucose uptake (solid line) and endogenous glucose production (dashed line) due to administration of insulin bolus at $t=0$ <i>min</i> (bottom).	101

4.15 Model prediction (solid line) versus published data ($\mu \pm \sigma$) (circle) [22] of total glucose concentration (endogenous and exogenous labeled-glucose) in response to a labeled-IVGTT (top); model prediction (solid line) versus published data ($\mu \pm \sigma$) (circle) [22] of tracer glucose concentration in response to a labeled-IVGTT (bottom)	102
4.16 Model prediction (solid line) versus published data ($\mu \pm \sigma$) (circle) [12] in response to mild exercise performed at $PVO_2^{max} = 40\%$ intensity lasting from $t_{Ex} = 0$ to 60 <i>min</i> . Top: glucose uptake rate (in deviation form) during exercise (Rd_G); Middle: glucose production rate (in deviation form) during exercise (Ra_G); Bottom: plasma glucose concentration during short-term exercise ($G(t)$).	105
4.17 Model prediction (solid line) versus published data [15] ($\mu \pm \sigma$) (circle) in response to moderate exercise performed at $PVO_2^{max} = 60\%$ intensity lasting from $t_{Ex} = 0$ to 210 <i>min</i> . Top: glucose uptake rate in deviation variables during exercise (Rd_G); Middle: glucose production rate in deviation variables during exercise (Ra_G); Bottom: plasma glucose concentration during prolonged exercise (G).	107
4.18 Parametric relative sensitivity analysis of the composite model for all the sixteen states.	110
4.19 Parametric relative sensitivity analysis of the composite model for the plasma insulin, $I(t)$ (top), FFA, $F(t)$ (middle), and glucose, $G(t)$ (bottom) states.	112
4.20 Plasma insulin concentration in response to mild exercise ($PVO_2^{max} = 30$) lasting from $t_{ex} = 0$ to 120 <i>min</i> . Model simulation validation (solid line) and published data [13] (circles) ($\mu \pm \sigma$) of plasma insulin [$R^2 = 0.936$].	113
4.21 Plasma FFA concentration in response to MI-FSIGT test where boluses of insulin were administered at time $t = 0$ and 20 <i>min</i> . Model simulation validation (solid line) and published data [23] (circles) ($\mu \pm \sigma$) of plasma insulin concentration [$R^2 = 0.999$] (top); model predictions of remote insulin x_{EFP1} (solid line) and x_{EFP2} (dashed line) concentrations (middle); model simulation validation (solid line) and published data [23] (circles) ($\mu \pm \sigma$) of plasma FFA concentration [$R^2 = 0.998$] (bottom).	114

4.22 Plasma FFA concentration in response to mild exercise ($PVO_2^{max} = 30$) lasting from $t_{ex} = 0$ to 120 *min*. Model prediction of plasma FFA uptake rate, Rd_F (top); model prediction (solid line) of plasma FFA production rate, Ra_F (middle); model simulation validation and published data [13] (circles) ($\mu \pm \sigma$) of plasma FFA concentration [$R^2 = 0.989$] (bottom). 115

4.23 Plasma insulin concentration in response to labeled-MI-FSIGT test where insulin boluses were administered at times $t = 0$ and 20 *min*. Model simulation validation (solid line) and published data [24] (circles) ($\mu \pm \sigma$) of plasma insulin concentration [$R^2 = 0.997$] (top); model predictions of normalized insulin action, x_G^N , (solid line) and x_{EGP}^N (dashed line) with respect to their basal values (bottom). 117

4.24 Plasma glucose concentration in response to labeled-MI-FSIGT test where a labeled-glucose bolus was infused at time $t = 0$ *min*. Model simulation validation (solid line) and published data [24] (circles) ($\mu \pm \sigma$) of plasma total glucose concentration [$R^2 = 0.999$] (top); model simulation validation (solid line) and published data [24] (circles) ($\mu \pm \sigma$) of labeled-glucose concentration [$R^2 = 0.99$] (bottom). 118

4.25 Model simulation validation (solid line) versus published data [15] ($\mu \pm \sigma$) (circles) in response to moderate exercise performed at $PVO_2^{max} = 50\%$ intensity lasting from $t_{Ex} = 0$ to 45 *min*. Glucose uptake rate (in deviation form) during exercise (Rd_G) [$R^2 = 0.935$] (top); glucose production rate (in deviation form) during exercise (Ra_G) [$R^2 = 0.955$] (middle); plasma glucose concentration during short-term exercise ($G(t)$) [$R^2 = 0.82$] (bottom). 119

4.26 Model simulation validation (solid line) versus published data [13] ($\mu \pm \sigma$) (circle) in response to mild arm exercise performed at $PVO_2^{max} = 30\%$ intensity lasting from $t_{Ex} = 0$ to 120 *min*. Glucose uptake rate in deviation variables during exercise (Rd_G) (top); glucose production rate in deviation variables during exercise (Ra_G) (middle); plasma glucose concentration during prolonged exercise (G) [$R^2 = 0.861$] (bottom). 120

4.27	Plasma FFA concentration due to infusion of intralipids at high rate (dotted line), low rate (dashed line), and saline (no intralipid infusion) (solid line) (top); published data [8, 21] ($\mu \pm \sigma$) (circle) versus model simulation validations of plasma glucose uptake rate at high (dotted line) [$R^2 = 0.923$] and low (dashed line) [$R^2 = 0.901$] intralipid infusion rates, as well as no intralipid infusion (solid line) [$R^2 = 0.944$] (bottom).	121
5.1	Physiologically-based metabolic model for glucose, adapted from [2]	127
5.2	Schematic representation of a physiologic compartment with no capillary wall resistance	128
5.3	Schematic representation of a typical physiologic compartment with capillary and interstitial space	128
5.4	Physiologically-based FFA model block diagram. B: Brain; H: Heart and lungs; G: Gut; L: Liver; K: Kidney; M: Muscle; AT: Adipose tissue.	138
5.5	Model fit (line) versus published data ($\mu \pm \sigma$) (circle) [25, 26, 27] of FFA uptake rate multiplier function in the heart/lungs compartment, M_{HFU}^F , as a function of normalized heart/lungs FFA concentration, F_H^N	145
5.6	Model fit (line) versus published data ($\mu \pm \sigma$) (circle) [28, 29] of FFA uptake rate multiplier function in the liver compartment, M_{LFU}^F , as a function of normalized liver FFA concentration, F_L^N	147
5.7	Model fit (line) versus published data ($\mu \pm \sigma$) (circle) [30, 31] of FFA uptake rate multiplier function in the muscle compartment, M_{MFU}^F , as a function of normalized muscle interstitial space FFA concentration, F_{MI}^N	148
5.8	Model fit (line) versus published data ($\mu \pm \sigma$) (circle) [16] of normalized FFA production rate in the AT compartment, $M_{AFP}^{I\infty}$, as a function of normalized adipocyte insulin concentration I_{AI}^N . The inset includes magnified coordinates, x-axis $\in [0 \text{ to } 45]$ and y-axis $\in [0 \text{ to } 2]$	150
5.9	Model predicted (line) and published ($\mu \pm \sigma$) (circle) [4] plasma FFA concentration in response to euglycemic hyperinsulinemic clamps. Plasma insulin concentration was maintained at $20 \frac{\mu U}{ml}$ (top), $30 \frac{\mu U}{ml}$ (middle), $100 \frac{\mu U}{ml}$ (bottom) 151	

5.10 Model fit (line) versus published data ($\mu \pm \sigma$) (circle) of glucose uptake rate multiplier function in the muscle compartment, $M_{M GU}^F$, as a function of normalized muscle interstitial space FFA concentration, F_{MI}^N , data obtained from [8, 21]	156
5.11 Model fit (line) versus published data ($\mu \pm \sigma$) (circle) of glucose uptake rate multiplier function in the liver compartment, $M_{H GU}^F$, as a function of normalized liver FFA concentration, F_L^N , data obtained from [8, 21]	157
5.12 Model fit (line) versus published data ($\mu \pm \sigma$) (circle) of glucose production rate multiplier function in the liver compartment, $M_{H GP}^F$, as a function of normalized liver FFA concentration, F_L^N , data obtained from [32, 33]	158
5.13 Surface plot of the multiplier function, $M_{H GP}^{IF\infty}$, as a function of normalized liver insulin, I_L^N , and FFA concentration, F_L^N , versus published data (cross) ($\mu \pm \sigma$) of normalized hepatic glucose production rate with respect to its basal value [19, 21, 32, 34, 35, 36]	159
5.14 Model fit (line) and experimental data ($\mu \pm \sigma$) (circle) [17] of a MI-FSIGT test. Glucose bolus was infused at time (t) = 0 min and insulin boluses were infused at $t = 0$ min and $t = 20$ min to obtain predictions of insulin (top); glucose (middle); and FFA (bottom) concentrations	161
5.15 Model validation (line) versus experimental data ($\mu \pm \sigma$) (circle) [37] of a MI-FSIGT test. Glucose bolus was infused at time (t) = 0 min and insulin boluses were infused at $t = 0$ min and $t = 20$ min to obtain predictions of insulin (top), glucose (middle), and FFA (bottom) concentrations.	162
5.16 Model validation (line) versus experimental data ($\mu \pm \sigma$) (circle) [33] of the effects of high FFA levels on plasma glucose concentration. Plasma glucose concentration reached hyperglycemic levels (top) due to elevation of FFA concentration by lipid infusion (bottom)	163
6.1 A schematic diagram of the closed-loop model-based insulin delivery system. Here, $r(t)$ is the desired glucose setpoint, $u(t)$ is the manipulated variable (exogenous insulin), $y(t)$ is the measured variable, and $\tilde{y}(t)$ is the model predicted output	166

6.2	A schematic diagram of the MPC algorithm implementation	170
6.3	Comparison between mixed meal disturbance rejection by LMPC _{E-LE} (solid line) and NMPC _{E-E} (dashed line) with input constraint. Setpoint (dotted line) is set at $81 \frac{mg}{dl}$	174
6.4	Comparison between mixed meal disturbance rejection by LMPC _{E-LE} (solid line), NMPC _{E-B} (dashed line), and LMPC _{E-LB} (dotted line) with input constraint. Setpoint (dotted line) is set at $81 \frac{mg}{dl}$	175
6.5	Comparison between mixed meal disturbance rejection by NMPC _{PB-C} (solid line) and LMPC _{PB-LC} (dashed line) with input constraints. Setpoint (dotted line) is set at $81 \frac{mg}{dl}$	177
6.6	Mixed meal disturbance rejection by NMPC _{PB-B} with input constraints. Setpoint (dotted line) is set at $81 \frac{mg}{dl}$. Controller model parameters were obtained from Bergman <i>et al.</i> [1].	178
6.7	Comparison between mixed meal disturbance rejection by NMPC _{PB-B} (solid line) and LMPC _{PB-LB} (dashed line) with input constraints. Setpoint (dotted line) is set at $81 \frac{mg}{dl}$. The Bergman minimal model parameters were obtained from Table 6.2.	179
6.8	Mixed meal disturbance rejection by NMPC _{PB-PB} with input constraints. Setpoint (dotted line) is set at $81 \frac{mg}{dl}$	181

PREFACE

The four years of graduate school in Pittsburgh has been one of the most exciting journeys of my life. I would like to take this opportunity to show my gratitude to all my mentors, friends, and loved ones who were always there for me at every corner of this eventful trip.

Let me start with my PhD advisor, Dr. Robert S. Parker. Bob has been an excellent mentor throughout my tenure at University of Pittsburgh as a graduate student. His guidance and constructive criticism has helped me to become a better researcher. The meticulous problem-solving approach that I adhered from Bob's laboratory is going to help me immensely for the rest of my career. I still remember my first meeting with Bob and the enthusiasm that he had in his voice while explaining me the challenges in curing diabetes as a systems engineer; which he has successfully passed on to me.

I would like to show my earnest appreciation to Dr. Gilles Clermont for showing confidence in me and allowing me to work in the inflammation project as a team member; furthermore, for being a vital member of my doctoral committee. In addition, I would like to extend my gratitude to professors Joseph J. McCarthy and Steven R. Little for serving as internal members of my doctoral committee.

I am extremely grateful to all of my laboratory members (Dr. John Harrold, Dr. Abhishek Soni, Dr. Jeff Florian, and Dr. Chad Kanick) for sharing their knowledge with me, especially during the initial stages. I would also like to thank my Masters advisor, Dr. Robert Beitle, from University of Arkansas for encouraging me to pursue the doctoral degree.

Of course, none of this would have been possible without the support of my family. I consider myself extremely blessed to have my mother and father beside me throughout my life. Whenever required, they have gone far beyond their reach to help me fulfill my dreams. It is a pity, that for these very dreams I have not been able to spend quality time with them

as their only child, especially now when they are growing older. Finally, I would like to take this opportunity to mention few words regarding my lovely wife, Arpita. She is the most amazing person that I have ever met in my entire life. Apu has provided me an enormous mental support with her love and care ever since we got married. She always amazes me with her grace and tolerance during the toughest of times. I feel the luckiest person in the world to have her beside me.

1.0 INTRODUCTION

The pancreas plays a vital role in regulating blood glucose concentration in the body. Gluco-regulatory hormones, such as insulin, secreted by the pancreatic β -cells facilitate transport of glucose from the circulatory system into the tissues [38]. Absolute or partial deficiency in insulin secretion by the pancreas, lack of gluco-regulatory action of insulin, or both, leads to a metabolic disease known as diabetes mellitus (DM) [3, 38, 39]. Several pathological processes contribute to the development of DM, such as: autoimmune destruction of the pancreatic β -cells; deficient insulin action resulting from diminished secretion by the pancreas; diminished tissue response to the gluco-regulatory action of insulin at one or more points of the complex pathways of hormone action; and genetic defects that prevent regulated secretion of hormone [38, 39].

DM is largely classified into two categories. Insulin dependent diabetes mellitus (IDDM), also known as Type 1 diabetes mellitus (T1DM), usually results from an absolute deficiency of insulin secretion due to auto-immune destruction of the pancreatic β -cells [38]. Patients with T1DM require exogenous insulin replacement therapy in order to regulate their blood glucose levels [38]. The much more prevalent form is termed non-insulin dependent diabetes mellitus (NIDDM), commonly known as Type 2 diabetes mellitus (T2DM). The cause of T2DM is a combination of resistance to insulin action and an inadequate compensatory insulin secretion response [38]. Most patients with this form of diabetes are obese, and obesity may itself cause some degree of insulin resistance [38, 39, 40]. Non-obese T2DM individuals often reflect elevated circulating levels of free fatty acids (FFA) and triglycerides (TG). In case of T2DM, initially and often throughout the lifetime, the patients do not require insulin replacement treatment to survive [38].

DM is becoming increasingly prevalent in U.S. and around the world. According to the American Diabetes Association (ADA), approximately 17.5 million people in the U.S. have been diagnosed with diabetes in 2007 [3]. This estimation is substantially higher than the 2002 estimate of 12.1 million people by the ADA [41]. About 5-10% of the diabetic patients have T1DM [38]. The total (direct plus indirect) estimated cost of diabetes has also significantly risen from \$132 billion in 2002 [41] to \$174 billion in 2007 [3].

DM is usually associated with wide blood glucose ($G(t)$) fluctuations, resulting in hyperglycemia ($G(t) > 120 \frac{mg}{dL}$) or hypoglycemia ($G(t) < 70 \frac{mg}{dL}$) [42, 43]. Long-term effects of DM are mainly caused by prolonged hyperglycemia, which may lead to complications such as loss of vision, peripheral neuropathy with a risk of foot ulcer or even amputation, cardio-vascular disease, nephropathy and sexual dysfunction [38, 42, 43]. Immediate disease consequences are primarily caused by hypoglycemia, which may lead to dizziness, unconsciousness, or even death [42, 43].

Over the years, researchers have shown that an intensive insulin therapy for diabetic patients can delay the onset of serious complications [44, 45]. According to the findings of the Diabetes Control and Complications Trial (DCCT) research group, intensive insulin treatment reduced the risk of retinopathy, nephropathy and neuropathy by 35% to 90% when compared with conventional treatment [44]. Intensive treatment was most effective when begun early, before complications were detectable. As shown in Figure 1.1, the most common insulin intensive treatment for T1DM involves self-monitoring of blood glucose (SMBG) by finger-pricking at least 3-4 times a day followed by subcutaneous insulin injection in order to achieve required glycemic goals (see Table 1.1) as recommended by the ADA [3].

Even with such intensive insulin therapy, wide glucose fluctuations persist mainly due to daily activities such as meal intake and exercise. In an experiment performed by Raskin *et al.* [46], the long-term effects of fast-acting insulin aspart (IAsp) and regular human insulin (HI) on glycemic control were studied on T1DM patients. Blood glucose was measured at 8 time points and insulin was injected before breakfast, before lunch, before dinner, and at bedtime. Their results revealed significant hyperglycemic events at post-prandial periods for both the insulin regimens, with HI being worse. The ultimate goal in diabetes treatment is the development of an automatic closed-loop insulin delivery system that can mimic the

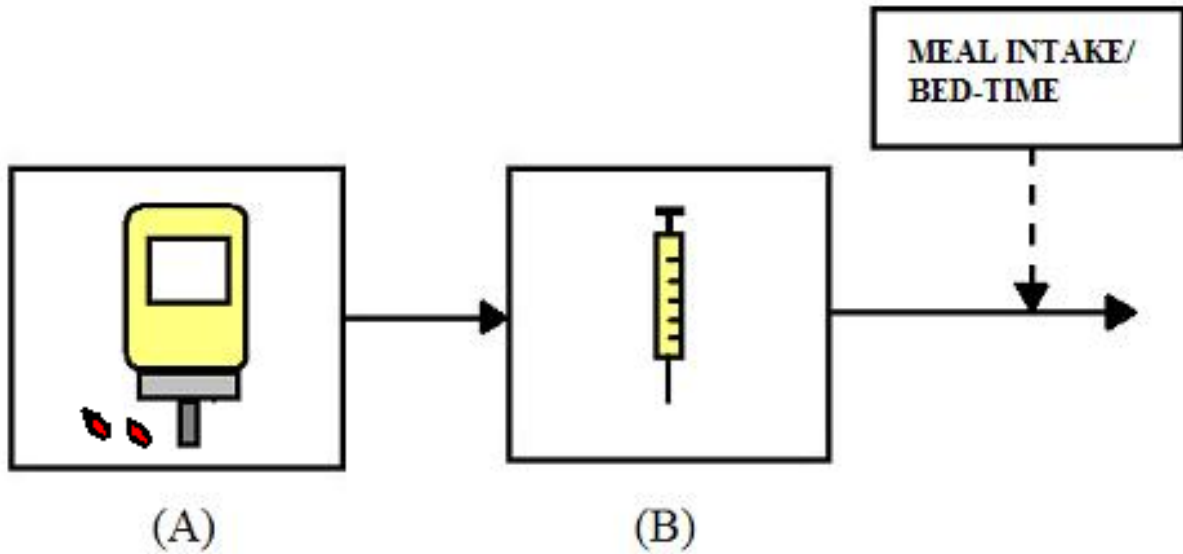


Figure 1.1: Schematic diagram of intensive insulin therapy: (A) blood glucose is measured by using a self-monitoring blood glucose device by finger-pricking before meal intake/bed-time; (B) estimated insulin dosage is injected subcutaneously via a syringe to achieve required glycemic goals. This procedure is repeated 3-4 times a day [3, 7]

Table 1.1: Summary of glycemic recommendations for adults with diabetes (adapted from [3])

Description	Value
Glycosylated hemoglobin (A1C)	<7.0%
Preprandial capillary plasma glucose	70-130 $\frac{mg}{dL}$
Peak post-prandial (1-2 hr after the beginning of meal) capillary plasma glucose	<180 $\frac{mg}{dL}$
A1C is the primary target for glycemic control	
More stringent glycemic goals (<i>i.e.</i> , A1C <6.0%) may further reduce complications at the cost of increased risk of hypoglycemia	

activity of a normal pancreas and is capable of maintaining physiological blood glucose levels for T1DM patients. Such an artificial pancreas system can theoretically produce tight glucose control without finger-stick blood glucose measurements, subcutaneous insulin injections, or hypo-/hyper-glycemic events [47], thereby dramatically improving the quality of life for an insulin-dependent diabetic patient. A device of this type would primarily contain three components: (i) an insulin pump, (ii) a continuous glucose sensor, and (iii) a mathematical algorithm to regulate the pump in order to maintain normoglycemia in presence of sensor measurements [48, 49], as shown in Figure 1.2. In the case of a model-based closed-loop insulin delivery system, the controller calculates the required insulin dosage for maintenance of normoglycemia based on the blood glucose predictions obtained from a mathematical model. Hence, model quality plays a vital role as theoretically available controller performance is limited by model accuracy [50]. In addition, superior quality mathematical models of DM provide numerous significant open-loop advantages. For example, a comprehensive mathematical model facilitates a better understanding of the complex relationship between insulin and the major energy-providing metabolic substrates [51]. High fidelity metabolic models can predict the time-course and effect of insulin on plasma glucose in presence of various external disturbances such as meal consumption, exercise, etc. Finally, an accurate T1DM patient-specific metabolic model might be used to adjust daily insulin therapy dosage for the same individual [51].

Over the years, numerous metabolic models have been published in the literature with a primary goal of capturing the dynamics of the insulin-glucose system. Such glucocentric (glucose-based) models largely ignore FFA metabolism and its interaction with glucose and insulin. FFA is a major metabolic source of energy for the human body. Almost 70-80 % of muscle energy is derived from FFA oxidation during rest [52, 53]. This is because the energy yield from 1 g of FFA is approximately 9 kcal, compared to 4 $\frac{kcal}{g}$ for proteins and carbohydrate (CHO) [54]. Moreover, significant interactions exist between glucose and FFA metabolism. To further complicate matters, the FFA, glucose, and insulin dynamics are significantly altered during exercise. In the development of a diabetes mellitus patient model, it is important to consider all the major energy-providing substrates (glucose and FFA) and their persisting metabolic interactions during rest and exercise. Such a complete

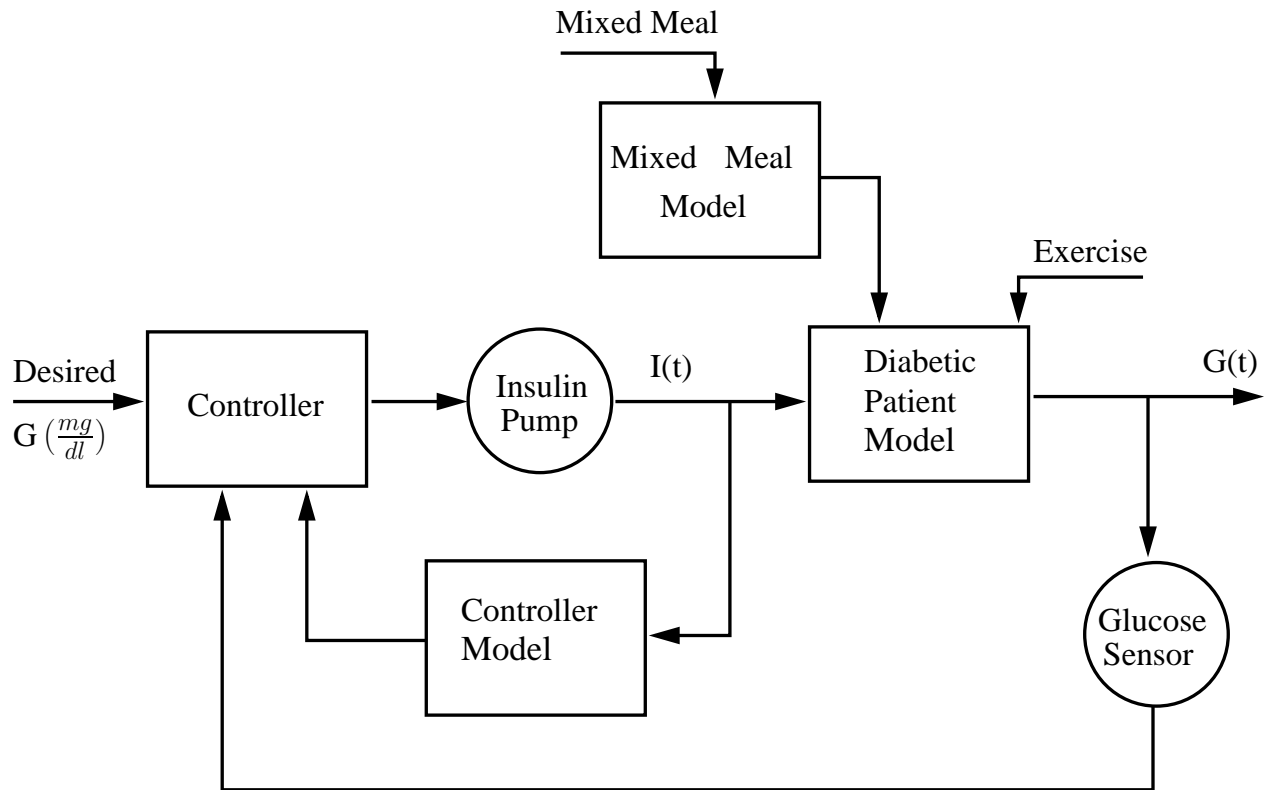


Figure 1.2: Block diagram of closed-loop insulin delivery system

metabolic model can provide more accurate glucose predictions under realistic conditions, such as disturbances provided from mixed meal (containing CHO, protein, and fat) ingestion and exercise. Finally, metabolic models describing the dynamics of insulin, glucose, and FFA during rest and exercise can provide the control community an excellent platform for the development of model-based controllers for maintenance of normoglycemia by rejecting the various external disturbances.

In the following Section (1.1), a brief overview of the major metabolic interactions taking place between the major energy-providing substrates and insulin at rest and during exercise is presented. Sections 1.2 and 1.3 are dedicated for a concise review of the glucose-insulin models and the closed-loop insulin delivery systems currently present in the literature, respectively. Finally, a brief overview of the rest of the dissertation Chapters is presented in Section 1.4.

1.1 A BRIEF OVERVIEW OF THE INSULIN-GLUCOSE-FFA SYSTEM

Glucose from the circulatory system is consumed by the hepatic tissues mostly for storage in the form of glycogen and by the extra-hepatic tissues for oxidation purpose [55]. To maintain plasma glucose homeostasis, stored glucose from the liver is released back into the circulation via a process known as glycogenolysis [56]. Plasma insulin secreted by the pancreas, or exogenously infused in the case of T1DM patients, facilitates the uptake of glucose in the tissues [55]. Plasma insulin also inhibits hepatic glucose production [57]. FFA from the circulatory system is consumed by the adipose tissue (AT) mostly for storage in the form of triglycerides and by the peripheral tissues (except brain) for oxidation purpose [54]. Whenever the body requires energy, stored FFA is released back into the circulatory system via a process known as lipolysis [54]. Insulin acts as a strong anti-lipolytic agent, in other words, it suppresses the lipolytic process [54]. In the early 1960s, Randle *et al.* [58, 59] proposed that glucose and FFA compete for oxidation in the muscle tissues. This phenomenon, popularly known as the glucose-FFA cycle, was later demonstrated in studies performed by several researchers [8, 21], where it has been shown that an increase in plasma

FFA concentration inhibits muscular glucose uptake rate. Several studies have also reported that an increase in FFA inhibits insulin-mediated suppression of glycogenolysis [32, 19]. In a recent publication, Ghanassia *et al.* [60] has mentioned that FFA and insulin act in synergy and provide a fine-tuning for regulation of endogenous glucose production rate. Exercise also plays a major role in influencing the dynamics of plasma glucose, FFA, and insulin. An elevated exercise level up-regulates plasma glucose and FFA uptake rates [13, 61]. At the same time, plasma insulin level decreases due to elevated insulin-mediated clearance rate [62]. To maintain glucose homeostasis, hepatic glucose production also increases during exercise [63]. Lactate production by working muscles is also increased during exercise [13]. Excess lactate in the plasma is absorbed by the liver for conversion to glucose (known as gluconeogenesis [64]) in order to support the elevated glucose production rate. The schematic diagram in Figure 1.3 captures all the major metabolic interactions between the insulin-glucose-FFA system at rest and during exercise.

1.2 PREVIOUS LITERATURE ON MATHEMATICAL MODELS OF METABOLISM

Metabolic models currently present in the literature can be classified into three groups (i) strictly empirical, (ii) semi-empirical, and (iii) physiologically-based. The sole purpose of a strictly empirical model is to capture the input-output data (insulin-glucose dynamics) without consideration of any physiology [23, 65, 66, 67]. Hence such models are also called black-box models. Since only the input-output data is used to develop the models, the identification of the structure and parameters could be much simpler. Hence, time required to synthesize these models can be short. As empirical model structures could be selected to facilitate controller design, a vast number of model-based controllers employ dynamical empirical models [68]. However, these models have several significant drawbacks. Since strictly empirical models do not consider any biology, separation of specific physiological effects of metabolic substrates taking place in the various tissues/organs is impossible. Also input-output models provide no insight regarding the mechanisms underlying the observed system

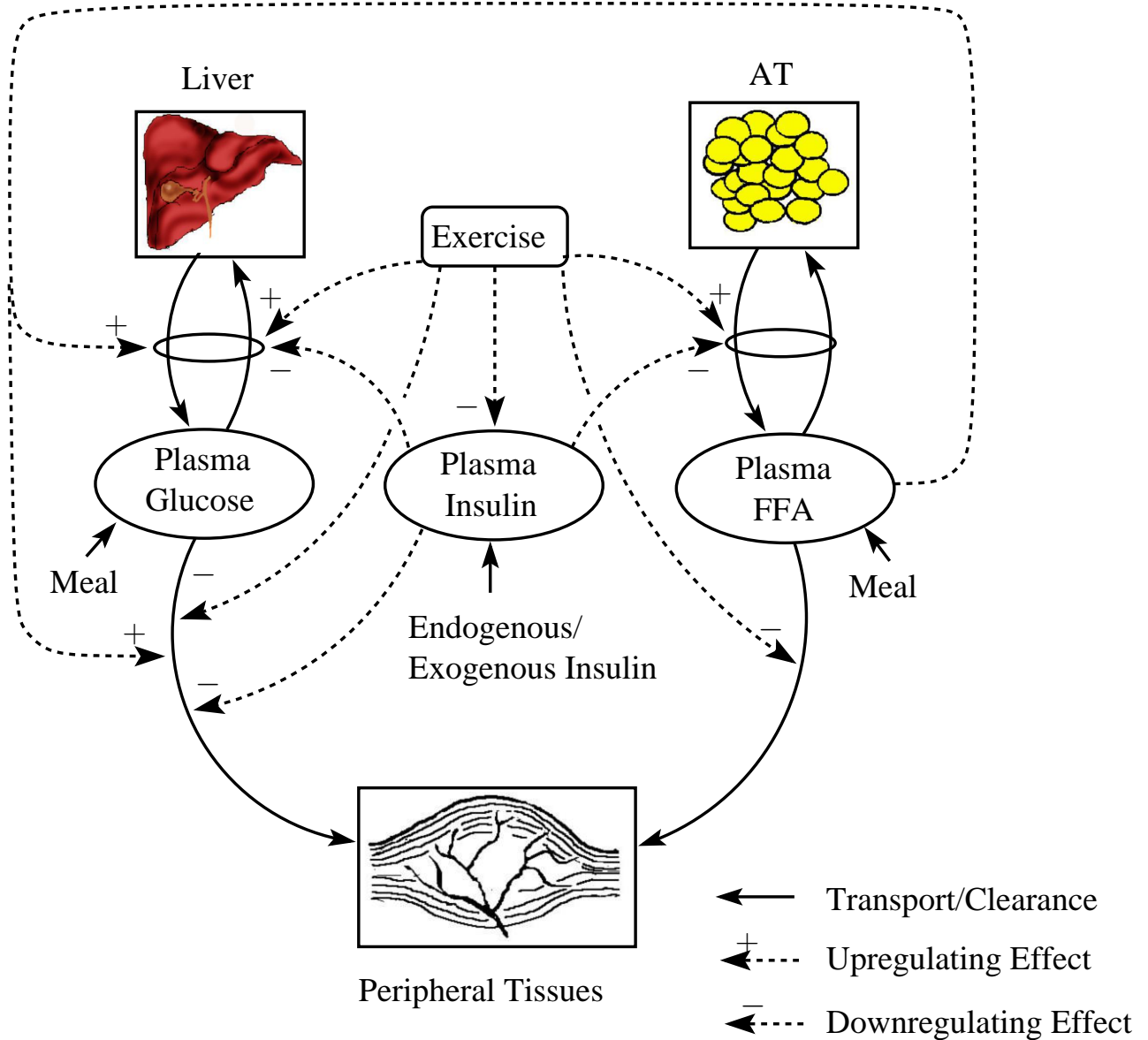


Figure 1.3: Schematic diagram of the major interactions taking place between plasma insulin, glucose, and FFA during rest and exercise. The arrows with a solid line represent transport/clearance of metabolites and hormones. Dashed line arrows with + and - signs represent upregulating and downregulating effects on plasma FFA, glucose, or insulin, respectively.

dynamics. Moreover, biological processes responsible for glucose dynamics are nonlinear and vary under many conditions; hence, simple linear input-output models are inadequate to provide credible predictions for extended future horizons under realistic disturbances, such as a meal [23].

The semi-empirical models consist of a minimum number of equations capturing the insulin glucose dynamics with a primary focus on emulating the data by considering only the necessary physiology [1, 69, 70, 71, 72, 73, 74, 75]. Unlike the strictly empirical models, minimal models include several macroscopic metabolic parameters, like peripheral tissue sensitivity to insulin and overall glucose effectiveness of extra-hepatic tissues [5]. However, these models do not differentiate the distribution of metabolic substrates at various organ/tissue levels, as that will add further model complexity. Hence, the goal in such models is to capture the major physiological interactions in order to reproduce the data without sacrificing the structural simplicity. Due to this very nature, semi-empirical models can be an ideal candidate for the synthesis of model-based controllers capable of maintaining glucose homeostasis by rejecting disturbances from mixed meal consumption and exercise.

Finally, the physiologically-based models are more detailed and complex in terms of number of parameters and equations providing an in depth description of the physiology behind the various metabolic interactions taking place in the body [2, 76, 77, 78]. In such models, the distribution of metabolic substrates is captured at the organ/tissue and intracellular levels. Physiologically-based models can be extremely useful, as they can promote insight, as well as motivation for experiments that could be performed to validate various model components. In terms of drawbacks, these models are usually time-intensive to develop. They typically have large number of nonlinear equations with many parameters that need to be estimated. Even though complexity is an issue, a valid physiologically-based model can not only describe the dynamics of measurable quantities, but also correctly predict all the unmeasurable variables relevant to the system.

1.2.1 Empirical Models

Strictly empirical models are developed based on the input-output data without considering the fundamental properties (physiology) of the system. Typically, the model structure is chosen to facilitate parameter estimation or design of model-based controller. Mitsis and Marmarelis [79] developed a non-parametric model of the glucose-insulin system by selecting the Volterra-Wiener approach. The first and second order kernels of the Volterra model were estimated from input-output data generated from a parametric model [1] by employing the Laguerre-Volterra Network (LVN) methodology. The simulation results revealed that synthesis of accurate nonlinear input-output models from insulin-glucose data generated from parametric models was feasible. The authors also demonstrated the robustness of the Volterra models under presence of additive output noise. Furthermore, such kind of models are accommodating to adaptive and patient-specific estimation, which could be necessary for a model-based blood glucose control algorithm.

A linear input-output model for glucose prediction based on recent blood glucose measurement history was proposed by Bremer and Gough [23]. Autocorrelation function (ACF) estimates at fixed time intervals were used to identify the model structure. An ACF estimate provides a statistical measure of the dependence between individual measurements of a process at different time points. Published data analyzed in their work indicated that blood glucose dynamics are not random, and that blood glucose values can be predicted from frequently sampled previous values, at least for the near future. However the model prediction of blood glucose for extended horizon (in excess of 30 *min*) was not acceptable.

Parker *et al.* [65] developed a linear input-output step-response model of insulin delivery rate (input) effects on glucose concentration (output) by filtering the impulse response coefficients via projection onto the Laguerre basis. The identified linear input-output model does not include all the gain information of the diabetic patient, but it does succeed in capturing the dynamic behavior. Inability to capture the steady state characteristics did not affect the closed-loop performance of the model. In a separate study, Florian and Parker [80] synthesized empirical Volterra series models of glucose and insulin behavior by considering input-output data generated from a physiologically-based metabolic model [2]. In absence

of noise, the identified Volterra models accurately predicted the data. However, addition of Gaussian distributed measurement noise significantly degraded the coefficient estimates. Significant noise filtering was achieved by projecting the Volterra models onto the Laguerre basis functions. Closed-loop performance of the nonlinear empirical model with measurement noise in rejecting 50 g oral glucose challenge was mediocre. Best closed-loop performance was achieved by a linear MPC with ability to filter noise effects by proper tuning.

Van Herpe *et al.* [66] developed a control-relevant black-box model for prediction of the glycemic levels of critically-ill patients in the intensive care unit (ICU) by using real clinical ICU input-output (insulin-glucose) data. An autoregressive exogenous input (ARX) model structure was used for predicting blood glucose concentration by considering the following input variables: insulin infusion rate, body temperature, total CHO calorie intake, total fat calorie intake, glucocorticoids level, adrenalin level, dopamine level, dobutamine level, and beta-blockers level. The estimated model coefficients showed clinical relevance with respect to the behavior of glycemia in relation to insulin, insulin resistance, intake of CHO calories, etc. However, the authors pointed out that further data is required to make the model more patient specific especially to capture the diurnal variation of insulin resistance for critically-ill patients.

In another study, several types of empirical models, like Auto-regressive with exogenous input (ARX) and Box-Jenkins (BJ), were developed by Finan *et al.* to evaluate the ‘infinite-step ahead’ glucose predictions [67]. The input-output models were identified from simulating a semi-empirical model developed by Hovorka *et al.* [75]. The higher- and lower-order ARX and BJ models described normal operating conditions with high accuracy. However, model accuracy during abnormal situations (*e.g.*, change in insulin sensitivity, underestimates in CHO content of meals, mismatch between actual and patient-reported timing of meals) were inaccurate, especially for the lower-order models.

A nonlinear neural network (NN) model of blood glucose concentration identified from subcutaneous glucose sensor and subcutaneous insulin infusion data was developed by Trajnski *et al.* [81]. The system identification framework combines a nonlinear autoregressive with exogenous input (NARX) model representation, regularization approach for constructing radial basis function NNs, and validation methods for nonlinear systems. Numerical

studies on system identification and closed loop control of glucose were carried out by using a comprehensive glucose model and pharmacokinetic model of insulin absorption from a subcutaneous depot. Closed-loop simulation results showed that stable control is achievable in the presence of large noise levels. However, one major drawback of the closed-loop system is that, due to the subcutaneous route of insulin administration, rapid control actions were not stable which are typically necessary after a standard OGTT.

Bellazzi *et al.* [82] proposed a fuzzy model for predicting blood glucose levels in T1DM patients. The underlying idea in their approach consists of the integration of qualitative modeling techniques with fuzzy logic systems. The resulting hybrid system uses *a priori* structural knowledge on the system to initialize a fuzzy inference procedure, which estimates a functional approximation of the system dynamics by using the experimental data in order to predict the patient's future blood glucose concentration. The results obtained showed that the presented framework generates fuzzy systems that may be used reliably and efficiently to predict blood glucose concentration for T1DM patients. A potential drawback is that, as the initialization of the fuzzy system requires *a priori* knowledge of the qualitative model, any erroneous approximation of unknown functions could lead to significant degradation of the fuzzy model performance.

Bleckert *et al.* [83] developed a model of glucose-insulin metabolism by identifying the system with stochastic linear differential equations using a mixed graphical models technique. The model was identified in terms of biological parameters and noise parameters. Density estimates of the unknown parameters were obtained from the input-output data by using the exact inference algorithm [83]. The parameter estimates were given as *a posteriori* distributions, which can be interpreted as fuzzy probability distributions. These density estimates convey much more information about the unknown parameters than a point estimate.

1.2.2 Semi-Empirical Models

The semi-empirical metabolic models consist of minimum number of equations capturing only the necessary physiology in order to better understand the mechanisms of the glucose-

insulin regulatory system. One of the pioneers in this field is Bolie. In 1961, he proposed a 2-dimensional (2-D) metabolic model consisting of ordinary differential equations (ODE) [69]. The two ODEs, one capturing glucose and the other capturing insulin concentration, consisted of 5 parameters. Parameter values were estimated from published data; predominantly average values obtained from human, as well as animal, experiments. Ackerman *et al.* [70] developed a similar 2-D glucose-insulin model which was published in 1965. The model considered the important fact that changes in insulin and glucose concentration depend on the concentration of both the components. Serge *et al.*, in the early 1970's, synthesized a metabolic model consisting of linear ODEs to capture blood glucose kinetics of normal T1DM and obese patients [84]. Although all these early models were easily identified from available data, they oversimplified the actual physiological effects between glucose-insulin.

A huge impact in the field of modeling glucose-insulin dynamics was initiated by the introduction of the “minimal” model developed by Bergman and colleagues in the late 1970's and early 1980's [1, 85]. There are approximately 500 studies published in the literature, that involve the Bergman minimal model [86]. The model consists of three ODEs that capture plasma glucose dynamics, plasma insulin dynamics, and insulin concentration in an unaccessible remote compartment (which can be conceptualized as interstitial insulin). Structurally, the model consisted of a minimum number of lumped compartments and parameters to accurately capture the various physiological phenomena, such as glucose effectiveness and insulin sensitivity, during an intra-venous glucose tolerance test (IVGTT) [1]. The addition of the remote insulin compartment and a bilinear term in the glucose state increased the accuracy of the model without sacrificing any simplicity. However, several shortcomings of the minimal model have been raised in the literature [87, 88]. Quon *et al.* reported that the Bergman minimal model tends to overestimate the effect of glucose on glucose uptake and underestimate the contribution of incremental insulin [87]. Researchers have also raised questions that the minimal model might be too minimal [73]. Despite its shortcomings, the Bergman minimal model [1] has gained enormous popularity in the diabetes research community, mainly because of its structural simplicity and easily identifiable parameters [86, 89]. Because of this very nature, the minimal model was selected in this work to provide a platform for the development of a lipid-based extended minimal

model and an exercise minimal model which are detailed in Chapter 2 and 3, respectively.

Cobelli and colleagues have developed numerous metabolic models capturing the various physiological interactions between glucose and insulin [5, 71, 72, 74, 90, 91]. The Bergman minimal model [1] does not allow the separation of glucose production from utilization. To overcome this limitation, Cobelli *et al.* proposed a revised minimal model which was fitted to cold and hot (radio-labeled) IVGTT data [5], as the hot data reflects glucose utilization only. In another publication by Cobelli *et al.* [74], the over-estimation of glucose effectiveness (S_G) and under-estimation of insulin sensitivity (S_I) of the Bergman minimal model due to under-modeling was addressed by adding a second non-accessible glucose compartment for a better description of the glucose kinetics. The two-compartment glucose model improved the accuracy of S_G and S_I estimates from a standard IVGTT in humans. In a series of publications Cobelli and co-authors [71, 72, 90] developed an extensive model of glucose and two hormones, insulin and glucagon. Glucagon is a counter-regulatory hormone secreted by the α -cells of the pancreas. Its role is to enhance the release of glucose from the liver into the plasma by speeding the breakdown of hepatic glycogen. The glucose sub-system explicitly considered the net hepatic glucose balance (NHGB), renal excretion of glucose, and insulin-dependent and insulin-independent glucose utilization by peripheral tissues, red blood cells and the central nervous system. The insulin sub-system is divided into five compartments, whereas the glucagon subsystem consisted of a single compartment. The nonlinear equations employed saturating functions (hyperbolic tangents) to capture the saturation behavior observed in biological systems (*e.g.*, hepatic glucose production). Incorporation of all these physiological interactions provided further insight into glucose-insulin metabolism.

Berger and Rodbard [92] developed a computer program for the simulation of plasma insulin and glucose dynamics after subcutaneous injection of insulin. A pharmacokinetic model was used to calculate the time courses of plasma insulin for various combinations of popular preparations. The program can predict the time course of plasma glucose in response to a change in CHO intake and/or insulin dose, with the use of a pharmacodynamic model describing the dependence of glucose dynamics on plasma insulin and glucose levels. A set of parameters for the model were estimated from the literature. The model can be used to theoretically explore the impact of various factors associated with glycemic control in T1DM.

Results of the glucose dynamics generated by the simulator were not exact, particularly after perturbations from larger CHO intake sizes. One potential drawback is that, due to the absence of FFA effects, the simulator may be incapable of predicting plasma glucose level accurately in the presence of disturbances from mixed meals containing CHO and fat.

In a much more recent work, Hovorka *et al.* [75] extended the 2-compartment minimal model developed by Cobelli *et al.* [74] by separating the effect of insulin on glucose distribution/transport, glucose disposal, and endogenous glucose production during an IVGTT by employing a dual-tracer dilution methodology. The model consisted of a two-compartment glucose sub-system, a single compartment for plasma insulin, and three remote insulin compartments capturing the different physiological effects of insulin on glucose. By using the dual-tracer technique along with the model, the authors demonstrated a novel approach of separating the three actions of insulin on glucose kinetics successfully. The results showed that the insulin-mediated suppression of endogenous glucose production accounts for approximately one-half of the overall insulin action on glucose after an IVGTT. However, the absence of any saturating functions, particularly for the mathematical expression capturing the endogenous glucose production rate, could generate erroneous predictions for experiments with higher insulin boluses.

Salzsieder *et al.* developed a biologically relevant model describing the *in vivo* glucose-insulin relationship of T1DM patients [93]. Four linear state variables were used to model the system. The physiologically relevant states represented the circulating concentration of insulin and glucose, net endogenous glucose balance, and peripheral insulin-dependent glucose uptake. The model was calibrated and validated using published data of dogs [94, 93, 95]. Slow dynamics, as well as steady state glucose behavior, were accurately captured by the model. However, this accuracy was absent during faster insulin dynamics. The original model was verified within the limit of linearity, which was the upper normoglycemic level. This might prove to be disadvantageous, as during the post-prandial period the blood glucose level often hovers in the hyperglycemic level, especially for T1DM patients.

In another glucose-insulin modeling effort, Boroujerdi *et al.* [96] developed a glucose kinetics model which represented glucose utilization as two processes: insulin dependent and insulin independent. The overall glucose disposal comprised of glucose transport and utiliza-

tion and the effect of insulin on these processes. The model consisted of five compartments representing, plasma glucose, insulin sensitive and insulin-insensitive glucose interstitial space, and a glucose-transporter limited metabolism compartment for each of the interstitial spaces. An important finding of their model was that saturation of the glucose-transporter mechanism in diabetic patients leads to hyperglycemia. Inclusion of such physiological phenomenon would definitely make the model more accurate. However, the model lacked in specifying tissue-specific saturating phenomena and its characterization of insulin effects on endogenous glucose production.

A semi-empirical model of glucose-insulin interaction was developed by Lehman and Deutsch for T1DM patient evaluation [97]. The purpose of the model was to simulate glycemic and plasma insulin responses to a given insulin therapy and dietary regimen for 24 *hr*. The model contains a single glucose pool into which glucose enters via both intestinal absorption and hepatic glucose production. Glucose is removed from this space by insulin-independent glucose utilization in red blood cells, insulin-dependent glucose utilization in liver and periphery, and renal glucose excretion. Since the introduction of this model in the World Wide Web (www.2aida.org) for noncommercial use, a significant number of copies of this model have been downloaded to assist T1DM treatment [98]. Although, the main purpose of the model is to provide valuable knowledge to T1DM patients regarding their glucose dynamics after meal consumption, absence of FFA absorption from a mixed meal intake might limit the accuracy of the model prediction. Also, the model was incapable of predicting the glucose dynamics accurately during a continuous steady state insulin infusion (to maintain basal level) experiment, as shown by Steil *et al.* [51]. Utilization of two glucose compartments might have improved the accuracy of the model.

Tolic *et al.* [99] developed a model to evaluate insulin-glucose feedback regulation under pulsatile supply of insulin. The feedback loops present in the model consist of glucose-stimulated pancreatic insulin secretion, insulin-stimulated glucose uptake, insulin-stimulated inhibition of hepatic glucose production, and glucose-stimulated enhancement of its own uptake. Delays are also incorporated in the model to represent the physiologic delay of insulin action on hepatic glucose production. The results obtained from the model have shown that when hepatic glucose release rate is operating at its upper limit, an oscillatory

insulin infusion will be more effective in lowering blood glucose level than constant infusion. As the authors pointed out, more work is required to refine the model. For example, the time delay between plasma insulin and hepatic glucose production needs to be replaced by more physiologically relevant states. Also, the pulsatile effect of insulin on down-regulation of the insulin receptors should be incorporated in the model.

Originally, the “minimal” model was developed to capture the glucose kinetics of a single individual [1] and was never used to estimate the metabolic portrait for a whole population. A population-based approach can be useful in the study of diabetes for classification of patients being in risk groups or not. Furthermore, information from population estimates can provide prior information for statistical analysis of a single individual. Vicini and Cobelli [100] were the first to propose a Bayesian approach to the population-based minimal model. They used IVGTT data from sixteen healthy individuals to obtain distributions of glucose effectiveness and insulin sensitivity in the population. The mean and standard deviation obtained from the distributions were used as *a priori* information for individual analysis. Their method produced precise glucose effectiveness and insulin sensitivity estimates, even with a small sampling size. However, the method was employed on only the glucose part of the model. Recently, Andersen and Hojbjerg [101], proposed a similar version of the stochastic minimal model, where they combined both the glucose and insulin parts of the model. The population-based minimal model accounted for error terms associated with the measurement and the process. The Markov chain Monte Carlo technique was successfully implemented in estimation of the parameters by using the Bayesian approach. The method was demonstrated on experimental IVGTT data performed on 19 normal glucose-tolerant subjects.

Engelborghs and co-authors [102] developed a semi-empirical model with two delayed differential equations (DDE) for the plasma glucose and insulin concentration in a diabetic patient connected to an exogenous insulin delivery system. The model has two delays: the intrinsic delay involved with the external device, and the physiological delay associated with the action of insulin on glucose. Bifurcation analysis of steady state solutions and periodic solutions revealed two categories of diabetic patients for which the insulin delivery system had different efficiencies.

For better understanding of the insulin absorption kinetics produced by continuous subcutaneous infusion of insulin, Kraegen and Chisholm [103] used a kinetic model to quantitate the dynamics. The authors used a two-pool system to reasonably capture the systemic insulin delivery profile following a subcutaneous infusion. The model revealed that subcutaneous insulin degradation is low regardless of the input profile. Such kinetic models of subcutaneous insulin absorption should be useful to predict the impact of programming strategies for continuous subcutaneous insulin infusion therapy. Later, Puckett and Lightfoot [104] developed a three-compartment model representing the link between dosage and blood insulin levels. A comparison study revealed that the 3-D model fitted the data of individual patients better than the 2-D model from [103]. They also performed parameter identification and sensitivity analysis which highlighted insulin kinetic features that may significantly influence glucose dynamics. Their results showed significant inter-, as well as intra-patient variability of insulin absorption kinetics.

A semi-empirical model capable of capturing the absorption kinetics of subcutaneously injected insulin was developed by Wach *et al.* [105]. The model consisting of partial differential equations (PDE), described the diffusion of soluble insulin, equilibration between monomeric and dimeric insulin, and absorption of monomeric insulin molecules. The authors solved the PDEs numerically by dividing the subcutaneous region into spherical shells for space distribution. Parameters of the model were estimated by fitting published glucose-clamp data. The model predictions of dose- and concentration-dependent insulin absorption within the therapeutic range were in good accordance with the experimental data. According to the authors, the model could be used in a clinical setup to describe the subcutaneous insulin absorption kinetics of individual patients.

1.2.3 Physiological Models

In the mid-70s, Tiran and co-authors [76, 106] were among the first to attempt to develop physiologically-based “circulation model” of the glucose-insulin system. Several compartments were used to represent major organs and tissues in the human body. Each compartment was divided into two regions representing the capillary and interstitial space.

Glucose and insulin were distributed in these compartments via the blood circulation pathways. Nonlinear effects of glucose metabolism were also incorporated in the model. The model performed reasonably well in predicting venous glucose concentration in response to perturbations from glucose boluses of small sizes ($<30\text{ g}$). However, the model over-predicted glucose concentration for bolus sizes in excess of 30 g . The model also lacked in capturing the threshold metabolic behaviors of the physiological system. As the authors pointed out, the whole body model has the potential to serve as a basis for examining hypothesis regarding the glucose-insulin system.

A physiologically-based model of metabolism was developed by Sorensen, in his Ph.D. dissertation [2], based on an earlier model by Guyton *et al.* [107]. The model is comprised of 19 differential equations: 11 are used to define the glucose system, 7 define the insulin system, and one models glucagon. The glucose model consists of compartments representing the vital glucose-utilizing body organs and tissues: brain, heart/lungs, gut, liver, kidney, and periphery. In the model, ‘periphery’ represents skeletal muscle as well as adipose tissues (AT). Blood pumped from the heart enters into each compartment through the arterial circulation and exits to the venous circulation. Mass balances were performed across each tissue or organ in order to capture the plasma glucose distribution. Some of the compartments (such as ‘brain’ and ‘periphery’) were divided into sub-compartments (capillary and interstitial space) to incorporate resistance to glucose transport. Metabolic sinks representing glucose uptake were added to all the compartments. As the liver consumes, as well as produces glucose, both metabolic sink and source were incorporated in the ‘liver’ compartment. Most of the metabolic sinks/sources were functions of glucose, insulin, or glucagon concentration. The model accepted exogenous glucose input in the form of meal consumption. The insulin model has a similar structure to the glucose model [2]. The only difference, is that the ‘brain’ in the insulin model had a single compartment, because insulin does not cross the brain capillary barrier. Metabolic sinks representing insulin clearance were added to the ‘liver’, ‘kidney’, and ‘periphery’ compartments. The model does an excellent job in capturing the glucose and insulin distributions in all the major organs and tissues. Validation studies revealed that the model accurately predicted plasma glucose concentrations after intravenous and oral glucose tolerance tests. Because of its high accuracy and structural integrity, the Sorensen model

[2] was selected to provide a platform for the development of a physiologically-based FFA model to capture the fatty acid distribution at organ/tissue levels, as described in Chapter 5.

A semi-physiologic nonlinear model of glucose and insulin was developed by Cobelli *et al.* [78]. The model consisted of mathematical functions capturing peripheral glucose consumption, renal glucose excretion, hepatic glucose production and utilization, glucose absorption from a meal, insulin secretion, and insulin degradation. Delay terms were also included in the model to incorporate the physiologic delay involved in the gluco-regulatory action of insulin on glucose. Simulation studies revealed that the model successfully described physiological events occurring in a normal human after the ingestion of standard meals on a 24 hour horizon. However, the model does not account for glucose distribution at the major glucose-consuming organ levels.

1.2.4 Metabolic Models Considering FFA and Exercise Effects

All the metabolic models so far discussed spanning five decades exclusively focus on the interactions between glucose and insulin. Effects of FFA and exercise on plasma glucose dynamics have been largely neglected. For the synthesis of high quality and robust closed-loop model-based controllers for maintenance of glucose homeostasis, it is essential to develop models that take into account the external disturbances encountered by a T1DM patient in his/her daily life, like mixed meal ingestion and exercise. There are only few metabolic models present in the literature that consider FFA and exercise effects on glucose dynamics.

A physiologically-based model of insulin, glucose, and fatty acids has been proposed by Srinivasan *et al.* [77]. The model is made of interconnected sub-systems, each representing one or more physiological processes. Known physiology was incorporated with an intention to reproduce the effects of FFA and glucose metabolism for a short-term period (< 2 hr). This complex model was the first of its kind to include FFA dynamics in the glucose-insulin system. The model, qualitatively, did a reasonable job in predicting glucose and FFA dynamics after an IVGTT. One potential drawback is that the model ignored the effects of blood circulation on metabolism. Also, as pointed out by the authors, the model lacked the ability

to adequately reproduce the finer details of plasma glucose, FFA, and insulin changes caused due to introduction of disturbances in the metabolic system. According to the authors, further refinement of the mathematical functions and inclusion of more hormonal controls might yield better results. From a control point of view, a major drawback of the model is its inability to predict plasma glucose and FFA dynamics at longer time periods (in excess of 2 *hr*).

Recently, Kim *et al.* [108] developed a physiologically-based model of metabolism to capture the whole-body fuel homeostasis during exercise. The model was divided into seven physiologic compartments representing the brain, heart, liver, GI (gastrointestinal) tract, muscle, AT, and other tissues. Dynamic mass balance equations along with cellular metabolic reactions were considered in each of the compartments. Hormonal control by insulin and glucagon over the cellular metabolic processes were incorporated in the model to predict the changes in fuel homeostasis during exercise. Model simulations were validated with experimental data where normal subjects performed moderate intensity exercise for 60 *min*. The model successfully captured the exercise-induced changes in hormonal signals at various tissues in order to regulate metabolic fluxes for maintenance of glucose homeostasis. The model also successfully captured the dynamics of variables like, hepatic glycogenolysis and gluconeogenesis, which are hard to measure. In addition, the model can also indicate the relative contributions to fuel oxidation of glucose and FFA in the muscle during exercise. This novel mechanistic model that links cellular metabolism to whole-body fuel homeostasis can be used for testing hypotheses of hormonal control and dynamical predictions of metabolite concentrations in various tissues during exercise. However, due to the scale and complexity in terms of number of equations and parameters, the model has limited applicability in a clinical setup to be calibrated to individual patients. Also, the model fails to capture the experimental data of arterial lactate concentration.

From a control prospective, the complexity of both the above mentioned models [77, 108] can prove to be a liability for the synthesis of a model-based control system for T1DM patients. Due to the sheer scale of the model, it is hard to design experimental protocols to identify parameters for individual patients. Hence, parametric identifiability can be a major issue. One potential method for overcoming the parameter estimation problem is *a*

priori identifiability, which is discussed as a potential direction of future work in Section 7.2.2. A further complication of the detailed models is the difficulty in using them in an adaptive control environment, as no identifiable parameter or combination of parameters are necessarily available to be updated online. As the long-term goal of the present work is to develop models that can be used for the synthesis of a model-based controller, development of accurate lower-order structurally simple metabolic models capturing the insulin, glucose, and FFA dynamics during rest and exercise is essential.

1.3 OVERVIEW OF CLOSED-LOOP INSULIN DELIVERY SYSTEMS

A fully automated closed-loop (CL) insulin delivery system (also known as an artificial pancreas) could potentially be the ultimate answer for blood glucose control in diabetic patients. According to Klonoff [47], the artificial pancreas is a system of integrated devices containing only synthetic materials, which substitutes for a pancreas by sensing plasma glucose concentration, calculating the amount of insulin needed, and then delivering the correct amount of insulin. Typically, such a device is comprised of a glucose monitoring sensor, an insulin pump, and a control algorithm to regulate the pump. Such an approach of glucose measurement, determination of proper insulin dose, and delivery of insulin can theoretically result in physiologic glycemic levels with a high level of precision.

The first CL insulin delivery device (an ‘on-off’ system) was developed by Kadish [109] in 1964. The device measured venous blood glucose concentration every 15 seconds and delivered either insulin (if the blood glucose level was above $150 \frac{mg}{dL}$) or glucagon (if the blood glucose level was below $50 \frac{mg}{dL}$) to maintain the glycemic level within a range of 50–150 $\frac{mg}{dL}$. The performance of the Kadish device was hampered due to the lack of computational power at the time. Also, the size of the device was equivalent to a large back-pack.

In the mid 1970’s, Albisser *et al.* [110, 111] synthesized a true artificial pancreas. In order to automate insulin delivery, the integrated device consisted of a continuous glucose monitor with control algorithms implemented on a micro-computer. The device used a two channel system, one of which was dedicated to dextrose infusion and the other one was

for insulin infusion. One of the major limitations of the device is that the control algorithm required several patient-dependent parameters. In addition, the initial controller response to a glucose surge was sluggish. The first commercially available CL insulin-delivery system, the Biostator (Miles laboratory), was available in 1977 [112]. A nonlinear proportional-derivative (PD) control algorithm was used to regulate a dual infusion system (insulin and dextrose) to maintain glucose homeostasis. For the feedback signal, venous blood was sampled at a regular interval to measure plasma glucose concentration and the associated measurement noise was filtered by using a 5-point moving average. The device suffers from serious limitations, mainly due its size, and necessity of constant supervision. Also, it requires individualization before use. The Biostator is no longer commercially available. A modified version of the Albisser [110] algorithm based on glucose measurement and rate of change of glucose was presented by Botz [113], Marliss [114], and Kragen *et al.* [115] to reduce post-prandial hypo-/hyper-glycemic events. In a review paper, Broekhuysse *et al.* [116] concluded that none of the above-mentioned algorithms were superior.

Fischer and colleagues have extensively studied closed-loop feedback control of blood glucose in T1DM [94]. They raised the question of whether or not only an adaptive algorithm would guarantee optimal feedback control of glycemia in insulin-dependent diabetes. In their experiment, insulin was applied intravenously and an oral glucose load was given to fasting diabetic dogs at rest. Three different control strategies were employed: (i) online identification of the glucose-insulin system for 4 *hr* followed by an adaptive feedback control algorithm where the control parameters were adapted continuously at every sampling time ($\Delta t=1 \text{ min}$), [Test A]; (ii) online system identification just like the previous test followed by a fixed command control using the initial estimates without any further changes in the control parameters [Test B]; and (iii) fixed command control employed on the basis of individually optimized offline control constants (no online system identification was performed) [Test C]. Normal glycemic profiles were obtained with the adaptive control setup (Test A) and the fixed command control optimized to meet individual needs (Test C).

Recently, Medtronic Minimed has developed an external physiological insulin delivery system (ePID) [117]. The fundamental design criterion of the controller is to emulate the characteristics of the β -cell, in particular the first and the second phase insulin secretion as

observed during hyperglycemic glucose clamps [118, 119]. This was achieved by adapting a proportional-integral-derivative (PID) controller [120] which can be considered to reproduce the first phase insulin secretion by linking insulin administration to the rate of change in glucose concentration (the derivative component of the controller) and the second phase by linking insulin administration to the difference between the actual and target glucose (the proportional and integral component of the controller). A recent evaluation of the ePID system on 6 T1DM patients revealed satisfactory performance. However, the controller was unable to prevent hypoglycemic events during the post-prandial periods [117].

In 1982, Swan [121] developed an optimal controller for maintenance of normoglycemia in diabetic patients. He used a linear diabetic patient model and a quadratic performance criterion to estimate the optimal insulin infusion rate by solving the nonlinear algebraic Riccati equation. The authors did not examine the controller performance during post-prandial conditions. Ollerton [122] applied optimal control theory to the minimal model developed by Bergman [1] for maintenance of glucose homeostasis, where he utilized an integral-squared error objective function based on deviation from the target glucose value. In order to reduce calculation time, the Bergman minimal model was discretized with a 10 *min* sampling time. The control formulation was sensitive to oscillations in the glucose profile about the basal state.

In another study by Fisher and Teo [123], blood glucose control during post-prandial, as well as fasting condition was examined. Various insulin infusion protocols were tested to minimize the objective function, which was basically the sum-squared error in glucose setpoint tracking. An insulin impulse at $t=0$ provided superior setpoint tracking if a good meal estimate was available.

One of the most promising control approaches is a model predictive controller (MPC). As the name suggests, MPC is a model-based control approach where a metabolic model of a patient is used to predict future plasma glucose concentration. The controller solves an optimization problem by minimizing a quadratic objective function at every sampling time. The terms in the objective function include setpoint error, which is the difference between predicted future blood glucose concentration and the desired reference trajectory, as well as a penalty for the insulin delivery rate. MPC performance depends largely on the ability of the

model to accurately predict future glucose concentration based on the current physiological condition [50] and available measurements.

Trajonski *et al.* [81] developed a MPC framework for glycemic control of diabetic patients. Using the subcutaneous route for insulin infusion and glucose measurement, a radial basis function (RBF) neural network model for glucose prediction was identified from past insulin infusion rates and glucose measurements. A nonlinear MPC was synthesized based on the identified model for maintenance of glucose homeostasis. According to the simulation results, stable control was achievable in the presence of large noise levels.

Parker *et al.* [65] used a linear version of the physiologically-based Sorensen model [2] to synthesize a MPC, both with and without state estimation, for glycemic control [65]. Input constraints were implemented for both input delivery rate and rate of change of insulin delivery rate. For simulation purposes, the full nonlinear Sorensen model was treated as the patient in order to represent the effects of plant-model mismatch. The control formulation was tested successfully to regulate blood glucose for both meal disturbance rejection and hyperglycemic initial condition. A linear MPC based on the input-output model was sufficient to maintain normoglycemia after a 50 g oral glucose tolerance test (OGTT).

Lynch and Bequette [124] synthesized a constrained MPC based on a modified version of the Bergman minimal model [1] developed by Fisher [125]. A Kalman filter was used for state estimation based on subcutaneous blood glucose measurements. In order to incorporate plant-model mismatch, the patient was represented by the higher-order Sorensen model [2]. With proper tuning, the closed-loop controller successfully returned blood glucose to the normoglycemic range by rejecting disturbances from meal consumption.

A nonlinear MPC was developed by Hovorka *et al.* [126] to maintain normoglycemia of T1DM patients during fasting conditions. The controller employed a compartment model developed by Hovorka *et al.* [75], which represents the glucoregulatory system, and included submodels representing absorption dynamics of the subcutaneous short-acting insulin. The controller used Bayesian parameter estimation to determine time-varying model parameters. The algorithm also employed gradually decreasing setpoint trajectory in order to facilitate controlled normalization of hyperglycemic glucose levels, and faster normalization of hy-

poglycemic glucose levels. The closed-loop system employed inta-venous glucose sampling every 15 *min* and subcutaneous infusion of insulin. For clinical evaluation, the controller was implemented on ten T1DM patients over a period of 8–10 *hr*. The authors concluded that the performance of the adaptive nonlinear MPC was promising for glucose control during the fasting state. However, the controller was not examined for the post-prandial state.

Advanced control strategies were developed by Parker *et al.* [6] by utilizing the MPC framework to deliver exogenous insulin to T1DM patients for maintenance of normoglycemia. To satisfy the performance requirement of a diabetic patient, an asymmetric objective function MPC was synthesized to minimize the post-prandial hypoglycemic events. This technique was compared to another formulation where a prioritized objective function MPC was synthesized to ensure desired objectives were met according to their level priority. The asymmetric objective function MPC performed well in avoiding hypoglycemia as compared to the PO MPC [6].

Out of all these control approaches, MPC is of particular interest as it has many potential advantages. An unconstrained MPC provides optimal insulin delivery by solving an optimization problem at every sampling time [127]; this optimality is purchased at the expense of computational effort, in general. One of the major benefits of a MPC controller is that it can adjust the insulin delivery rate in response to a predicted future hyper- or hypoglycemic event much before the actual incident has actually occurs. A MPC controller has the capability, within reason, to compensate for the dynamics associated with the glucose sensor and the appearance of insulin in the circulatory system after being released from the pump [51]. Also, the lower and upper constraints for insulin delivery rate can be intrinsically formulated in the MPC algorithm [127], which is an important safety issue for such biomedical systems. Finally, the MPC framework can be tailored to fulfill inherent requirements of a physiological system by altering the objective function [6, 128].

1.4 THESIS OVERVIEW

The goal of this dissertation is to incorporate the FFA dynamics and its physiologic interactions with glucose and insulin at rest, as well as during exercise, into the published glucose-insulin metabolic models [1, 2]. This will be accomplished by synthesizing physiologically-relevant mathematical expressions (ordinary differential and algebraic equations) calibrated to experimental data obtained from the literature. Validation of the models will be performed by comparing model predictions with new data sets procured from the literature.

Chapter 2 concentrates on a minimalistic approach for the synthesis of a lipid-based (FFA) model. The “minimal” model developed by Bergman [1] was extended to incorporate the FFA dynamics and the physiological interactions that exist between FFA, glucose, and insulin. This enables the model to provide valuable insight regarding the disturbance provided by FFA on plasma glucose level after consumption of a mixed meal, *i.e.* meal containing CHO, protein, and fat. Hence, a mixed meal model has also been developed in Chapter 2 to capture the absorption of CHO, protein, and fat (as FFA) from gut into the circulatory system. The mixed meal model served as a disturbance to the extended minimal model.

The exercise effects on glucose and insulin dynamics were addressed in Chapter 3. Here, once again the Bergman minimal model was modified to incorporate the physiological effects of mild-to-moderate exercise on plasma glucose and insulin levels. Chapter 4 focuses on a lower-order model of the insulin-glucose-FFA system which is capable of predicting plasma insulin, glucose, and FFA concentrations at rest, as well as during exercise. Basically, this model combines the FFA model from Chapter 2 and the exercise model from Chapter 3 with relevant physiologically-motivated modifications to form a lower-order composite model.

In Chapter 5, the focus was shifted from developing minimal models to physiologically-based metabolic models. A physiological multi-compartmental FFA model was synthesized and coupled with the glucose-insulin model developed by Sorensen [2]. This model is more complex than the FFA minimal model (developed in Chapter 2), in terms of number of equations and parameters. The model is capable of predicting insulin, glucose, and FFA dynamics at the organ/tissue levels.

One objective of developing accurate metabolic models is to synthesize model-based insulin delivery systems for maintaining normoglycemia [65, 124]. The current treatment procedure for T1DM (insulin intensive treatment) is unable to produce tight glucose control causing prolonged periods of hypoglycemic and/or hyperglycemic events. To minimize the glucose fluctuations caused due to meal intake, a part of the thesis focused on the development of a model-based closed-loop insulin delivery system, which have been shown to produce superior glucose control [126]. Hence, in Chapter 6 the loop was closed by employing a MPC algorithm based on the metabolic models for meal disturbance rejection and maintenance of normoglycemia. A summary of all the conclusions of this work, as well as possible future directions are presented in the penultimate Chapter (Chapter 7).

2.0 AN EXTENDED “MINIMAL” MODEL OF FFA, GLUCOSE, AND INSULIN¹

One of the most widely used and validated metabolic models of glucose-insulin dynamics is the so-called “minimal” model developed by Bergman and colleagues [1, 85]. The model was proposed more than 25 years ago, and over the years it has become a major clinical tool for analyzing glucose effectiveness (ability of glucose to promote its own disposal) and insulin sensitivity (ability of insulin to enhance glucose effectiveness) during an IVGTT for diabetic patients [1, 131]. Prior to the Bergman minimal model [1], only few mathematical models of metabolism existed [69, 70, 77, 84]. These models were either too simple [69, 70, 84] or too complex [77], as discussed in Chapter 1. Hence, Bergman *et al.* hypothesized the existence of a metabolic model with “optimal” complexity. In other words, a model complex enough to account for the feedback relationship between insulin and glucose, but simple enough so that it can be used to evaluate metabolic functions of a diabetic patient with a simple clinical protocol. Because of these characteristics, the Bergman minimal model [1] has gained immense popularity in the diabetes treatment and research community, despite of its shortcomings as pointed by Quon *et al.* [87] and others [5, 73].

The primary focus of the Bergman minimal model [1] was to describe the feedback relationship within the glucose-insulin system. The model has proven to be effective particularly in quantifying the glucose disposal process, by providing a measure of insulin sensitivity and glucose effectiveness [5]. Such non-invasive measurements of glucose kinetics are essential to understand the etiology of various forms of impaired glucose tolerances.

Historically, insulin was believed to be the exclusive regulator of blood glucose concentration, hence, majority of the published mathematical models dealt with the glucose-insulin

¹Portions of this chapter have been published in [129] and [130]

feedback system only. However, in the last three decades researchers have demonstrated that FFA plays a significant role in altering the glucose-insulin system [132, 133, 8, 134]. Despite FFA being an important metabolite, its incorporation in the metabolic models has been largely overlooked. This void in the literature has motivated us to synthesize “lipid-based” metabolic models with a long-term goal of developing model-based controllers for maintaining normoglycemia by rejecting disturbances from mixed meal ingestion.

FFA in the human plasma pool is mostly composed of long chain carbon molecules with varying numbers of unsaturated bonds. The primary constituents of this mixture are: palmitate (16:0), stearate (18:0), oleate (18:1), linolate (18:2), palmitoleate (16:1), and myristate (14:0) [135]. The nomenclature (A:B) describes the length of the carbon chain, A, and the number of unsaturated bonds, B. Approximately 80% of the muscle energy is derived from FFA metabolism when the body is at rest [52, 53]. The main reason for this is because FFA, when compared with plasma glucose, accounts for a greater energy flux [54]; ATP yield from the breakdown of 16-carbon fatty acid is approximately 2.5 times greater than glucose per gram [136].

Significant interactions exist between FFA, glucose, and insulin. Randle *et al.* proposed that an increased delivery of FFA to muscle tissue enhanced the rate of fat oxidation, which led to increased acetyl-CoA and resulted in downregulation of the rate-limiting glucose metabolizing enzymes, thereby attenuating glucose uptake into the tissues [58, 59]. *In vitro* studies have also revealed that prolonged hyperglycemia promotes release of stored FFA from the AT into the the circulatory system [9, 137]. As a first step towards the synthesis of lipid-based models, the Bergman minimal model [1] was extended to include plasma FFA dynamics, and its interactions with glucose and insulin, with a primary focus on T1DM patients. Care was taken to include all the major physiological interactions between glucose, insulin, and FFA without sacrificing the simplifying approach of the minimal model.

The following Section (2.1) provides a detailed description regarding the structure of the Bergman minimal model [1]. The structure of the extended minimal model capturing the dynamics of FFA, glucose, and insulin is introduced in the Section 2.2. Section 2.3 presents a detailed description of the parameter estimation technique and goodness of fit. Results of the extended minimal model along with structural justifications are provided in Section

2.4. One of the objectives in synthesizing the extended minimal model is to evaluate the effects of mixed meal ingestion on closed-loop glucose control. Hence, in Section 2.5 a mixed meal model was developed to capture the gut absorption of glucose, protein, and FFA from a mixed meal into the circulatory system. The outputs of the meal model served as disturbance inputs to the extended minimal model. Finally, the chapter ends with a brief summary 2.6.

2.1 BERGMAN MINIMAL MODEL

In order to quantify the insulin sensitivity and glucose effectiveness of a T1DM patient during an IVGTT, Bergman *et al.* [1] developed a three compartment mathematical model, as shown in Figure 2.1. Compartment $I(t)$, $X(t)$, and $G(t)$ represent the plasma insulin ($\frac{\mu U}{ml}$), remote insulin ($\frac{\mu U}{ml}$), and plasma glucose concentration ($\frac{mg}{dl}$), respectively. The model as written assumes that all the necessary insulin is infused exogenously ($u_1(t)$), thereby modeling the insulin-dependent diabetic patient. A portion of the infused insulin enters into the remote compartment, $X(t)$, from the circulatory system, $I(t)$. The inaccessible remote insulin ($X(t)$) actively takes part in promoting uptake of plasma glucose ($G(t)$) into the liver and peripheral (extra-hepatic) tissues.

The Bergman minimal model, adapted from [1], is mathematically given by:

$$\frac{dI(t)}{dt} = -nI(t) + p_5 u_1(t); \quad I(0) = I_b = \frac{p_4}{n} u_{1b} \quad (2.1)$$

$$\frac{dX(t)}{dt} = -p_2 X(t) + p_3 [I(t) - I_b]; \quad X(0) = 0 \quad (2.2)$$

$$\frac{dG(t)}{dt} = -p_1 G(t) - p_4 X(t) G(t) + p_1 G_b + \frac{u_2(t)}{Vol_G}; \quad G(0) = G_b \quad (2.3)$$

Here, I_b and G_b are the basal plasma insulin and glucose concentrations, respectively. The exogenous insulin infusion rate to maintain I_b is represented by u_{1b} (mU/min). The rate constant n represents clearance of plasma insulin. Parameter p_5 represents the inverse of

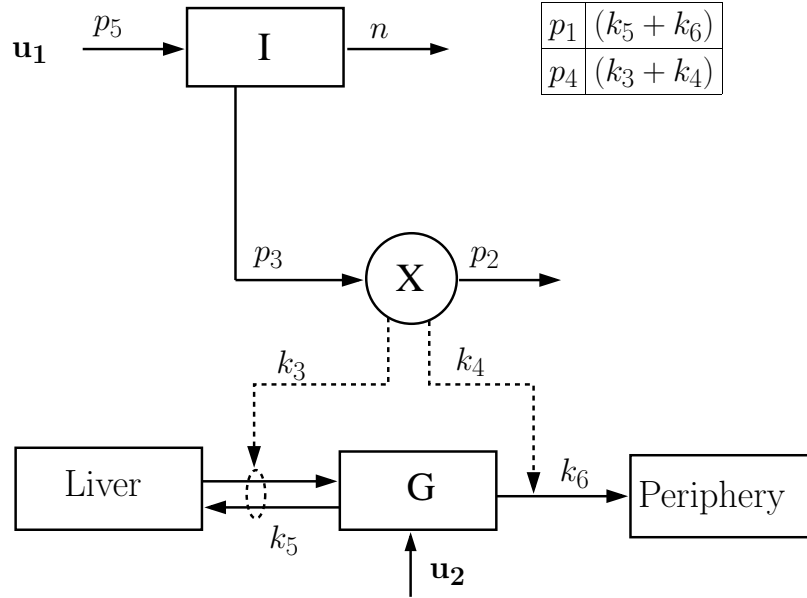


Figure 2.1: Bergman minimal model of insulin and glucose dynamics, adapted from [1]

insulin distribution space. The rates of appearance of insulin in, and disappearance of remote insulin from, the remote insulin compartment ($X(t)$) are governed by the parameters p_2 and p_3 , respectively. Dietary absorption or external infusion of glucose is indicated by $u_2(t)$, and the glucose distribution space is indicated by Vol_G . Parameter p_1 represents the rate at which glucose is removed from the plasma space into the liver (mostly for storage) or into the periphery (mostly for oxidation) independent of the influence of insulin. Glucose uptake under the influence of insulin is governed by the parameter p_4 . Parameter values for the Bergman minimal model [1] are provided in Table 2.1.

2.2 EXTENDED MINIMAL MODEL

The Bergman minimal model [1] was extended to incorporate FFA dynamics and its interaction with glucose and insulin. Modifications were made to the original model structure

Table 2.1: Parameters of the Bergman minimal model, from [1]

Parameter	Value	Units	Parameter	Value	Units
p_1	0.068	$\frac{1}{min}$	p_5	0.000568	$\frac{1}{mL}$
p_2	0.037	$\frac{1}{min}$	n	0.142	$\frac{1}{min}$
p_3	0.000012	$\frac{1}{min}$	G_b	98.0	$\frac{mg}{dL}$
p_4	1.0	$\frac{mL}{min \cdot \mu U}$	Vol_G	117.0	dL

by adding extra compartments, as shown in Figure 2.2. Compartment $F(t)$ represents the plasma FFA concentration. Similar to compartment $X(t)$ in the Bergman minimal model, an unaccessible compartment $Y(t)$ was added to the FFA model representing the remote insulin concentration inhibiting FFA release from the AT into the circulatory system. An additional first order filter, compartment $Z(t)$, was added to the model to represent the remote FFA concentration affecting glucose uptake dynamics.

Similar to the Bergman minimal model, the extended minimal model assumes that no insulin is produced endogenously. Equations, (2.1) and (2.2) from the Bergman minimal model (Section 2.1) are used to describe the dynamics of plasma insulin and remote insulin concentration for the extended minimal model, respectively.

The plasma glucose dynamics are represented by the following equation:

$$\frac{dG(t)}{dt} = -p_1G(t) - p_4X(t)G(t) + p_6G(t)Z(t) + p_1G_b - p_6G_bZ_b + \frac{u_2(t)}{Vol_G} \quad (2.4)$$

Parameters p_1 , p_4 , G_b , Vol_G and $u_2(t)$ are same as in equation (2.3). The additional impairing action of plasma FFA on glucose uptake is represented by the parameter p_6 .

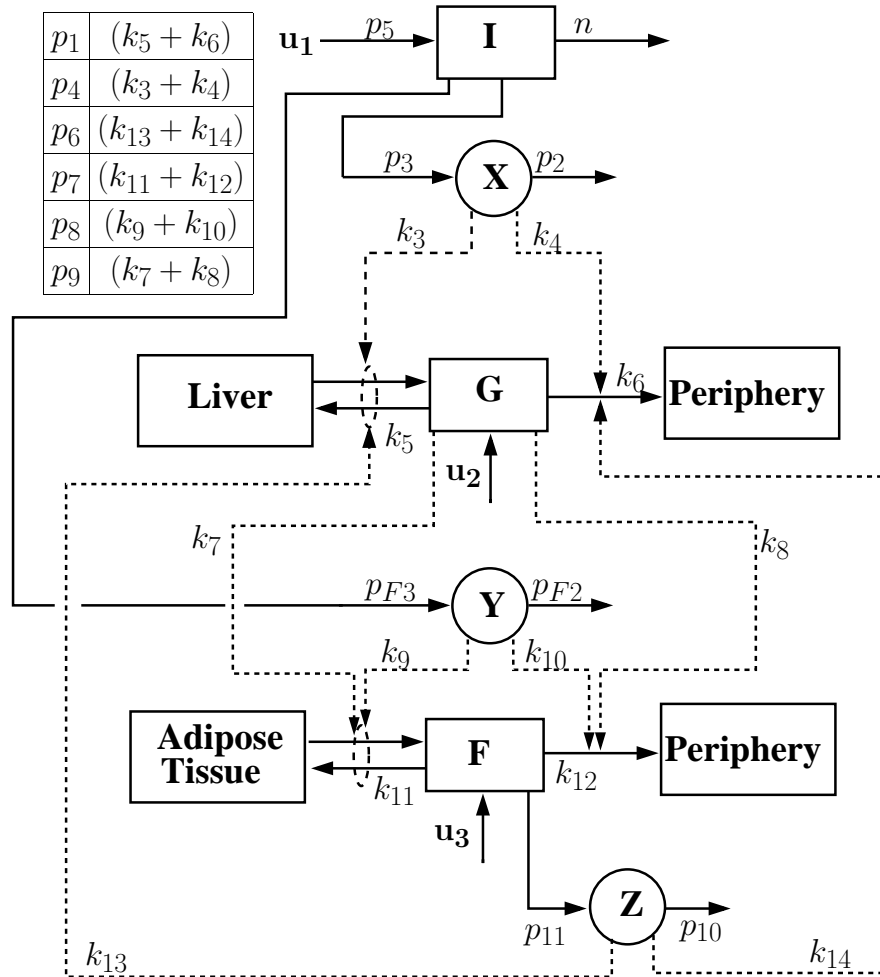


Figure 2.2: Extended minimal model of insulin, glucose, and free fatty acid dynamics

The release of stored FFA into the circulatory system, which is known as lipolysis, is inhibited by the insulin in the unaccessible compartment $Y(t)$. The remote insulin dynamics for FFA ($Y(t)$) are represented as follows:

$$\frac{dY(t)}{dt} = -p_{F2}Y(t) + p_{F3}[I(t) - I_b] \quad (2.5)$$

The rate of disappearance of insulin from this remote insulin compartment is governed by the parameter p_{F2} , and the rate at which plasma insulin enters into the remote insulin compartment is governed by the parameter p_{F3} .

Plasma FFA is taken up by the periphery (for oxidation) and by the AT (for storage). Prolonged hyperglycemia, *i.e.*, high glucose levels, induces lipolysis, thereby promoting release of FFA from the AT into the circulatory system. The dynamical equation representing plasma FFA is given by:

$$\frac{dF(t)}{dt} = -p_7F(t) - p_8Y(t)F(t) + p_9(G)F(t)G(t) + p_7F_b - p_9(G)F_bG_b + \frac{u_3(t)}{Vol_F} \quad (2.6)$$

Here, the basal FFA concentration and FFA distribution space are given by F_b and Vol_F , respectively. Dietary FFA absorption or external lipid infusion is represented by $u_3(t)$. The combined rate at which FFA is taken up by the AT and periphery without the influence of insulin is governed by the parameter p_7 . Similarly, parameter p_8 represents the rate of disappearance of plasma FFA under the influence of insulin, or, in other words, the anti-lipolytic effect of insulin. The lipolytic effect of plasma glucose concentration level is indicated by the parameter $p_9(G)$, which is a function of glucose concentration, as follows:

$$p_9(G(t)) = ae^{-bG(t)} \quad (2.7)$$

FFA from the circulatory system enters in the unaccessible compartment $Z(t)$, which affects glucose uptake in the liver and peripheral tissues. The remote FFA dynamics ($Z(t)$) are represented by:

$$\frac{dZ(t)}{dt} = -k_2[Z(t) - Z_b] + k_1[F(t) - F_b] \quad (2.8)$$

Here, Z_b represents the basal remote FFA concentration. The rate of FFA concentration disappearance from, and appearance in compartment $Z(t)$ are governed by the parameters k_2 and k_1 , respectively.

2.3 PARAMETER ESTIMATION AND GOODNESS OF FIT TECHNIQUE

The parameters for the extended model were estimated using the nonlinear ‘least square’ technique as described by Carson and Cobelli [138]. The normalized residual is obtained as:

$$\chi^2 \equiv \sum_{i=1}^N \left[\frac{y_i - y(t_i, \theta_1 \dots \theta_M)}{\sigma_i} \right]^2 \quad (2.9)$$

Here, y_i is the measured data at time t_i , which has a standard deviation of σ_i . The model prediction is given by $y(t_i, \theta_1 \dots \theta_M)$, where θ_i represent model parameters. Equation (2.9) is the objective of a weighted minimization having $(\frac{1}{\sigma})^2$ as the weights and θ_i as the degrees of freedom. N is the number of data points, and M is the total number of estimated model parameters.

The parameters n , p_1 , p_2 , p_3 , p_4 , p_5 , and n , were fixed to the values in Table 2.1. First, the rate constants representing plasma FFA concentration with (p_8 , p_{F2} , and p_{F3}) and without (p_7) the influence of insulin were estimated in order to fit published data [4]. Next, the lipolytic effect of glucose ($p_9(G)$) was estimated using data from the literature [9]. Finally, the parameters representing the effect of plasma FFA on glucose uptake (p_6) and the remote FFA concentration (k_1 and k_2) were estimated from published data [8]. All the estimated parameter values of the extended model are given in Table 2.2.

Table 2.2: Parameters of the extended minimal model, in addition to those in Table 2.1. 95% confidence interval (CI) bounds were calculated by using the *nlparci.m* MATLAB function.

Parameter	Value	Lower 95% CI	Upper 95% CI	Units
p_6	0.00006	$4.5e - 5$	$7.5e - 5$	L/(min · μ mol)
p_7	0.03	0.026	0.033	1/min
p_8	4.5	3.86	5.14	mL/(min · μ U)
a	$0.21e - 3$	$0.2079e - 3$	$0.2121e - 3$	dL/(min · mg)
b	0.0055	0.00536	0.00563	dL/mg
k_1	0.02	0.0158	0.0242	1/min
k_2	0.03	0.0231	0.0369	1/min
p_{F2}	0.17	0.1438	0.1961	1/min
p_{F3}	0.00001	$8.577e - 6$	$1.1423e - 5$	1/min
F_b	380	–	–	μ mol/L
Vol_F	11.7	–	–	L

The quality of the model fits was assessed by measuring the statistical correlation between data and model predictions (R^2). R^2 can be defined as:

$$R^2 = 1 - \frac{\chi^2}{SST} \quad (2.10)$$

Here, χ^2 is the weighted sum squared error from equation (2.9), and SST is the weighted sum of squares about the data mean. SST can be calculated using the following equation:

$$SST \equiv \sum_{i=1}^N \left[\frac{y_i - \bar{y}}{\sigma_i} \right]^2 \quad (2.11)$$

Here, N is the number of data points and \bar{y} is the mean of all the data points. R^2 takes values between 0 and 1, with a value closer to 1 indicating a better fit.

Akaike's Information Criterion (AIC) [139] was employed to establish a statistical comparison between the extended model with and without the remote insulin compartment,

$Y(t)$, and remote fatty acid compartment, $Z(t)$, as described below in Section 2.4.5. The value of AIC can be calculated from the following equation:

$$AIC = (N) \ln \left(\frac{\chi^2}{N} \right) + 2(M) \quad (2.12)$$

Here, M is the number of model parameters. The criterion may be minimized over choices of M to form a tradeoff between the fit of the model, which lowers the sum squared error (χ^2), and the model's complexity, which is quantitated by M . Hence, AIC not only rewards goodness of fit, it discourages over-parameterizing. When comparing two models having different values of M , it is always desirable to prefer the model that has a lower AIC value. However, in settings where the sample size (N) is small, AIC tends to favor inappropriately the high-dimensional candidate models [140].

2.4 RESULTS OF THE EXTENDED MINIMAL MODEL

2.4.1 Antilipolytic Effect of Insulin

FFA movement across AT capillary walls is bi-directional, unlike any other tissue [54]. In other words, plasma FFA is taken up by the AT for storage purposes, and at the same time, stored FFA from AT is released back into the circulatory system whenever necessary. Insulin plays a major role in altering the balance between lipid storage and release in AT, by acting as a strong antilipolytic agent. Basically, insulin inhibits the release of stored FFA into the circulatory system. This antilipolytic effect of insulin was well demonstrated by an *in vivo* study performed by Howard *et al.* [4].

In the experiment, an euglycemic hyperinsulinemic clamp was employed in healthy subjects, as shown in Figure 2.3. Insulin was infused at three different rates in order to maintain the plasma insulin concentration at 20, 30, and 100 $\frac{\mu U}{ml}$ [4]. The plasma FFA concentration decreased significantly below the basal state in response to the insulin clamps. Parameters p_7 , p_8 , p_{F2} , and p_{F3} of equations (2.5) and (2.6) were adjusted in order to

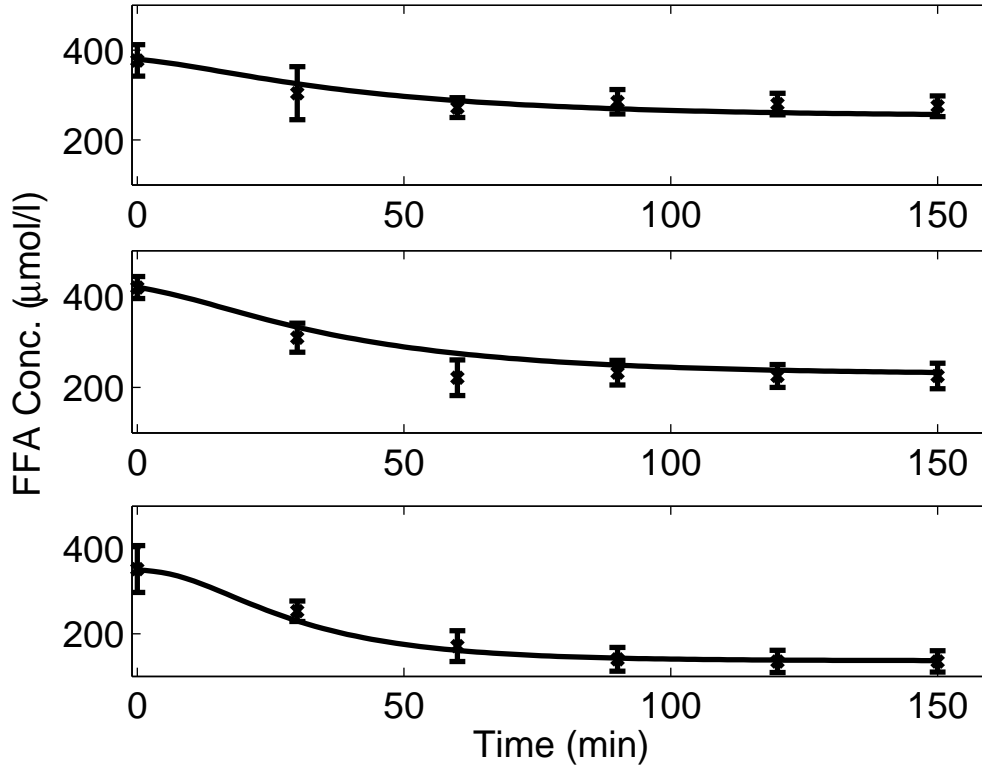


Figure 2.3: Predicted (solid lines) and published (cross) [4] ($\mu \pm \sigma$) plasma FFA concentration in response to euglycemic hyperinsulinemic clamp. Plasma insulin concentration was maintained at $20 \frac{\mu U}{ml}$ [$R^2 = 0.77$] (top), $30 \frac{\mu U}{ml}$ [$R^2 = 0.94$] (middle), $100 \frac{\mu U}{ml}$ [$R^2 = 0.98$] (bottom)

minimize equation (2.9) using the published data from [4], as described in Section 2.3. The resulting model predictions of plasma FFA concentration are consistent with the published data, as shown in Figure 2.3. Estimated parameter values are provided in Table 2.2.

2.4.2 Lipolytic Effect of Hyperglycemia

Prolonged hyperglycemia enhances lipolysis in adipocytes [9, 137]. The rate-limiting step of adipocyte lipolysis is due to the hydrolysis of stored triglycerides by hormone-sensitive lipase

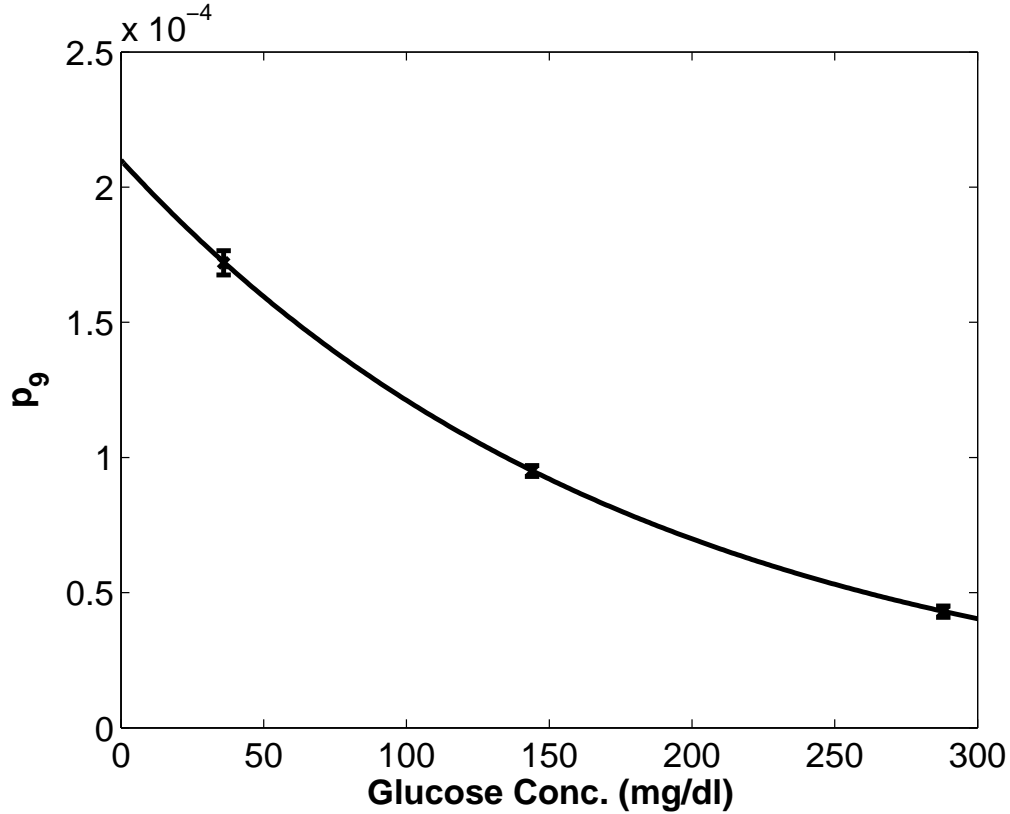


Figure 2.4: Predicted values of parameter p_9 in response to increasing glucose clamps for 90 min. [$R^2 = 1$]

(HSL) enzyme [137]. Hyperglycemia induces activation of HSL, which in turn enhances lipolysis [137]. In an *in vitro* study by Szkudelski *et al.*, isolated rat adipocytes were treated with increasing glucose concentration (36, 144, and 288 $\frac{mg}{dl}$) [9]. After 90 min of incubation the increment in lipolysis was measured by analyzing the total glycerol released in the incubating medium (recorded as, 342 ± 7 , 445 ± 5 , and $506 \pm 12 \frac{nmol}{ml-10^6 cells-90min}$, respectively). In order to estimate the value of parameter p_9 , the glucose concentration of the FFA minimal model during a 90 min simulation was held constant at 36, 144, or 288 $\frac{mg}{dl}$, and p_9 was adjusted to acquire the respective increment in FFA concentration. The variation of p_9 with increasing glucose concentration clamps is shown in Figure 2.4. The

relationship of p_9 with G is provided in equation (2.7) and Table 2.2. In a separate *in vitro* study, Moussalli *et al.* [141] treated isolated human adipocytes with $36 \frac{mg}{dl}$ of glucose. The glycerol released from the human AT ($331 \pm 15 \frac{nmol}{ml-10^6 cells-90min}$) was similar to that of the rat AT ($342 \pm 7 \frac{nmol}{ml-10^6 cells-90min}$) treated at the same glucose concentration in [9]. Due to the comparable glycerol release rates, the lipolytic effects of glucose on rat and human adipocytes were treated as equivalent for the present study. The validation of this assumption at higher glucose concentrations requires additional experimental data.

2.4.3 Impairing Effect of FFA on Glucose Uptake Rate

Studies as early as 1963 [58] had revealed that high plasma FFA concentration impairs net glucose uptake rate. The postulated mechanism is that increased FFA oxidation causes accumulation of glucose-6-phosphate in the muscle and AT, which would inhibit hexokinase II expression (an important enzyme required for glycolysis) resulting in decreased glucose uptake [142]. To demonstrate this impairing effect of elevated FFA concentration, Thiebaud *et al.* [8] performed an *in vivo* experiment with 25 healthy subjects where plasma glucose and insulin concentrations were maintained at $93 \pm 2 \frac{mg}{dl}$ and $60 \pm 4 \frac{\mu U}{ml}$, respectively (euglycemic-hyperinsulinemic condition). Intralipid was infused at low and high rates to achieve plasma FFA concentrations of 340 ± 13 and $650 \pm 10 \frac{\mu mol}{l}$, respectively. It can be observed from Figure 2.5 that the total glucose uptake rate increased to a maximum level of $3.53 \pm 0.012 \frac{mg}{dl \cdot min}$ for the control (no intralipid infusion) as soon as the insulin clamps were applied. Furthermore, glucose uptake rate was lowest ($2.09 \pm 0.013 \frac{mg}{dl \cdot min}$) when the intralipid infusion rate was highest. The net glucose uptake rate, G_{UP} ($\frac{mg}{dl \cdot min}$), obtained from equation (2.4) can be written as;

$$G_{UP}(t) = -p_1 G(t) - p_4 X(t)G(t) + p_6 G(t)Z(t) + p_1 G_b - p_6 G_b Z_b \quad (2.13)$$

Parameters p_6 , k_1 , and k_2 were estimated in order to fit the data [8] (see Table 2.2 for the estimated parameter values). While the model slightly over-predicts G_{UP} at the 20 *min* time point, the remainder of the model prediction is consistent with the experimental

data (Figure 2.5). Improving the model fit is possible through the inclusion of additional dynamics; however, this is at the expense of model complexity and an increased number of parameters, thereby decreasing confidence in parameter estimates.

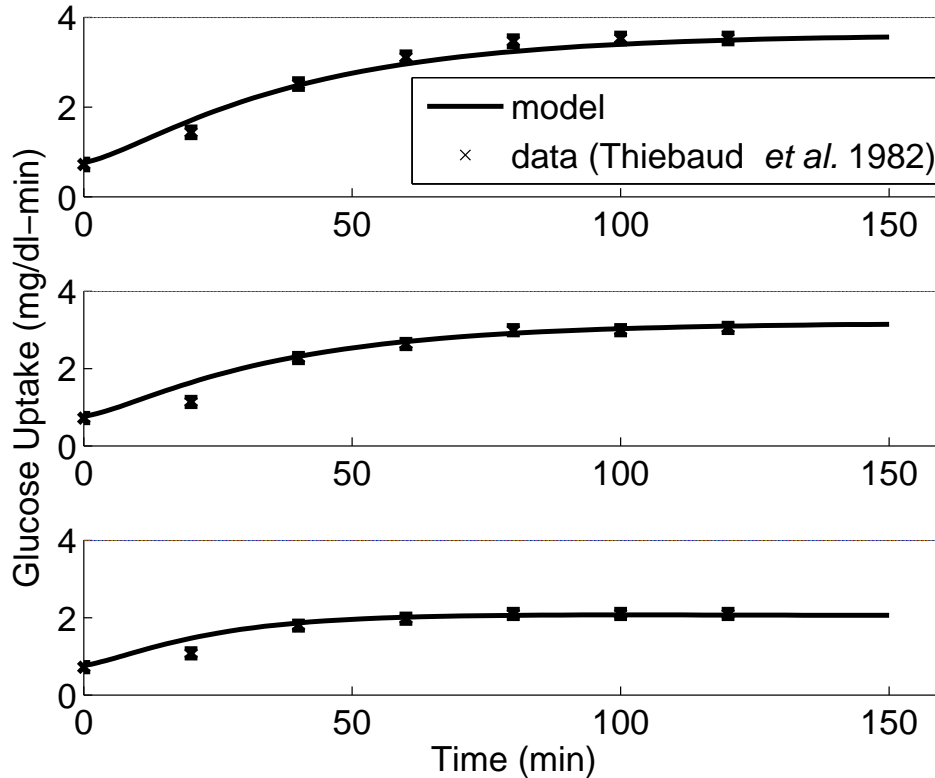


Figure 2.5: Predicted and published ($\mu \pm \sigma$) glucose uptake rate in response to no intralipid infusion - control [$R^2 = 0.9771$] (top); low intralipid infusion rate [$R^2 = 0.9528$] (middle); and high intralipid infusion rate [$R^2 = 0.9115$] (bottom)

2.4.4 Model Validation

2.4.4.1 Anti-lipolytic action of insulin: In order to verify the anti-lipolytic action of insulin in the model, an euglycemic hyperinsulinemic clamp simulation was performed. Insulin concentration was elevated to $100 \frac{\mu U}{ml}$, thereby matching the conditions of a study on healthy subjects by Coon *et al* [143]. The conditions employed in the experimental

study [143] are identical to that of Figure 2.3 (bottom). After allowing the simulated initial condition to match the study data (see Figure 2.6), the insulin clamp led to a decrease in simulated plasma FFA concentration below its basal level. The model predictions (without parameter value changes) are consistent with this data set [143].

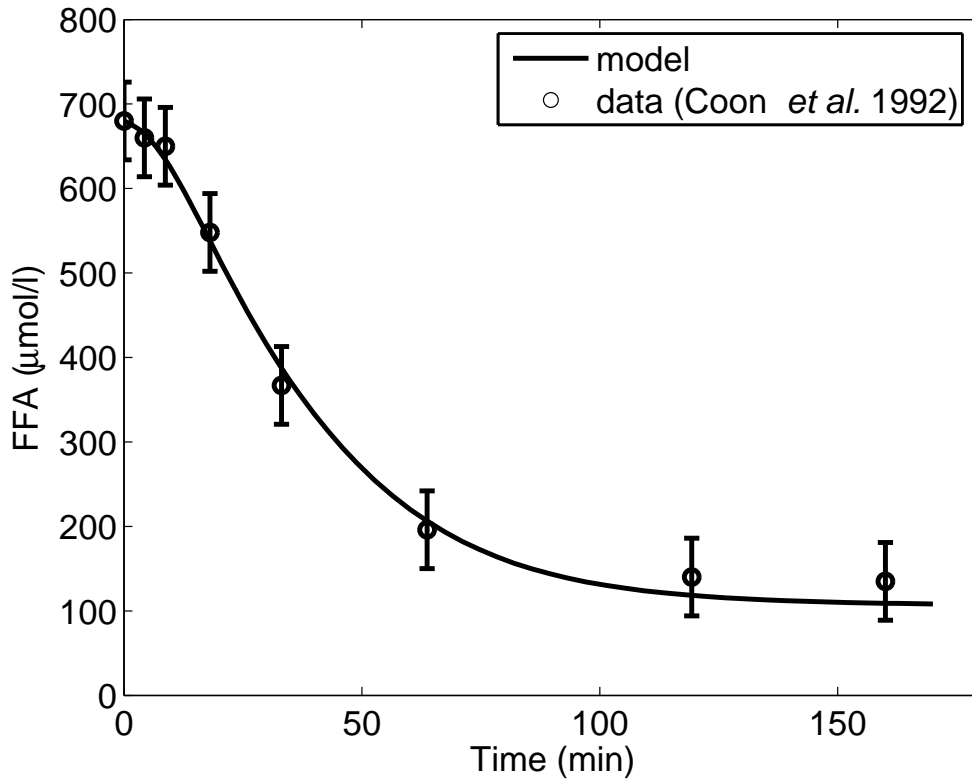


Figure 2.6: Model simulation validation versus published data ($\mu \pm \sigma$) of plasma FFA concentration in response to euglycemic hyperinsulinemic clamp ($100 \frac{\mu U}{ml}$) [$R^2 = 0.901$]

2.4.4.2 Intra-venous glucose tolerance test: In an IVGTT simulation, the model was subjected to a bolus of glucose, as shown in Figure 2.7. Exogenous insulin infusion (bolus at $t = 0$, then constant infusion at $24 \frac{mU}{min}$) yielded a decline in plasma glucose concentration until it returned to its basal level of $87 \pm 6 \frac{mg}{dl}$. Comparison between the model predictions of plasma glucose and insulin concentrations with published data [1] are shown in Figure 2.7. It can be observed that the simulated results are consistent with the published data, which

is to be expected as the glucose-insulin dynamics of the extended model are essentially those of Bergman *et al.* [1], except for modifications to equation (2.3), as shown in (2.4).

In response to the IVGTT, the simulated plasma FFA concentration declined significantly below its basal level. Comparison between the model prediction and published data of FFA concentration in response to an IVGTT [144] are shown in Figure 2.8. It can be observed that the model predictions are within the measurement error.

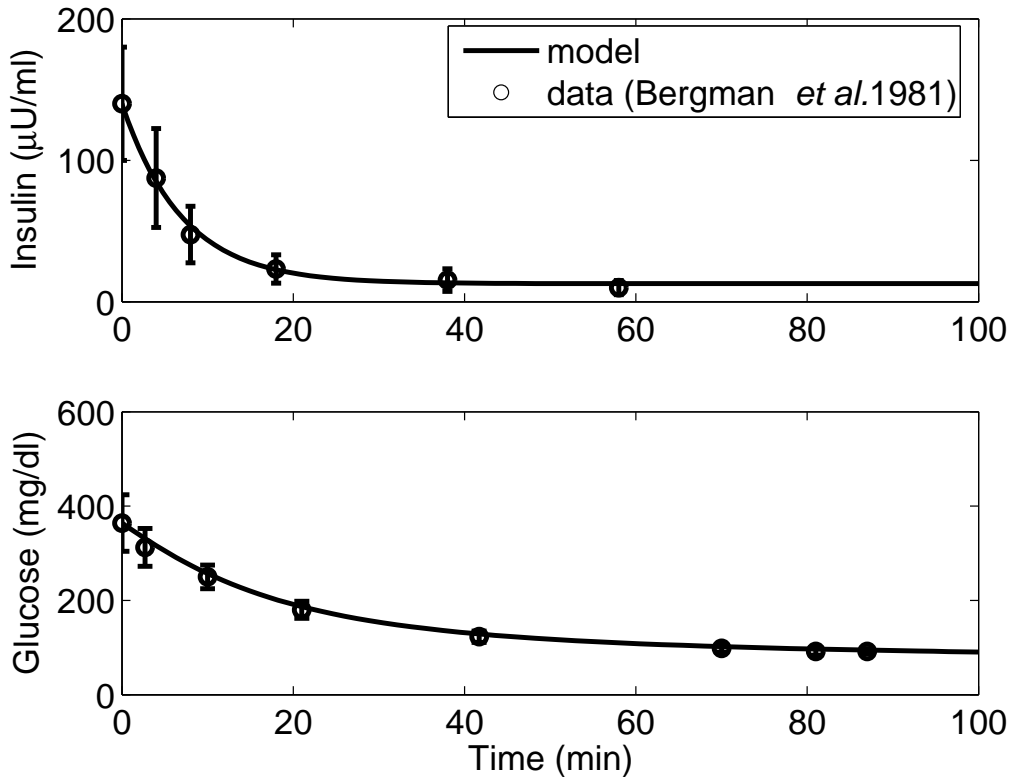


Figure 2.7: Model simulation validation versus published data ($\mu \pm \sigma$) of plasma insulin [$R^2 = 0.974$] (top) and glucose [$R^2 = 0.98$] (bottom) concentration dynamics in response to an intra-venous glucose tolerance test

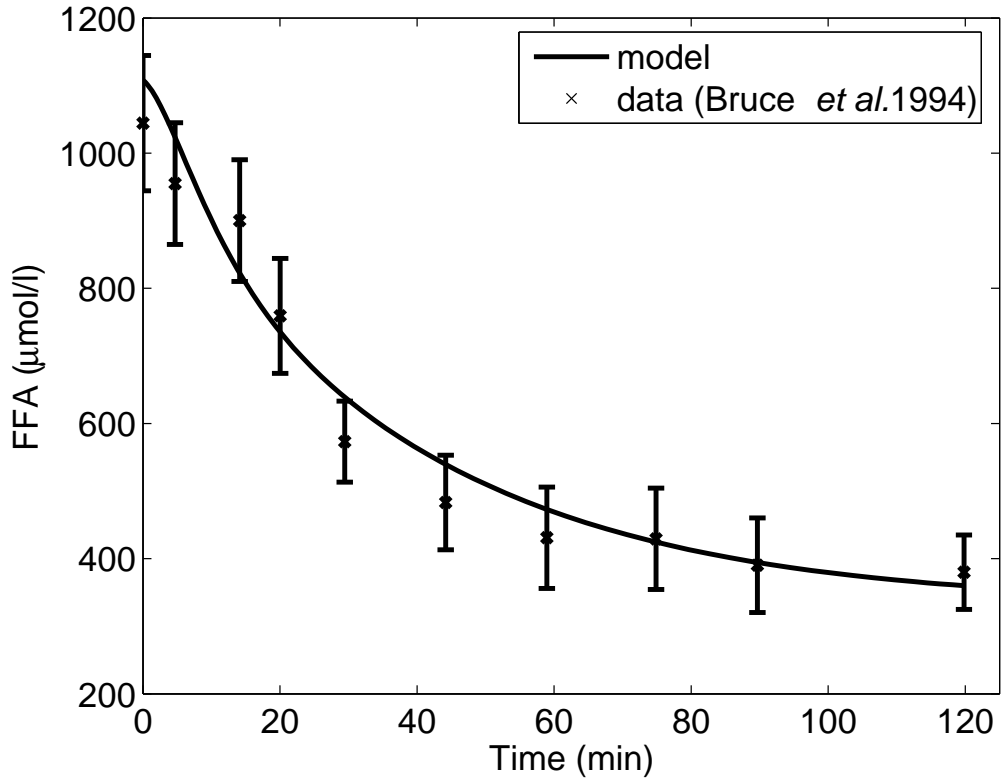


Figure 2.8: Model simulation validation versus published data ($\mu \pm \sigma$) of FFA concentration dynamics in response to an intra-venous glucose tolerance test [$R^2 = 0.8756$]

2.4.5 Model Structure Justification

While designing an empirical mathematical model, it is generally preferable to decrease the complexity of the model by reducing the number of parameters. Simultaneously, it is equally important to capture the observed dynamics of the system, *i.e.*, to have high model accuracy. The trade-off between the fit of the model and model complexity, as measured by the number of parameters, can be quantified by using the AIC as discussed in Section 2.3.

A remote insulin compartment $Y(t)$ was added to the model to slow down the insulin-mediated FFA uptake from the circulatory system into the AT. This addition was necessary to capture the dynamic response observed in the published data [4]. The extended model

prediction of FFA dynamics with and without the compartment $Y(t)$ is shown in Figure 2.9. By omitting $Y(t)$ from the extended model structure, equation (2.6) becomes:

$$\begin{aligned} \frac{dF(t)}{dt} = & -p_7F(t) - p_8X(t)F(t) + p_9(G)F(t)G(t) + p_7F_b \\ & -p_9(G(t))F_bG_b + \frac{u_3(t)}{Vol_F} \end{aligned} \quad (2.14)$$

AIC [139] was employed to establish a statistical comparison between the extended model with and without the $Y(t)$ compartment, as shown in Table 2.3. As it can be observed, the model with the $Y(t)$ compartment has a lower AIC value and hence is more desirable.

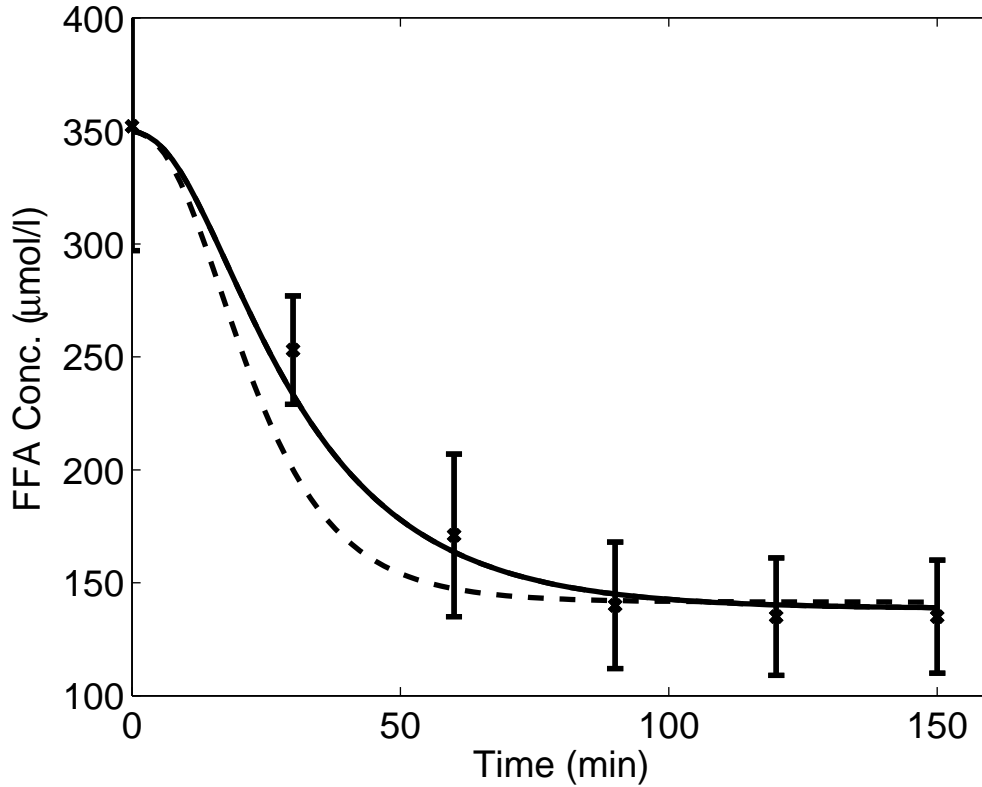


Figure 2.9: Extended model prediction versus data (cross) [4] ($\mu \pm \sigma$) of plasma FFA concentration in response to euglycemic hyperinsulinemic clamp ($100 \frac{\mu U}{ml}$) with (solid line) and without (dashed line) the $Y(t)$ sub-compartment

Similarly, to slow down the impairing effect of FFA on glucose uptake, a remote compartment $Z(t)$ was added to the extended model based on the published data [8]. The extended model prediction of glucose uptake rate with (solid line) and without (dashed line) the $Z(t)$ compartment is shown in Figure 2.10. By excluding $Z(t)$ from the extended model structure, equation (2.4) changes to:

$$\frac{dG(t)}{dt} = -p_1G(t) - p_4X(t)G(t) + p_6G(t)F(t) + p_1G_b - p_6G_bF_b + \frac{u_2(t)}{Vol_G} \quad (2.15)$$

Hence, the net glucose uptake rate, equation (2.13), can be written as:

$$G_{UP}(t) = -p_1G(t) - p_4X(t)G(t) + p_6G(t)F(t) + p_1G_b - p_6G_bF_b \quad (2.16)$$

AIC comparison of the extended model with and without the $Z(t)$ sub-compartment is also in Table 2.3. Again, it can be observed that the AIC value favors the extended model having the $Z(t)$ compartment. However, Figure 2.10 clearly reveals that the model overpredicts glucose uptake rate at the 20 *min* time point. This can be rectified by incorporating additional FFA filter equations at the cost of model complexity. An AIC comparison was used to quantitate the worthiness of an extra FFA filter compartment in order to achieve better $G_{UP}(t)$ fit, especially at the 20 *min* point. Hence the net glucose uptake rate (equation 2.13) with a second FFA filter ($Z_2(t)$) can be re-written as:

$$G_{UP}(t) = -p_1G(t) - p_4X(t)G(t) + p_6G(t)Z_2(t) + p_1G_b - p_6G_bZ_{2b} \quad (2.17)$$

$$\frac{dZ(t)}{dt} = -k_2[Z(t) - Z_b] + k_1[F(t) - F_b] \quad (2.18)$$

$$\frac{dZ_2(t)}{dt} = k_3(Z(t) - Z_2(t)) \quad (2.19)$$

The additional unmeasurable variable, $Z_2(t)$, adds an extra lag in the dynamics of plasma FFA effects on $G_{UP}(t)$, as shown in Figure 2.10 (dotted line). At basal steady state, Z_{2b} is equal to Z_b .

Table 2.3: Calculated AIC values of the extended minimal model with and without the $Y(t)$ and $Z(t)$ sub-compartments

<i>AIC</i>	<i>Extended Minimal Model</i>	
	<i>without</i>	<i>with</i>
FFA dynamics ($Y(t)$)	Eq. (2.14) 22.7782	Eq. (2.6) 14.8778
Glucose uptake dynamics ($Z(t)$)	Eq. (2.16) 36.5598	Eq. (2.13) 33.2001
Glucose uptake dynamics ($Z_2(t)$)	Eq. (2.13) 33.2001	Eq. (2.19) 32.90

Table 2.3 indicates that two FFA filters in series, $Z(t)$ and $Z_2(t)$ (AIC = 32.90), only marginally improves the model fit as compared to only one filter, $Z(t)$ (AIC = 33.2001). Hence, it is probably not worth incorporating the added complexity in terms of the new parameter (k_3).

In order to justify the selection of an exponential function to capture the effect of glucose on parameter $p_9(G(t))$ (equation (2.7)) as opposed to a linear fit, an AIC evaluation was performed. A linear expression capturing the glucose effects on $p_9(G(t))$ can be mathematically written as:

$$p_9(G(t)) = -5.232 \times 10^{-7}G(t) + 1.869 \times 10^{-4} \quad (2.20)$$

The dynamics of $p_9(G(t))$ as a function of glucose obtained from the equations (2.7) and (2.20) are indicated in Figure 2.11. It is clear from the data that higher values of glucose will generate negative values for parameter $p_9(G(t))$ in case of the equation (2.20), thereby making the system unstable; a phenomenon which will be absent in case of equation (2.7). Moreover, the calculated AIC value for equation (2.7) (-54.509) is much lower than that of equation (2.20) (-25.461).

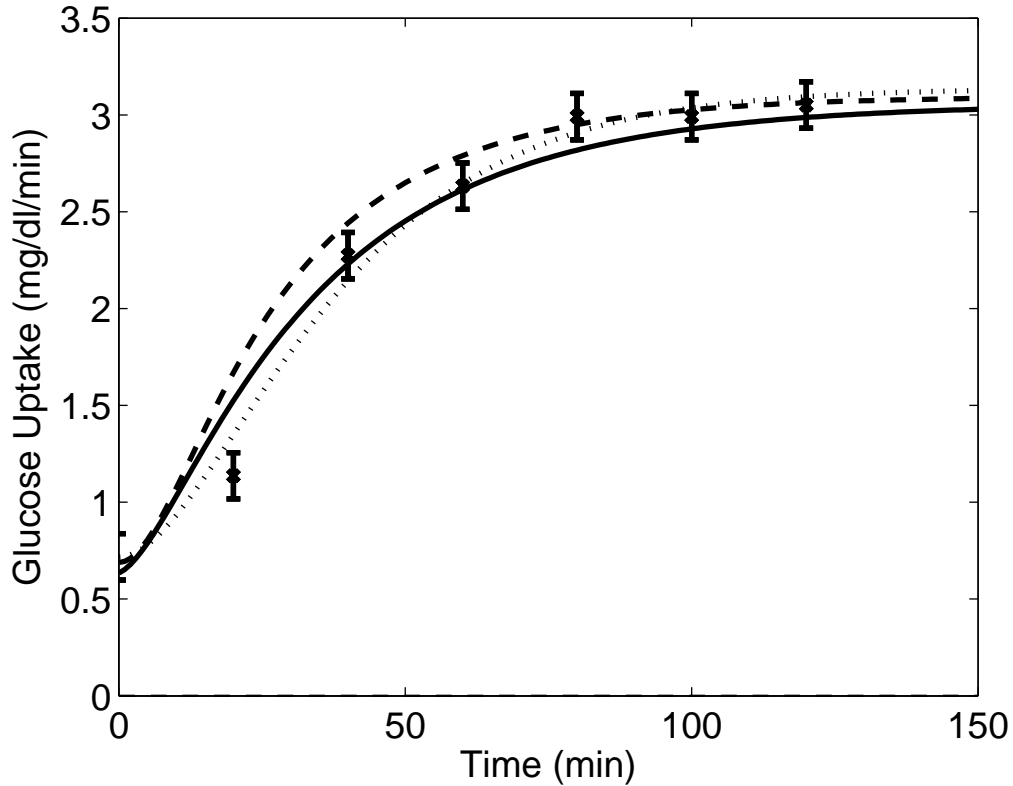


Figure 2.10: Extended model prediction versus data (cross) [8] ($\mu \pm \sigma$) of plasma glucose uptake rate in response to low intralipid infusion rate ($0.5 \frac{ml}{min}$) with only $Z(t)$ sub-compartment (solid line), with $Z(t)$ and $Z_2(t)$ sub-compartments (dotted line), and without any filter sub-compartment ($Z(t)$ or $Z_2(t)$) (dashed line) sub-compartment

2.5 MIXED MEAL MODELING

A diabetic patient consume meals at least three times a day causing substantial fluctuations of the plasma glucose and FFA levels. One of the key objective of developing the extended minimal model was to evaluate the physiological response of the major energy-providing metabolites to disturbances from mixed meal ingestion. Hence, a mixed meal model was developed to capture the absorption of CHO (as glucose), protein, and fat (as FFA) from

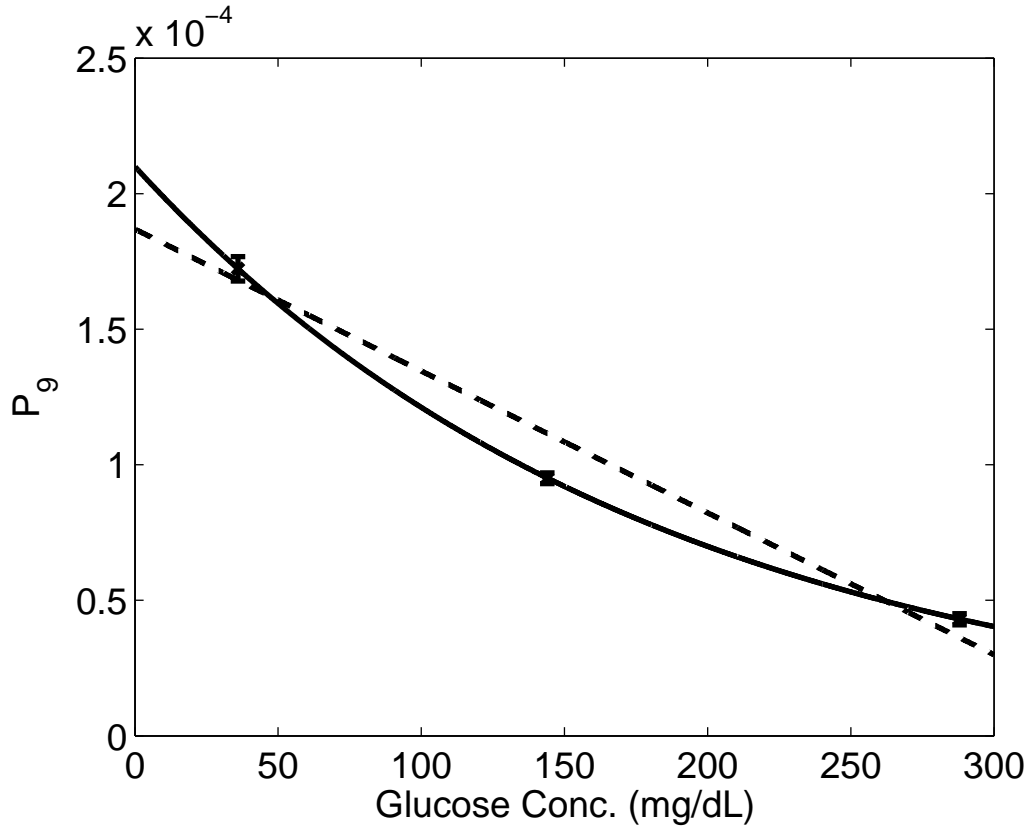


Figure 2.11: Published data [9] (cross) versus predicted values of parameter $p_9(G(t))$ from equation (2.7) (solid line) and equation (2.20) (dashed line) in response to increasing glucose clamps for 90 min

the gut into the circulatory system. The meal model outputs served as disturbance inputs to the extended minimal model.

2.5.1 Mixed Meal Modeling

A mixed meal usually consist of all the three major nutrients: glucose, protein, and fat. After ingestion, the stomach converts the meal contents to chyme via a combination of mechanical and chemical processes. The partly digested meal then empties into the intestine for further digestion and absorption into the circulatory system. The extended minimal model accepts

meal-induced disturbance in the form of glucose ($u_2(t)$), as well as, FFA ($u_3(t)$) absorption from the gut into the circulatory system. The meal models proposed in the literature typically focus on the gut absorption of glucose only [145, 146]. Thus, a mixed meal model describing CHO, protein, and FFA absorption is needed to test the accuracy of the extended minimal model. The present study employs the Lehmann and Deutsch meal model [145] structure to explicitly account for protein, fat, and CHO, absorption from the gut into the circulatory system.

The model assumes that the gastric emptying rate (G_{emp}) has a trapezoidal shape (adapted from [145]), which can be mathematically written as:

$$G_{emp}(t) = \begin{cases} \frac{V_{max}}{T_{asc}} t & t < T_{asc} \\ V_{max} & T_{asc} < t \leq T_{asc} + T_{max} \\ V_{max} - \frac{V_{max}}{T_{des}}(t - T_{asc} - T_{max}) & T_{asc} + T_{max} \leq t < T_{max} + T_{asc} + T_{des} \\ 0 & otherwise \end{cases} \quad (2.21)$$

$$V_{max} = \frac{2N_{tot}}{T_{asc} + 2T_{max} + T_{des}} \quad (2.22)$$

Here, V_{max} is the maximum rate of gastric emptying. The duration for which G_{emp} is maximum (V_{max}) and constant is given by T_{max} (*min*). T_{asc} (*min*) and T_{des} (*min*) are the respective ascending and descending periods of G_{emp} . Total nutrient consumed is given by N_{tot} (*g*). The gastric emptying function is an input to the model of intestinal absorption. Nutrient absorption from the gut into the circulatory system is given by the following differential equations:

$$\dot{N}_G(t) = x_G G_{emp}(t) - k_G N_G(t) \quad (2.23)$$

$$\dot{N}_P(t) = x_P G_{emp}(t) - k_P N_P(t) \quad (2.24)$$

$$\dot{N}_F(t) = x_F G_{emp}(t) - k_F N_F(t) \quad (2.25)$$

Here, $N_G(t)$, $N_P(t)$, and $N_F(t)$ are the amount of digestible glucose, protein and FFA in the gut, respectively. The mass fraction of digestible glucose, protein and FFA in the meal are given by x_G , x_P , and x_F , respectively. Similarly, the intestinal absorption rate constant for digestible glucose, protein, and FFA are given by k_G , k_P , and k_F , respectively. The model

assumes that 60% of the protein is converted to glucose [147]. Hence, the rates of appearance of glucose and FFA in the circulatory system, *i.e.*, $u_2(t)$ from equation (2.4) and $u_3(t)$ from equation (2.6), are given by:

$$u_2(t) = k_G N_G(t) + 0.6[k_P N_P(t)] \quad (2.26)$$

$$u_3(t) = k_F N_F(t) \quad (2.27)$$

The second part of the right hand side (RHS) of equation (2.26) enabled the model to capture the effects of protein on plasma glucose and FFA concentrations after ingestion of a mixed meal. Graphical representations of the G_{emp} of the total meal, and rate of appearance of the three nutrients in the circulatory system are given in Figure 2.12, based on the simulation conditions described in the next section (Section 2.5.2).

2.5.2 Mixed Meal Tolerance Test (MTT)

A mixed meal (CHO = 70 g, protein = 18 g, and FFA = 20 g) was consumed by healthy subjects in 10 min in an MTT study by Owens *et al.* [10]. Blood samples were taken at various times after the meal consumption to measure glucose and insulin concentrations. To investigate MTT response in simulation, the mixed meal model was coupled with the extended minimal model from Section 2.2. Since insulin concentration measurements were available, the insulin dynamics, equation (2.1) from Section 2.1, were replaced by a piecewise linear approximation of the normal subject's insulin profile (Figure 2.13, top). Parameters T_{max} , k_G , k_P , and k_F of the mixed meal model were estimated using the nonlinear least square technique (Section 2.3) to fit the glucose profile obtained from [10] (as shown in Figure 2.13, bottom). Parameters of the FFA minimal model were directly obtained from Table 2.2. The parameter values of the meal model are $T_{max} = 35 \text{ min}$, $k_G = 0.022 \text{ min}^{-1}$, $k_P = 0.015 \text{ min}^{-1}$, and $k_F = 0.0097 \text{ min}^{-1}$. V_{max} calculated from equation (2.22) is $2.2 \frac{\text{g}}{\text{min}}$. This is similar in value to other maximum G_{emp} rates reported in the literature using similar meal sizes [148]. Literature data also suggested that the time to reach V_{max} for a medium size mixed meal, such as the one used here, is typically 10 - 15 min [149]. Based

on that, the T_{asc} and T_{des} values were fixed at 10 *min*. It can be observed that the meal model, when coupled to the FFA minimal model, yielded glucose concentration predictions consistent with experimental data (see Figure 2.13). The slight underprediction of glucose in the first 50 *min* could be due to differences in dynamics between the patients modeled in the FFA minimal model and the patient responses in [10]. More accurate glucose predictions could be achieved by reducing T_{asc} to a lower value; however this would violate generally accepted physiological limits on T_{asc} [149].

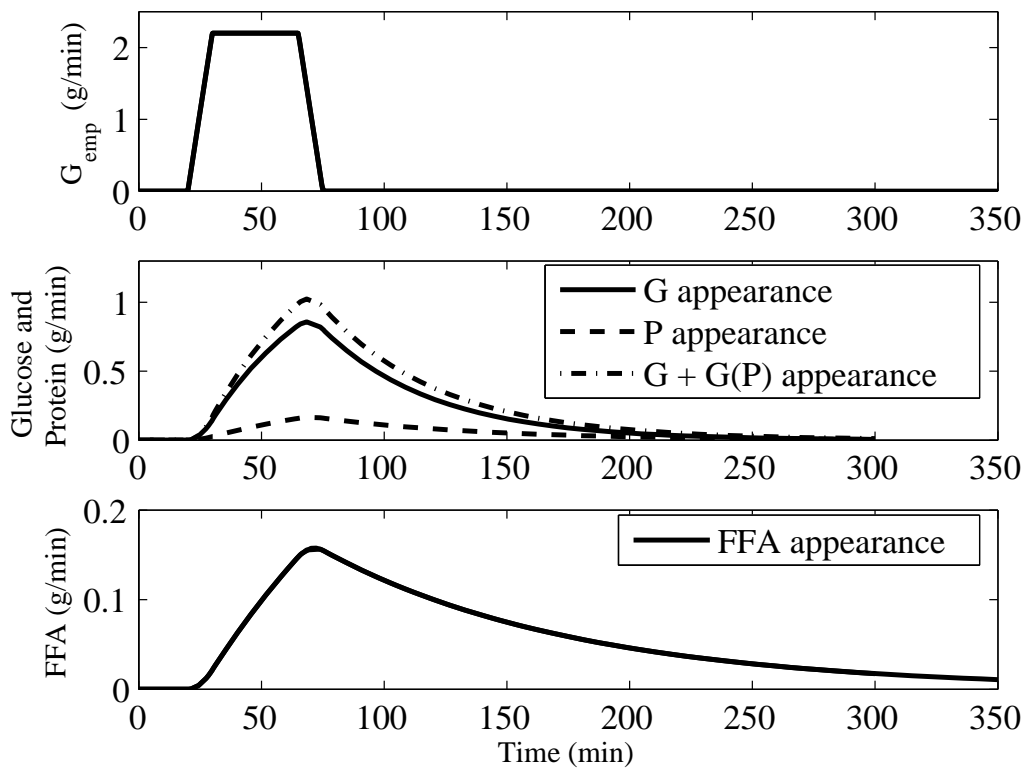


Figure 2.12: Model simulation of total meal gastric emptying rate (top); glucose (G) appearance, protein (P) appearance, and G plus glucose derived from protein (G(P)) appearance (middle); and FFA appearance (bottom), in response to 108 *g* mixed meal tolerance test.

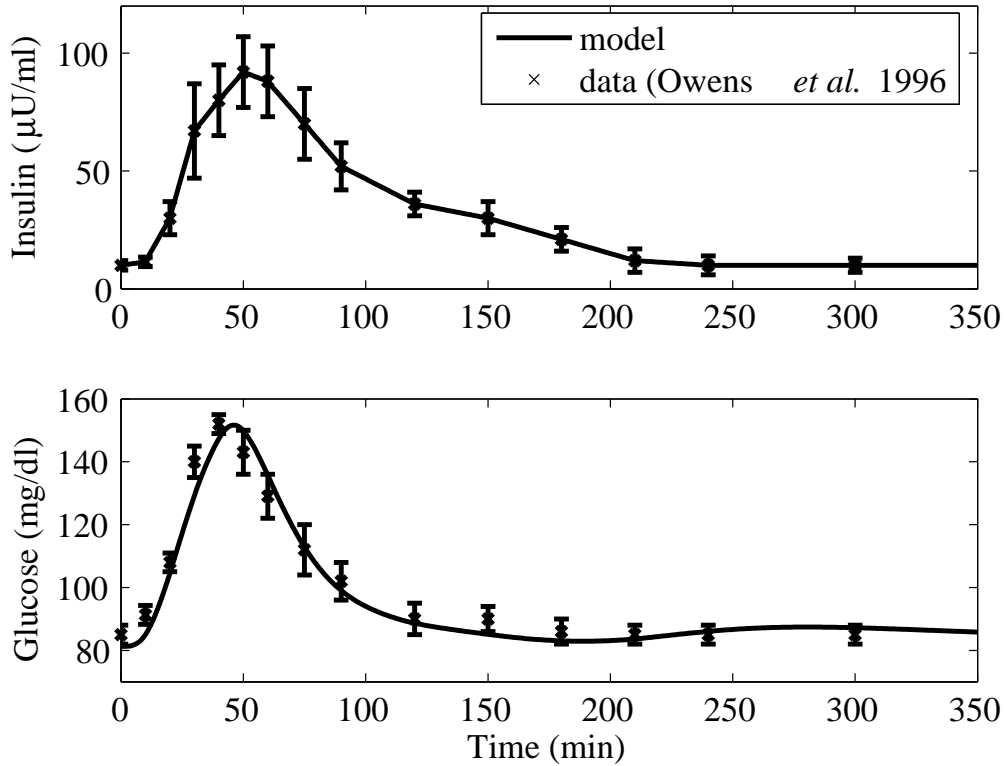


Figure 2.13: Insulin concentration data from normal subjects [10] ($\mu \pm \sigma$) and piecewise linear approximation (top), model simulation versus published data [10] ($\mu \pm \sigma$) of plasma glucose concentration dynamics in response to mixed meal tolerance test (bottom).

2.6 SUMMARY

Bergman’s minimal model [1] was extended to include FFA dynamics. Differential equations representing FFA dynamics, as well as remote insulin and fatty acid concentrations, were added to the minimal model. This model successfully captured plasma FFA concentration behavior, plasma glucose and insulin concentrations, and the physiological interactions that exist between these species. The addition of parameter p_6 in equation (2.4) made it possible to capture the impairing effect of FFA on net glucose uptake. The model also successfully

predicted the anti-lipolytic effect of insulin. This was possible due to the addition of parameter p_8 in equation (2.6).

By incorporating the FFA dynamics and its effect on plasma glucose, the ability of the model to predict glucose concentration dynamics after a mixed meal (meal containing carbohydrates (CHO) and fat) has been increased. With the given structure, the extended model is capable of predicting the fluctuations in FFA level due to meal intake. This broadens the scope of further investigation regarding plasma FFA disturbance effects on glucose dynamics and the glucoregulatory action of insulin. Also, when coupled with a mixed meal model, the extended model can be utilized to determine the different dynamics of glucose and FFA absorption and distribution via the circulatory system when ingested in various proportions.

With the long term goal of synthesizing an automatic closed-loop insulin delivery system comprised of a continuous glucose measuring device, an insulin pump, and a model-based control algorithm, it is necessary to develop accurate models that characterize expected physiological conditions [50]. Hence, this more complete model of the major energy providing metabolic substrates provides the control community with a more detailed model for use in control design. Also, due to the easily identifiable parameters, the model could be used in an adaptive control environment, thus facilitating patient specificity. The extended minimal model could be considered as an important step towards the development of an externally wearable pancreas which will be capable of maintaining normoglycemia by rejecting mixed meal (CHO and fat) disturbances. However, validation of the extended model requires additional experimental data. For example, *in vivo* studies involving human adipocytes are needed to verify the lipolytic effect of hyperglycemia.

3.0 “MINIMAL” MODEL WITH EXERCISE EFFECTS ON GLUCOSE AND INSULIN¹

Exercise induces several fundamental metabolic changes in the body [62]. Elevated physical activity promotes a drop in plasma insulin concentration from its basal level [151]. This suppression of insulin level could be necessary to enhance hepatic glucose production and lipolysis of free fatty acids from AT to meet the augmented energy uptake by the working tissues [12]. It has been shown by Seals *et al.* (1984) that exercise reduces insulin secretion [152]. In addition, a more recent study [153] has demonstrated that exercise augments clearance of insulin from the plasma in both healthy as well as T1DM patients. A study performed by Wolfe *et al.* (1986) [12] has revealed that clamping insulin at its basal level during exercise increased the rate of glucose uptake above normal, and the rate of glucose production was not sufficient to fully compensate the elevated muscle glucose uptake rate.

An increase in exercise intensity also amplifies glucose uptake by the working tissues [154]. In order to maintain plasma glucose homeostasis, hepatic glucose release increases with increasing work intensity [155]. During mild-to-moderate exercise (also known as the aerobic exercise range, *i.e.*, when the body utilizes oxygen to breakdown glucose [156]), the increased splanchnic glucose release is primarily due to by elevated hepatic glycogenolysis. Glycogenolysis is a metabolic process in which stored glycogen (a polymeric form of glucose) is catabolized into glucose. As the duration of exercise increases, the rate of hepatic glycogenolysis diminishes due to the limited supply of liver glycogen stores [15]. Simultaneously, hepatic gluconeogenesis is accelerated during elevated physical work [13]. Gluconeogenesis is the generation of glucose from non-sugar carbon substrates like pyruvate, lactate, glycerol, and glucogenic amino acids. However, the rate of glucose produced via

¹Portions of this chapter have been published in [150]

liver gluconeogenesis does not fully compensate for the decrease in glucose release by liver glycogenolysis (the former is a slower process), thereby resulting in a net decrease in hepatic glucose release during prolonged exercise [157]. Due to this imbalance between glucose uptake and hepatic glucose release, the plasma glucose concentration declines, and hypoglycemia occurs [13, 15]. As an added complication in glucose regulation, studies have shown that liver glycogen content declines more rapidly with increasing exercise intensity [15, 11].

During the recovery period after short term exercise, both the elevated glucose uptake rate by working muscles and the rate of hepatic glucose release, decline gradually to their respective basal levels. On the other hand, glucose fluxes after prolonged exercise are quite different. Due to the substantial depletion of liver glycogen stores during prolonged exercise, the rate of glycogenolysis is significantly suppressed leading to a net decrease in hepatic glucose release rate. During the recovery period, the elevated muscle glucose uptake rate gradually declines to the basal level. The already suppressed hepatic glucose release rate also declines back to its basal level [157]. *In vivo* studies have revealed a significant increment in hepatic lactate consumption immediately after prolonged exercise, and this lactate serves as a substrate for the repletion of the liver glycogen stores [158, 15].

The existing control-relevant metabolic models present in the literature fail to consider most of the above-mentioned physiologic effects of exercise on glucose and insulin dynamics. With the ultimate goal of developing a closed-loop model-based insulin delivery system, it is essential to synthesize lower-order metabolic models which are capable of predicting fluctuations in glucose dynamics during exercise. Open-loop simulations from such models can also give prior intimation to T1DM patients regarding the time-span during which exercise could be performed at a given intensity without reaching hypoglycemia.

In this chapter, the various effects of exercise were incorporated into the classical Bergman minimal model [1] (described in Section 2.1) in order to capture the plasma glucose and insulin dynamics during, as well as after, periods of mild-to-moderate exercise. In Section 3.1, a technique to quantitate exercise intensity is presented. In the following Section (3.2), a detailed description regarding the structure of the exercise minimal model is introduced. The data fitting results along with model validation simulations are presented in Section 3.3. Finally, Section (3.4) explores model structure justification by employing AIC technique.

3.1 QUANTITATING EXERCISE INTENSITY

The maximum rate of oxygen consumption for an individual during exercise is given by VO_2^{max} ($\frac{ml}{kg-min}$). Oxygen consumption is approximately linearly proportional to energy expenditure [159]. Hence, it is possible to indirectly measure the maximum capacity of an individual for aerobic work by measuring oxygen consumption. When physical activity is expressed as a percentage of VO_2^{max} (PVO_2^{max}), exercise effects may be compared between individuals of the same sex and similar body weight at the same PVO_2^{max} . The average PVO_2^{max} for a person in the basal state is 8% [151]. Ahlborg *et al.* [63] demonstrated that PVO_2^{max} increases rapidly at the onset of exercise, reaches its ultimate value within 5-6 *min* and remains constant for the duration of exercise. The exercise model developed in this study uses PVO_2^{max} to quantify exercise intensity. The ordinary differential equation for PVO_2^{max} is given by:

$$\frac{dPVO_2^{max}(t)}{dt} = -0.8PVO_2^{max}(t) + 0.8u_{Ex}(t); \quad PVO_2^{max}(0) = 0 \quad (3.1)$$

Here, $PVO_2^{max}(t)$ is the exercise level above basal as experienced by the individual, and $u_{Ex}(t)$ is the ultimate exercise intensity above the basal level – an input to the model with a maximum span of 0 to 92%. However, for the proposed model the range of $u_{Ex}(t)$ is valid only within the mild-to-moderate exercise level ($\leq 68\% PVO_2^{max}(t)$). The parameter value of 0.8 ($\frac{1}{min}$) was selected to achieve a $PVO_2^{max}(t)$ settling time of approximately 5 *min*, consistent with the observations in [63].

3.2 EXERCISE MINIMAL MODEL

The glucose and insulin dynamics adapted from the Bergman minimal model [1], when coupled with the major mild-to-moderate exercise effects, are mathematically given by:

$$\frac{dI(t)}{dt} = -nI(t) - I_e(t) + p_5u_1(t) \quad (3.2)$$

$$\frac{dX(t)}{dt} = -p_2X(t) + p_3[I(t) - I_b]$$

$$\begin{aligned} \frac{dG(t)}{dt} = & -p_1[G(t) - G_b] - p_4X(t)G(t) + \frac{W}{Vol_G}[G_{prod}(t) - G_{gly}(t)] \\ & - \frac{W}{Vol_G}G_{up}(t) + \frac{u_2(t)}{Vol_G} \end{aligned} \quad (3.3)$$

$$\frac{dG_{prod}(t)}{dt} = a_1PVO_2^{max}(t) - a_2G_{prod}(t) \quad (3.4)$$

$$\frac{dG_{up}(t)}{dt} = a_3PVO_2^{max}(t) - a_4G_{up}(t) \quad (3.5)$$

$$\frac{dI_e(t)}{dt} = a_5PVO_2^{max}(t) - a_6I_e(t) \quad (3.6)$$

The insulin dynamics, equation (3.2), have been modified from the Bergman minimal model, equation (2.1), by adding the final term. Here, $I_e(t)$ ($\frac{\mu U}{ml-min}$) is the rate of insulin removal from the circulatory system due to exercise-induced physiological changes. The plasma glucose dynamics, equation (3.3), differ from equation (2.3) of the Bergman minimal model by addition of the following terms: $\frac{W}{Vol_G}[G_{prod}(t) - G_{gly}(t)] - \frac{W}{Vol_G}G_{up}(t)$. Variables $G_{up}(t)$ ($\frac{mg}{kg-min}$) and $G_{prod}(t)$ ($\frac{mg}{kg-min}$) represent the rates of glucose uptake and hepatic glucose production induced by exercise, respectively. W (kg) represents the weight of the subject. Variable $G_{gly}(t)$ ($\frac{mg}{kg-min}$) represents the decline of glycogenolysis rate during prolonged exercise due to depletion of liver glycogen stores. The dynamics of hepatic glucose production, glucose uptake, and plasma insulin removal induced by exercise are represented in equations (3.4), (3.5), and (3.6), respectively. Initial conditions of the above ODEs are listed in Table 3.1.

The rate of glycogenolysis ($G_{gly}(t)$) starts to decrease when the energy expenditure exceeds a critical threshold value (A_{TH}) which is a function of exercise intensity and duration. A_{TH} can be mathematically represented as:

$$A_{TH} = u_{Ex}(t)t_{gly}(u_{Ex}(t)) \quad (3.7)$$

Here, $t_{gly}(u_{Ex}(t))$ is the duration of exercise that can be performed at intensity $u_{Ex}(t)$ before the rate of hepatic glycogenolysis starts to decrease. The rate of hepatic glycogen depletion increases with increasing exercise intensity [15, 11]. Hence, $t_{gly}(u_{Ex}(t))$ is a function of

Table 3.1: Initial condition of the equations belonging to the exercise minimal model

Variable	Value	Units
$I(0)$	$\frac{p_5}{n} u_{1b}$	$\frac{m\mu U}{ml}$
$X(0)$	0	$\frac{m\mu U}{ml}$
$G(0)$	G_b	$\frac{mg}{dl}$
$G_{prod}(0)$	0	$\frac{mg}{kg \cdot min}$
$G_{up}(0)$	0	$\frac{mg}{kg \cdot min}$
$I_e(0)$	0	$\frac{\mu U}{ml \cdot min}$

exercise intensity, as shown in Figure 3.1. A linear equation, decreasing with increasing work intensity, captures the dependence of $t_{gly}(u_{Ex}(t))$ on $u_{Ex}(t)$, as follows:

$$t_{gly} = -1.1521u_{Ex}(t) + 87.471 \quad (3.8)$$

By substituting equation (3.8) into equation (3.7),

$$A_{TH} = -1.1521[u_{Ex}(t)]^2 + 87.471u_{Ex}(t) \quad (3.9)$$

Hence, the dynamics of glycogenolysis during prolonged exercise can be mathematically represented as follows:

$$\frac{dG_{gly}(t)}{dt} = \begin{cases} 0 & A(t) < A_{TH} \\ k & A(t) \geq A_{TH} \\ -\frac{G_{gly}(t)}{T_1} & u_{Ex}(t) = 0 \end{cases} \quad (3.10)$$

Here, $A(t)$ is the integrated exercise intensity ($u_{Ex}(t)$), which is calculated by the following set of equations:

$$\frac{dA(t)}{dt} = \begin{cases} u_{Ex}(t) & u_{Ex}(t) > 0 \\ -\frac{A(t)}{T_2} & u_{Ex}(t) = 0 \end{cases} \quad (3.11)$$

With the onset of exercise ($u_{Ex}(t) > 0$), $A(t)$ will increase at a rate proportional to $u_{Ex}(t)$. At the end of physical activity ($u_{Ex}(t) = 0$), $A(t)$ will return back to its initial

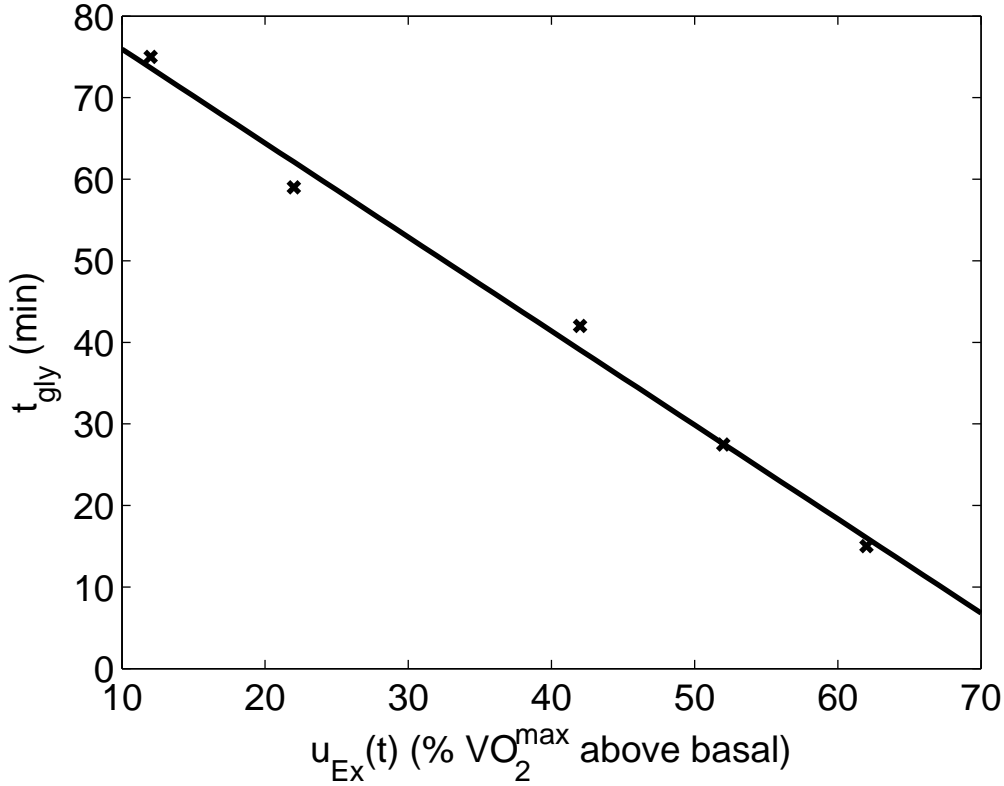


Figure 3.1: Dependence of time at which hepatic glycogen starts to deplete, t_{gly} , on exercise intensity ($u_{Ex}(t)$). Published data (cross) from Pruett *et al.* [11] and linear fit (solid line) [$R^2 = 0.9908$]

condition (which is zero) at rate governed by T_2 . Both rat and human studies have revealed that majority of the liver glycogen stores are repleted within 1 *hr* of the recovery period [160, 161]. Hence, the time constant T_2 was assigned a value of 10 *min*. As long as $A(t)$ is less than the critical threshold value (A_{TH}), enough glycogen is still available to maintain a sufficient rate of hepatic glucose release. However, once $A(t)$ reaches A_{TH} , the rate of glycogenolysis rate starts to decline at a rate given by k , due to the depletion of available liver glycogen stores. The end of exercise (when $u_{Ex}(t)$ returns to zero), which is also the beginning of the recovery period, marks the commencement of repletion of glycogen stores

via a continued elevation in the rate of hepatic gluconeogenesis. The time required for $G_{gly}(t)$ to return to its basal value after exercise is governed by the pseudo-time constant T_1 .

3.2.1 Parameter Estimation Technique

Parameters for the exercise minimal model were estimated using the nonlinear least square technique, as described in Section 2.3 (equation (2.9)). Data from [12] were used to estimate the parameters a_5 and a_6 , thereby quantifying the depletion of plasma insulin during exercise and its repletion during the recovery period. After fixing a_5 and a_6 , the insulin model was validated by comparing with the data from [13]. Parameters a_1 and a_2 for G_{prod} dynamics and a_3 and a_4 for $G_{up}(t)$ dynamics were also estimated from [12]. The glucose model was validated by comparing the model predictions of $G_{prod}(t)$, $G_{up}(t)$ and $G(t)$ with T1DM patient data from [14]. After fixing the parameters a_{1-6} to their estimated values, the effects of glycogen depletion during prolonged exercise, and recovery were modeled. In order to capture these effects, data from [13] was used to estimate the parameters k and T_1 in equation (3.10). For further validation of the model during prolonged exercise, plasma glucose concentration was compared with the data from another study performed at higher exercise intensity [15]. All the parameter values for the exercise minimal model along with their 95% confidence interval (CI) bounds calculated by using the *nlparci.m* function from the MATLAB Statistics Toolbox (©2008 The Mathworks Inc., Natick, MA) are given in Table 3.2. The quality of the model fits was assessed by using the R^2 technique (for details see Section 2.3). Calculated R^2 values for every model fit and validation are provided in the figure legends.

3.3 RESULTS OF THE EXERCISE MINIMAL MODEL

3.3.1 Plasma Insulin Dynamics During Exercise

Simulation study of mild exercise ($PVO_2^{max}(t) = 40$) for 60 *min* was performed to evaluate the physiological effects of exercise on plasma insulin concentration. With the onset of exercise, plasma insulin declined from its basal level ($12.2 \frac{\mu U}{mL}$), and continued to do so along

Table 3.2: Parameters of the exercise minimal model with 95% confidence intervals (CI), in addition to those in Table 2.1

Parameter	Value	Lower Limit 95% CI	Upper Limit 95% CI	Unit
a_1	0.00158	0.0013	0.0019	mg/kg·min ²
a_2	0.056	0.0441	0.0679	1/min
a_3	0.00195	0.0015	0.0024	mg/kg·min ²
a_4	0.0485	0.0355	0.0617	1/min
a_5	0.00125	0.001	0.0015	μ U/mL·min
a_6	0.075	0.0588	0.0912	1/min
k	0.0108	0.0085	0.0131	mg/kg·min ²
T_1	6.0	1.86	10.14	min

a first-order-type response trajectory until the end of the experiment, as shown in Figure 3.2. During the recovery period ($t > 60 \text{ min}$), the plasma insulin concentration climbed back to its basal level. Quantitatively, the model predictions were consistently within one standard deviation of the mean of experimental data [12] from which the relevant parameters (a_5 and a_6) were estimated. The 95% CI bounds of plasma insulin concentration were simulated by choosing a set of parameter values from Table 3.2 that had the maximum overestimation ($a_5 = 0.001$, $a_6 = 0.0912$) and maximum underestimation ($a_5 = 0.0015$, $a_6 = 0.0588$) of insulin concentration, as shown in Figure 3.2 (dotted lines).

For validation of the model, a separate simulation study was performed keeping the parameter values of a_5 and a_6 unchanged with a different exercise intensity level ($PVO_2^{max}(t) = 30$) which lasted for a longer time duration ($t_{ex} = 0$ to 120 min). With the onset of exercise, the insulin level declined well below the basal level ($10.2 \frac{\mu\text{U}}{\text{mL}}$), and this hypoinsulinemic state persisted until the end of the experiment. A comparison between model prediction of insulin and experimental data [13] with same exercise protocol is shown in Figure 3.3. Plasma insulin gradually returned back to the basal level during the recovery period ($t > 120 \text{ min}$). Overall, the insulin model fits the experimental data sets.

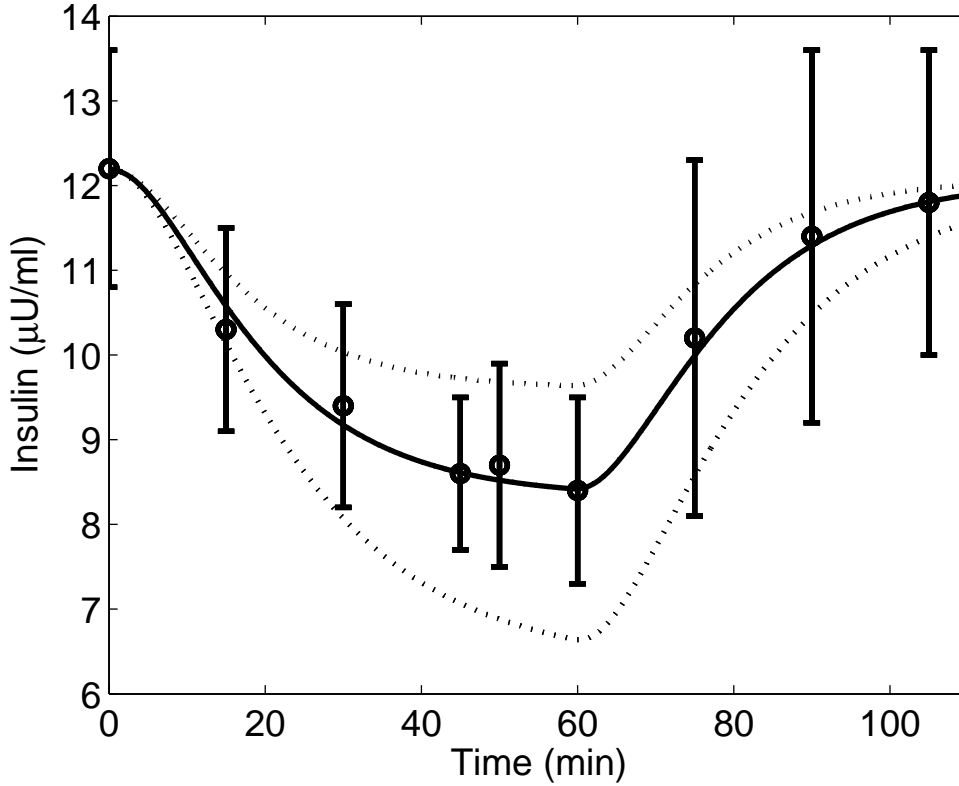


Figure 3.2: Plasma insulin concentration in response to mild exercise ($PVO_2^{max} = 40$) lasting from $t_{ex} = 0$ to 60 *min*. Published data (circles) ($\mu \pm \sigma$) from Wolfe *et al.* [12], model fit (solid line), and 95% confidence interval of the model output (dotted line).

3.3.2 Plasma Glucose Dynamics During Exercise

To evaluate the exercise effects on plasma glucose concentration, a simulation study of mild exercise was performed ($PVO_2^{max}(t) = 40$) for 60 *min*. With the onset of exercise, $G_{up}(t)$ increased from its basal state to $1.15 \frac{mg}{kg \cdot min}$. During the recovery period ($t > 60$ *min*), G_{up} returned to its basal level. Model prediction of $G_{up}(t)$ along with experimental data [12] with same exercise protocol from which parameters a_3 and a_4 were estimated is shown in Figure 3.4 (Top). The 95% CIs of $G_{up}(t)$ were simulated by choosing a set of parameter values from Table 3.2 that had the maximum underestimation ($a_3 = 0.0015$, $a_4 = 0.0617$) and maximum

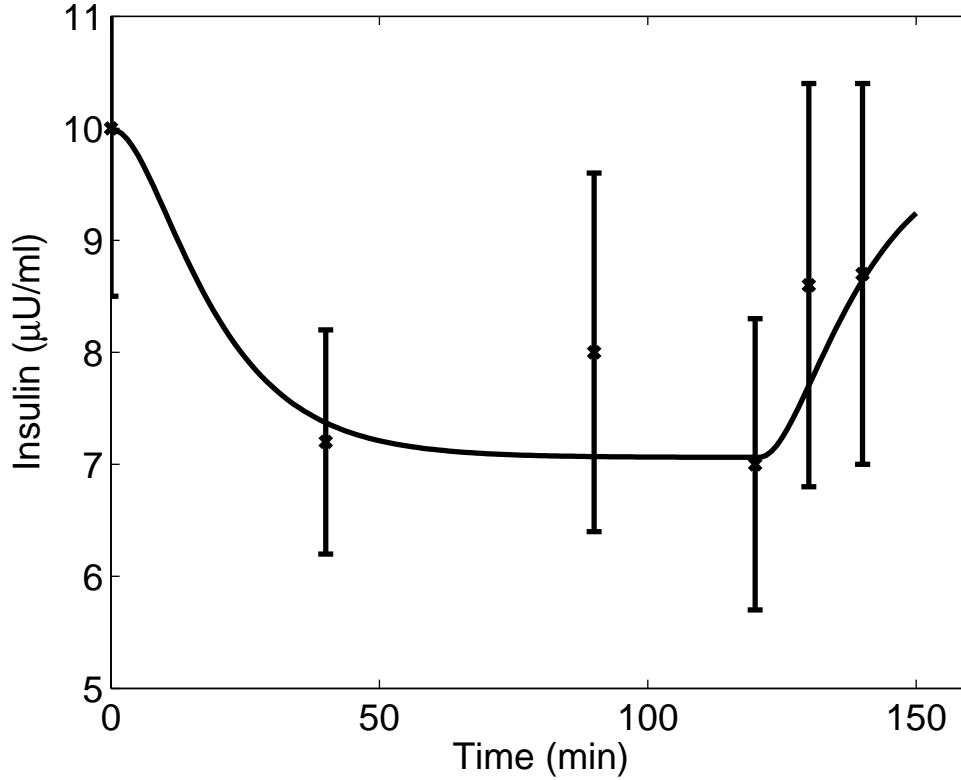


Figure 3.3: Plasma insulin concentration in response to mild exercise ($PVO_2^{max} = 30$) lasting from $t_{ex} = 0$ to 120 *min*. Model simulation validation (solid line) and published data (cross) ($\mu \pm \sigma$) from Ahlborg *et al.* [13]

overestimation ($a_3 = 0.0024$, $a_4 = 0.0355$) of glucose uptake rate, as shown by the dotted lines in Figure 3.4 (Top). In order to maintain plasma glucose homeostasis, hepatic glucose production rate ($G_{prod}(t)$, $\frac{mg}{kg \cdot min}$) also increased from its basal level to $0.95 \frac{mg}{kg \cdot min}$ for the duration of exercise. In conjunction with glucose uptake rate, $G_{prod}(t)$ decreased to its basal level after the end of exercise. Parameters a_1 and a_2 were estimated to fit the data, as shown in Figure 3.4 (Bottom). Again, 95% CIs of $G_{prod}(t)$ were simulated by choosing a set of parameter values from Table 3.2 that had the maximum underestimation ($a_1 = 0.0013$, $a_2 = 0.0679$) and the maximum overestimation ($a_1 = 0.0019$, $a_2 = 0.0441$) of glucose production

rate, as shown by the dotted lines in Figure 3.4 (Bottom). Both $G_{up}(t)$ and $G_{prod}(t)$ are represented in deviation form in Figure 3.4.

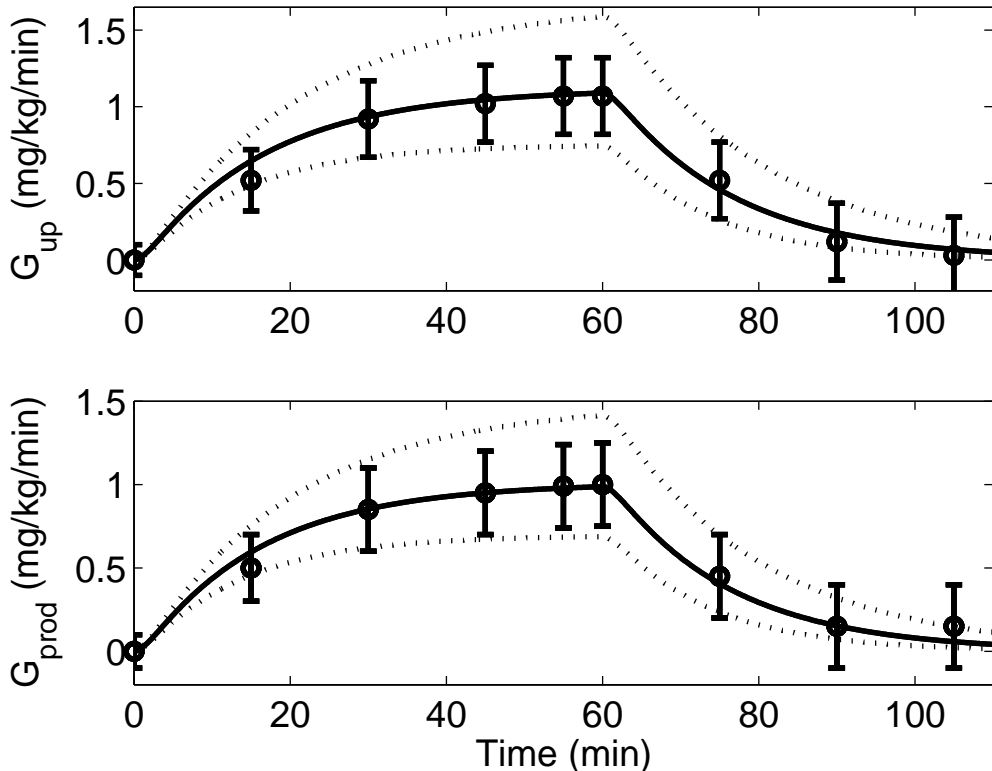


Figure 3.4: Model simulation (solid lines), 95% confidence intervals of model outputs (dotted lines) and published data (circles) ($\mu \pm \sigma$) from Wolfe *et al.* [12] in response to mild exercise ($PVO_2^{max} = 40$) lasting from $t_{ex} = 0$ to 60 min. Top: hepatic glucose uptake rate (G_{up}), and Bottom: hepatic glucose production rate (G_{prod}). Both G_{up} and G_{prod} are plotted in deviation form.

The accelerated glucose uptake rate during exercise is compensated for by enhanced hepatic glucose production; hence, normoglycemia is maintained throughout the course of physical activity. A comparison between the model prediction of glucose concentration including $G_{up}(t)$ plus $G_{prod}(t)$ effects and experimental data [12] is provided in Figure 3.5. The predictions of the glucose model are in good accordance with the published data. In order to simulate the 95% CIs for plasma glucose concentration, a combination of parameter

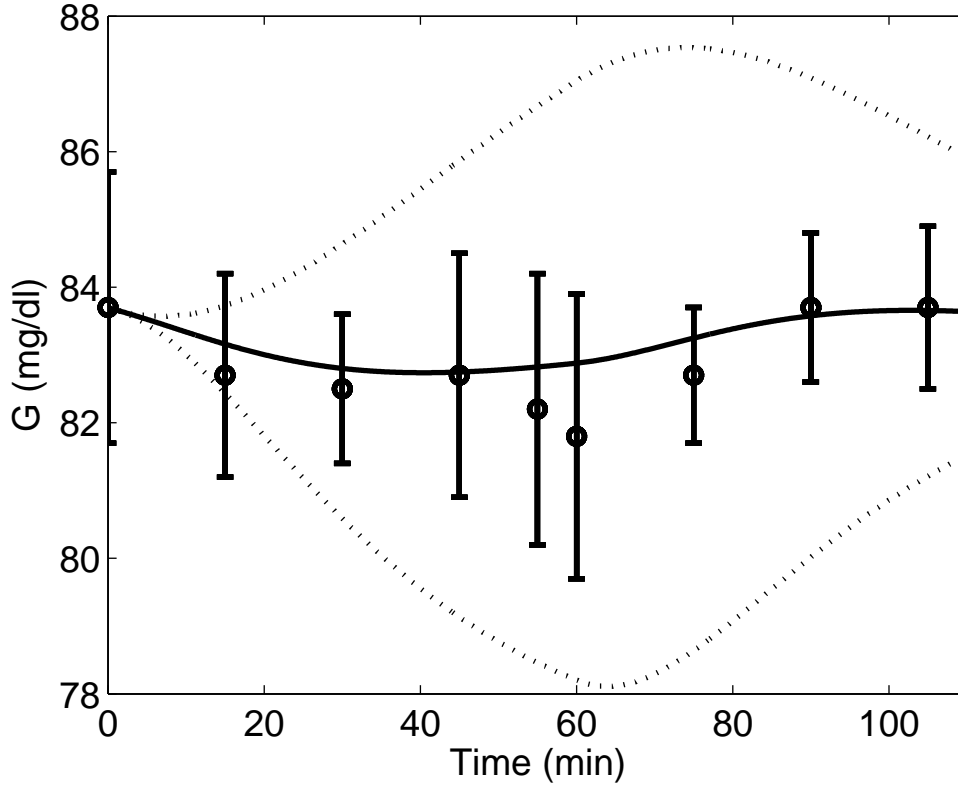


Figure 3.5: Plasma glucose concentration (G) in response to mild exercise ($PVO_2^{max} = 40$) lasting from $t_{ex} = 0$ to 60 min . Model simulation (solid line), 95% confidence intervals of model output (dotted lines), and published data (circles) ($\mu \pm \sigma$) from Wolfe et al. [12].

values were chosen from Table 3.2 that generated the maximum underestimation ($a_1 = 0.0013$, $a_2 = 0.0679$, $a_3 = 0.0024$, $a_4 = 0.0355$, $a_5 = 0.001$, $a_6 = 0.0912$) and the maximum overestimation ($a_1 = 0.0019$, $a_2 = 0.0441$, $a_3 = 0.0015$, $a_4 = 0.0617$, $a_5 = 0.0015$, $a_6 = 0.0588$) of plasma glucose, as indicated by the dotted lines in Figure 3.5.

For the validation of the glucose model, another simulation test was performed at moderate level of exercise for 45 min at $PVO_2^{max}(t) = 50$. Again, with the onset of exercise, both $G_{up}(t)$ and $G_{prod}(t)$ increased. During the recovery period ($t > 45 \text{ min}$), $G_{up}(t)$ and $G_{prod}(t)$ gradually declined to their respective basal levels. Model validation simulations (*i.e.*,

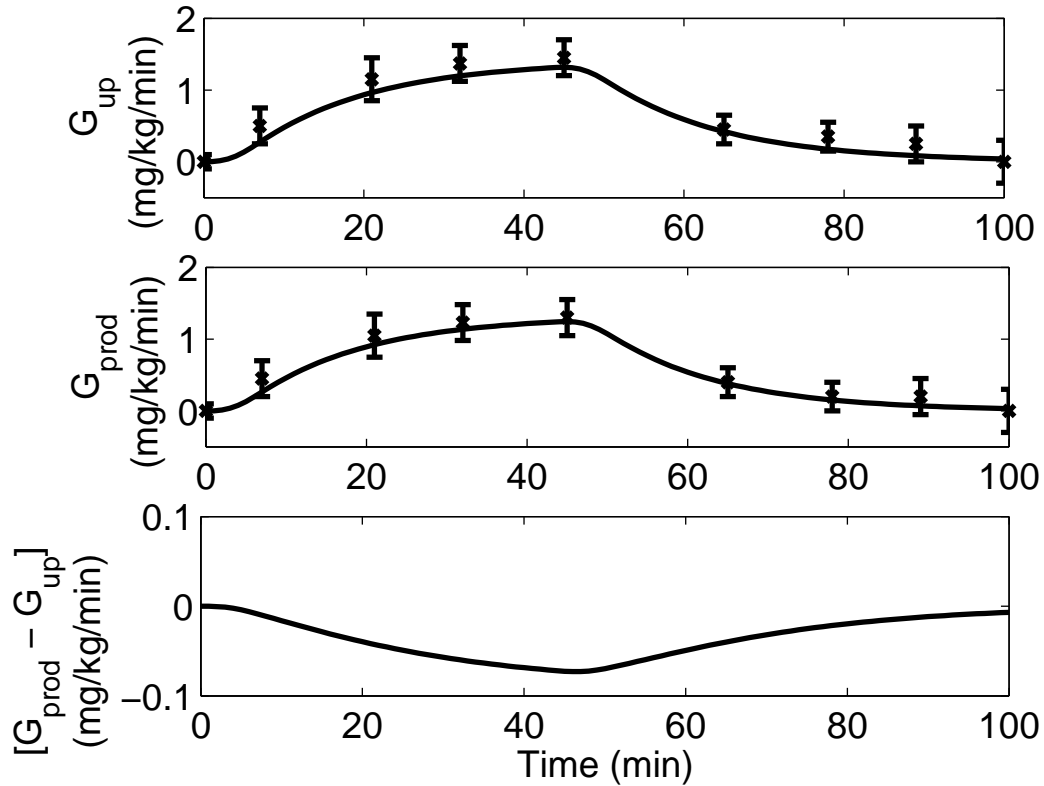


Figure 3.6: Response to moderate exercise ($PVO_2^{max} = 50$) lasting from $t_{ex} = 0$ to 45 min. Model simulation validation (solid lines) and published data (cross) ($\mu \pm \sigma$) from Zinman *et al.* [14]. Top: glucose uptake rate (G_{up}); Middle: hepatic glucose production rate (G_{prod}); Bottom: difference $[G_{prod} - G_{up}]$. Both G_{up} and G_{prod} are shown in deviation form.

no model parameter changes) are plotted alongside experimental data of T1DM patients [14] in Figure 3.6, top and bottom (both in deviation form). Figure 3.7 reveals the model prediction of plasma glucose concentration including the combined effects of $G_{up}(t)$ and $G_{prod}(t)$ during exercise along with experimental data [14] with the same group of patients.

To evaluate the plasma glucose dynamics during prolonged exercise, data from Ahlborg *et al.* [13] was considered (see Figure 3.8). With the onset of exercise, both $G_{up}(t)$ and $G_{prod}(t)$ rates were elevated from the basal level; this resulted in the maintenance of glucose

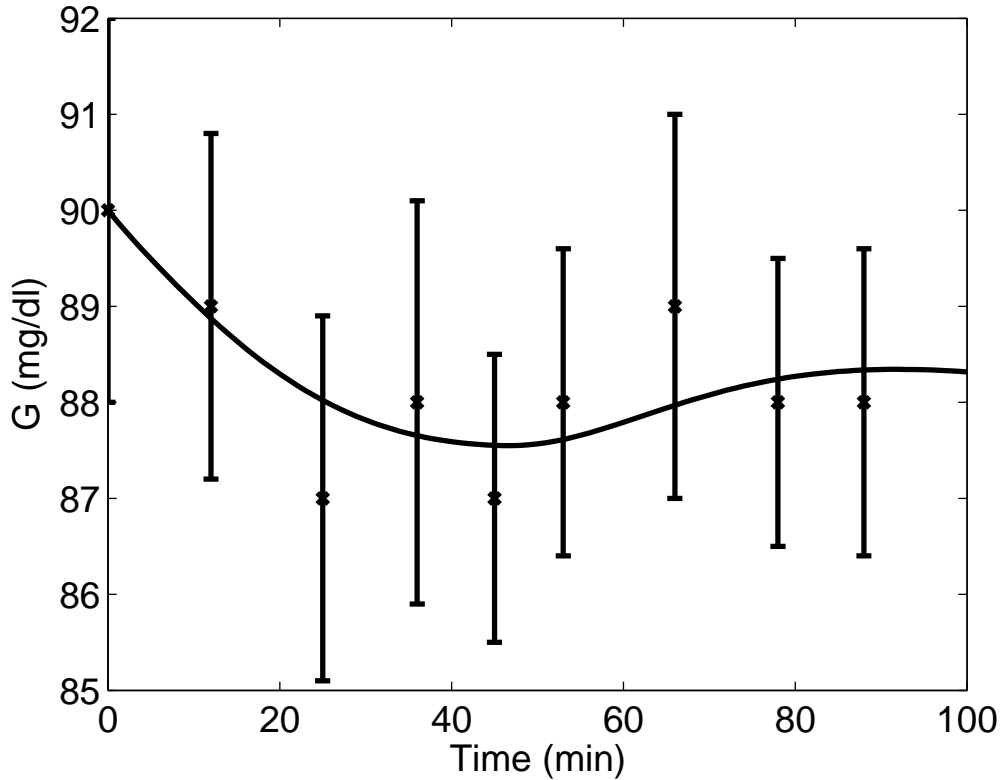


Figure 3.7: Plasma glucose concentration (G) in response to moderate exercise ($PVO_2^{max} = 50$) lasting from $t_{ex} = 0$ to 45 *min*. Model simulation validation (solid line) versus published data (cross) ($\mu \pm \sigma$) from Zinman *et al.* [14].

homeostasis during the first hour of exercise. As the integrated exercise intensity exceeded a critical threshold (which is a function of exercise intensity and duration), the hepatic glycogenolysis rate started to decline as a result of which net liver glucose production rate, $[G_{prod}(t) - G_{gly}(t)]$, decreased until the end of exercise (Figure 3.8: Bottom). However, G_{up} remained elevated due to continuing physical activity (Figure 3.8: Middle). This mismatch between $G_{up}(t)$ and $G_{prod}(t)$ resulted in a net decrease of plasma glucose level (Figure 3.8: Top). During the post-exercise recovery period, lactate consumption by the liver increases significantly, serving as a substrate for accelerated post-exercise gluconeogenesis [157]. It is

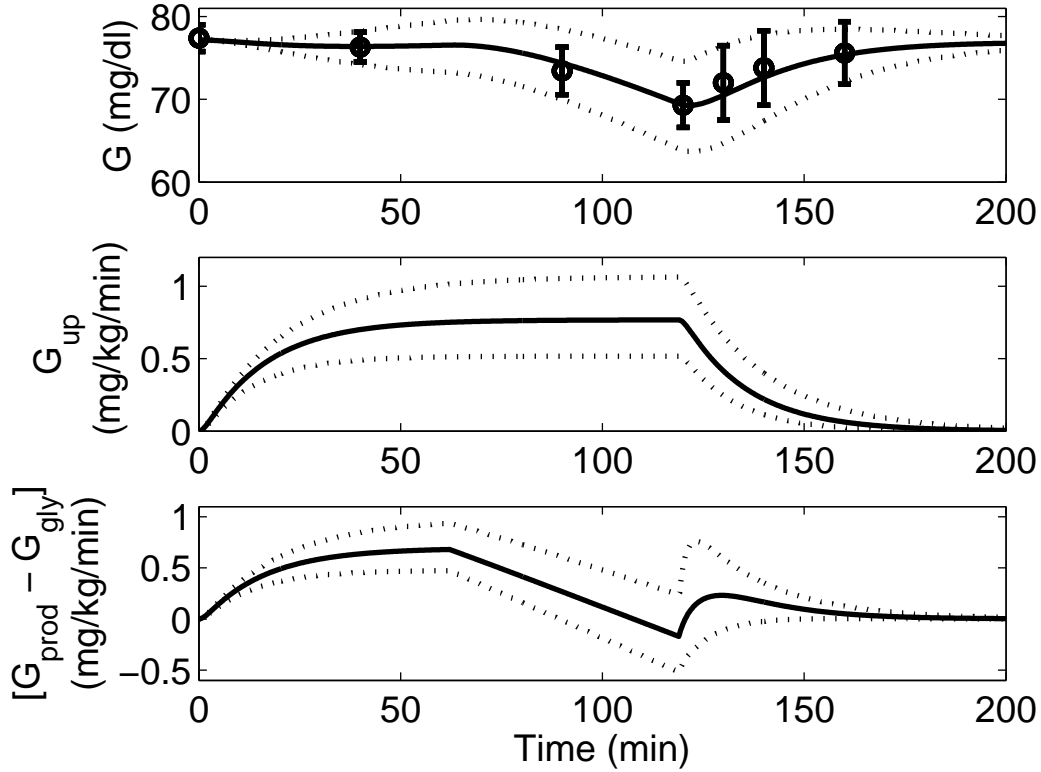


Figure 3.8: Model response to mild exercise ($PVO_2^{max} = 30$) lasting from $t_{ex} = 0$ to 120 min. Published data (circles) ($\mu \pm \sigma$) from Ahlborg *et al.* [13], model fit (solid line), and 95% confidence interval of fit (dashed line). Top: model prediction of plasma glucose (G); Middle: model prediction of hepatic glucose uptake rate (G_{up}); and Bottom: model prediction of net liver glucose production. Both G_{up} and $[G_{prod} - G_{gly}]$ are shown in deviation form.

believed that the purpose of this elevated gluconeogenesis is to replete the liver glycogen stores and restore normoglycemia [157]. Keeping parameters a_{1-6} unchanged, parameters k and T_1 from equation (3.10) were adjusted to capture the dynamical behavior of plasma glucose concentration. To simulate the 95% CIs for plasma glucose concentration during prolonged exercise, the same combination of parameter values were chosen from Table 3.2 as in Figure 3.5, with the addition of ($k = 0.0131$, $T_1 = 10.14$) for maximum underestimation

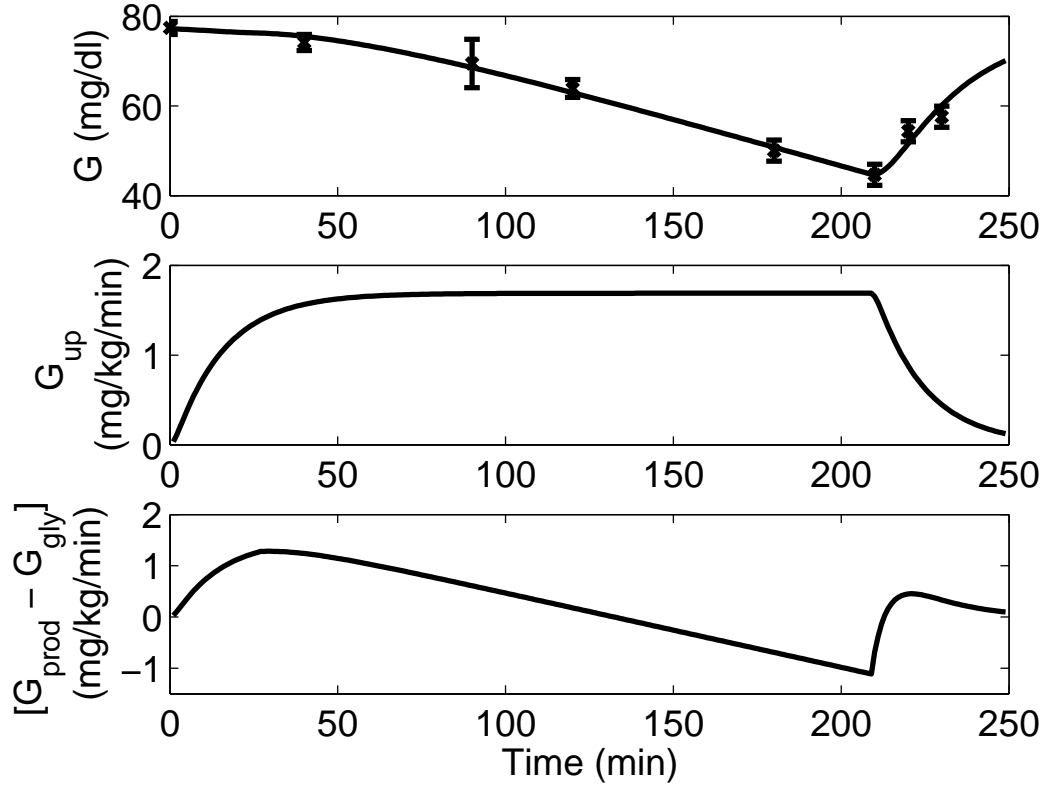


Figure 3.9: Model response to moderate exercise ($PVO_2^{max} = 60$) lasting from $t_{ex} = 0$ to 210 *min*. Published data (cross) ($\mu \pm \sigma$) from Ahlborg *et al.* [15] and model prediction validation (solid line). Top: model prediction of plasma glucose (G); Middle: model prediction of hepatic glucose uptake rate (G_{up}); and Bottom: model prediction of net liver glucose production. Both G_{up} and $[G_{prod} - G_{gly}]$ are shown in deviation form.

and ($k = 0.0085$, $T_1 = 1.86$) for the maximum overestimation, as shown by the dotted lines in Figure 3.8 (Top). To simulate the CIs for $G_{up}(t)$, the same parameter value sets as those used in Figure 3.4 (Top), were chosen (see Figure 3.8: Middle). Finally, to simulate the 95% CIs of net liver glucose production rate, a combination of parameter values were chosen from Table 3.2 to generate the maximum underestimation ($a_1 = 0.0013$, $a_2 = 0.0679$, $k = 0.0131$, $T_1 = 10.14$) and the maximum overestimation ($a_1 = 0.0019$, $a_2 = 0.0441$, $k = 0.0085$, $T_1 =$

1.86) of $[G_{prod}(t) - G_{gly}(t)]$, as shown by the dotted lines in Figure 3.8 (Bottom). In order to validate the model during prolonged exercise, a separate simulation study was performed where exercise was performed for 3 hours at a moderate exercise intensity ($PVO_2^{max} = 60$). Due to the higher exercise intensity, glycogen stores depleted at a faster rate; the result is an inability to maintain glucose homeostasis beyond $t_{ex} = 30 \text{ min}$ (see Figure 3.9: Top). A comparison between model simulations (without changing any parameters) and data [15] are given in Figure 3.9.

3.4 MODEL STRUCTURE JUSTIFICATION

The purpose of the proposed model was to extend the classical minimal model [1] in order to capture the vital physiological effects induced by mild-to-moderate exercise on glucose and insulin dynamics during and immediately after physical activity. The states added (equations (3.4), (3.5), (3.6), and (3.10)) were essential to describe accurately the acute exercise effects on plasma insulin and glucose concentrations. However, including extra equations certainly added complexity to the proposed model. Hence, this Section explores reduced versions of the proposed exercise model. AIC (see Section 2.3) was employed to establish a statistical comparison between the proposed model and its reduced versions.

3.4.1 Validity of $I_e(t)$ (Equation 3.6)

Equation (3.6) was added to the proposed model to capture the dynamics of $I_e(t)$, which represents the rate of insulin clearance from the circulatory system due to exercise. As mentioned in Section 3.2.1, parameters a_5 and a_6 from equation (3.6) were estimated using the data from Wolfe *et al.* [12] (for the values, refer to Table 3.2). In the reduced version, $I_e(t)$ (equation 3.6) was omitted. Hence, the exercise induced plasma insulin clearance was captured directly by the $PVO_2^{max}(t)$ variable coupled with a new parameter, b_1 . Thus, equation (3.2) could be re-written as follows:

$$\frac{dI(t)}{dt} = -nI(t) + p_4u_1(t) - b_1PVO_2^{max}(t) \quad (3.12)$$

The parameter value of $b_1 = 0.0148 \frac{\mu U}{ml \cdot min}$ was estimated from the data [12] via the nonlinear least square technique (Section 2.3). The calculated AIC values with and without the variable $I_e(t)$ (equation (3.6)) are presented in Table 3.3. It is clearly evident that the proposed model is superior to the reduced version, in terms of their AIC values. Simulation of these two models, along with the experimental data [12] are shown in Figure 3.10. Insulin dynamics during exercise without the filter equation (3.6) is much faster as compared to the data [12].

3.4.2 Validity of $G_{up}(t)$ (Equation 3.5)

In the proposed model, exercise-induced glucose uptake ($G_{up}(t)$) was captured by equation (3.5). Parameters a_3 and a_4 belonging to equation (3.5) were estimated by using the data from [12], as mentioned in Section 3.2.1 (for the values, refer Table 3.2). In the reduced version, equation (3.5) ($G_{up}(t)$), was omitted. Hence, the exercise induced glucose uptake rate, $G_{up}(t)$, was captured by the term $b_2PVO_2^{max}(t)$, which is a product of a new gain parameter, b_2 , and exercise intensity, $PVO_2^{max}(t)$. Therefore, equation (3.3) could be re-written as follows:

$$\begin{aligned} \frac{dG(t)}{dt} &= -p_1[G(t) - G_b] - X(t)G(t) + \frac{W}{Vol_G}[G_{prod}(t) - G_{gly}(t)] \\ &\quad - \frac{W}{Vol_G}G_{up}(t) + \frac{u_2(t)}{Vol_G} \end{aligned} \quad (3.13)$$

$$G_{up}(t) = b_2PVO_2^{max}(t) \quad (3.14)$$

The value of parameter b_2 ($0.03114 \frac{mg}{kg \cdot min}$) was estimated by using the data obtained from [12] via the nonlinear least square technique. The calculated AIC values of the proposed and reduced models are provided in Table 3.3. Once again, from the AIC values it is clearly

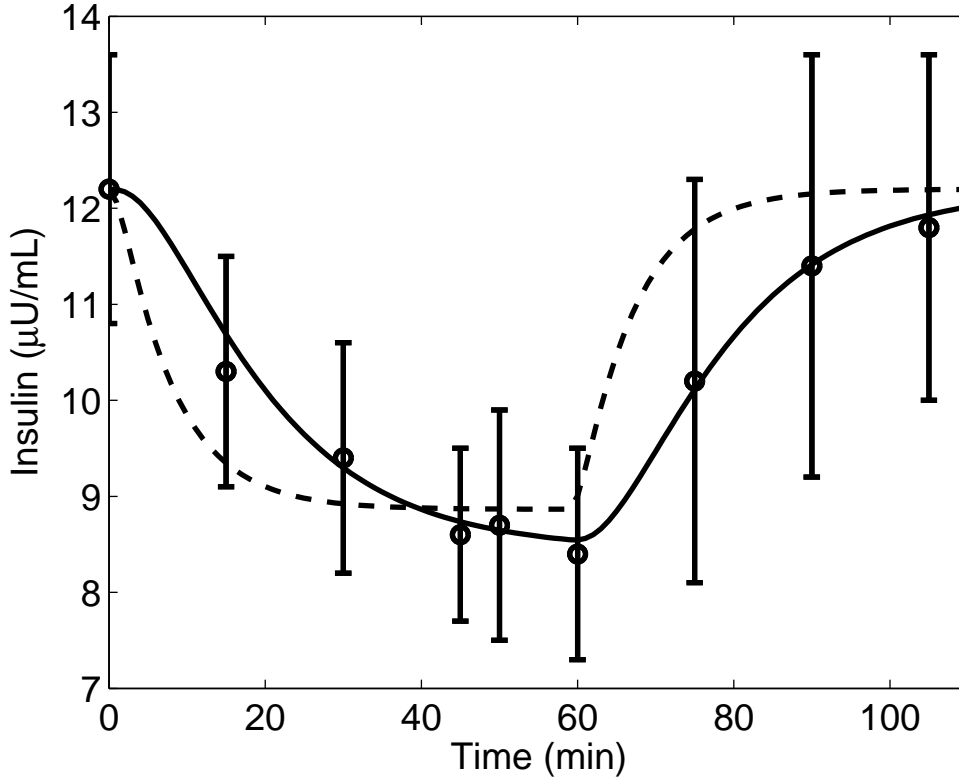


Figure 3.10: Plasma insulin concentration in response to mild exercise ($PVO_2^{max} = 40$) lasting from $t_{ex} = 0$ to 60 min. Published data (circles) ($\mu \pm \sigma$) from Wolfe *et al.* [12], proposed model fit [AIC = -32.194] (solid line), and reduced model fit [AIC = -11.83] (dashed line).

evident that the proposed model is superior to the reduced version. By not including equation (3.5) makes the model prediction of exercise-induced glucose uptake rate significantly faster than the observed data [12] (see Figure 3.11: Top).

3.4.3 Validity of $G_{prod}(t)$ (Equation 3.4)

In order to maintain glucose homeostasis, hepatic glucose production rate ($G_{prod}(t)$) is also increased during exercise. In the proposed model, the dynamics of $G_{prod}(t)$ are captured by

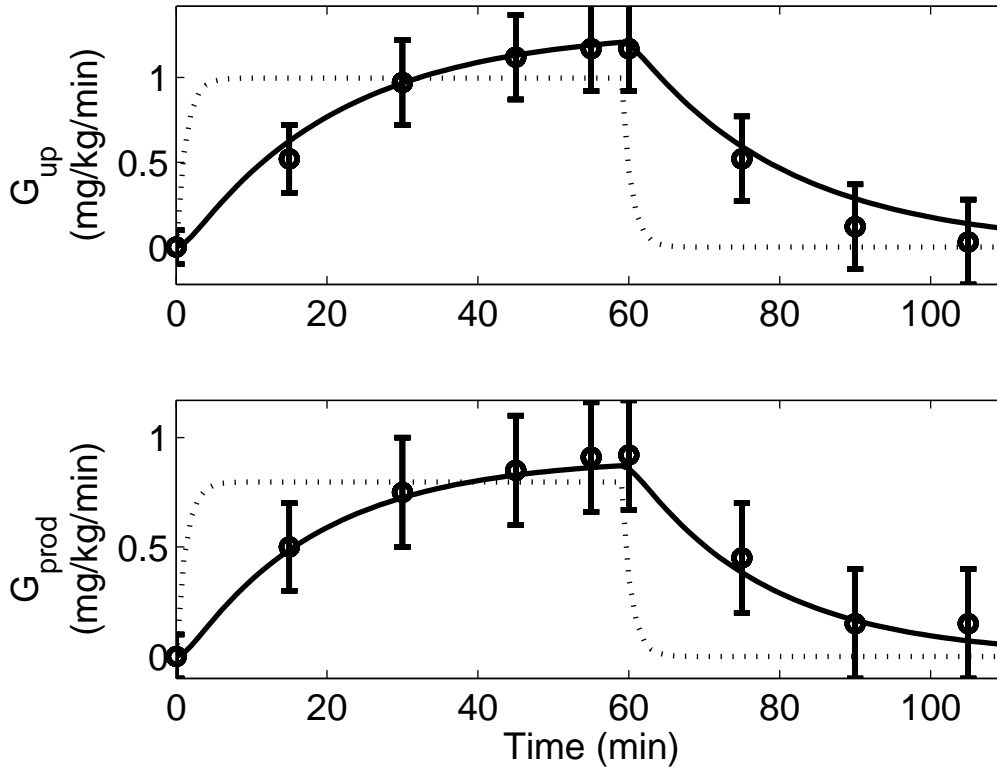


Figure 3.11: Proposed model simulation (solid lines), reduced model simulation (dotted lines) and published data (circles) ($\mu \pm \sigma$) from Wolfe *et al.* [12] in response to mild exercise ($PVO_2^{max} = 40$) lasting from $t_{ex} = 0$ to 60 min. Top: glucose uptake rate (G_{up}), and Bottom: hepatic glucose production rate (G_{prod}). Both G_{up} and G_{prod} are plotted in deviation form.

equation (3.4). As mentioned earlier, parameters a_1 and a_2 belonging to equation (3.4) were estimated by using the data from [12] via nonlinear least square algorithm.

In the reduced version, equation (3.4) ($G_{prod}(t)$) is eliminated. Therefore, the accelerated plasma glucose production induced by exercise is captured directly by the $PVO_2^{max}(t)$ variable coupled with the new parameter, b_3 . Hence, equation (3.3) could be re-written as shown below:

$$\begin{aligned} \frac{dG(t)}{dt} &= -p_1[G(t) - G_b] - X(t)G(t) + \frac{W}{Vol_G}[G_{prod}(t) - G_{gly}(t)] \\ &\quad - \frac{W}{Vol_G}G_{up}(t) + \frac{u_2(t)}{Vol_G} \end{aligned} \quad (3.15)$$

$$G_{prod}(t) = b_3 PVO_2^{max}(t) \quad (3.16)$$

Data from [12] was utilized to estimate the parameter, $b_3 = 0.02491 \frac{mg}{kg \cdot min}$ via the nonlinear least square technique. From the AIC values it is clearly evident that the proposed model is superior to the reduced model. The model prediction of exercise-induced glucose production ($G_{prod}(t)$) without equation 3.4 is significantly faster than the observed data [12] (see Figure 3.11: Bottom).

By comparing all the AIC values of the proposed exercise model and its reduced versions, it is evident that the originally proposed additional states (equation (3.4), (3.5), and (3.6)) are essential to accurately capture the dynamics of plasma glucose and insulin concentrations under the influence of exercise. Any further simplification than the proposed structure will compromise the quality of the model.

Table 3.3: Calculated AIC values of the exercise minimal model with and without the $I_e(t)$, $G_{up}(t)$ and $G_{prod}(t)$ filter equations

<i>AIC</i>	<i>Exercise Minimal Model</i>	
	<i>without</i>	<i>with</i>
Insulin clearance dynamics ($I_e(t)$)	Eq. (3.12) -11.830	Eq. (3.2) -32.194
Glucose uptake dynamics ($G_{up}(t)$)	Eq. (3.14) 8.880	Eq. (3.5) -15.705
Glucose production dynamics ($G_{prod}(t)$)	Eq. (3.16) 4.20	Eq. (3.4) -26.78

3.5 SUMMARY

A model of exercise effects on plasma glucose-insulin dynamics was developed. The principal goal was to extend the Bergman minimal model [1] by adding state equations in order to predict plasma glucose and insulin concentrations. This was accomplished by mathematically capturing the necessary physiological phenomenon induced by exercise. All the added equations in the proposed model are linear in nature thus maintaining the simplifying approach of the original minimal model [1]. The model successfully captured the effects of mild-to-moderate aerobic exercise on plasma glucose and insulin concentrations. Inclusion of separate dynamics in the model for glucose uptake (equation (3.5)) and hepatic glucose production (equation (3.4)) made it possible to capture the simultaneous rise of these rates with the onset of short term exercise in order to maintain glucose homeostasis. These equations were also successful in capturing the dynamics of glucose fluxes during the post-exercise recovery period. As the integrated exercise intensity extends beyond a critical threshold (which is a function of exercise intensity and duration), a decline in splanchnic glucose release is expected. As glucose uptake rate remains elevated, maintenance of glucose homeostasis is no longer possible. Due to this, plasma glucose continues to decline until the end of physical activity. At the end of prolonged exercise, the hepatic gluconeogenesis rate is increased, and this facilitates repletion of glycogen stores and helps to achieve normoglycemia [157]. A substantial amount of lactate is released from the post-exercising muscles during the recovery period, which serves as a substrate for gluconeogenesis. To capture the dynamics of plasma glucose during the various stages of prolonged exercise, equation (3.10) was incorporated. The model also successfully captured the clearance of plasma insulin from the circulatory system during physical exercise due to the addition of equation (3.6).

With a focus on closed-loop insulin delivery systems for T1DM patients, it is necessary to develop models that can accurately predict plasma glucose concentration during rest, as well as during physical exercise. Hence, this model provides the control community with an alternative benchmark problem in glucose control for diabetic patients by allowing the analysis of meal and exercise disturbances alone or in combination. The exercise model can also be used to predict the duration of exercise at a given intensity that can be executed while

keeping plasma glucose within the normoglycemic range. However, a prospective validation of the components of the minimal exercise model is necessary before the model, or a model-based controller, is employed in any clinical setting.

The proposed model as presented in this Chapter does not include the FFA dynamics and its interactions with blood glucose. As discussed in Chapter 2, FFA plays a significant role in influencing plasma glucose concentration. Also, FFA dynamics is profoundly altered during physical activity. Hence, in the following Chapter a lower-order composite model was synthesized by combining the FFA model from Chapter 2 and the exercise model from this Chapter. The composite model, as proposed in Chapter 4, is capable of predicting plasma FFA, glucose, and insulin dynamics during rest, as well as exercise.

4.0 A LOWER-ORDER MODEL OF FFA, GLUCOSE, AND INSULIN AT REST AND DURING EXERCISE

So far in the dissertation, two different metabolic models were developed by modifying the Bergman minimal model [1] in order to incorporate various physiological effects of FFA and exercise on the insulin-glucose system [129, 150]. The extended minimal model developed in Chapter 2 is capable of predicting FFA along with glucose dynamics during pre- and post-prandial states. The model is also equipped to capture the inhibitory effects of FFA on glucose uptake rate by the peripheral and hepatic tissues. However, the extended minimal model does not consider the exercise effects on insulin, glucose, and FFA kinetics. In Chapter 3, an exercise minimal model was developed to capture the effects of exercise on glucose and insulin dynamics. The model successfully captured insulin-glucose concentrations during and immediately after mild-to-moderate exercise. The model is also capable of predicting the plasma glucose excursion towards hypoglycemia during prolonged exercise periods. The major drawback of this model is the absence of FFA dynamics and its interactions with glucose and insulin.

Instead of having two different minimal models capturing the effects of FFA and exercise on the glucose-insulin system separately, a single low-order metabolic model capturing all the physiological effects on the glucose-insulin system can be developed. Hence, in this Chapter a composite metabolic model capable of predicting plasma glucose, insulin, and FFA dynamics at rest, as well as during mild-to-moderate exercise was developed.

One objective of the model was to represent the physiology more accurately. Hence, necessary modifications were made to the original model structures obtained from Chapters 2 and 3. For example, insulin action on glucose was divided into two parts having separate dynamics: one capturing the insulin-mediated tissue glucose uptake, and the other part

capturing the insulin-mediated suppression of endogenous glucose production. Moreover, saturating functions were used to represent the effects of insulin on endogenous glucose and FFA production rates. In order to accurately model literature data, unobservable filter equations capturing the interactions between insulin, glucose, FFA, and exercise were added wherever necessary. However, addition of extra equations increased the complexity of the model in terms of number of parameters which are required to be estimated. Hence, the trade-off between model accuracy and model complexity was measured by using AIC (equation (2.12)) as described in Section 2.3. The model structure with a lower AIC value was selected in synthesizing the composite model. The resulting composite model consisted of four parts: insulin, glucose, FFA, and exercise sub-models.

In the following Section (4.1), a brief overview of the physiological interactions between the plasma insulin, glucose, and FFA at rest and during exercise is presented. In Section 4.2, a detailed description of the structure of the composite model is introduced. A parametric sensitivity analysis is performed in Section 4.3. Finally, the results of model validation simulations are presented in Section 4.4.

4.1 INTERACTIONS BETWEEN INSULIN, GLUCOSE, AND FFA DURING REST AND EXERCISE

The major metabolic interactions captured by the composite model are given in Figure 4.1. Basically, the lower-order model is divided into four parts capturing the plasma insulin (section-I), plasma glucose (section-II), plasma FFA (section-III), and exercise (section-IV) dynamics, as shown in the schematic diagram. The continuous lines in the diagram represent transport or clearance of metabolic substrates and hormones; the dashed lines represent interactions taking place between the substrates, hormones, and exercise.

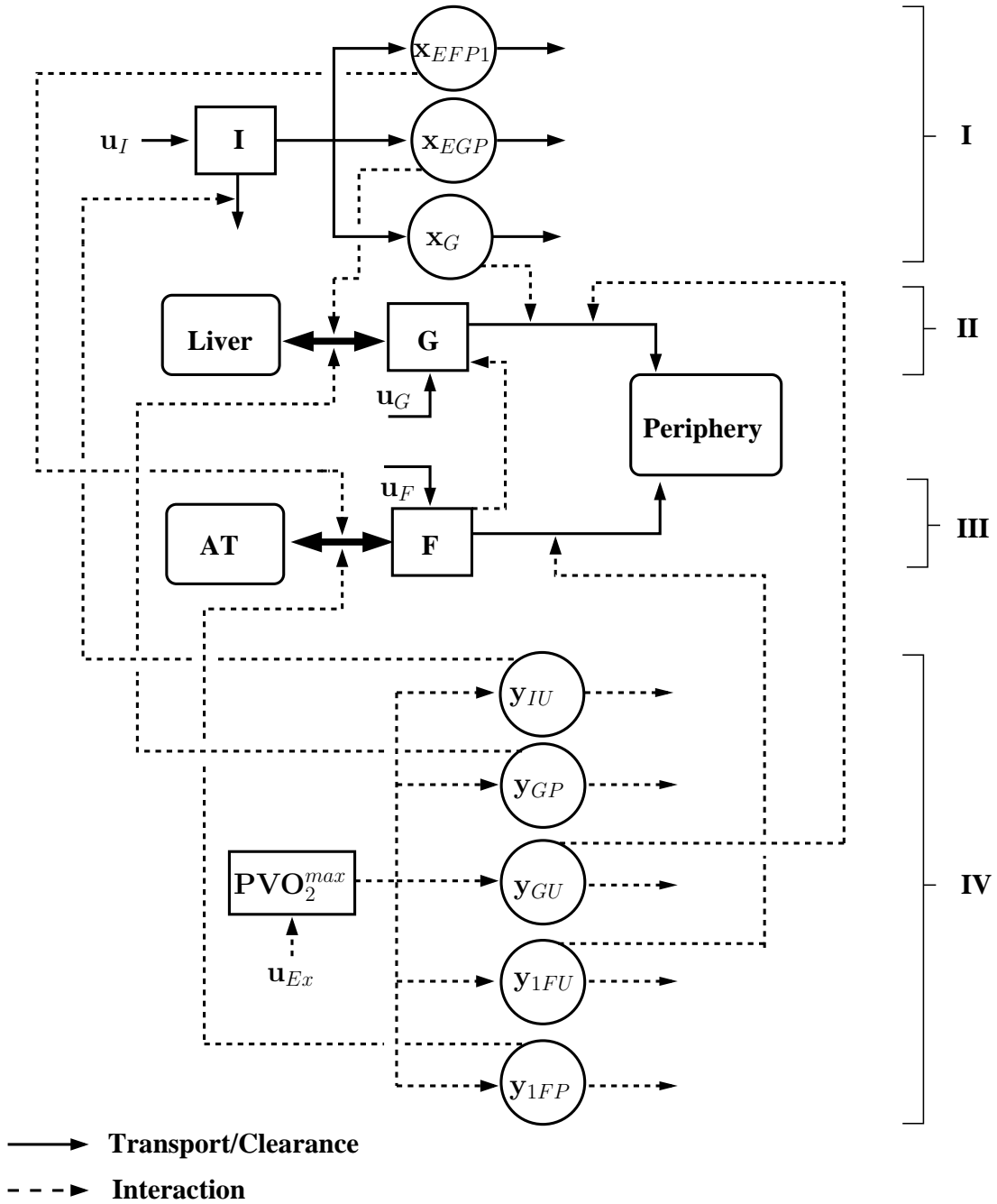


Figure 4.1: Schematic diagram of the composite model. Sections I, II, III, and IV represent the insulin, glucose, FFA, and exercise sub-models, respectively. I: Insulin; G: Glucose; F: FFA; u_I : Exogenously infused insulin; u_G , u_F : Glucose or FFA absorbed from meal or infused; u_{Ex} : Exercise intensity; PVO_2^{max} : Percentage of maximum rate of oxygen uptake; x_G , x_{EGP} , x_{EFP1} : Remote insulin compartments; y_{IU} , y_{GU} , y_{GP} , y_{1FU} , y_{1FP} : 1st-order filters capturing exercise effects.

The insulin model assumes that all of the insulin present in the system is infused exogenously, as indicated by u_I ($\frac{mU}{min}$). Compartment I, in section-I (Figure 4.1), represents the observable insulin concentration at the systemic level. Insulin from the plasma space enters into three unobservable remote insulin compartments, x_i (where, $i \in G, EGP, EFP1$). Insulin-mediated glucose uptake in the tissues is governed by x_G . Insulin also plays a major role in suppressing the hepatic glucose production [57], which is captured by x_{EGP} . Finally, the inhibitory action of insulin on endogenous FFA production rate (anti-lipolysis) is captured by x_{EFP1} .

In section-II (Figure 4.1), compartment G represents circulating plasma glucose concentration. Glucose from the circulatory system is consumed by the peripheral tissues for oxidation purposes and by the hepatic tissues mostly for storage purposes in the form of glycogen [55]. Whenever the body requires energy, stored glycogen is catabolized into glucose which is then released back into the circulatory system; a process commonly known as glycogenolysis [56]. Glucose infused intravenously or absorbed from meal is represented by u_G ($\frac{g}{min}$).

The plasma FFA dynamics is captured in section-III (Figure 4.1), where compartment F represents measurable FFA level in the circulatory system. FFA is consumed by the peripheral tissues for oxidation purposes, while uptake by the AT is mostly for storage in the form of triglycerides [54]. FFA absorbed from the meal or infused intravenously is captured by u_F ($\frac{g}{min}$). The inhibitory effects of FFA on the glucose uptake rate, as proposed by Randle *et al.* [58, 59], is indicated by the dashed line initiating from the F compartment and terminating at the G compartment.

The dynamics of exercise intensity in terms of PVO_2^{max} is captured in section-IV (Figure 4.1). The significant effects of physical activity on insulin, glucose, and FFA are captured by the first-order filter compartments y_i (where, $i \in IU, GP, 1FU$, and $1FP$). As mentioned in the previous chapter, exercise accelerates the clearance of plasma insulin, which is captured by y_{IU} in the composite model. Alterations in the glucose kinetics due to exercise is captured by y_{GU} and y_{GP} ; where, the former represents exercise-induced increase in muscle glucose uptake rate and the latter represents increased hepatic glucose production rate due to exercise. During mild-to-moderate exercise, fat oxidation in the muscle increases

approximately 4-5 folds above its resting amount [162, 61]. This increased FFA oxidation due to exercise is captured by y_{1FU} in the model. Availability of FFA also increases significantly during exercise [61]. Majority of the increased supply of FFA is provided by lipolysis which typically exceeds the FFA uptake rate [162, 18]. In the model, y_{1FP} governs the increased FFA production rate during exercise.

In the following section, the mathematical structure of the composite model is introduced. Most of the parameter values were estimated from published data by using the nonlinear least square technique, as described in Section 2.3 (Chapter 2), and the rest were directly obtained from the literature. All the parameter values of the composite model in its final form are provided in Table 4.1.

4.2 COMPOSITE MODEL STRUCTURE

4.2.1 Insulin Dynamics

The model assumes an absolute deficiency of the pancreatic β -cells to secrete any insulin; hence, all of the gluco-regulatory hormone is externally infused ($u_I(t)$). Exercise promotes the clearance of insulin, causing a drop in the plasma insulin level. This phenomenon is essential to enhance the hepatic glucose production and lipolysis during exercise [12]. The insulin dynamics along with exercise effects can be mathematically written as:

$$\frac{dI(t)}{dt} = -nI(t) - y_{IU}(t)I(t) + \frac{u_I(t)}{V_I} \quad (4.1)$$

$$\frac{dPVO_2^{max}(t)}{dt} = m_{PV}(u_{Ex}(t) - PVO_2^{max}(t)) \quad (4.2)$$

$$\frac{dy_{IU}(t)}{dt} = m_{IU1}PVO_2^{max}(t) - m_{IU2}y_{IU}(t) \quad (4.3)$$

Here, equation (4.1) captures the plasma insulin concentration ($I(t)$, $\frac{\mu U}{ml}$), similar to equation (3.2) in Chapter 3. The insulin clearance rate, n , and the insulin distribution space, V_I , are directly obtained from the literature [1]. Notice, the only difference in this equation from equation (3.2) in Chapter 3 is the 2^{nd} term in the right hand side (RHS) of both the

equations representing the exercise-induced clearance rate of insulin. Unlike the exercise minimal model in Chapter 3, introduction of the bilinear term ($y_{IV}(t)I(t)$) in the composite model will prevent $I(t)$ from reaching negative values during exercise in absence of any plasma insulin, which might happen for T1DM patients. Equation (4.2), which quantifies the exercise intensity above its basal level, is same as equation (3.1) in Chapter 3. The dynamics of the unobserved variable $y_{IV}(t)$ ($\frac{1}{min}$) is represented by equation (4.3). Parameters m_{IV1} and m_{IV2} were estimated by utilizing data obtained from Wolfe *et al.* [12], where healthy subjects performed bicycle exercise for 60 *min* at an intensity $PVO_2^{max} = 40\%$. Blood samples were collected during exercise and the recovery period to measure the plasma insulin concentration, as shown in Figure 4.2. With the onset of exercise, plasma insulin declined below its basal level due to the elevated clearance rate and remained low until the end of exercise. During the recovery period, plasma insulin climbed back to its basal value.

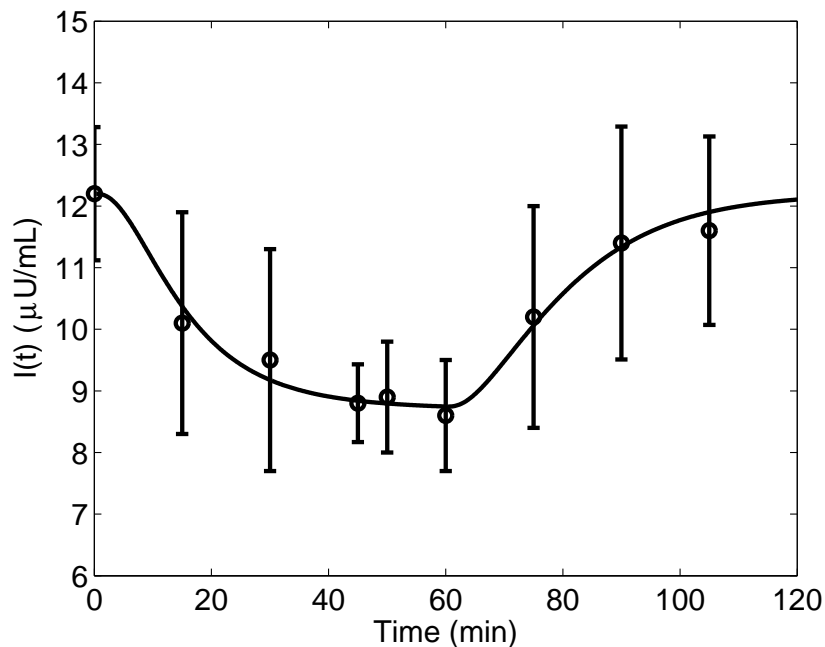


Figure 4.2: Plasma insulin concentration in response to mild exercise ($PVO_2^{max} = 40\%$) lasting from time $t_{Ex} = 0$ to 60 *min*. Published data (circles) ($\mu \pm \sigma$) from Wolfe *et al.* [12] and model fit (solid line)

4.2.2 FFA Dynamics

FFA is released from the AT into the plasma via the lipolytic process. The circulating FFA is consumed by the various organs and tissues mostly for oxidation, except the AT where it is consumed for storage purposes. Insulin is one of the major hormones that regulates the lipolytic process by suppressing the activation of hormone sensitive lipase (HSL), which is the primary enzyme responsible for lipolysis [137]. The following equations capture the FFA dynamics at rest.

$$\frac{dF(t)}{dt} = -p_{F1}F(t) + EFP(t) + \frac{u_F}{V_F} \quad (4.4)$$

$$EFP(t) = EFP_0 \left(1 - k_{EFP} \left(\frac{x_{EFP1N}(t)}{x_{EFP1N}(t) + s_{EFPN}} \right) \right) \quad (4.5)$$

$$\frac{dx_{EFP1}(t)}{dt} = p_{F2}(I(t) - x_{EFP1}(t)) \quad (4.6)$$

$$x_{EFP1N}(t) = \frac{x_{EFP1}(t)}{x_{EFP1B}} \quad (4.7)$$

Here, equation (4.4) represents the plasma FFA concentration ($F(t)$, $\frac{\mu\text{mol}}{l}$). The plasma FFA distribution volume (V_F , l) is directly obtained from the literature [18]. Parameter p_{F1} represents the rate at which FFA is consumed by the tissues. The rate of endogenous FFA production (*i.e.*, lipolysis) is captured by the variable $EFP(t)$ ($\frac{\mu\text{mol}}{l \cdot \text{min}}$), which is a function of insulin concentration as shown in equations (4.5)–(4.7). The unobserved variable x_{EFP1} ($\frac{\mu\text{mol}}{l}$) represents the effect of remote insulin concentration on lipolysis. Variable $x_{EFPN}(t)$ is the remote insulin concentration normalized with respect to its basal level (x_{EFPB} , $\frac{\mu\text{mol}}{l}$), as shown in equation (4.7).

To establish the correlation between endogenous FFA production rate and insulin concentration, data was obtained from Campbell et al. [16], where the lipolytic rate of healthy humans was measured at various steady state hyperinsulinemic levels. As we can see in Figure 4.3, an increasing insulin level significantly suppressed the FFA production rate. In fact, saturation was reached for the EFP when insulin level was approximately 40 fold above its basal level. The rate of lipolysis at zero insulin in equation (4.5), EFP_0 ($\frac{\mu\text{mol}}{l \cdot \text{min}}$), was obtained from the literature [16]. The gain parameter, k_{EFP} , was also extracted from the

data [16] by considering the data-point having the lowest EFP value (EFP_{lo}), as indicated by the point (a) in Figure 4.3, as follows: When,

$$EFP(t) = EFP_{lo}$$

$$x_{EFP1N} \gg s_{EFPN}$$

Hence,

$$\frac{x_{EFP1N}(t)}{x_{EFP1N}(t) + s_{EFPN}} \approx 1$$

As a result, equation (4.5) reduces to:

$$k_{EFP} = 1 - \frac{EFP_{lo}}{EFP_0} \quad (4.8)$$

In order to fit the data [16] in Figure 4.3, only the saturation constant, s_{EFPN} , from equation (4.5) was estimated.

The value of parameter p_{F1} representing the plasma uptake rate of FFA can be directly obtained from equation (4.4) at the basal steady state condition, as shown below:

$$p_{F1} = \frac{EFP_B}{F_B} \quad (4.9)$$

Here, EFP_B ($\frac{\mu mol}{l \cdot min}$) is the lipolytic rate at basal conditions and F_B ($\frac{\mu U}{ml}$) is the basal plasma FFA concentration. Both these values were directly obtained from the literature [16].

In order to capture the dynamical effects of insulin on endogenous FFA production, parameter p_{F2} in equation (4.6) was estimated by utilizing data from two different studies simultaneously [4, 17]. In [4], euglycemic-hyperinsulinemic clamps were employed on normal subjects. Plasma insulin concentration was elevated to 20, 30, and 100 $\frac{\mu U}{ml}$, as shown in the top, middle, and bottom panels in Figure 4.4, respectively. Due to the antilipolytic action of elevated insulin levels, plasma FFA was suppressed in all the three cases. In the second study

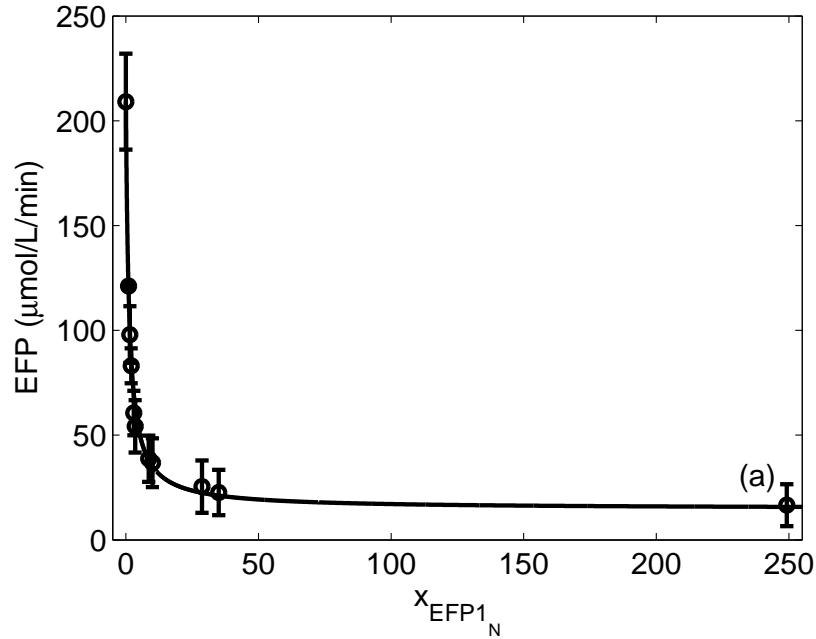


Figure 4.3: Model fit (solid line) versus published data ($\mu \pm \sigma$) (circle) [16] of steady state endogenous FFA production rate, EFP , as a function of normalized remote insulin concentration x_{EFP1_N} . Data-point (a) indicates the lowest FFA production rate, EFP_{lo} .

[17], a modified insulin frequently sampled intravenous glucose tolerance test (MI-FSIGT) was performed, where boluses of insulin at time $t = 0$ and 20 min were administered to normal subjects, as indicated by the top panel of Figure 4.5. Due to the insulin boluses, plasma FFA concentration was suppressed well below its basal level as shown in the bottom panel of Figure 4.5. The model predictions indicated in Figure 4.4 and 4.5 were obtained by adjusting the parameter $p_{F2} = 0.014782 \frac{1}{\text{min}}$. The AIC value of the model estimated by using the technique as discussed in Section 2.3 is -22.74 . By analyzing the model performances in both the studies, it is evident that the model predictions underestimate the FFA data, particularly in the first 50 min of the bottom panels in both the Figures (4.4 and 4.5). Therefore, to delay the FFA action on lipolysis a second filter compartment (x_{EFP2}) was introduced in series, as shown in Figure 4.6.

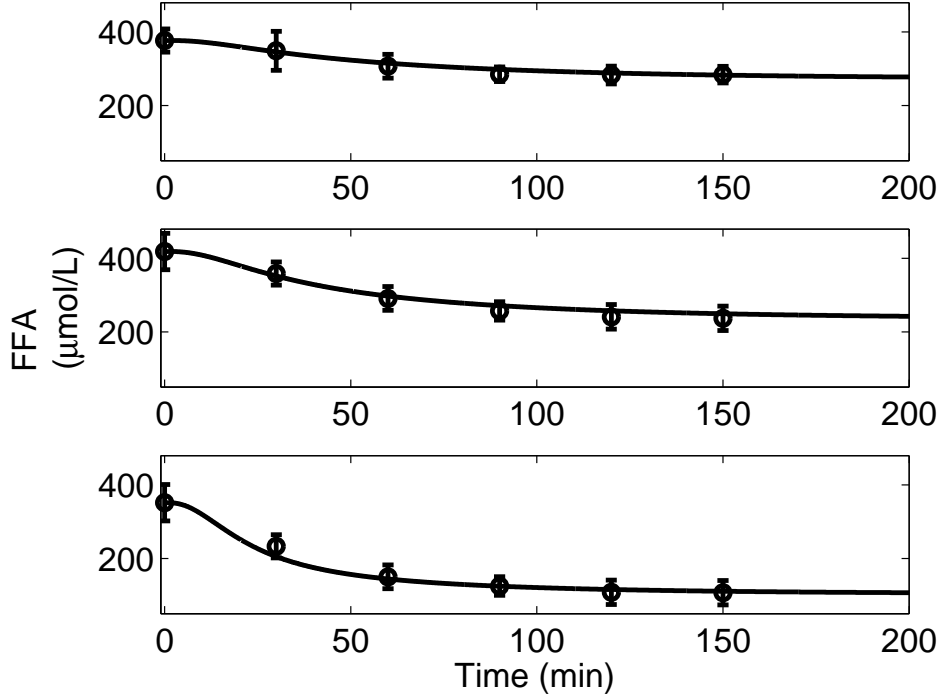


Figure 4.4: Euglycemic hyperinsulinemic clamp study, where plasma insulin concentration was maintained at $20 \frac{\mu U}{ml}$ (top); $30 \frac{\mu U}{ml}$ (middle); and, $100 \frac{\mu U}{ml}$ (bottom). Model prediction (solid line) using only one insulin filter (x_{EFP1}) and published data ($\mu \pm \sigma$) (circle) [4] of plasma FFA concentration.

Hence, the endogenous FFA production rate after addition of the extra lag can be mathematically expressed as follows:

$$EFP(t) = EFP_0 \left(1 - k_{EFP} \left(\frac{x_{EFP2N}(t)}{x_{EFP2N}(t) + s_{EFPN}} \right) \right) \quad (4.10)$$

$$\frac{dx_{EFP2}(t)}{dt} = p_{F3}(x_{EFP1}(t) - x_{EFP2}(t)) \quad (4.11)$$

$$x_{EFP2N}(t) = \frac{x_{EFP2}(t)}{x_{EFP2B}} \quad (4.12)$$

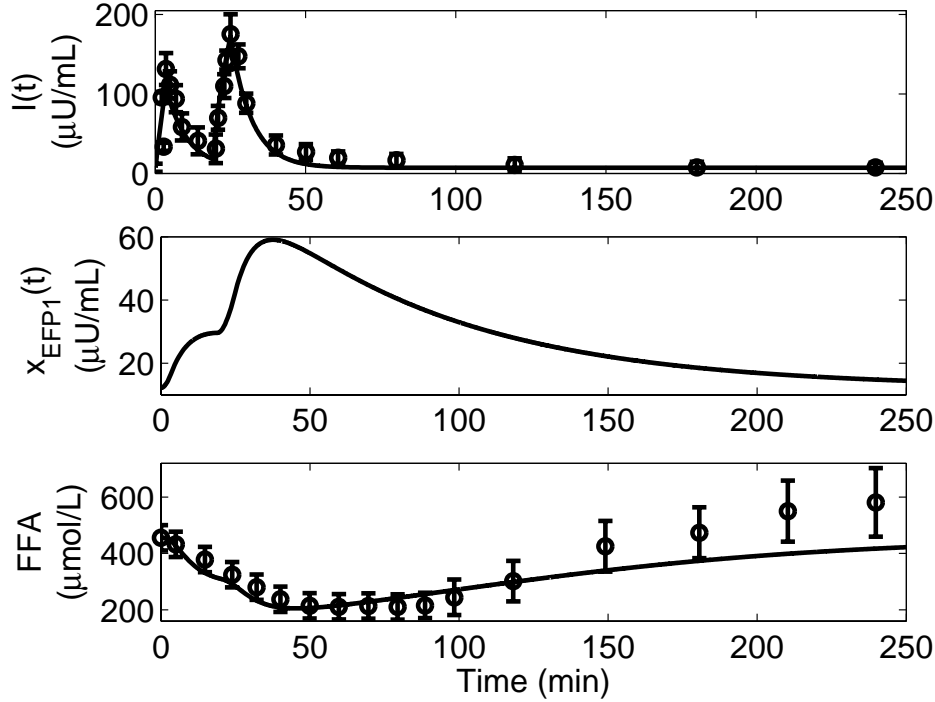


Figure 4.5: MI-FSIGTT study, where plasma insulin boluses were administered at $t = 0$ and 20 min . Model prediction (solid line) and published data ($\mu \pm \sigma$) (circle) [17] of plasma insulin concentration (top); model prediction (solid line) of the unobserved remote insulin concentration x_{EFP1} (middle); model prediction using only one insulin filter (x_{EFP1}) (solid line) and published data ($\mu \pm \sigma$) (circle) [17] of plasma FFA concentration (bottom)

The additional filter equation (4.11) introduced a new parameter, p_{F3} . Once again, parameters p_{F2} and p_{F3} were adjusted to capture the data from [4] and [17], simultaneously. Introduction of the new lag slowed down the FFA dynamics significantly thereby increasing the accuracy of the model predictions, as indicated in Figures 4.7 and 4.8. Although, in Figure 4.8 the FFA data seems to have reached a pseudo-basal level which is higher than the initial basal concentration. This could be due to diurnal variations of plasma FFA, which are unrelated to the insulin or glucose kinetics, as pointed out by the authors [17]. The two separate filter equations in the insulin dynamics could be visualized as the lag associated

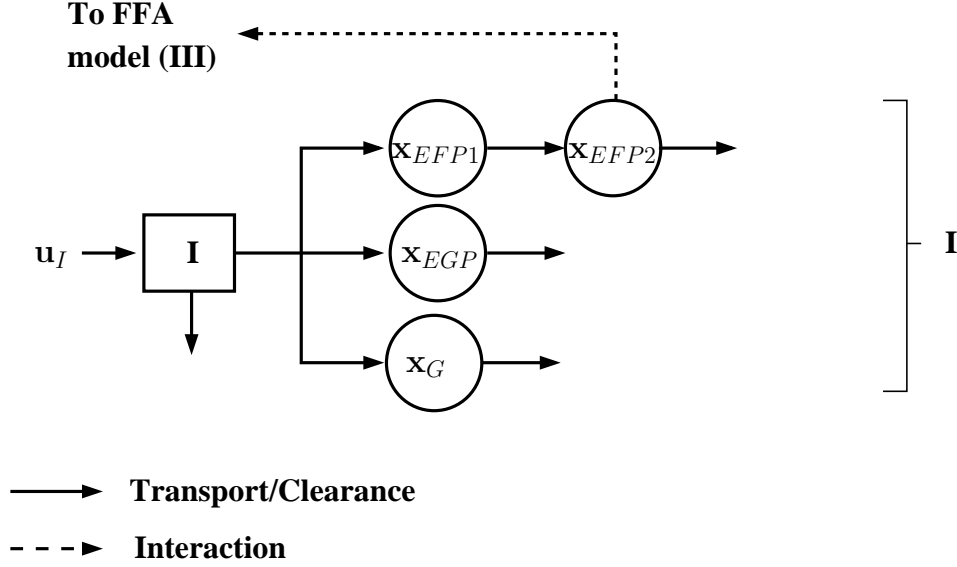


Figure 4.6: Schematic diagram of the modified insulin model section (I) of the composite model with modifications

with transport of insulin in the adipocyte from the circulatory system and the lag associated with the action of insulin on deactivation of HSL, due to which lipolysis is suppressed. Even with the added complexity (in terms of the one added parameter), the AIC value of the modified model is -54.42 , which is much lower than the AIC value of the previous insulin model structure.

Exercise increases FFA uptake, as well as production in the body. In order to incorporate the effects of exercise on FFA dynamics, equation (4.4) can be re-written as follows:

$$\frac{dF(t)}{dt} = -p_{F1}F(t) - \frac{W}{V_F}y_{1FU}(t) + EFP(t) + \frac{W}{V_F}y_{1FP}(t) + \frac{u_F(t)}{V_F} \quad (4.13)$$

$$\frac{dy_{1FU}(t)}{dt} = m_{FU1}PVO_2^{max}(t) - m_{FU2}y_{1FU}(t) \quad (4.14)$$

$$\frac{dy_{1FP}(t)}{dt} = m_{FP1}PVO_2^{max}(t) - m_{FP2}y_{1FP}(t) \quad (4.15)$$

Here, $y_{1FU}(t)$ ($\frac{\mu\text{mol}}{\text{kg}\cdot\text{min}}$) represents the rate of disappearance of FFA by the working tissues due to exercise. Exercise-induced production of FFA is captured by $y_{1FP}(t)$ ($\frac{\mu\text{mol}}{\text{kg}\cdot\text{min}}$). W

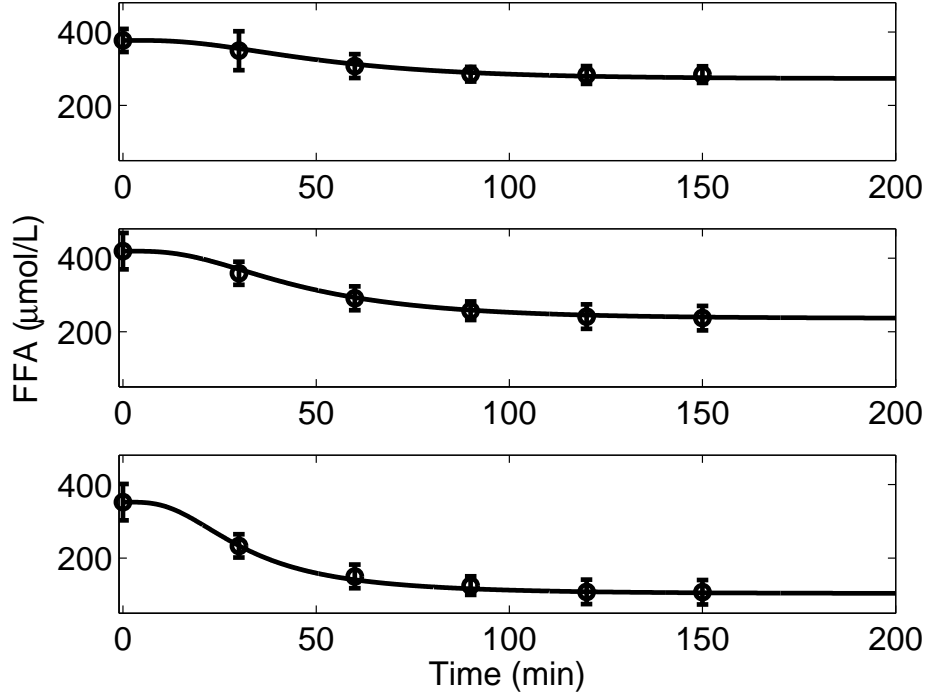


Figure 4.7: Euglycemic hyperinsulinemic clamp study, where plasma insulin concentration was maintained at $20 \frac{\mu U}{ml}$ (top); $30 \frac{\mu U}{ml}$ (middle); $100 \frac{\mu U}{ml}$ (bottom). Model prediction (solid line) using two insulin filters (x_{EFP1} and x_{EFP2}) and published data ($\mu \pm \sigma$) (circle) [4] of plasma FFA concentration.

(kg) is the weight of the patient. In order to estimate the parameters of equations (4.14) and (4.15), data was obtained from an experiment performed by Klein *et al.* [18] where healthy subjects performed exercise at $PVO_2^{max} = 45\%$ intensity for 240 min . FFA kinetics were measured during and immediately after the physical activity, to measure the whole-body plasma FFA appearance rate, Ra_F ($\frac{\mu mol}{l \cdot min}$), and plasma disappearance rate, Rd_F ($\frac{\mu mol}{l \cdot min}$), was measured along with the FFA concentration at the systemic level. With the onset of exercise, both Rd_F and Ra_F increased rapidly over the first 30 min . Thereafter, Rd_F and Ra_F gradually increased until the end of exercise. As Ra_F exceeded Rd_F , plasma FFA concentration increased steadily throughout the duration of exercise. During the recovery

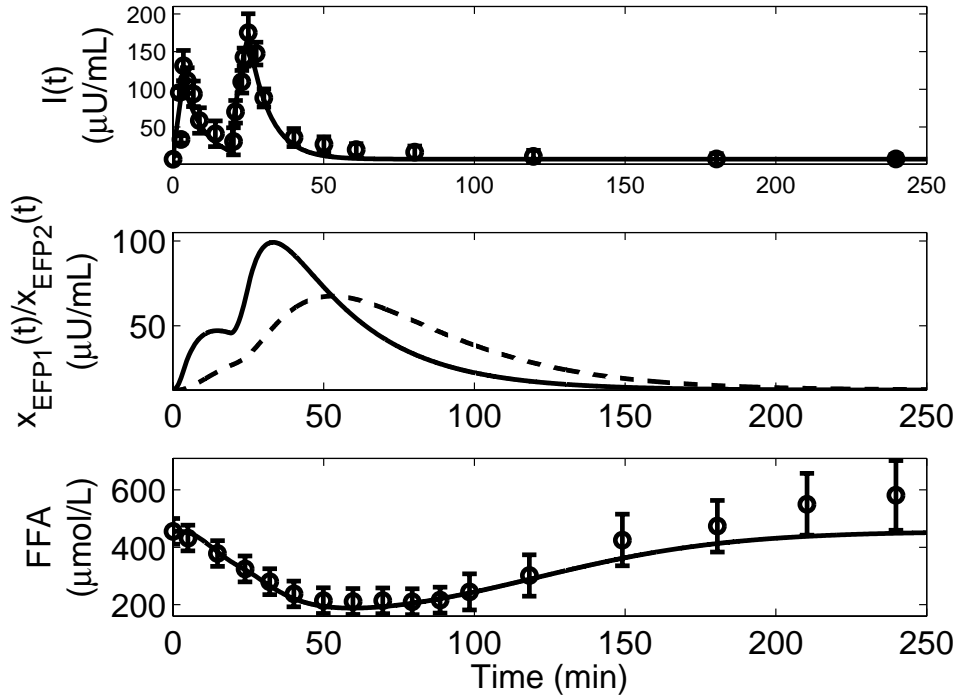


Figure 4.8: MI-FSIGTT study, where plasma insulin boluses were administered at $t = 0$ and 20 min . Model prediction (solid line) and published data ($\mu \pm \sigma$) (circle) [17] of plasma insulin concentration (top); model predictions of the first, x_{EFP1} (solid line), and second x_{EFP2} (dashed line) remote insulin concentrations (middle); model prediction (solid line) using both the insulin filters (x_{EFP1} and x_{EFP2}) and published data ($\mu \pm \sigma$) (circle) [17] of plasma FFA concentration (bottom)

period, the FFA returned to its basal level slowly. On the RHS of equation (4.13), the first two terms represent the rate of disappearance of plasma FFA (Rd_F); whereas, the third and fourth terms represent the rate of appearance of plasma FFA (Ra_F). Parameters $m_{FU1} = 0.0093287 \left(\frac{\mu\text{mol}}{\text{kg}\cdot\text{min}^2}\right)$, $m_{FU2} = 0.021622 \left(\frac{1}{\text{min}}\right)$, $m_{FP1} = 0.0094836 \left(\frac{\mu\text{mol}}{\text{kg}\cdot\text{min}^2}\right)$, and $m_{FP2} = 0.019745 \left(\frac{1}{\text{min}}\right)$ were estimated to obtain the model predictions as shown in Figure 4.9. The calculated AIC value of the model is -14.6116 . By closely analyzing the top and middle panels of Figure 4.9, it is quite evident that equations (4.14) and (4.15) are inadequate to

capture the rapid initial rise in Rd_F and Ra_F during exercise (especially the 30 *min* point). To increase the model accuracy in terms of capturing the FFA kinetics during physical activity, the exercise model structure was modified by incorporating two extra compartments (y_{2FU} and y_{2FP}), as shown in Figure 4.10. All the parameter values of the model are provided in Table 4.1.

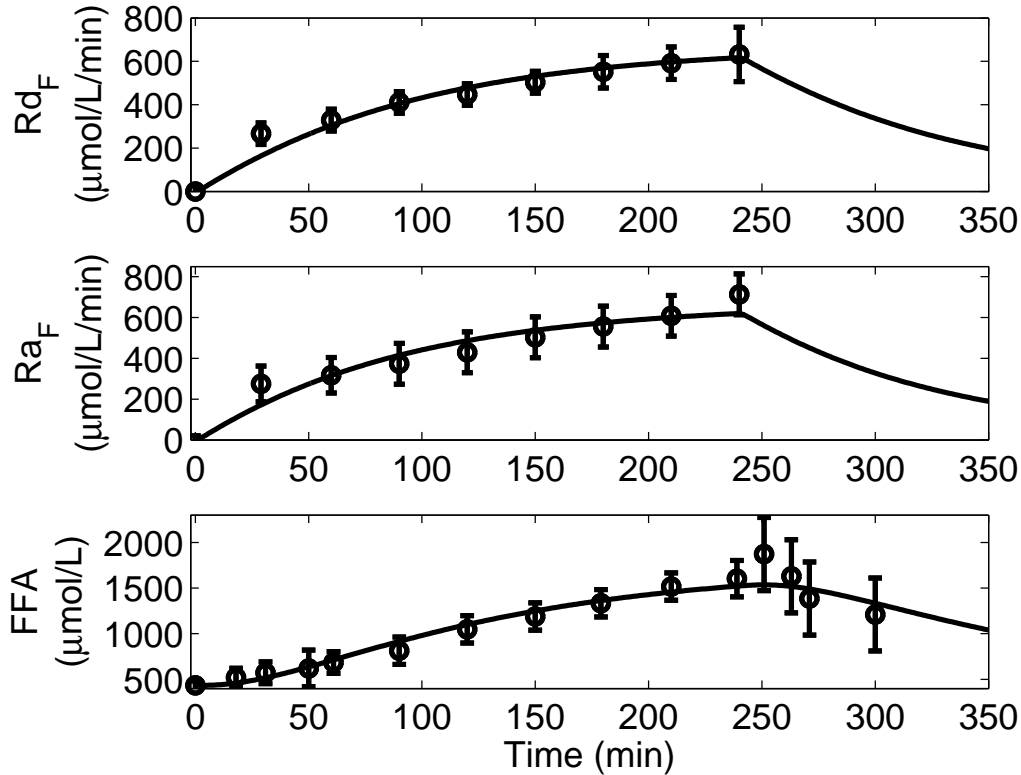


Figure 4.9: Plasma FFA kinetics in response to mild exercise ($PVO_2^{max} = 45\%$) lasting from $t_{ex} = 0$ to 240 *min*. The exercise model is comprised of two compartments, y_{1FU} and y_{1FP} , to capture the FFA kinetics during exercise. Model prediction (solid line) and published data ($\mu \pm \sigma$) (circle) [18] of plasma FFA uptake rate (Rd_F) (top); model prediction (solid line) and published data ($\mu \pm \sigma$) (circle) [18] of plasma FFA production rate (Ra_F) (middle); model prediction (solid line) and published data ($\mu \pm \sigma$) (circle) [18] of plasma FFA concentration (bottom)

————> **Transport/Clearance**

- - - -> **Interaction**

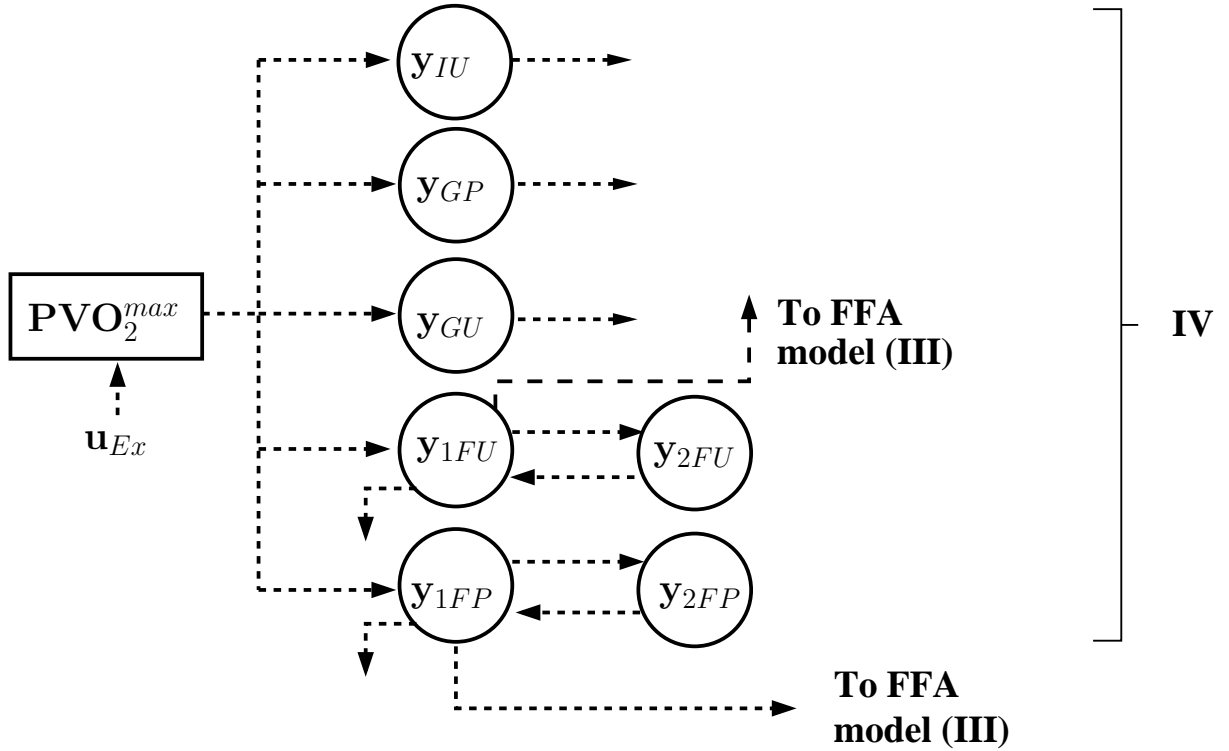


Figure 4.10: Schematic diagram of the exercise section (IV) of the composite model with modifications

Hence, the equations capturing FFA kinetics during exercise for the updated model can be written as follows:

$$\frac{dy_{1FU}(t)}{dt} = m_{FU1}PVO_2^{max}(t) - m_{FU2}y_{1FU}(t) - m_{FU3}(y_{1FU}(t) - y_{2FU}(t)) \quad (4.16)$$

$$\frac{dy_{2FU}(t)}{dt} = m_{FU3}(y_{1FU}(t) - y_{2FU}(t)) \quad (4.17)$$

$$\frac{dy_{1FP}(t)}{dt} = m_{FP1}PVO_2^{max}(t) - m_{FP2}y_{1FP}(t) - m_{FP3}(y_{1FP}(t) - y_{2FP}(t)) \quad (4.18)$$

$$\frac{dy_{2FP}(t)}{dt} = m_{FP3}(y_{1FP}(t) - y_{2FP}(t)) \quad (4.19)$$

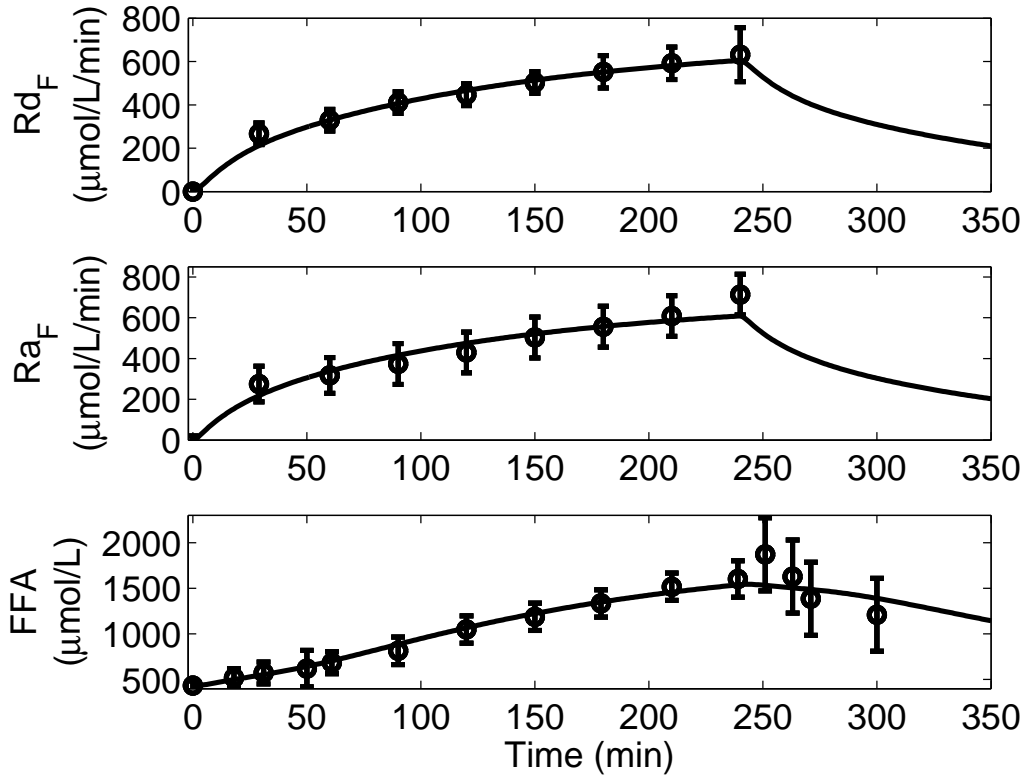


Figure 4.11: Plasma FFA kinetics in response to mild exercise ($PVO_2^{max} = 45\%$) lasting from $t_{ex} = 0$ to 240 *min*. The exercise model is comprised of four compartments, y_{1FU} , y_{2FU} , y_{1FP} and y_{2FP} , to capture the FFA kinetics during exercise. Model prediction (solid line) and published data ($\mu \pm \sigma$) (circle) [18] of plasma FFA uptake rate (Rd_F) (top); model prediction (solid line) and published data ($\mu \pm \sigma$) (circle) [18] of plasma FFA production rate (Ra_F) (middle); model prediction (solid line) and published data ($\mu \pm \sigma$) (circle) [18] of plasma FFA concentration (bottom).

Due to the addition of two new compartments, two extra parameters were introduced (m_{FU3} and m_{FP3}). Once again, all the parameters ($m_{FU1-FU3}$ and $m_{FP1-FP3}$) capturing the exercise effects on FFA kinetics were estimated by using data from Klein *et al.* [18]. As it can be seen in Figure 4.11, the new structure of the exercise model provided a better fit of Rd_F

and Ra_F during exercise. The superiority of the modified structure is further suggested by calculating the AIC value (-34.35), which is far less than the previous exercise model structure. However, the proposed model was unable to capture the sudden burst in plasma FFA concentration at the commencement of the recovery period, as observed in the mean data (Figure 4.11: bottom). In order to capture such kind of plasma FFA dynamics at the end of the exercise period, additional equations are required. Incorporation of extra equations will increase the number of unknown parameters which are required to be estimated, thereby increasing the complexity of the model.

4.2.3 Glucose Dynamics

Glucose is taken up from the circulating pool by hepatic tissues for storage (primarily) and by the peripheral tissue for oxidation purposes. Glucose influences its own uptake in the hepatic and extra-hepatic tissue (known as glucose effectiveness [5]). Glucose uptake into the tissues is further facilitated by insulin (known as insulin sensitivity [5]). To maintain plasma glucose homeostasis, stored glucose in the liver is released back into the circulatory system via glycogenolysis. The rate of hepatic glucose production (HGP) is indirectly regulated by insulin [57]. Plasma insulin inhibits glucagon secretion from the pancreatic α -cells [163, 164], and the latter is a crucial hormone for maintaining HGP [165]. Furthermore, increased availability of FFA has an inhibitory effect on tissue glucose uptake [58, 59, 166, 167]. The dynamics of plasma glucose at rest along with the actions of insulin on glucose uptake and endogenous glucose production, plus the inhibitory effect of FFA on glucose uptake at the systemic level can be mathematically expressed as given below:

$$\frac{dG(t)}{dt} = (-p_{G1}G(t) - x_G(t)G(t)) f_{FG}(t) + EGP(t) + \frac{u_G(t)}{V_G} \quad (4.20)$$

$$\frac{dx_G(t)}{dt} = p_{G2}I(t) - p_{G3}x_G(t) \quad (4.21)$$

$$f_{FG}(t) = f_{FG0} \left(1 - k_{FG} \left(\frac{F_N^3(t)}{F_N^3(t) + s_{FGN}^3} \right) \right) \quad (4.22)$$

$$F_N(t) = \frac{F(t)}{F_B} \quad (4.23)$$

$$EGP(t) = EGP_0 \left(1 - k_{EGP} \left(\frac{x_{EGP_N}^3(t)}{x_{EGP_N}^3(t) + s_{EGP_N}^3} \right) \right) \quad (4.24)$$

$$\frac{dx_{EGP}(t)}{dt} = p_{GA}(I(t) - x_{EGP}(t)) \quad (4.25)$$

$$x_{EGP_N}(t) = \frac{x_{EGP}(t)}{x_{EGP_B}} \quad (4.26)$$

Here, equation (4.20) represents plasma glucose concentration, $G(t)$ ($\frac{mg}{dl}$). The first term in the parenthesis on the RHS of equation (4.20) represents the glucose uptake rate under its own influence. The bilinear term, $x_G(t)G(t)$, captures glucose uptake under the influence of insulin; $x_G(t)$ ($\frac{1}{min}$) represents the action of insulin on tissue glucose uptake. The dynamics of $x_G(t)$ are captured by equation (4.21). The multiplier function $f_{FG}(t)$ is a dimensionless variable that captures the inhibitory effect of FFA on glucose uptake rate (Rd_G). Variables x_{EGP_N} and F_N are the remote insulin and FFA concentrations normalized with respect to their basal levels, x_{EGP_B} and F_B , respectively. The rate of endogenous glucose production is represented by $EGP(t)$, which is a function of plasma insulin as shown in equation (4.24). EGP_0 ($\frac{mg}{dl \cdot min}$) is the rate of hepatic glucose production in the absence of insulin. The dynamical effect of insulin on $EGP(t)$ is captured by the unobserved remote insulin concentration, $x_{EGP}(t)$ ($\frac{\mu U}{ml}$).

To establish the correlation between HGP and insulin concentration, data was obtained from [19, 20]. In these studies, the rate of glucose production was estimated by measuring the arterial-venous glucose concentration difference across the liver along with the hepatic blood flow rate. Due to the nature of the EGP dynamics with respect to the normalized remote insulin concentration (x_{EGP_N}), a 3rd-order Hill function was selected for superior model accuracy, as indicated in equation (4.24). The value of EGP_0 and k_{EGP} were directly obtained from the literature [20]. Only the saturation constant s_{EGP_N} was estimated to fit the data, as shown in Figure 4.12.

Randle *et al.* were the first to introduce the glucose-FFA cycle [58, 59] to explain the interaction between CHO and fat metabolism. It was proposed that an increase in FFA availability will enhance fat oxidation, thus causing an increase in acetyl-CoA production, which will result in downregulating the rate-limiting CHO metabolizing enzymes. Due to

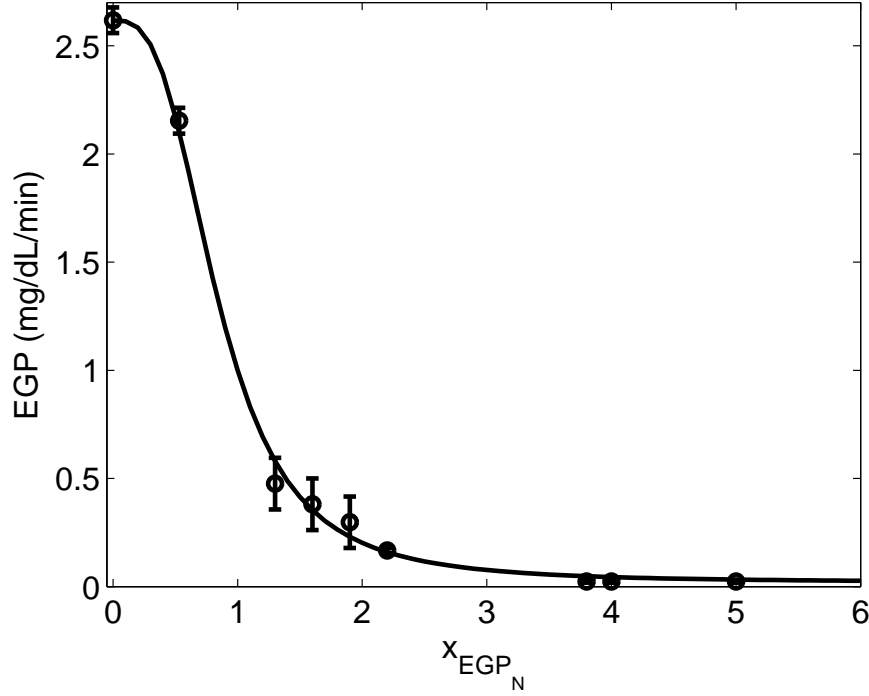


Figure 4.12: Model fit (solid line) versus published data ($\mu \pm \sigma$) (circle) [19, 20] of endogenous glucose production rate, EGP , as a function of normalized insulin concentration x_{EGP_N}

this phenomenon, tissue glucose uptake will decrease [168]. The correlation between glucose uptake rate, Rd_G , and plasma FFA was captured by utilizing data from [8, 21], where experiments were performed on healthy subjects by employing euglycemic-hyperinsulinemic clamps. The overall glucose uptake rate was measured at various plasma FFA levels (Figure 4.13). In Figure 4.13, the y-axis represents glucose uptake rate normalized with respect to its basal level (f_{FG}). The x-axis represents normalized plasma FFA concentration (F_N). The gain parameter, k_{FG} , from equation (4.22) was directly obtained from the data [8, 21]. Only the saturation constant, s_{FG_N} , was estimated to fit the data. Once again, due to the nature of the dynamics of f_{FG} with respect to the normalized FFA concentration, a 3rd-order Hill function was selected, as shown in equation (4.22). All the parameter values are given in Table 4.1.

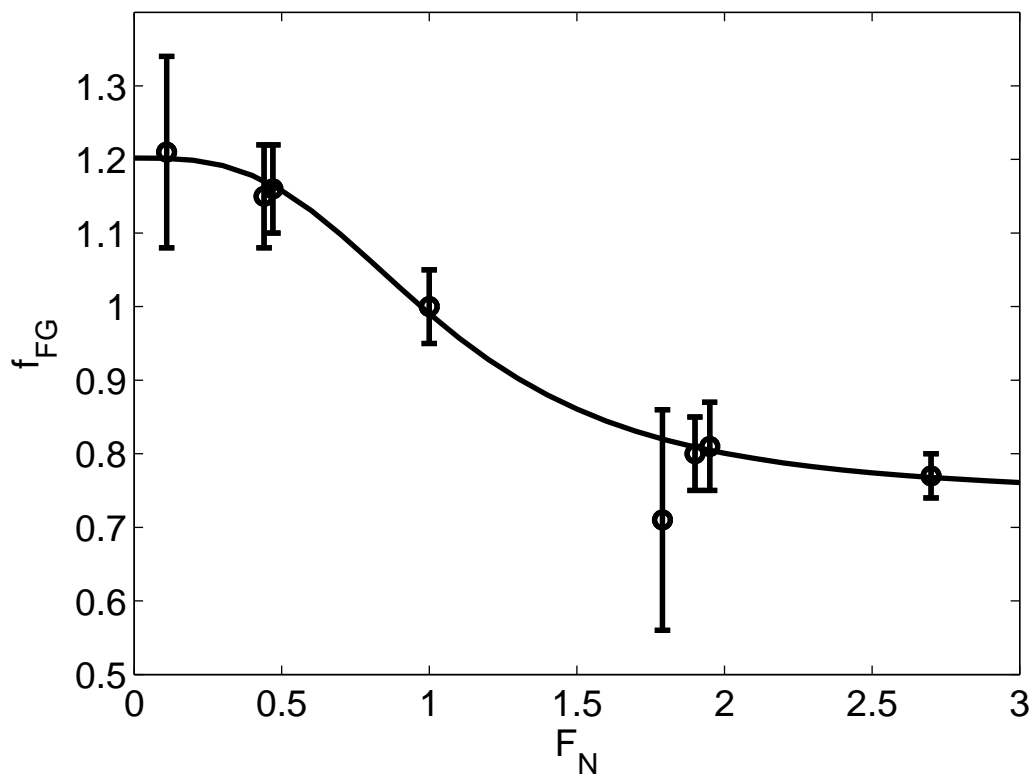


Figure 4.13: Model fit (solid line) versus published data ($\mu \pm \sigma$) (circle) [8, 21] of normalized glucose uptake rate, f_{FG} , as a function of normalized FFA concentration F_N

At basal steady state conditions (*i.e.*, $F(t) = F_B$), the value of f_{FG} becomes equal to 1. Hence, equations (4.20) and (4.21) reduce to:

$$p_{G1} = \frac{EGP_B}{G_B} - x_{G_B} \quad (4.27)$$

$$x_{G_B} = \frac{p_{G2}}{p_{G3}} I_B \quad (4.28)$$

Here, EGP_B , G_B , and I_B are the endogenous glucose production rate, plasma glucose concentration, and plasma insulin concentration at the basal level, respectively.

Parameters p_{G2} and p_{G3} from equation (4.21), representing the insulin action on tissue glucose uptake, and parameter p_{G4} from equation (4.25), capturing the dynamical effect of insulin mediated-suppression on hepatic glucose production, were estimated by using data from Regittnig *et al.* [22]. In this study, a labeled-IVGTT was performed in T1DM patients. At time $t=0$ *min*, a bolus of glucose labeled with a stable isotope tracer, D-[6,6²H₂]glucose, (hot glucose) was administered intravenously. A bolus of insulin was also injected at $t=0$ *min*, followed by a continuous insulin infusion at constant rate to maintain the basal level (Figure 4.14). Blood samples were gathered at regular intervals to measure the concentrations of plasma insulin, tracer glucose, and total glucose (endogenous glucose plus the labeled exogenous glucose), as shown in Figure 4.14 and 4.15. Parameters estimated from the labeled-IVGTT data provide a significant advantage over the unlabeled-IVGTT [5]. Due to the presence of tracer, it is possible to monitor the dynamics of glucose disappearance only. Hence, labeled IVGTT data can separate the individual contributions of insulin on glucose production and utilization, which is impossible to achieve from unlabeled-IVGTT data. This technique was first introduced by Cobelli *et al.* [5] to minimize model errors and ambiguities that may arise when estimating parameters of the classical minimal model [1] from the unlabeled data only.

To estimate the parameters (p_{G2} , p_{G3} , and p_{G4}) from the labeled-IVGTT data [22], two glucose models were used simultaneously. The total glucose concentration was captured by using equations (4.20), (4.21), (4.24), (4.25), and (4.22); this forms the cold glucose model. On the other hand, the tracer glucose concentration was captured by a new ODE as shown below:

$$\frac{dG_h(t)}{dt} = (-p_{G1}G_h(t) - x_G(t)G_h(t)) f_{FG} \quad (4.29)$$

Here, $G_h(t)$ ($\frac{mg}{dl}$) represents concentration of the tracer glucose. Equation (4.29) along with equations (4.21) and (4.22) forms the hot glucose model. Simultaneous fitting of the total and tracer glucose data (as shown in Figure 4.15) by using the cold and hot glucose models, respectively, should provide better informed parameter estimates.

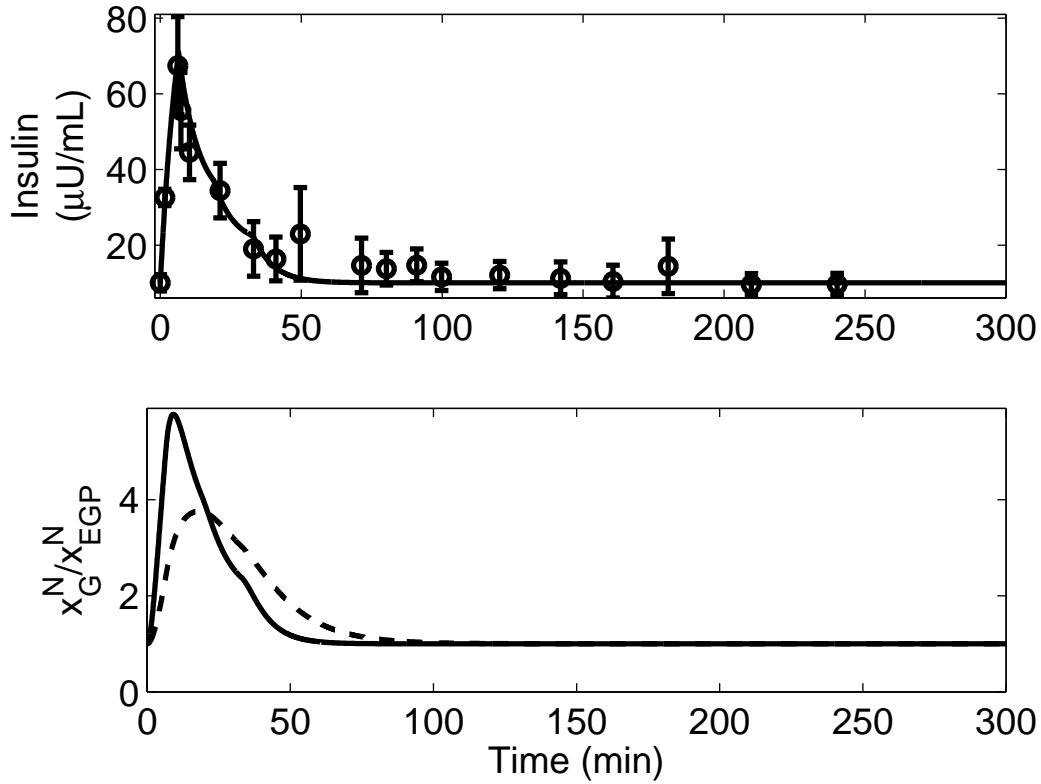


Figure 4.14: Model prediction (solid line) versus published data ($\mu \pm \sigma$) (circle) [22] of plasma insulin concentration in response to a labeled-IVGTT (top); normalized insulin action with respect to their basal values on glucose uptake (solid line) and endogenous glucose production (dashed line) due to administration of insulin bolus at $t=0 \text{ min}$ (bottom).

Exercise induces an elevation in glucose uptake rate, Rd_G ($\frac{mg}{dl \cdot min}$), by the working muscles. To maintain glucose homeostasis in the systemic level, glucose production rate (Ra_G , $\frac{mg}{dl \cdot min}$) is also elevated during exercise due to the accelerated rate of glycogenolysis. As mentioned earlier, an increased FFA oxidation results in downregulation of pyruvate dehydrogenase (PDH) [168]; this is an important enzyme for glucose oxidation. This regulatory mechanism, which is true at rest, is overridden by other factors during exercise [168]. Hence, studies have revealed no effect of elevated FFA on glucose uptake during exercise [168, 169]. In order to

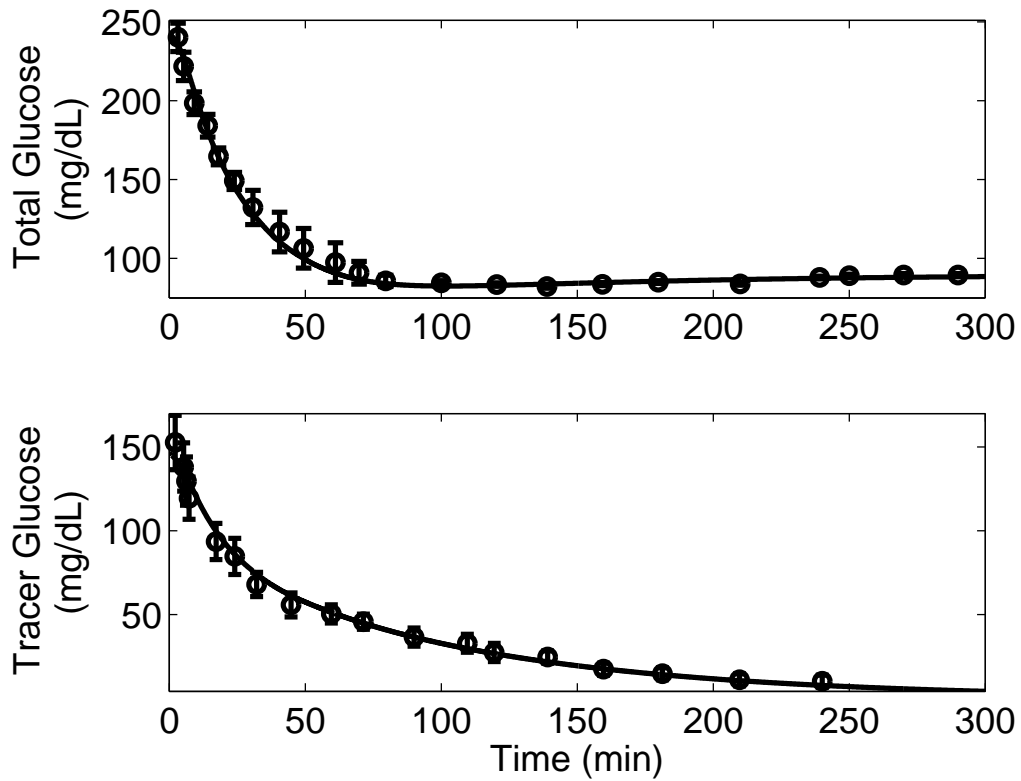


Figure 4.15: Model prediction (solid line) versus published data ($\mu \pm \sigma$) (circle) [22] of total glucose concentration (endogenous and exogenous labeled-glucose) in response to a labeled-IVGTT (top); model prediction (solid line) versus published data ($\mu \pm \sigma$) (circle) [22] of tracer glucose concentration in response to a labeled-IVGTT (bottom)

incorporate all these important physiological effects of mild-to-moderate short-term exercise on glucose dynamics, equations (4.20) and (4.23) were modified as follows:

$$\begin{aligned} \frac{dG(t)}{dt} = & (-p_{G1}G(t) - x_G(t)G(t)) f_{FG}(t) - \frac{W}{V_G}y_{GU}(t) + EGP(t) + \frac{W}{V_G}y_{GP}(t) \\ & + \frac{u_G(t)}{V_G} \end{aligned} \quad (4.30)$$

$$F_N(t) = \frac{1}{F_B} ((1 - b)F(t) + bF_0) \quad (4.31)$$

The dynamics of the new terms $y_{GU}(t)$, $y_{GP}(t)$, and b , can be written as:

$$\frac{y_{GU}(t)}{dt} = m_{GU1}PVO_2^{max}(t) - m_{GU2}y_{GU}(t) \quad (4.32)$$

$$\frac{y_{GP}(t)}{dt} = m_{GP1}PVO_2^{max}(t) - m_{GP2}y_{GP}(t) \quad (4.33)$$

$$b = \frac{PVO_2^{max}(t)}{PVO_2^{max}(t) + s_{PV}} \quad (4.34)$$

Here, the variables $y_{GU}(t)$ and $y_{GP}(t)$ ($\frac{mg}{kg \cdot min}$) represent the exercise-induced glucose uptake and production rates. F_0 represents the FFA concentration at initial (or basal) conditions ($F_0 = F(0)$). At rest, b becomes equal to zero, as $PVO_2^{max} = 0$. Hence, equation (4.31) reduces to equation (4.23). However, during exercise ($PVO_2^{max} \gg 1$) b approaches 1, as s_{PV} is assigned a value of 1. Therefore, equation (4.31) becomes $F_N(t) = F_0/F_B$ at $PVO_2^{max}(t) \gg 1$. As the normalized FFA concentration is fixed at its initial condition during physical activity, f_{FG} remains unperturbed at its initial condition. As a result of this, the increasing concentration of plasma FFA during exercise has no effect on glucose uptake rate. The motivation behind selecting $s_{PV} = 1$ is that at $PVO_2^{max} = 40\%$ almost 97% of $F_N(t)$ is contributed by the second part of the RHS of equation 4.31 (*i.e.*, $\frac{F_0}{F_B}$), which concur with the experiment performed by Odland *et al.* [168] where elevated FFA had no significant effect on glucose uptake rate at the same level of exercise.

In order to capture the exercise-induced changes in glucose kinetics, data was procured from Wolfe *et al.* [12], where healthy subjects performed exercise at $PVO_2^{max} = 40\%$ for 60 *min.* Blood samples were obtained at regular intervals to measure glucose uptake rate and

hepatic glucose production rate during and after exercise, as shown in Figure 4.16. From equation (4.30), plasma glucose uptake (Rd_G) and production (Ra_G) rate can be written as:

$$Rd_G = - \left[(-p_{G1}G(t) - x_G(t)G(t)) f_{FG}(t) - \frac{W}{V_G} y_{GU}(t) \right] \quad (4.35)$$

$$Ra_G = EGP(t) + \frac{W}{V_G} y_{GP}(t) \quad (4.36)$$

In order to obtain the model prediction of glucose uptake rate during exercise, parameters m_{GU1} and m_{GU2} were estimated, as shown in Figure 4.16 (top). To capture the glucose production rate during exercise, parameters m_{GP1} and m_{GP2} were adjusted, as shown in Figure 4.16 (middle). With the onset of exercise, both Rd_G and Ra_G were elevated. As the production matched utilization, the overall plasma glucose homeostasis was maintained (Figure 4.16: bottom).

During prolonged exercise, the rate of hepatic glycogenolysis diminishes due to the limited supply of liver glycogen stores [15]. As a result of this, the net endogenous glucose production rate also decreases. As glucose production can no longer match the uptake rate, plasma glucose concentration declines and reaches hypoglycemic levels during prolonged exercise [13, 15]. In order to capture the glucose dynamics during prolonged exercise, equation (4.30) can be re-written as follows:

$$\begin{aligned} \frac{dG(t)}{dt} = & (-p_{G1}G(t) - x_G(t)G(t)) f_{FG}(t) - \frac{W}{V_G} y_{GU}(t) + EGP(t) \\ & + \frac{W}{V_G} (y_{GP}(t) - y_{Gly}(t)) + \frac{u_G(t)}{V_G} \end{aligned} \quad (4.37)$$

The new variable $y_{Gly}(t)$ ($\frac{mg}{kg \cdot min}$) represents the dynamics associated with the rate of glycogenolysis due to depletion of the available hepatic glycogen stores. It captures the same physiological effects of prolonged exercise on plasma glucose level as the variable $G_{gly}(t)$ (equation 3.10) used in the exercise minimal model in Section 3.2.

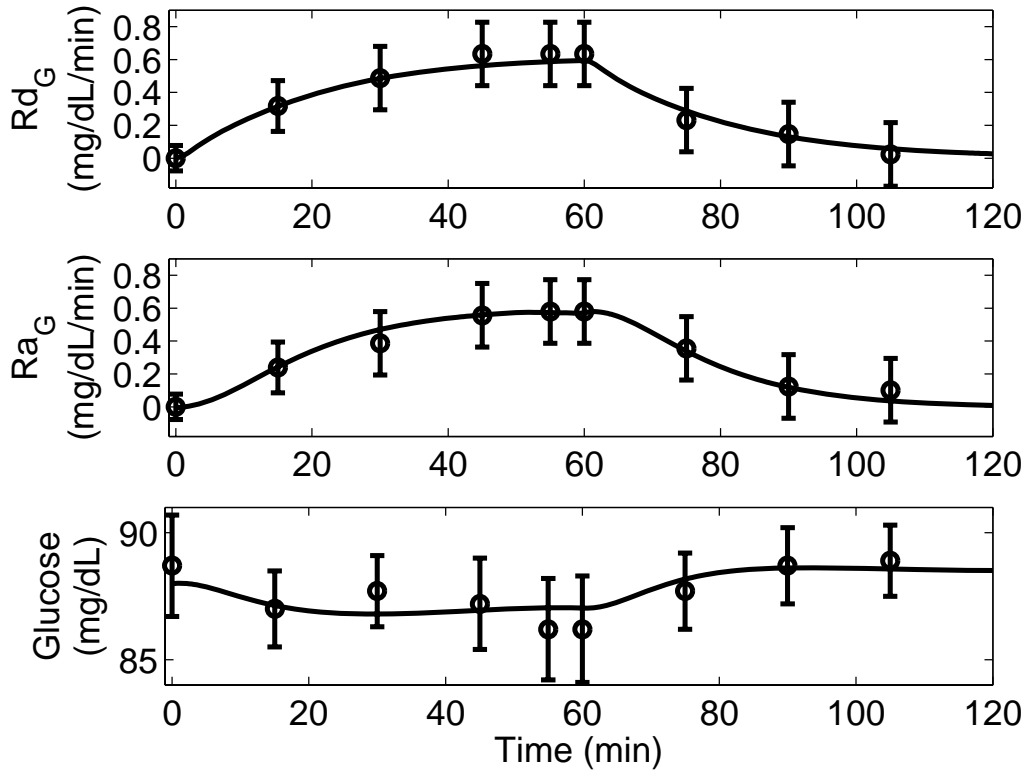


Figure 4.16: Model prediction (solid line) versus published data ($\mu \pm \sigma$) (circle) [12] in response to mild exercise performed at $PVO_2^{max} = 40\%$ intensity lasting from $t_{Ex} = 0$ to 60 min. Top: glucose uptake rate (in deviation form) during exercise (Rd_G); Middle: glucose production rate (in deviation form) during exercise (Ra_G); Bottom: plasma glucose concentration during short-term exercise ($G(t)$).

Hence, the dynamics of glycogenolysis during prolonged exercise can be mathematically expressed as follows, adapted from equation (3.10):

$$\frac{dy_{Gly}(t)}{dt} = \begin{cases} 0 & A(t) < A_{TH} \\ k & A(t) \geq A_{TH} \\ -\frac{y_{Gly}(t)}{T_1} & u_{Ex}(t) = 0 \end{cases} \quad (4.38)$$

Here, $A(t)$ is the integrated exercise intensity ($u_{Ex}(t)$) having the same mathematical expression as equation (3.11) in Section 3.2. A_{TH} is the critical threshold value of energy expenditure which is a function of exercise intensity and duration, same as equation (3.9) (Section 3.2). After the commencement of exercise, as long as A is less than A_{TH} , the rate of glycogenolysis (y_{Gly}) remains unaffected due to the presence of sufficient hepatic glycogen stores. However, y_{Gly} starts to decline at a rate k , once A exceeds the threshold value (A_{TH}). At the end of exercise, *i.e.*, the recovery period, liver glycogen stores are replenished back to its basal level. The time required for y_{Gly} to return back to its basal level after exercise is represented by the pseudo-time constants T_1 and T_2 (equation (3.11) from Section 3.2).

In order to estimate the parameter values of k and T_1 , data was obtained from an experiment performed by Ahlborg *et al.* [15], where healthy subjects performed moderate level exercise ($PVO_2^{max} = 60\%$) lasting for 210 *min*. Blood samples were taken at regular intervals during and immediately after exercise to measure blood glucose concentration, as shown in Figure 4.17 (bottom). With the onset of exercise, both Rd_G and Ra_G are elevated above their basal levels, as shown in Figure 4.17 (top) and (middle) panels, respectively. As the duration of exercise exceeded a certain threshold, the rate of glycogenolysis started to decrease from its original value. As a result of this, Ra_G started to decline until the end of exercise, causing plasma glucose to reach hypoglycemic levels (Figure 4.17: bottom).

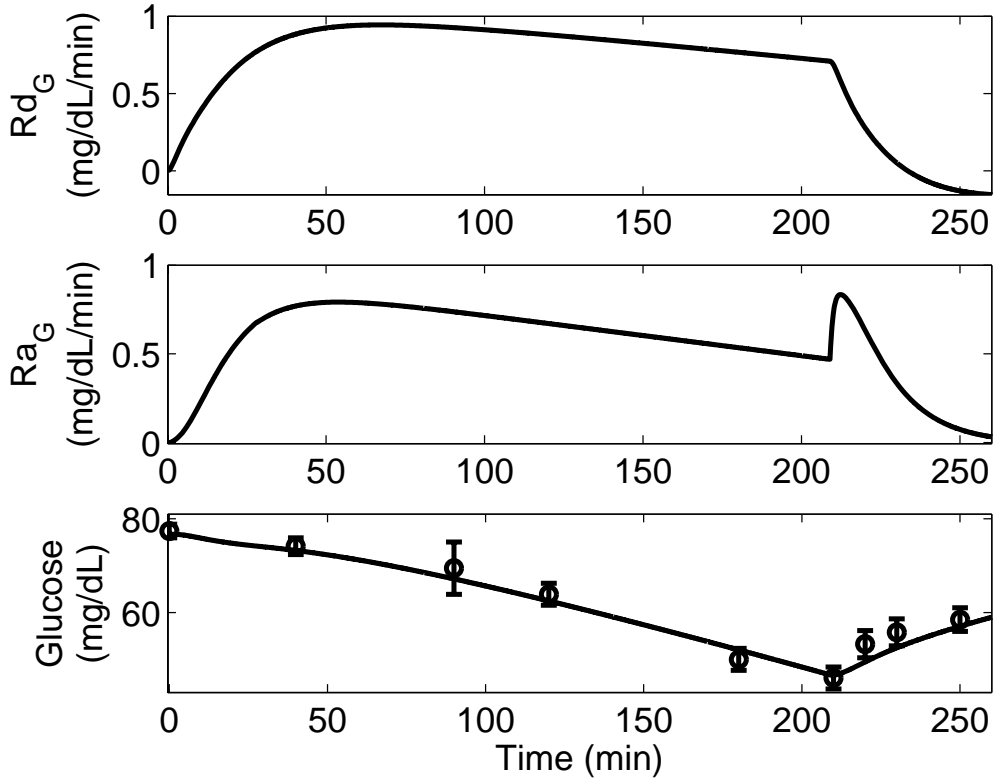


Figure 4.17: Model prediction (solid line) versus published data [15] ($\mu \pm \sigma$) (circle) in response to moderate exercise performed at $PVO_2^{max} = 60\%$ intensity lasting from $t_{Ex} = 0$ to 210 *min*. Top: glucose uptake rate in deviation variables during exercise (Rd_G); Middle: glucose production rate in deviation variables during exercise (Ra_G); Bottom: plasma glucose concentration during prolonged exercise (G).

4.3 PARAMETRIC SENSITIVITY ANALYSIS BY FINITE DIFFERENCE METHOD

The composite model can be expressed as a set of N_x differential equations with N_x states (x) and M parameters (θ). The N_x by M parameter sensitivity matrix can be calculated by using the finite difference approximation method, in which the sensitivity coefficients ($s_{i,j}$)

Table 4.1: Parameter values of the composite model.

Nos.	Parameters	Values	Source	Nos.	Parameters	Values	Source
1	k_{EFP}	0.92889	[16]	20	$p_{G3} \left(\frac{1}{min}\right)$	0.35	–
2	s_{EFP_N}	1.169	[16]	21	$p_{G4} \left(\frac{1}{min}\right)$	0.073535	–
3	$EFP_0 \left(\frac{\mu mol}{L \cdot min}\right)$	209.09	[16]	22	$m_{IU1} \left(\frac{1}{min^2}\right)$	0.0028176	–
4	k_{EGP}	0.9909	[20, 19]	23	$m_{IU2} \left(\frac{1}{min}\right)$	1.7354	–
5	s_{EGP_N}	0.84115	[20, 19]	24	$m_{FU1} \left(\frac{mmol}{kg \cdot min^2}\right)$	0.013736	–
6	$EGP_0 \left(\frac{mg}{dL \cdot min}\right)$	2.618	[20, 19]	25	$m_{FU2} \left(\frac{1}{min}\right)$	0.032272	–
7	s_{FG}	1.0472	[8, 21]	26	$m_{FU3} \left(\frac{1}{min}\right)$	0.0023229	–
8	f_{FG_0}	1.202	[21]	27	$m_{FP1} \left(\frac{mmol}{kg \cdot min^2}\right)$	0.016831	–
9	k_{FG}	0.38075	[8, 21]	28	$m_{FP2} \left(\frac{1}{min}\right)$	0.018241	–
10	$n \left(\frac{1}{min}\right)$	0.38075	[1]	29	$m_{FP3} \left(\frac{1}{min}\right)$	0.024841	–
11	$V_I (mL)$	10.133	[1]	30	$m_{GU1} \left(\frac{mg}{kg \cdot min^2}\right)$	0.0021874	–
12	$p_{F1} \left(\frac{1}{min}\right)$	0.18727	–	31	$m_{GU2} \left(\frac{1}{min}\right)$	0.058974	–
13	$W (kg)$	70.0	[18]	32	$m_{GP1} \left(\frac{mg}{kg \cdot min^2}\right)$	0.0009152	–
14	$V_F (L)$	3.0	[18]	33	$m_{GP2} \left(\frac{1}{min}\right)$	1.3073	–
15	$V_G (dL)$	117.0	[1]	34	$T_1 (min)$	1	–
16	$p_{F2} \left(\frac{1}{min}\right)$	0.036513	–	35	$k \left(\frac{1}{min}\right)$	0.0038	–
17	$p_{F3} \left(\frac{1}{min}\right)$	0.03909	–	36	s_{PV}	1	–
18	$p_{G1} \left(\frac{1}{min}\right)$	0.0076	–	37	$T_2 (min)$	10	–
19	$p_{G2} \left(\frac{mL}{\mu U \cdot min^2}\right)$	0.00010259	–	38	$m_{PV} \left(\frac{1}{min}\right)$	0.8	[63]

are calculated from the difference of nominal and perturbed solutions [170, 171].

$$s_{i,j}(t) = \frac{\partial x_i(t)}{\partial \theta_j} = \frac{x_i(\theta_j + \Delta\theta_j, t) - x_i(\theta_j, t)}{\Delta\theta_j} \quad (4.39)$$

Here, $i \in [1, N_x]$ and $j \in [1, M]$. To facilitate direct comparison of responses across different parameters, a normalized sensitivity coefficient ($\bar{s}_{i,j}$) is calculated [170]:

$$\bar{s}_{i,j}(t) = \frac{\partial x_i(t)}{\partial \theta_j} \cdot \frac{\theta_j}{x_i} \quad (4.40)$$

For the evaluation of dynamic sensitivity, a L^2 -norm operation is performed to calculate the relative sensitivity (RS) along the time axis. RS can be mathematically expressed as:

$$RS_{i,j} = \frac{1}{N_P} \sqrt{\sum_{k=1}^{N_P} |\bar{s}_{i,j}(k)|^2} \quad (4.41)$$

Here, k is the point in time when a sample is collected and N_P is the total number of sample points observed.

By using this method, a parametric relative sensitivity matrix ($RS_{i,j}$) of the composite model was generated. The matrix was comprised of 16 rows ($i \in [1 \text{ to } 16]$), representing the states, and 38 columns ($j \in [1 \text{ to } 38]$), representing all the parameters of the model. A graphical representation of the $RS_{i,j}$ values is provided in Figure 4.18. The y-axis lists the parameters by number; this mapping is provided in Table 4.1. The x-axis lists the states of the model as per Table 4.2, and the z-axis represents the parametric relative sensitivity values corresponding to each state. A higher $RS_{i,j}$ value indicates the state is more sensitive to the specified parameter.

By closely observing the insulin state ($I(t)$), $RS_{1,1:38}$, reveals that the plasma insulin is highly sensitive to its own parameters, n and V_I , which is expected (Figure 4.19: top). The FFA state ($F(t)$), $RS_{2,1:38}$, indicates that plasma FFA is most sensitive to parameter p_{F1} followed by parameter EFP_0 (Figure 4.19: middle). Plasma FFA also exhibits significant sensitivity towards the parameters associated with $I(t)$. The parameters associated with FFA production during exercise (m_{FP1} , m_{FP2} , and m_{FP3}) are relatively more sensitive than the parameters associated with FFA uptake during exercise (m_{FU1} , m_{FU2} , and m_{FU3}). For the glucose state ($G(t)$), $RS_{3,1:38}$, the most sensitive parameters are the ones associated with $I(t)$, as shown in Figure 4.19 (bottom). Parameters associated with the endogenous glucose production rate (k_{EGP} , s_{EGP} , and EGP_0) are more sensitive than the parameter p_{G1} , which captures the effect of glucose on its own uptake rate. Parameters representing insulin action on glucose uptake by the tissues (p_{G2} and p_{G3}) are more sensitive than the parameter representing the insulin action on suppression of endogenous glucose production rate (p_{G4}). Also, the parameters representing glucose uptake during exercise (m_{GU1} and

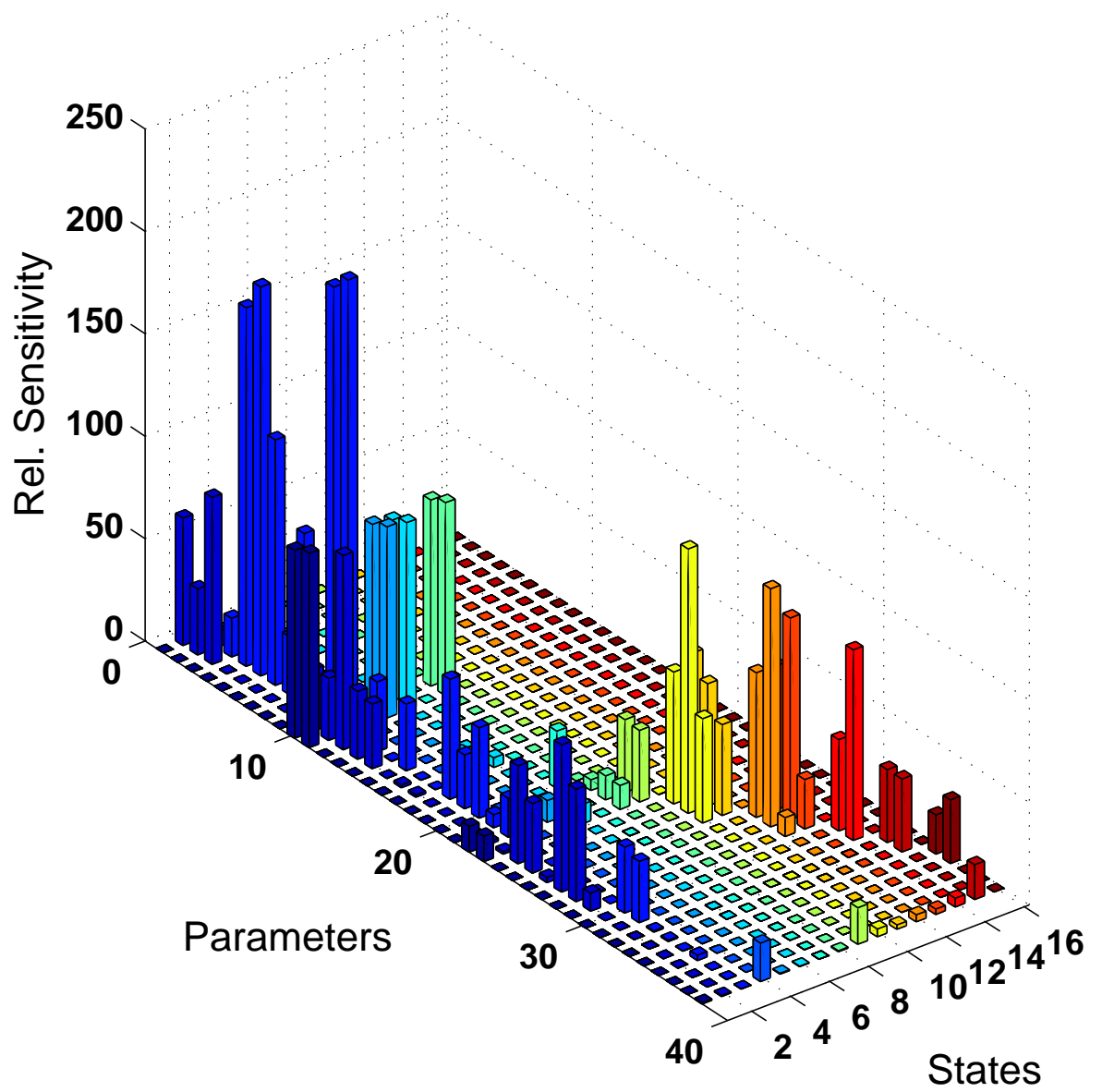


Figure 4.18: Parametric relative sensitivity analysis of the composite model for all the sixteen states.

Table 4.2: List of states of the composite model used in the parametric sensitivity analysis

Nos.	Equations	Nos.	Equations
1	(4.1)	9	(4.3)
2	(4.13)	10	(4.16)
3	(4.37)	11	(4.17)
4	(4.2)	12	(4.18)
5	(4.6)	13	(4.19)
6	(4.11)	14	(4.32)
7	(4.21)	15	(4.33)
8	(4.25)	16	(4.38)

m_{GU2}) are significantly more sensitive than the parameters representing glucose production during exercise (m_{GP1} and m_{GP2}).

Lots of important informations can be extracted from the parametric sensitivity analysis. For example, endogenous glucose production plays a major role in maintaining glucose homeostasis. Hence, more experiments are required to accurately define the correlation between $EGP(t)$ and $I(t)$. Moreover, the $RS_{i,j}$ matrix indicates that the suppression of insulin plays a bigger role in elevating endogenous glucose production rate during physical activity than the exercise-mediated glucose production. However in case of FFA, the exercise-mediated fat production was more prominent than the elevated lipolysis due to insulin suppression during exercise. Experimental studies could be performed to verify the extent of hypoglycemia that might be reached during short-term exercise by clamping the plasma insulin at basal level.

4.4 VALIDATION OF THE LOWER-ORDER COMPOSITE MODEL

Once the model was formulated and the parameters were estimated from the literature data, simulation studies were performed to validate the various components of the model. Model predictions were compared with new data sets (*i.e.*, data different from the ones used for

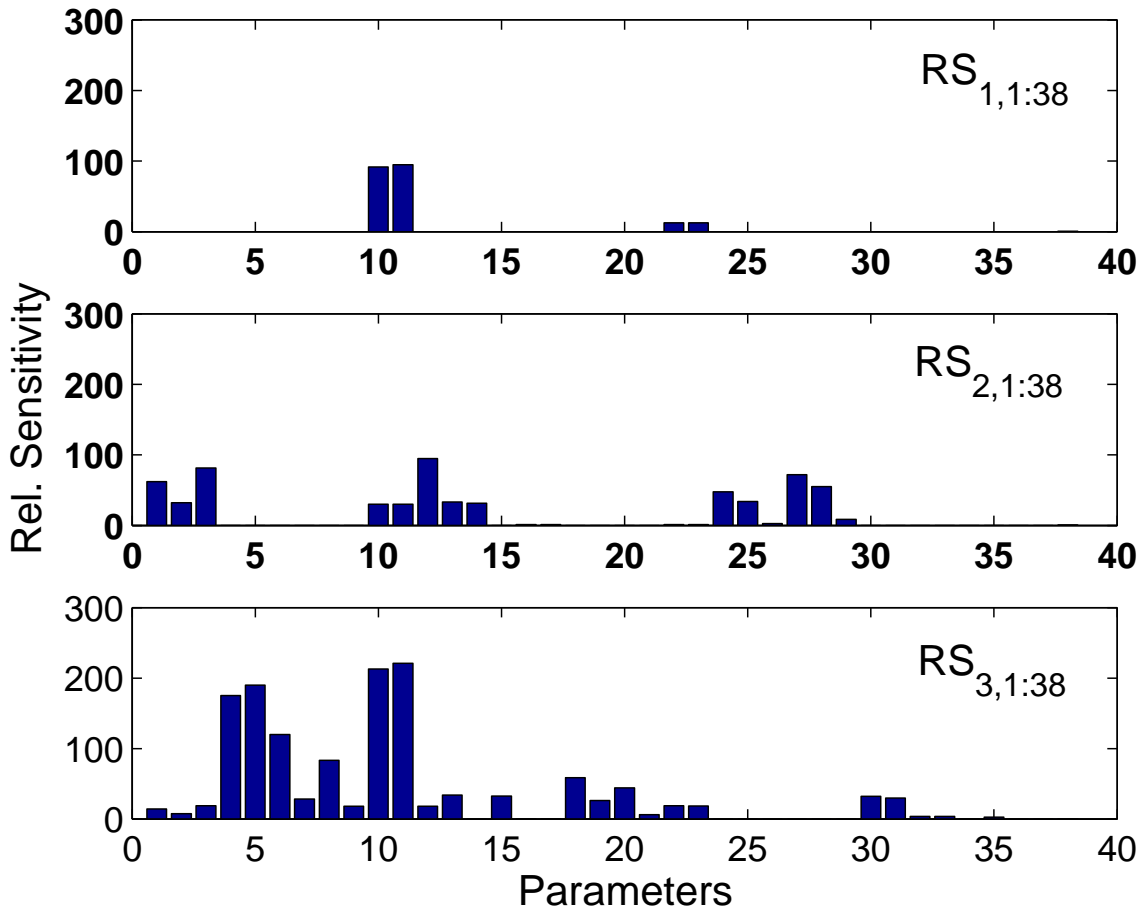


Figure 4.19: Parametric relative sensitivity analysis of the composite model for the plasma insulin, $I(t)$ (top), FFA, $F(t)$ (middle), and glucose, $G(t)$ (bottom) states.

parameter estimation), without manipulating the estimated parameter values. As described in Section 2.3, R^2 was used to quantitate the goodness of fit.

4.4.1 Effect of Exercise on Plasma Insulin Concentration

For validation of the insulin model, a simulation test was performed at a mild level of exercise, $PVO_2^{max} = 30\%$, lasting for 120 min. With the onset of exercise, plasma insulin

level declined due to the accelerated insulin clearance rate. During the recovery period, plasma insulin concentration climbed back to its basal level. Model validation along with experimental data of healthy individuals subjected to same exercise protocol [13] is shown in Figure 4.20. The model prediction emulates the data well. Although, at the 40 *min* mark the model slightly underpredicts the data.

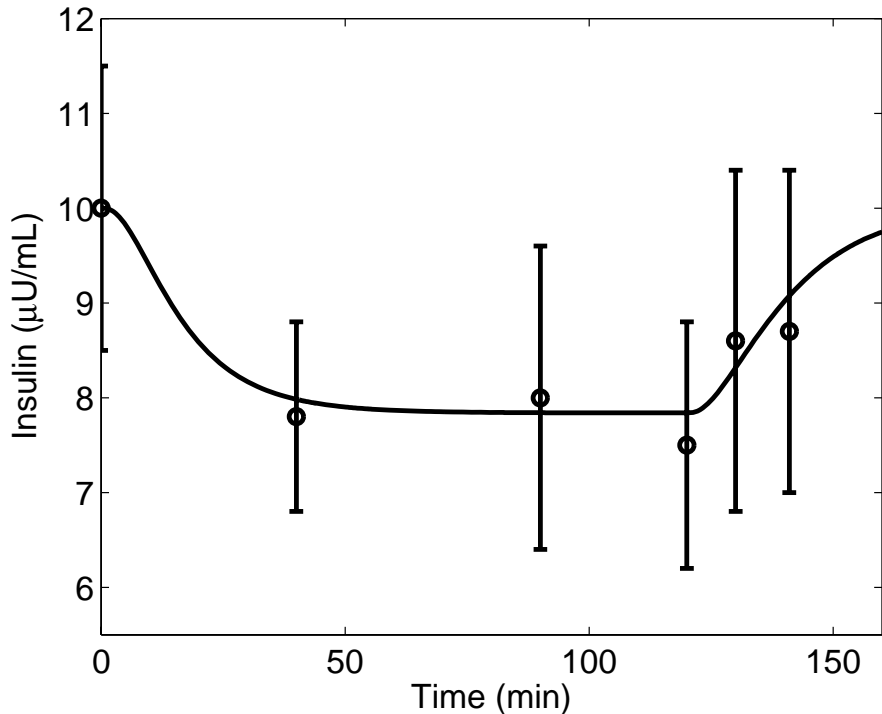


Figure 4.20: Plasma insulin concentration in response to mild exercise ($PVO_2^{max} = 30$) lasting from $t_{ex} = 0$ to 120 *min*. Model simulation validation (solid line) and published data [13] (circles) ($\mu \pm \sigma$) of plasma insulin [$R^2 = 0.936$].

4.4.2 Effect of Insulin on Plasma FFA Dynamics

In order to validate the insulin effects on FFA dynamics, a MI-FSIGT simulation test was performed, where boluses of insulin were infused at time $t = 0$ and 20 *min* at a rate similar to the experiment performed by Brehm *et al.* [23] (Figure 4.21: top). Due to the anti-lipolytic

action of insulin, plasma FFA declined well below its basal level (Figure 4.21: bottom). The model predictions, as shown in Figure 4.21, are within one standard deviation of the data. After the two hour mark, however, the model seems to slightly underpredict the plasma FFA data.

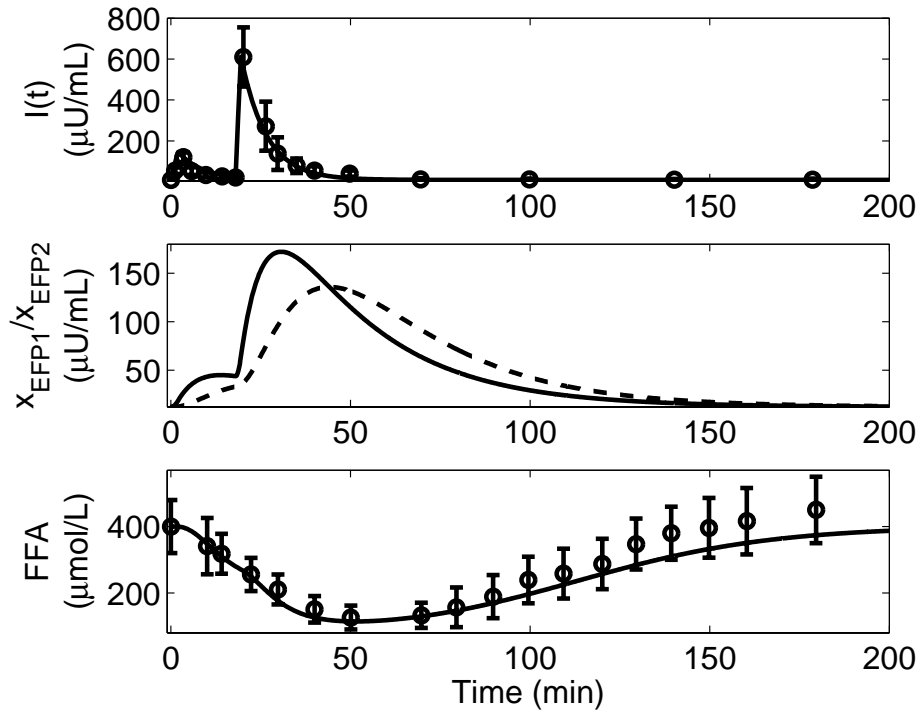


Figure 4.21: Plasma FFA concentration in response to MI-FSIGT test where boluses of insulin were administered at time $t = 0$ and 20 min . Model simulation validation (solid line) and published data [23] (circles) ($\mu \pm \sigma$) of plasma insulin concentration [$R^2 = 0.999$] (top); model predictions of remote insulin x_{EFP1} (solid line) and x_{EFP2} (dashed line) concentrations (middle); model simulation validation (solid line) and published data [23] (circles) ($\mu \pm \sigma$) of plasma FFA concentration [$R^2 = 0.998$] (bottom).

4.4.3 Effect of Exercise on Plasma FFA Dynamics

For validation of the exercise effects on plasma FFA, a simulation study of a mild level of exercise, $PVO_2^{max} = 30\%$, was performed for 2 hours. With the onset of exercise, plasma

FFA utilization (Rd_F) and production (Ra_F) rate continuously increased until the end of physical activity. As the lipolytic rate was more than the uptake rate, FFA concentration increased steadily until the end of exercise. During the recovery period, FFA level remained elevated for about 20-30 *min* before it started to gradually decline toward its basal level. A comparison of the model prediction and experimental data from subjects undergoing the same exercise protocol [13] is provided in Figure 4.22. The model performed well during the exercise period, however, the model predictions during the recovery period were slower than the data.

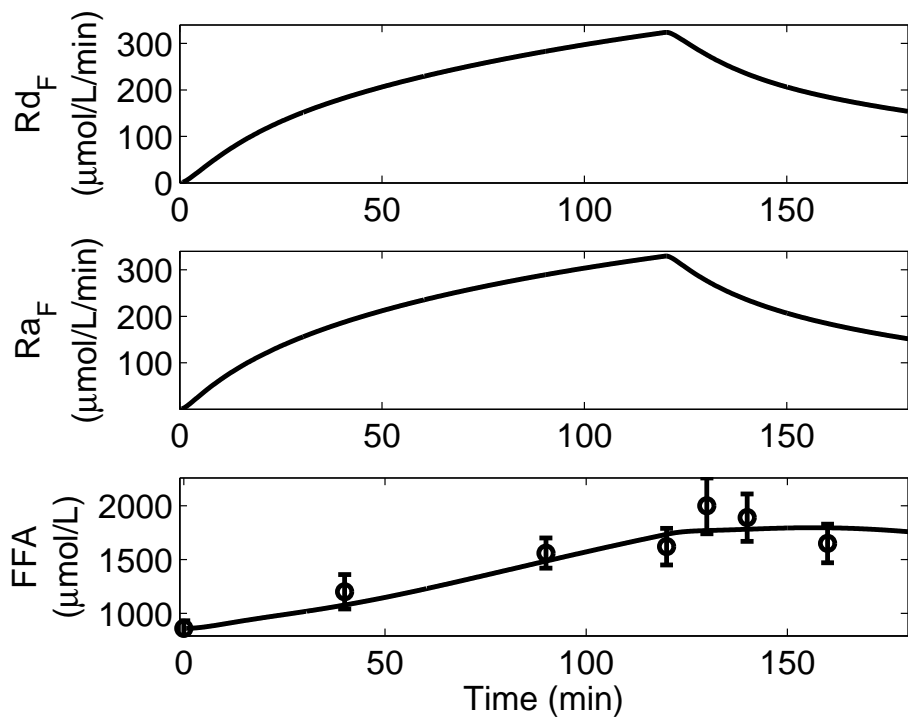


Figure 4.22: Plasma FFA concentration in response to mild exercise ($PVO_2^{max} = 30$) lasting from $t_{ex} = 0$ to 120 *min*. Model prediction of plasma FFA uptake rate, Rd_F (top); model prediction (solid line) of plasma FFA production rate, Ra_F (middle); model simulation validation and published data [13] (circles) ($\mu \pm \sigma$) of plasma FFA concentration [$R^2 = 0.989$] (bottom).

4.4.4 Effect of Insulin on Plasma Glucose Dynamics

For the glucose model validation, a labeled MI-FSIGT simulation test was performed, where boluses of insulin were administered at time $t = 0$ and 20 min (Figure 4.23) and a bolus of labeled glucose was infused at $t = 0 \text{ min}$, at a rate similar to the experiment performed by Nagasaka *et al.* [24]. Model predictions of the total glucose concentration (*i.e.*, endogenous glucose plus the labeled exogenous glucose) and tracer glucose concentrations obtained from the cold (equation (4.20)) and hot glucose model (equation (4.29)), respectively, along with the data [24] are provided in Figure 4.24. The model predicted glucose kinetics after the first insulin bolus seems to be marginally slower than the data. However, the model performed quite well in emulating the data after the second insulin bolus.

4.4.5 Effect of Exercise on Glucose Dynamics

In order to validate the short-term exercise effects on glucose kinetics, a simulation test was performed at moderate level exercise, $PVO_2^{max} = 50\%$, for 45 min . With the onset of exercise, both Rd_G and Ra_G were elevated. As production matched uptake, the overall plasma glucose concentration remained within the normoglycemic range. The model predictions alongside experimental data of T1DM patients [14] are plotted in Figure (4.25). The model predicted glucose kinetics are well within one standard deviation of the data. Validation of the composite model using T1DM patient data increased the confidence in the model.

To validate the glucose model during prolonged exercise, a separate simulation study of mild exercise was performed at $PVO_2^{max} = 30\%$ which lasted for 120 min . As the integrated exercise intensity exceeded the threshold value, hepatic glycogen stores started to deplete; this caused a net reduction in glucose production. Due to this imbalance between production and utilization, plasma glucose concentration started to decline at the later stages of exercise. A comparison between the model predictions and data obtained from a study performed by Ahlborg *et al.* on healthy subjects using the same exercise protocol are provided in Figure 4.26. Once again, the model predictions are well within one standard deviation of the data.

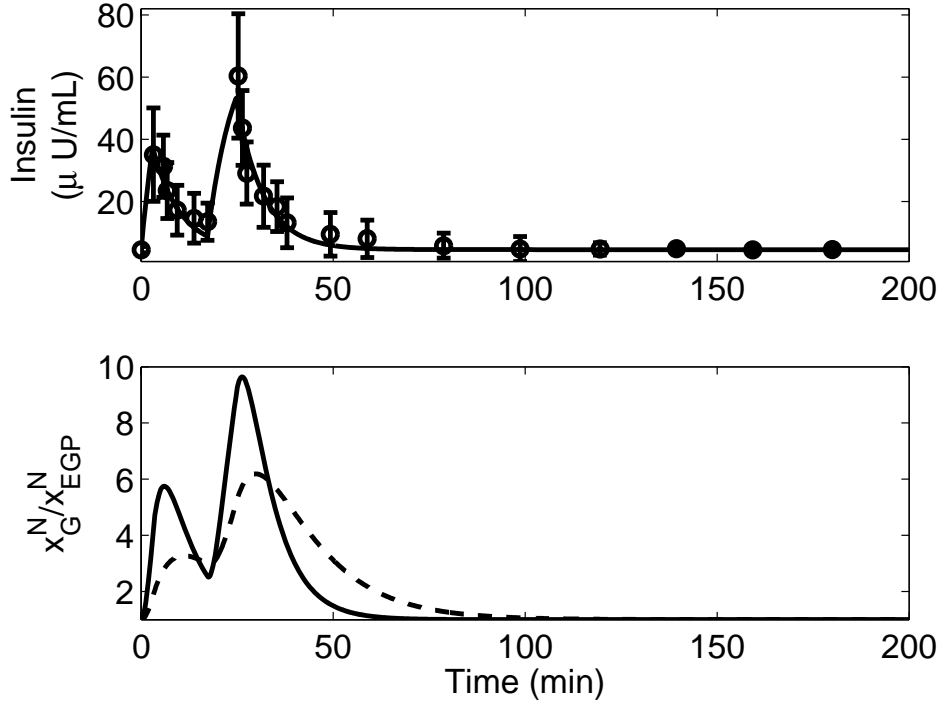


Figure 4.23: Plasma insulin concentration in response to labeled-MI-FSIGT test where insulin boluses were administered at times $t = 0$ and 20 min . Model simulation validation (solid line) and published data [24] (circles) ($\mu \pm \sigma$) of plasma insulin concentration [$R^2 = 0.997$] (top); model predictions of normalized insulin action, x_G^N , (solid line) and x_{EGP}^N (dashed line) with respect to their basal values (bottom).

4.4.6 Effect of FFA on Glucose Uptake Rate at Rest

At rest, an increasing FFA concentration suppresses plasma glucose uptake rate. This inhibitory effect of FFA on Rd_G is captured by the dimensionless multiplicative function, f_{FG} (equation (4.22)). In order to validate this physiological interaction between FFA and glucose, a simulation study was performed where euglycemic-hyperinsulinemic clamps were employed. Insulin was elevated up to $62 \frac{\mu\text{U}}{\text{ml}}$ to match the data obtained from an experimental study performed by Thiebaud *et al.* [8]. Intralipids were infused at either:)i) a low rate

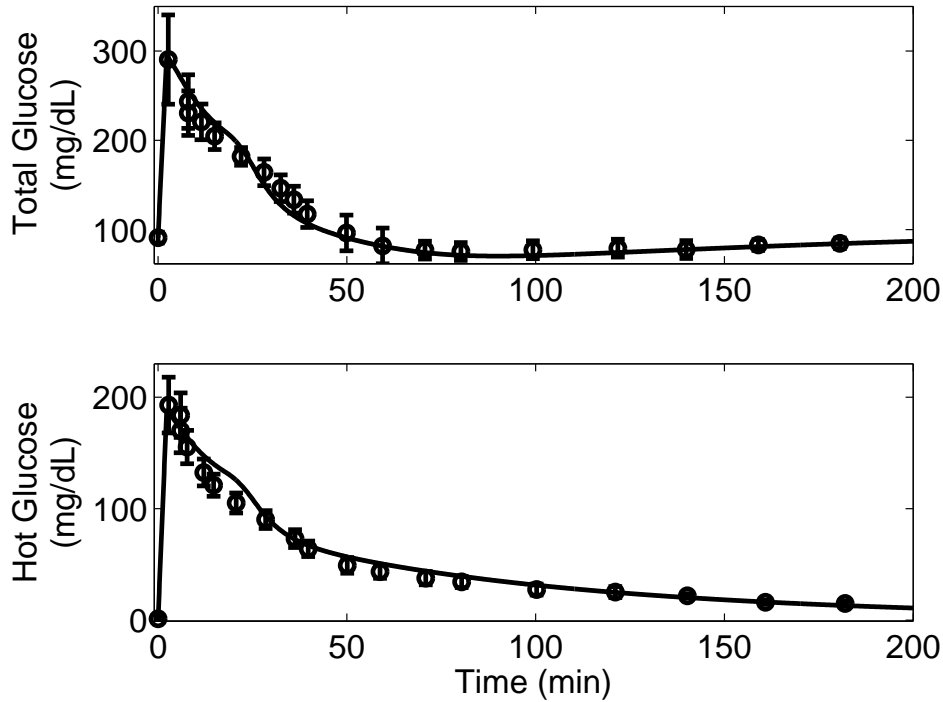


Figure 4.24: Plasma glucose concentration in response to labeled-MI-FSIGT test where a labeled-glucose bolus was infused at time $t = 0 \text{ min}$. Model simulation validation (solid line) and published data [24] (circles) ($\mu \pm \sigma$) of plasma total glucose concentration [$R^2 = 0.999$] (top); model simulation validation (solid line) and published data [24] (circles) ($\mu \pm \sigma$) of labeled-glucose concentration [$R^2 = 0.99$] (bottom).

to maintain basal levels of $340 \frac{\mu\text{mol}}{l}$ FFA, or (ii) a high rate elevating FFA levels to $650 \frac{\mu\text{mol}}{l}$. These FFA model predictions are shown by the dashed and dotted lines in Figure 4.27 (top). In absence of intralipid infusion (control study), FFA declined freely without any restrictions, as shown by the solid line in Figure 4.27 (top). Due to the elevated plasma FFA levels, glucose uptake rate was suppressed as shown by the dashed and dotted lines in Figure 4.27 (bottom). The model predictions are well within one standard deviation of the experimental data [8], thus indicating the capability of the model to accurately predict the glucose-FFA cycle.

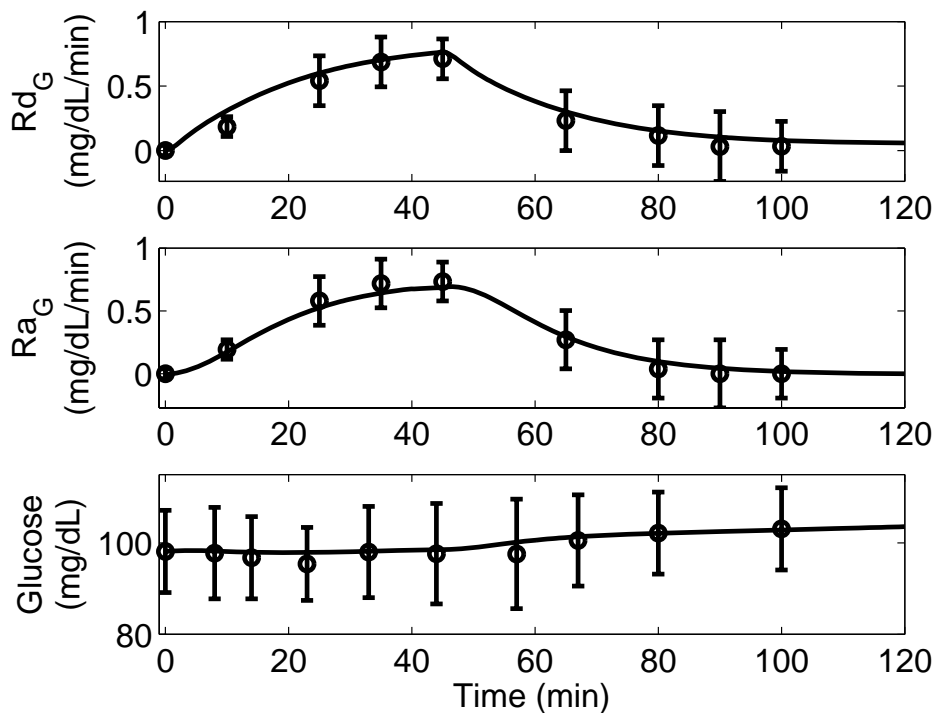


Figure 4.25: Model simulation validation (solid line) versus published data [15] ($\mu \pm \sigma$) (circles) in response to moderate exercise performed at $PVO_2^{max} = 50\%$ intensity lasting from $t_{Ex} = 0$ to 45 min. Glucose uptake rate (in deviation form) during exercise (Rd_G) [$R^2 = 0.935$] (top); glucose production rate (in deviation form) during exercise (Ra_G) [$R^2 = 0.955$] (middle); plasma glucose concentration during short-term exercise ($G(t)$) [$R^2 = 0.82$] (bottom).

4.5 SUMMARY

In this chapter, a 16-state metabolic model of insulin, glucose, and FFA was developed. The primary goal was to characterize the dynamics of the major energy-providing substrates and insulin at rest, as well as during exercise. The model successfully captured the physiological effects of FFA and mild-to-moderate exercise on plasma glucose concentration. This novel approach of incorporating both FFA and exercise effects in the glucose-insulin metabolic

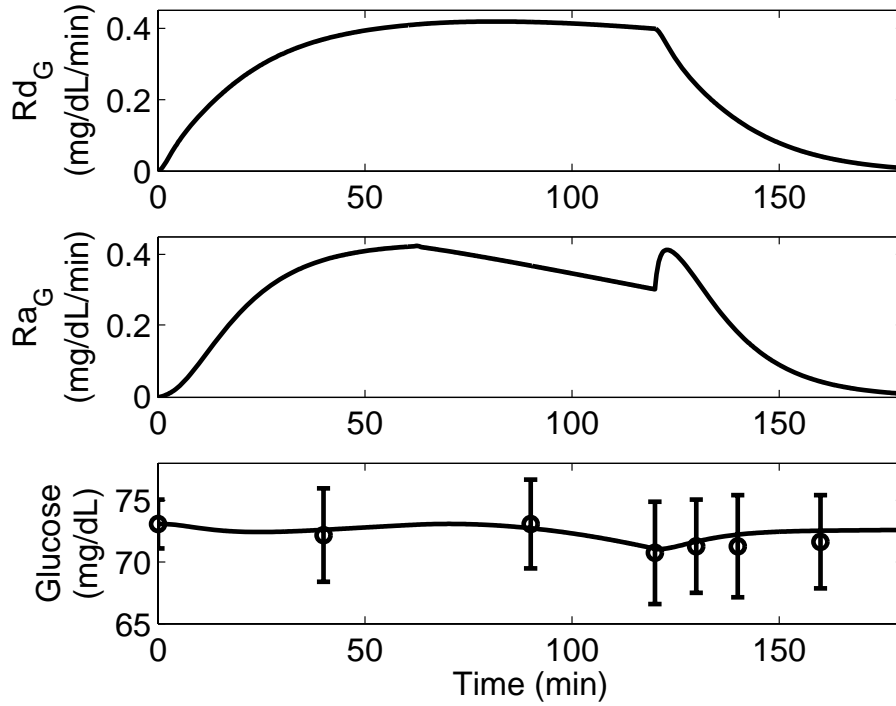


Figure 4.26: Model simulation validation (solid line) versus published data [13] ($\mu \pm \sigma$) (circle) in response to mild arm exercise performed at $PVO_2^{max} = 30\%$ intensity lasting from $t_{Ex} = 0$ to 120 min. Glucose uptake rate in deviation variables during exercise (Rd_G) (top); glucose production rate in deviation variables during exercise (Ra_G) (middle); plasma glucose concentration during prolonged exercise (G) [$R^2 = 0.861$] (bottom).

model provides the diabetes research community with an excellent tool to investigate the fluctuations in glucose dynamics after consumption of mixed meal or performing exercise.

The model consisted of four parts capturing the insulin, glucose, FFA, and exercise dynamics. The plasma insulin action on FFA and glucose was divided into three sections. The dynamical effect of insulin on lipolysis was captured by the two first-order filters (x_{EFP1} and x_{EFP2}) in series. The model successfully emulated the plasma FFA dynamics during a MI-FSIGT test and during hyperinsulinemic clamp studies. The insulin effects on glucose were divided into two parts. The first part captured the gluco-regulatory action of insulin

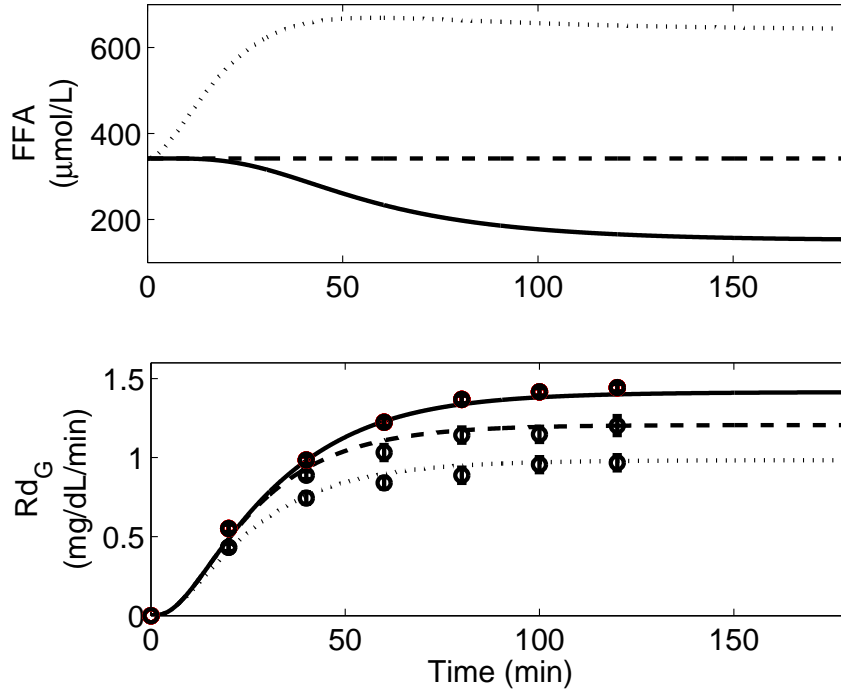


Figure 4.27: Plasma FFA concentration due to infusion of intralipids at high rate (dotted line), low rate (dashed line), and saline (no intralipid infusion) (solid line) (top); published data [8, 21] ($\mu \pm \sigma$) (circle) versus model simulation validations of plasma glucose uptake rate at high (dotted line) [$R^2 = 0.923$] and low (dashed line) [$R^2 = 0.901$] intralipid infusion rates, as well as no intralipid infusion (solid line) [$R^2 = 0.944$] (bottom).

in promoting glucose uptake into the tissues via the filter x_G . The second part captured the insulin-mediated suppression of endogenous glucose production by considering the saturating function $EGP(t)$, along with the filter x_{EGP} . Parameters of the filter equations were estimated by using a labeled-IVGTT. This technique of using hot and cold IVGTT data facilitates separation of the insulin action on glucose utilization and production [75, 5], thus providing more confidence in the estimated parameters.

The exercise effects on insulin, glucose, and FFA were divided into five sections. The exercise-induced clearance of insulin was captured by the first-order filter, y_{IU} . For the

glucose dynamics, the elevated rates of glucose production and utilization during exercise were captured by y_{GP} and y_{GU} , respectively. During short-term mild-to-moderate exercise, plasma glucose typically remains within the normoglycemic range as glucose production matches the utilization rate. However, as the integrated exercise intensity exceeded a certain threshold, the rate of glycogenolysis is expected to decline due to the depletion of available hepatic glycogen stores. As a result of this, the net glucose production rate will also decrease. This phenomenon was captured by incorporating the y_{Gly} variable. In order to capture the exercise effects on FFA kinetics, four compartments were used as shown in Figure 4.10. A set of two compartments represented the exercise-induced FFA uptake rate (y_{1FU} and y_{2FU}), and the remaining two compartments captured the elevated rate of FFA production during exercise (y_{1FP} and y_{2FP}).

The model also successfully captured the inhibitory effects of FFA on glucose uptake rate at rest. This phenomenon is also known as the glucose-FFA cycle, which was first introduced by Randle *et al.* [58, 59] in the early 1960's.

This more complete metabolic model has the potential to provide an excellent platform for the control community in development of model-based closed-loop insulin delivery systems for T1DM patients. The primary advantage of utilizing the composite model in the development of an artificial pancreas instead of other metabolic models present in the literature, is because of its unique ability to predict plasma glucose concentration in response to disturbances from mixed meals (CHO and fat) consumption and from exercise. The model can also accurately predict the interactions taking place between the major energy-providing metabolites and hormones during rest and exercise.

5.0 A PHYSIOLOGICALLY-BASED FFA, GLUCOSE, AND INSULIN MODEL

In the earlier chapters, semi-empirical metabolic models were developed to capture the effects of FFA and exercise on glucose-insulin dynamics. In Chapter 2, the extended minimal model was synthesized by modifying the classical minimal model [1] to incorporate plasma FFA dynamics and the interactions of FFA with glucose and insulin. The model consisted of lumped compartments and parameters capturing the systemic physiological interactions between FFA, glucose, and insulin. Only the necessary metabolic processes of FFA were considered in order to maintain the simplifying approach of the minimal model. Due to the minimum number of equations, a lesser number of parameters needed to be estimated, which generally makes simplified models easily identifiable, as well as less time intensive to build. However, these models do not differentiate the distribution of metabolic substrates at the various organ/tissue levels. Typically, in such models the entire body is treated as a single well-mixed space. Hence, the semi-empirical model fails to provide a detailed explanation of the biology that is actually taking place in the body, particularly at the organ/tissue scale.

In contrast, physiologically-based models are much more complex in terms of number of equations and parameters. These models provide a great deal of insight into the system as they are derived from known physiology. Typically in such models, the body is divided into compartments representing the major organs and tissues. Biologically relevant organ-specific metabolism can be captured, thereby making the model more structurally accurate. Physiologically-based models can also provide motivation to perform new experiments in order to validate certain model components, thereby incorporating biological understanding of tissue metabolic processes. However, such detailed models come at a price. Usually,

these models are very time intensive to develop, and often a large number of parameters are required to be estimated from limited available data sets.

Tiran *et al.* were the first to attempt to develop a physiologically-based glucose-insulin model in the mid 1970s [76, 106]. Compartments representing the major glucose utilizing organs/tissues were used. Glucose and insulin were distributed into each of these compartments via the circulatory system. Constant glucose uptake or production rates were incorporated in each of the physiological compartments. Later, a pharmacokinetic-pharmacodynamic model of metabolism was developed by Sorensen [2] in the mid 1980s, which was based on an earlier model by Guyton *et al.* [107]. The model was comprised of two sub-units capturing the glucose and insulin concentrations just like the Guyton model; in addition it also included the glucagon dynamics and its interactions with the glucose-insulin system. In the glucose and insulin sub-units, distribution of the energy-providing substrate and the gluco-regulatory hormone were modeled at the organ/tissue levels, respectively. The glucagon sub-unit consisted of a single well-mixed compartment representing the glucagon concentration at the systemic level. Metabolic rates causing addition or removal of glucose were assigned to each of the compartments. Hyperbolic tangent functions were used to represent the sigmoidal nonlinearities observed in the experimental data between the metabolic sinks/sources and the regulatory hormones.

Later in the 1990s, Cobelli *et al.* [78] developed another semi-physiological glucose-insulin model. The model consisted of several components representing physiologically-based glucose and insulin interactions; however, glucose distribution at the organ level was not considered. Most of the detailed metabolic models present in the literature do not consider FFA dynamics. As mentioned earlier, FFA plays a vital role in providing energy to the tissues. Also fluctuations in FFA dynamics alter glucose dynamics to a significant level. Hence, in this chapter a physiologically-based FFA model was developed and was coupled with the existing glucose-insulin model developed by Sorensen [2], which has a similar structure. The objective is to predict FFA distribution at the organ/tissue levels and to capture the interactions between glucose, insulin, and FFA through out the body.

In Section 5.1, the glucose-insulin model developed by Sorensen [2] is presented in detail. The physiologically-based FFA model is presented in Section 5.2. The original Sorensen

model was modified in order to integrate the FFA model, as indicated in Section 5.3. Metabolic sinks and sources of the FFA model are presented in Section 5.4. In Section 5.5, the interconnection points between the FFA and the glucose model are discussed in details. Finally, the simulation results of the physiologically-based model are presented in Section 5.6.

5.1 GLUCOSE-INSULIN PHYSIOLOGICAL MODEL OF SORENSEN

The model is comprised of three sub-systems: glucose, insulin, and glucagon. Eleven ODEs are used to define the glucose sub-system, seven define the insulin sub-system, and one models the glucagon dynamics. The glucose model consisted of several compartments representing the vital glucose-utilizing organs/tissues: brain, heart/lungs, kidney, liver, gut, and periphery, as shown in Figure 5.1. The peripheral compartment represents skeletal muscle, as well as adipose tissue (AT). The heart/lungs, kidney, liver, and gut compartments consist of a single well-mixed space where the substrate concentrations are assumed to be homogeneous, as shown in Figure 5.2. Each compartment is fed by the arterial blood influx and drained by the venous blood efflux. In some organs and tissues (mainly the brain and periphery) the capillary wall permeability is sufficiently low, thereby causing a slow equilibration of substrates between the capillary and the interstitial spaces. Hence, compartments representing such organs/tissues included two well-mixed spaces (capillary and interstitial space) where the substrate concentrations are assumed to be homogeneous (see Figure 5.3). Once again, substrates enter the capillary space via the arterial route and is drained by the venous route. The substrates diffuse through the capillary wall into the interstitial space from where they are ultimately consumed by the cells. Metabolic sinks, representing the rate of glucose consumption due to oxidation or storage, were added to each of these compartments. In the liver glucose flux is bi-directional, as it consumes glucose mostly for storage purposes in the form of glycogen, as well as releases the stored glucose in the circulatory system whenever the body requires energy. Hence, both metabolic sink and source were incorporated in the liver compartment. The insulin model had a similar structure

like the glucose model. Only difference is that, the brain had a single compartment unlike the glucose model, as studies have shown that the capillary wall of the brain is impermeable to insulin passage to the interstitial fluid space [172]. Metabolic sinks representing insulin clearance were added to the liver, kidney, and periphery compartments. Glucagon was modeled using a single ODE capturing the systemic glucagon concentration.

Mass balances were performed across each physiologic compartment to capture the solute distribution. Typically, where the capillary wall resistance is negligible thus allowing a rapid equilibration of the solute (X) between the capillary and the interstitial fluid spaces, only one mass balance equation is sufficient to capture the dynamics, as given below:

$$V_J^X \frac{dC_J(t)}{dt} = Q_J^X (C_{Ji}(t) - C_J(t)) - R_{JU} \quad (5.1)$$

As indicated in the left hand side (LHS) of the above equation (5.1), the rate of mass accumulation in the homogeneously mixed single compartment is equal to the product of organ/tissue volume, V_J^X (l^3), and the rate of change of solute concentration. $C_{Ji}(t)$ (mass/ l^3) is the arterial blood solute concentration and $C_J(t)$ (mass/ l^3) is the solute concentration in the organ/tissue and the outlet port, *i.e.*, the vein. Finally, R_{JU} (mass/time) is the rate of solute uptake by the cells (metabolic sink). Subscript J represents the compartment. The first term in the right hand side (RHS) of equation (5.1) represents convection and the second term represents metabolic sink/source.

In some cases where the capillary wall resistance is significantly high (Figure 5.3), two mass balance equations can be written to capture the solute concentrations in the capillary and interstitial space as shown below:

$$V_{JV}^X \frac{dC_{PV}(t)}{dt} = Q_J^X (C_{Ji}(t) - C_{JV}(t)) - \frac{V_{PI}^X}{T_J^X} (C_{JV}(t) - C_{JI}(t)) \quad (5.2)$$

$$V_{JI}^X \frac{dC_{PI}(t)}{dt} = \frac{V_{PI}^X}{T_J^X} (C_{JV}(t) - C_{JI}(t)) - R_{JU} \quad (5.3)$$

Here, V_{JV}^X (l^3) is the capillary blood volume and V_{JI}^X (l^3) is the interstitial fluid volume. The volumetric blood flow rate is given by Q_J^X (l^3 /time). $C_{JV}(t)$ (mass/ l^3) is the venous

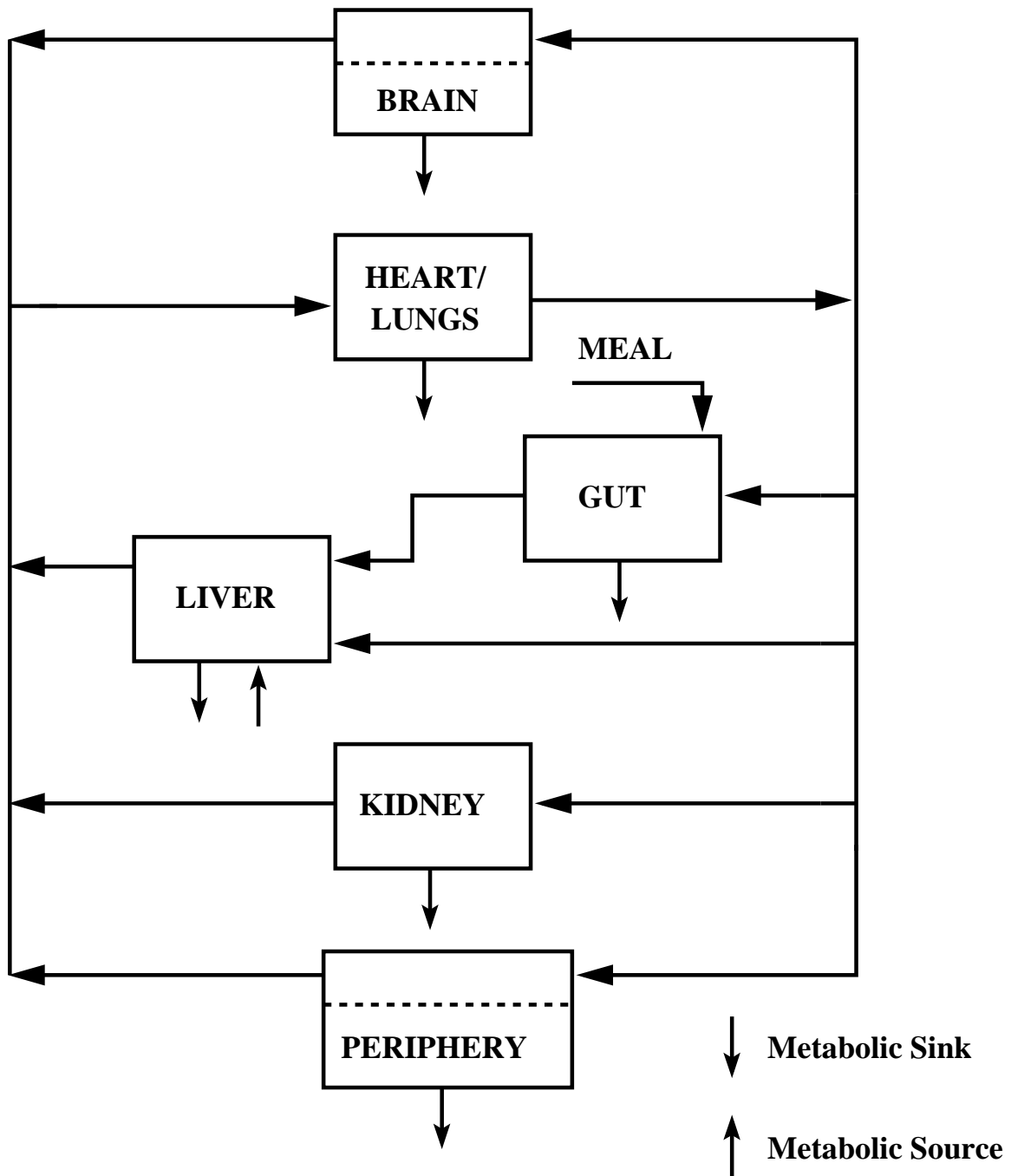


Figure 5.1: Physiologically-based metabolic model for glucose, adapted from [2]

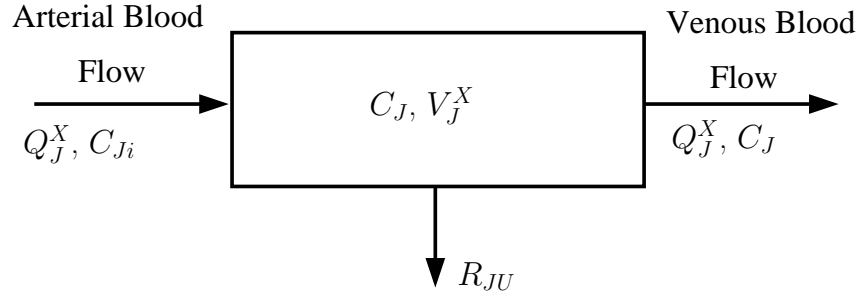


Figure 5.2: Schematic representation of a physiologic compartment with no capillary wall resistance

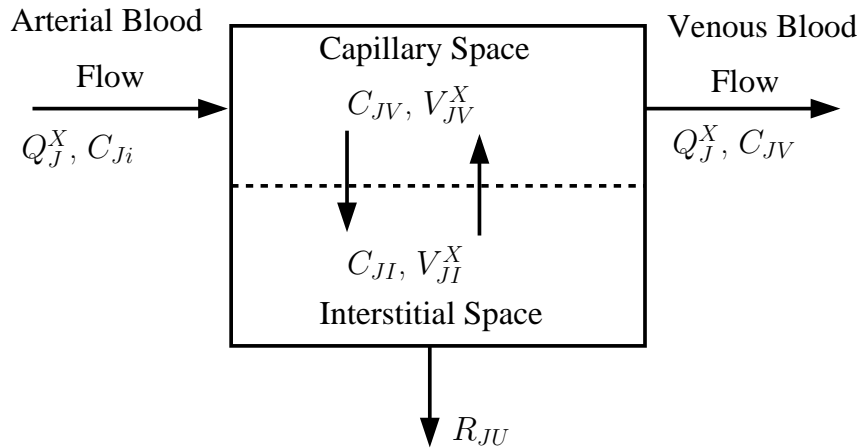


Figure 5.3: Schematic representation of a typical physiologic compartment with capillary and interstitial space

solute concentration, assumed in equilibrium with the capillary space solute concentration. The interstitial fluid solute concentration is given by $C_{JI}(t)$ (mass/ l^3). T_J^X (time) is the transcapillary diffusion time constant.

The rate of mass accumulation in the capillary space is equal to the product of the capillary blood volume and the rate of change of solute concentration in the capillary (equation 5.2). This rate of mass accumulation is the net additive result of contributions by

convection (first term on the RHS of equation (5.2)) and diffusion (second term on the RHS of equation (5.2)). A similar mass balance equation is written for the interstitial fluid space, as indicated by equation (5.3). In this case, the rate of mass accumulation is the result of contribution by diffusion (first term on the RHS of equation (5.3)) and any metabolic sink or source (second term on the RHS of equation (5.3)). Convection does not influence the interstitial fluid space.

By applying the above mathematical analysis, mass balance equations were generated for the glucose and insulin models at each physiologic compartments. Following are the physiologically-based model equations along with the nomenclature (Table 5.2) and parameter values (Table 5.1) adapted from [2]:

Glucose model

Brain:

$$\frac{dG_{BV}(t)}{dt} = \frac{Q_B^G}{V_{BV}^G}(G_H(t) - G_{BV}(t)) - \frac{V_{BI}}{V_{BV}^G T_B^G}(G_{BV}(t) - G_{BI}(t)) \quad (5.4)$$

$$\frac{dG_{BI}(t)}{dt} = \frac{1}{T_B^G}(G_{BV}(t) - G_{BI}(t)) - \frac{R_{BGU}}{V_{BI}} \quad (5.5)$$

Heart and Lungs:

$$\frac{dG_H(t)}{dt} = \frac{1}{V_H^G}(Q_B^G G_{BV}(t) + Q_L^G G_L(t) + Q_K^G G_K(t) + Q_P^G G_{PV}(t) - Q_H^G G_H(t)) \quad (5.6)$$

$$- \frac{R_{RBCU}}{V_H^G} \quad (5.7)$$

Gut:

$$\frac{dG_G(t)}{dt} = \frac{Q_G^G}{V_G^G}(G_H(t) - G_G(t)) - \frac{R_{GGU}}{V_G^G} \quad (5.8)$$

Liver:

$$\frac{dG_L(t)}{dt} = \frac{1}{V_L^G}(Q_Y^G G_H(t) + Q_G^G G_G(t) - Q_L^G G_L(t) + R_{HGUP}) - \frac{R_{HGUL}}{V_L^G} \quad (5.9)$$

Kidney:

$$\frac{dG_K(t)}{dt} = \frac{Q_K^G}{V_K^G}(G_H(t) - G_K(t)) - \frac{R_{KGE}}{V_K^G} \quad (5.10)$$

$$(5.11)$$

Periphery:

$$\frac{dG_{PV}(t)}{dt} = \frac{Q_P^G}{V_{PV}^G}(G_H(t) - G_{PV}(t)) - \frac{V_{PI}^G}{V_{PV}^G T_P^G}(G_{PV}(t) - G_{PI}(t)) \quad (5.12)$$

$$\frac{dG_{PI}(t)}{dt} = \frac{1}{T_P^G}(G_{PV}(t) - G_{PI}(t)) - \frac{R_{PGU}}{V_{PI}^G} \quad (5.13)$$

Metabolic sources and sinks:

$$R_{PGU} = M_{PGU}^I \times M_{PGU}^G \times 35 \quad (5.14)$$

$$M_{PGU}^I = 7.03 + 6.52 \times \tanh[0.338(I_{PI}^N(t) - 5.82)] \quad (5.15)$$

$$M_{PGU}^G = G_{PI}^N(t) \quad (5.16)$$

$$R_{HGP} = M_{HGP}^I \times M_{HGP}^X \times M_{HGP}^G \times 155 \quad (5.17)$$

$$\frac{dM_{HGP}^I}{dt} = \frac{1}{\tau_I}(M_{HGP}^{I\infty} - M_{HGP}^I) \quad (5.18)$$

$$M_{HGP}^{I\infty} = 1.2793 - 1.0647 \times \tanh[1.733(I_L^N(t) - 0.849)] \quad (5.19)$$

$$M_{HGP}^X = M_{HGP}^{X0} - f_2 \quad (5.20)$$

$$M_{HGP}^{X0} = 2.7 \times \tanh[0.39X^N(t)] \quad (5.21)$$

$$\frac{df_2}{dt} = \frac{1}{\tau_X} \left[\frac{M_{HGP}^{X0} - 1}{2} - f_2 \right] \quad (5.22)$$

$$M_{HGP}^G = 1.42 - 1.41 \times \tanh[0.62(G_L^N(t) - 0.497)] \quad (5.23)$$

$$R_{HGU} = M_{HGU}^I \times M_{HGU}^G \times 20 \quad (5.24)$$

$$\frac{dM_{HGU}^I}{dt} = \frac{1}{\tau_I}(M_{HGU}^{I\infty} - M_{HGU}^I) \quad (5.25)$$

$$M_{HGU}^{I\infty} = 2.0 \times \tanh[0.55I_L^N(t)] \quad (5.26)$$

$$M_{HGU}^G = 5.66 + 5.66 \times \tanh[2.44(G_L^N(t) - 1.48)] \quad (5.27)$$

$$R_{KGE} = 71 + 71 \times \tanh[0.11(G_K(t) - 460)] \quad 0 < G_K(t) < 460 \quad \text{mg/dL} \quad (5.28)$$

$$R_{KGE} = -330 + 0.872G(t)_K \quad G_K(t) \geq 460 \quad \text{mg/dL} \quad (5.29)$$

Insulin model

Brain:

$$\frac{dI_B(t)}{dt} = \frac{Q_B^I}{V_B^I}(I_H(t) - I_B(t)) \quad (5.30)$$

Heart and Lungs:

$$\frac{dI(t)_H}{dt} = \frac{1}{V_H^I}(Q_B^I I_B(t) + Q_L^I I_L(t) + Q_K^I I_K(t) + Q_P^I I_P(t) - Q_H^I I_H(t)) \quad (5.31)$$

Gut:

$$\frac{dI_G(t)}{dt} = \frac{Q_G^I}{V_G^I}(I_H(t) - I_G(t)) \quad (5.32)$$

Liver:

$$\frac{dI_L(t)}{dt} = \frac{1}{V_L^I}(Q_Y^I I_H(t) + Q_G^I I_G(t) - Q_L^I I_L(t)) - \frac{R_{LIC}}{V_L^I} \quad (5.33)$$

Kidney:

$$\frac{dI_K(t)}{dt} = \frac{Q_K^I}{V_K^I}(I_H(t) - I_K(t)) - \frac{R_{KIC}}{V_K^I} \quad (5.34)$$

Muscle:

$$\frac{dI_{PV}(t)}{dt} = \frac{Q_P^I}{V_{PV}^I}(I_H(t) - I_{PV}(t)) - \frac{V_{PI}^I}{V_{PV}^I T_P^I}(I_{PV}(t) - I_{PI}(t)) \quad (5.35)$$

$$\frac{dI_{PI}(t)}{dt} = \frac{1}{T_P^I}(I_{PV}(t) - I_{PI}(t)) - \frac{R_{PIC}}{V_{PI}^I} \quad (5.36)$$

Metabolic sources and sinks:

$$R_{LIC} = f_{LIC}(Q_Y^I I_H(t) + Q_G^I I_G(t)) \quad (5.37)$$

$$R_{KIC} = f_{KIC}(Q_K^I I_K(t)) \quad (5.38)$$

$$R_{PIC} = \frac{I_{PI}(t)}{\left(\frac{1-f_{PIC}}{f_{PIC}}\right) \left(\frac{1}{Q_P^I}\right) - \frac{T_P^I}{V_{PI}}} \quad (5.39)$$

Glucagon model

$$\frac{dX^N(t)}{dt} = \frac{1}{V_X}(R_{M_X C} R_{P_X R}^N - R_{P_X C}(t)) \quad (5.40)$$

Metabolic sources and sinks:

$$R_{P_X C}(t) = R_{M_X C} X^N(t) \quad (5.41)$$

$$R_{P_X R}^N = M_{P_X R}^I M^G P_X R \quad (5.42)$$

$$M^G P_X R = 2.93 - 2.10 \times \tanh[4.18(G_H^N(t) - 0.61)] \quad (5.43)$$

$$M^I P_X R = 1.31 - 0.61 \times \tanh[1.06(I_H^N(t) - 0.47)] \quad (5.44)$$

Table 5.1: Parameter values of the Sorensen model, adapted from [2]

Parameters	Values	Parameters	Values
R_{BGU} (mg/min)	70	T_P^G (min)	5.0
R_{RBCU} (mg/min)	10	f_{LIC}	0.4
R_{GGU} (mg/min)	20	f_{KIC}	0.3
τ_I (min)	25	f_{PIC}	0.15
τ_X (min)	65	V_B^I (L)	0.26
V_{BV}^G (dL)	3.5	V_H^I (L)	0.99
V_{BI}^G (dL)	4.5	V_G^I (L)	0.94
V_H^G (dL)	13.8	V_L^I (L)	1.14
V_L^G (dL)	25.1	V_K^I (L)	0.51
V_G^G (dL)	11.2	V_{PV}^I (L)	0.74
V_K^G (dL)	6.6	V_{PI}^I (L)	6.74
V_{PV}^G (dL)	10.4	Q_B^I (L/min)	0.45
V_{PI}^G (dL)	63.0	Q_H^I (L/min)	3.35
Q_B^G (dL/min)	5.9	Q_Y^I (L/min)	0.18
Q_H^G (dL/min)	43.7	Q_K^I (L/min)	0.72
Q_Y^G (dL/min)	2.5	Q_P^I (L/min)	1.28
Q_L^G (dL/min)	12.6	Q_G^I (L/min)	0.72
Q_G^G (dL/min)	10.1	Q_L^I (L/min)	0.9
Q_K^G (dL/min)	10.1	T_P^I (min)	20.0
Q_P^G (dL/min)	15.1	R_{MxC} (L/min)	0.91
T_B^G (min)	2.1	V^X (L)	9.94

Table 5.2: Nomenclature of the Sorensen model [2]

Variables	Description
G	Glucose concentration ($\frac{mg}{dL}$)
Q	Vascular blood flow ($\frac{dL}{min}$)
R	Metabolic source or sink ($\frac{mg}{min}$)
M	Multiplier function
T	Transcapillary diffusion time (min)
V	Volume (L)
τ	time constant
t	Time (min)
I	insulin concentration ($\frac{\mu U}{mL}$)
f	fractional clearance
X	glucagon concentration ($\frac{pg}{mL}$)
First Subscript: Physiologic Compartment	Description
B	Brain
H	Heart and Lungs
G	Gut
L	Liver
K	Kidney
P	Periphery
Y	Hepatic Artery tissue
Second Subscript Physiologic Subcompartment	Description
I	Interstitial fluid space
V	Vascular blood space
Metabolic Rate Subscript	Description
BGU	Brain glucose uptake
GGU	Gut glucose uptake
HGU	Hepatic glucose uptake
HGP	Hepatic glucose production
KGE	Kidney glucose excretion
PGU	Periphery glucose uptake
RBCU	Red blood cell glucose uptake
KIC	Kidney insulin clearance
LIC	Liver insulin clearance
PIC	Periphery insulin clearance
P _X C	Plasma glucagon clearance
M _X C	Metabolic glucagon clearance
P _X R	Pancreatic glucagon release
Superscript	Description
G	glucose
I	insulin
X	glucagon
B	basal value
N	normalized value (divided by basal value)

5.2 PHYSIOLOGICAL FFA MODEL STRUCTURE

A physiologically-based FFA model similar in structure to the existing glucose-insulin model of Sorensen [2] was developed to capture FFA distribution in various tissues and its interactions with other metabolic substrates and hormones. The model consists of compartments representing the major FFA utilizing tissues and organs, as shown in Figure 5.4. In this case, unlike the original glucose-insulin Sorensen model, the periphery compartment was divided into AT and muscle compartments, as these have different roles in FFA dynamics. For example, FFA movement across AT is bi-directional, unlike muscle tissues [54]. During fasting, FFA is predominantly generated within the AT by breaking down stored triglycerides (TG), and there is a net outflow of FFA from AT into the systemic circulation. However in the fed state, FFA released from circulating TG is taken up by the AT for esterification and storage as TG [173]. As shown in Figure 5.4, only the muscle and AT compartments were divided into two sub-compartments representing the capillary and interstitial fluid spaces. Blood pumped from the heart entered into the compartments via the arterial route and is drained out through the venous route. The rate of consumption of FFA at the various compartments is represented by the vertically-downward pointing arrows, as shown in Figure 5.4 (metabolic sinks). The only vertically-upward pointing arrow at the AT compartment captured the rate of lipolysis, or, the rate of production of FFA (metabolic source). The brain is the only organ which neither consumes nor produces FFA [174]. The mass balance equations across each of the physiologic compartments are formulated as follows:

Brain:

$$\frac{dF_B(t)}{dt} = \frac{Q_B^F}{V_B^F}(F_H(t) - F_B(t)) \quad (5.45)$$

Heart and lungs:

$$\frac{dF_H(t)}{dt} = \frac{1}{V_H^F}(Q_B^F F_B(t) + Q_L^F F_L(t) + Q_K^F F_K(t) + Q_M^F F_{MV}(t) + Q_A^F F_{AV}(t) - Q_H^F F_H(t)) - \frac{R_{HFU}}{V_H^F} \quad (5.46)$$

Gut:

$$\frac{dF_G(t)}{dt} = \frac{Q_G^F}{V_G^F}(F_H(t) - F_G(t)) - \frac{R_{GFU}}{V_G^F} \quad (5.47)$$

Liver:

$$\frac{dF_L(t)}{dt} = \frac{1}{V_L^F}(Q_Y^F F_H(t) + Q_G^F F_G(t) - Q_L^F F_L(t)) - \frac{R_{LFU}}{V_L^F} \quad (5.48)$$

Kidney:

$$\frac{dF_K(t)}{dt} = \frac{Q_K^F}{V_K^F}(F_H(t) - F_K(t)) - \frac{R_{KFE}}{V_K^F} \quad (5.49)$$

Muscle:

$$\frac{dF_{MV}}{dt} = \frac{Q_M^F}{V_{MV}^F}(F_H - F_{MV}) - \frac{V_{MI}}{V_{MV}^F T_M^F}(F_{MV} - F_{MI}) \quad (5.50)$$

$$\frac{dF_{MI}}{dt} = \frac{1}{T_M^F}(F_{MV} - F_{MI}) - \frac{R_{MFU}}{V_{MI}} \quad (5.51)$$

AT:

$$\frac{dF_{AV}(t)}{dt} = \frac{Q_A^F}{V_{AV}^F}(F_H(t) - F_{AV}(t)) - \frac{V_{AI}}{V_{AV}^F T_A^F}(F_{AV}(t) - F_{AI}(t)) \quad (5.52)$$

$$\frac{dF_{AI}(t)}{dt} = \frac{1}{T_A^F}(F_{AV}(t) - F_{AI}(t)) - \frac{R_{AFU}}{V_{AI}} + \frac{R_{AFP}}{V_{AI}} \quad (5.53)$$

Table 5.3: Nomenclature of the physiologically-based FFA model

Variables	Description
F	FFA concentration ($\frac{\mu\text{mol}}{L}$)
Q	Vascular blood flow ($\frac{L}{\text{min}}$)
R	Metabolic source or sink ($\frac{\mu\text{mol}}{\text{min}}$)
T	Transcapillary diffusion time (<i>min</i>)
V	Volume (<i>L</i>)
t	Time (<i>min</i>)
First Subscript: Physiologic Compartment	Description
B	Brain
H	Heart and Lungs
G	Gut
L	Liver
K	Kidney
M	Muscle
A	Adipose tissue
Y	Hepatic Artery tissue
Second Subscript Physiologic Subcompartment	Description
I	Interstitial fluid space
V	Vascular blood space
Metabolic Rate Subscript	Description
BFU	Brain FFA uptake
HFU	heart/lungs FFA uptake
GFU	Gut FFA uptake
LFU	Liver FFA uptake
KFE	Kidney FFA uptake
MFU	Muscle FFA uptake
AFU	AT FFA uptake
AFP	AT FFA production
Superscript	Description
F	FFA model

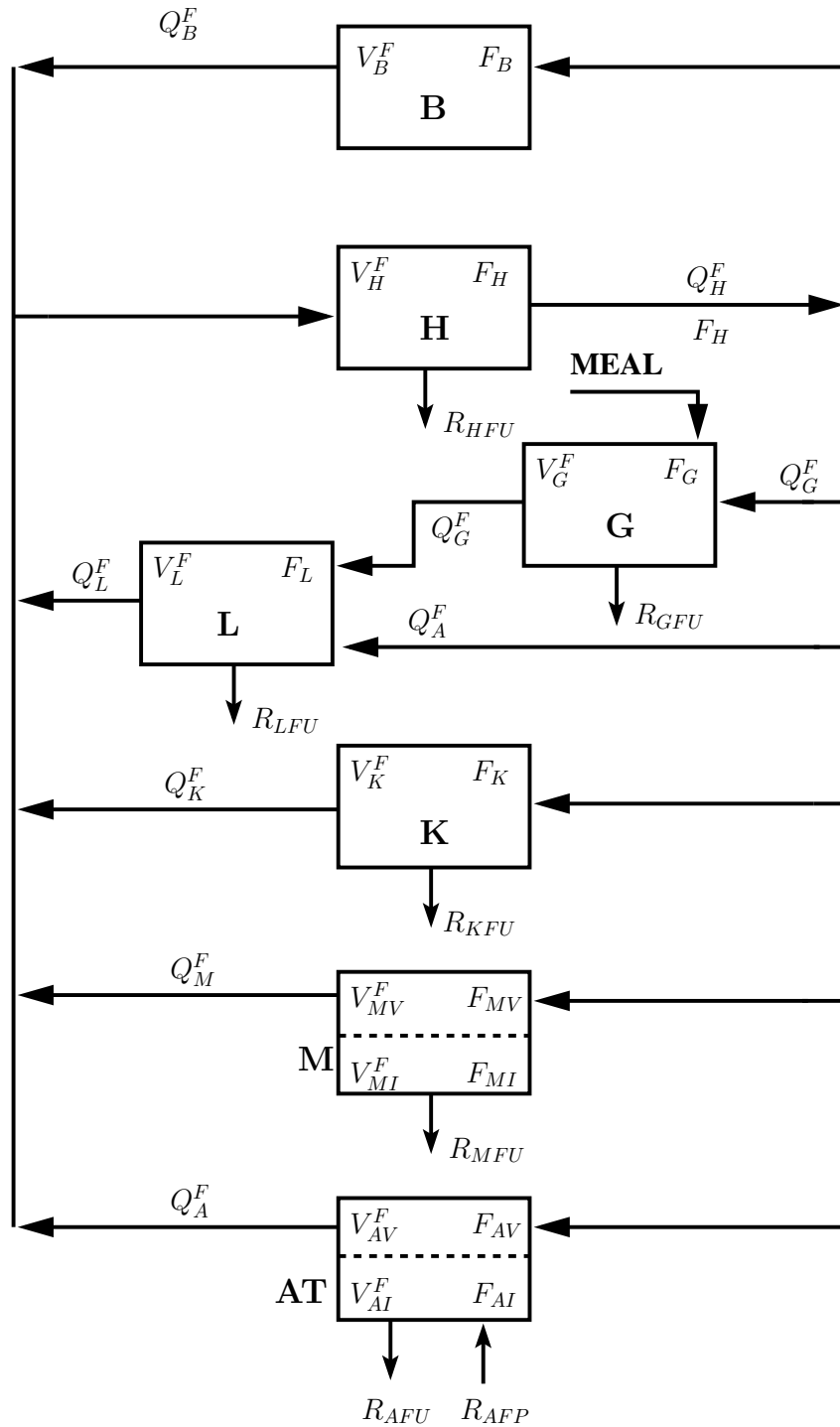


Figure 5.4: Physiologically-based FFA model block diagram. B: Brain; H: Heart and lungs; G: Gut; L: Liver; K: Kidney; M: Muscle; AT: Adipose tissue.

Table 5.4: Parameter values of the physiologically-based FFA model

Parameters	Values	Source	Parameters	Values	Source
Q_B^F (L/min)	0.4	[175]	V_H^F (L)	0.84	[175]
Q_K^F (L/min)	0.7	[175]	V_G^F (L)	0.94	[175]
Q_M^F (L/min)	0.42	[175]	V_L^F (L)	1.02	[175]
Q_A^F (L/min)	0.15	[175]	V_{MV}^F (L)	0.51	[176]
Q_Y^F (L/min)	0.2	[175]	V_{MI}^F (L)	2.4	[176]
Q_G^F (L/min)	0.62	[175]	V_{AV}^F (L)	0.057	[176]
Q_L^F (L/min)	0.82	[175]	V_{AI}^F (L)	0.77	[176]
Q_H^F (L/min)	2.49	[175]	T_M^F (min)	2.95	–
V_B^F (L)	0.82	[175]	T_A^F (min)	15.45	–
V_K^F (L)	0.16	[175]	T_{AFP} (min)	0.11	–

The FFA model with 7 physiologic compartments consist of 9 ODEs (including the sub-compartments of muscle and AT). The nomenclature of the FFA model is provided in Table 5.3 and corresponds with the symbols used in the schematic diagram (Figure 5.4). In general the first subscript represents the various organs/tissues, and if required, the second subscript represents the fluid spaces within the physiologic compartments. The superscript ‘F’ indicates the FFA model in order to distinguish similar parameter nomenclature used in different models (glucose, insulin, glucagon, and FFA) having different numeric values. All the physiologic parameters (flow rates, Q_i^F , and volumes, V_i^F) were directly obtained from the published literature [175, 176], as shown in Table 5.4. The metabolic rate at which FFA is consumed from, or released back into, the circulatory system is predominantly a function of its own concentration [54] and the concentration of insulin [54, 173]. This phenomenon was captured in the model by using the metabolic sink and source functions. In general, the rates for consumption or release of FFA have the following mathematical formulation (adapted from Sorensen [2]):

$$R_j = M_j^G \times M_j^I \times M_j^F \times R_j^B \quad (5.54)$$

Here, R_j (mass/time) is the metabolic rate of mass addition/removal via process j . M_j^G , M_j^I , and M_j^F (dimensionless) are the multiplicative effects of glucose, insulin, and FFA, respectively on process R_j . Finally, R_j^B (mass/time) is the metabolic rate of mass addition/removal in the basal state. Since hyperbolic tangent functions have been found to be readily suitable for representing the sigmoidal nonlinearities commonly observed in biological systems, the rate multiplier functions will have the following mathematical form (adapted from [2]):

$$M_j^q = A + B \times \tanh[C(q(t) - D)] \quad (5.55)$$

Here, $q(t)$ is insulin, glucose, or FFA concentration, and A , B , C , and D are the parameters.

Wherever sufficient data was available to support the relationship between metabolic rates and glucose/insulin/FFA concentration, the multiplier functions were fitted using the nonlinear least square technique (see Section 2.3) by adjusting the four parameters. Data were obtained primarily from published literature where regional FFA uptake rates were calculated by measuring the arterial-venous FFA concentration difference coupled with blood flow rate across a particular organ or tissue [25, 26, 28].

5.3 MODIFIED VERSION OF THE SORENSEN GLUCOSE-INSULIN MODEL

Some modifications were made to the original glucose-insulin model of Sorensen [2] in order to facilitate the incorporation of the FFA model. Mainly, the periphery compartment in the glucose and insulin models (which consists of 0.75 weight fraction of muscle tissue and the remaining is adipocytes [2, 177]) was partitioned into two compartments: muscle and AT. This facilitated the separate capture of the glucose and insulin distributions and dynamics in the muscle and adipose tissues, respectively. Just like the periphery compartment, both the muscle and AT compartments were further divided into two subcompartments representing

the capillary and interstitial fluid spaces, in order to incorporate the effect of capillary wall resistance.

In the glucose model (Section 5.1), equations (5.12) and (5.13) representing the glucose dynamics in the periphery compartment were replaced by new equations capturing the glucose dynamics in the muscle and AT compartments. Hence, the mass balance equations for the muscle compartment can be written as follows:

$$\frac{dG_{MV}(t)}{dt} = \frac{Q_M^G}{V_{MV}^G}(G_H(t) - G_{MV}(t)) - \frac{V_{MI}^G}{V_{MV}^G T_M^G}(G_{MV}(t) - G_{MI}(t)) \quad (5.56)$$

$$\frac{dG_{MI}(t)}{dt} = \frac{1}{T_M^G}(G_{MV}(t) - G_{MI}(t)) - \frac{R_{MGU}}{V_{MI}^G} \quad (5.57)$$

Here, the first subscript M for the physiologic parameters represents the muscle compartment and the subscript MGU in the metabolic sink term (R_{MGU}) represents muscle glucose uptake. Peripheral glucose uptake rate (equation (5.14)) in Section 5.1 is replaced by the rate of muscle glucose uptake which can be written as follows:

$$R_{MGU} = M_{MGU}^I \times M_{MGU}^G \times 35 \times f_M \quad (5.58)$$

$$M_{MGU}^I = 7.03 + 6.52 \times \tanh[0.338(I_{MI}^N(t) - 5.82)] \quad (5.59)$$

$$M_{MGU}^G = G_{MI}^N(t) \quad (5.60)$$

The term f_M represents the mass fraction of muscle in the periphery compartment, which is considered to be 0.75 [2, 177]. The multiplier functions M_{MGU}^I and M_{MGU}^G capture the muscle glucose uptake rate as a function of insulin and glucose concentrations, respectively.

Similarly, the mass balance equation for the AT compartment can be written as shown below:

$$\frac{dG_{AV}(t)}{dt} = \frac{Q_A^G}{V_{AV}^G}(G_H(t) - G_{AV}(t)) - \frac{V_{AI}^G}{V_{AV}^G T_A^G}(G_{AV}(t) - G_{AI}(t)) \quad (5.61)$$

$$\frac{dG_{AI}(t)}{dt} = \frac{1}{T_A^G}(G_{AV}(t) - G_{AI}(t)) - \frac{R_{AGU}}{V_{AI}^G} \quad (5.62)$$

In this case, the first subscript A for the physiologic parameters represents the AT compartment. Subscript AGU in the metabolic sink term (R_{AGU}) represents AT glucose uptake. The AT glucose uptake rate can be written as follows:

$$R_{AGU} = M_{AGU}^I \times M_{AGU}^G \times 35 \times f_A \quad (5.63)$$

$$M_{AGU}^I = 7.03 + 6.52 \times \tanh[0.338(I_{AI}^N(t) - 5.82)] \quad (5.64)$$

$$M_{AGU}^G = G_{AI}^N(t) \quad (5.65)$$

Mass fraction of AT in the periphery compartment is given by $f_A = 0.25$ [2, 177]. The AT glucose uptake rate as a function of insulin concentration is captured by M_{AGU}^I , whereas M_{AGU}^G represents the effect of glucose concentration on AT glucose uptake rate. All the physiologic parameters of the muscle and AT compartments belonging to the glucose model are provided in Table 5.5. The flow rate and volumes of the muscle compartment were obtained by multiplying f_M with the equivalent parameters of the periphery compartment, while the physiologic parameters of the AT compartment were calculated by multiplying f_A with the equivalent parameters of the periphery compartment in the glucose model.

Table 5.5: Parameter values of the modified glucose model

Parameters	Values	Parameters	Values
Q_M^G (dL/min)	11.33	Q_A^G (dL/min)	3.77
V_{MV}^G (dL)	7.8	V_{AV}^G (dL)	2.6
V_{MI}^G (dL)	47.25	V_{AI}^G (dL)	15.75
T_M^G (min)	5.0	T_A^G (min)	5.0

Similarly, in the insulin model (Section 5.1), equations (5.35) and (5.36) representing the insulin dynamics in the periphery compartment were replaced by new equations capturing the insulin dynamics in the muscle and AT compartments. Hence, the mass balance equations for the muscle compartment can be written as follows:

$$\frac{dI_{MV}(t)}{dt} = \frac{Q_M^I}{V_{MV}^I} (I_H(t) - I_{MV}(t)) - \frac{V_{MI}^I}{V_{MV}^I T_M^I} (I_{MV}(t) - I_{MI}(t)) \quad (5.66)$$

$$\frac{dI_{MI}(t)}{dt} = \frac{1}{T_M^I} (I_{MV}(t) - I_{MI}(t)) - \frac{R_{MIC}}{V_{MI}^I} \quad (5.67)$$

Once again, the first subscript M in the physiologic parameters represent the muscle compartment and the subscript MIC in the metabolic sink term (R_{MIC}) indicates muscle insulin clearance. Hence, the peripheral insulin clearance rate (equation (5.39)) is replaced by muscle insulin clearance rate, as shown below:

$$R_{MIC} = \frac{I_{MI}(t)}{\left(\frac{1-f_{MIC}}{f_{MIC}}\right) \left(\frac{1}{Q_M^I}\right) - \frac{T_M^I}{V_{MI}^I}} \quad (5.68)$$

Similarly, the mass balance equation for the AT compartment can be written as:

$$\frac{dI_{AV}(t)}{dt} = \frac{Q_A^I}{V_{AV}^I} (I_H(t) - I_{AV}(t)) - \frac{V_{AI}^I}{V_{AV}^I T_A^I} (I_{AV}(t) - I_{AI}(t)) \quad (5.69)$$

$$\frac{dI_{AI}(t)}{dt} = \frac{1}{T_A^I} (I_{AV}(t) - I_{AI}(t)) - \frac{R_{AIC}}{V_{AI}^I} \quad (5.70)$$

Again, the first subscript A for the physiologic parameters represents the AT compartment. Subscript AIC in the metabolic sink term (R_{AIC}) represents AT insulin clearance. The AT insulin clearance rate can be written as follows:

$$R_{AIC} = \frac{I_{AI}(t)}{\left(\frac{1-f_{AIC}}{f_{AIC}}\right) \left(\frac{1}{Q_A^I}\right) - \frac{T_A^I}{V_{AI}^I}} \quad (5.71)$$

The fractional insulin clearance by the muscle tissues and the AT are represented by f_{MIC} (equation (5.68)) and f_{AIC} (equation (5.71)), respectively. All the parameter values of the insulin model are given in Table 5.6. Once again, the flow rates and volumes of the muscle compartment were obtained by multiplying f_M with the equivalent parameters of the periphery compartment, while the physiologic parameters of the AT compartment were calculated by multiplying f_A with the equivalent parameters of the periphery compartment in the insulin model (Table 5.6).

Table 5.6: Parameter values of the modified insulin model

Parameters	Values	Parameters	Values
Q_M^I (L/min)	1.01	Q_A^I (L/min)	0.27
V_{MV}^I (L)	0.55	V_{AV}^I (L)	0.19
V_{MI}^I (dL)	5.05	V_{AI}^I (dL)	1.68
T_M^I (min)	20.0	T_A^I (min)	20.0
f_{MIC}	0.15	f_{AIC}	0.15

5.4 METABOLIC SINKS AND SOURCES OF THE FFA MODEL

5.4.1 Heart and Lungs FFA Uptake Rate (R_{HFU})

FFA is a major energy source for myocardial oxidative metabolism in the resting, postabsorptive state [27]. Uptake of FFA across the heart was calculated by measuring the myocardial blood flow together with venous and arterial FFA concentration difference [25, 26, 27]. Basal heart and lungs uptake rate of FFA (R_{HFU}^B) was estimated from published literature and was fixed at $18 \frac{\mu\text{mol}}{\text{min}}$ [25, 26]. The rate of FFA uptake by the heart and lungs is mediated by changes in FFA concentration at the heart/lungs compartment [178], and it is largely unaffected by fluctuations in glucose or insulin concentrations [54]. It can be mathematically expressed as:

$$R_{HFU} = M_{HFU}^F \times R_{HFU}^B \quad (5.72)$$

The FFA multiplicative function, M_{HFU}^F , can be written as:

$$M_{HFU}^F = 0.8894 + 1.0674 \times \tanh(1.2617(F_H^N(t) - 0.9497)) \quad (5.73)$$

Here F_H^N is the normalized FFA concentration at heart and lungs with respect to its basal value ($F_H^N = F_H/F_H^B$, where F_H^B is the basal FFA concentration at heart/lungs). The

parameters of equation (5.73) were estimated from published data [25, 26, 27] as shown in Figure 5.5. The figure indicates the effect of FFA concentration on FFA uptake rate in the heart/lungs compartment.

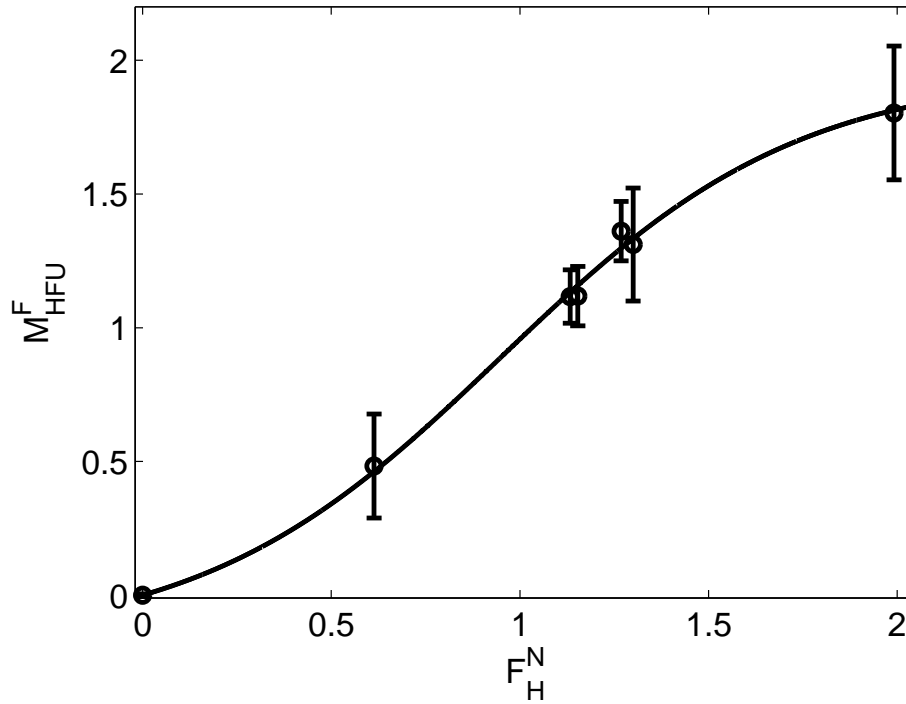


Figure 5.5: Model fit (line) versus published data ($\mu \pm \sigma$) (circle) [25, 26, 27] of FFA uptake rate multiplier function in the heart/lungs compartment, M_{HFU}^F , as a function of normalized heart/lungs FFA concentration, F_H^N

5.4.2 Gut FFA Uptake Rate (R_{GFU})

The gut, mainly comprised of the gastrointestinal tract, pancreas, and spleen, metabolizes FFA at a rate of $27 \frac{\mu\text{mol}}{\text{min}}$ [179]. FFA utilization by gut tissue appears to be relatively insensitive to FFA, glucose, or insulin concentration. Hence, the value of R_{GFU} was fixed at $27 \frac{\mu\text{mol}}{\text{min}}$.

5.4.3 Liver FFA Uptake Rate (R_{LFU})

Liver is an important site for removal of FFA from plasma [29]. Other than β -oxidation, a substantial amount of the consumed FFA in the liver is converted to glucose by a process known as gluconeogenesis [180]. Liver FFA uptake rate is calculated by measuring the arterial-venous difference of FFA concentration along with hepatic blood flow rate [28]. Once again, the liver FFA uptake rate is predominantly a function of the liver FFA concentration. The mathematical expression for R_{LFU} can be written as:

$$R_{LFU} = M_{LFU}^F \times R_{LFU}^B \quad (5.74)$$

$$M_{LFU}^F = 0.6007 + 0.6931 \times \tanh(1.4279(F_L^N(t) - 0.91324)) \quad (5.75)$$

The basal rate of liver FFA uptake rate, R_{LFU}^B , was fixed at $232 \frac{\mu\text{mol}}{\text{min}}$ [28]. In equation (5.75), F_L^N represents the normalized liver FFA concentration. Parameters in equation (5.75) were estimated from published literature [29, 28], as shown in Figure 5.6.

5.4.4 Kidney FFA Uptake Rate (R_{KFU})

Studies have revealed that the kidney is an important organ for FFA disposal [181]. Arterial-venous differences of plasma FFA concentration across the kidney have indicated a significant drop in venous FFA concentration. Data obtained from both animal and human studies have not indicated any significant change in FFA uptake rate with varying arterial FFA concentration [181]. Hence, the rate of kidney FFA uptake, R_{KFU} , was fixed at $20 \frac{\mu\text{mol}}{\text{min}}$ [181].

5.4.5 Muscle FFA Uptake Rate (R_{MFU})

FFA is the major source of skeletal muscle energy at rest [30]. Almost 75-80% of the resting muscle energy is provided by FFA oxidation [178]. The importance of FFA as an energy source is best highlighted by their rapid plasma turnover that allows for the transfer of high energy carbons from the AT stores to the muscle cells. Once FFA diffuses into the

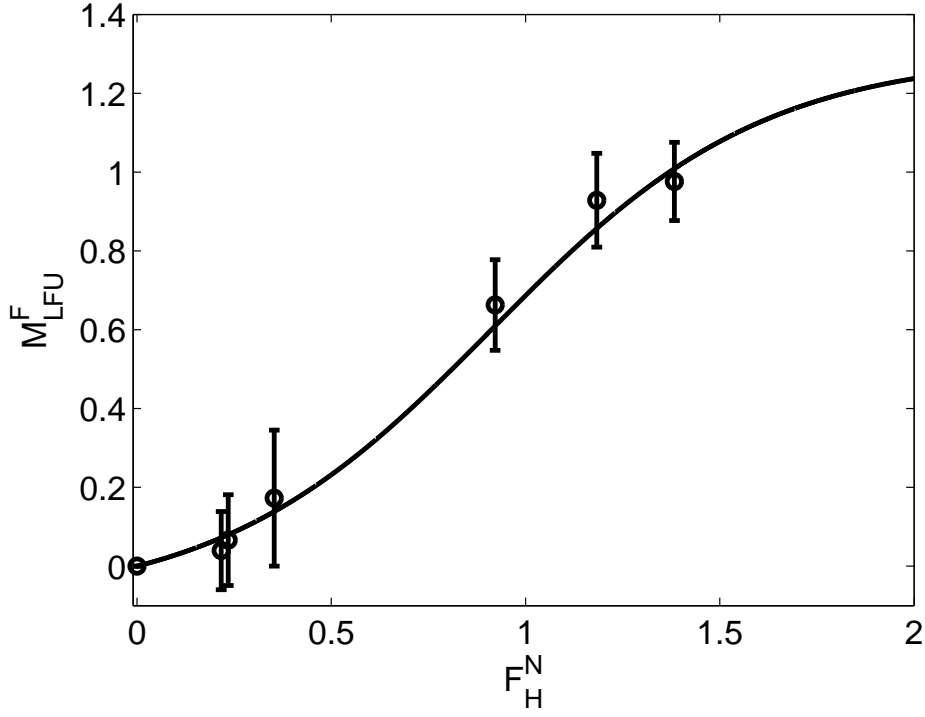


Figure 5.6: Model fit (line) versus published data ($\mu \pm \sigma$) (circle) [28, 29] of FFA uptake rate multiplier function in the liver compartment, M_{LFU}^F , as a function of normalized liver FFA concentration, F_L^N

muscle cells, FFA is oxidized to acetyl CoA, which then enters the Krebs cycle and results in production of ATP [178]. Arterial-venous FFA concentration measurement along with blood flow rate across the muscle tissue was used to estimate muscle FFA uptake rates [30, 31]. Muscular FFA uptake is primarily a function of the muscle FFA concentration. Mathematically, R_{MFU} can be expressed as:

$$R_{MFU} = M_{MFU}^F \times R_{MFU}^B \quad (5.76)$$

$$M_{MFU}^F = 0.78016 + 0.88336 \times \tanh(1.4145(F_{MI}^N(t) - 0.98)) \quad (5.77)$$

Here, M_{MFU}^F is the multiplier function capturing the effect of muscle interstitial space FFA concentration on the rate of muscle FFA uptake. F_{MI}^N is the normalized FFA concentration at the interstitial space of muscle tissue. The parameters of equation (5.77) were estimated from published data [30, 31], as shown in Figure 5.7. Basal rate of FFA uptake, R_{MFU}^B , was fixed at $130 \frac{\mu\text{mol}}{\text{min}}$ [31].

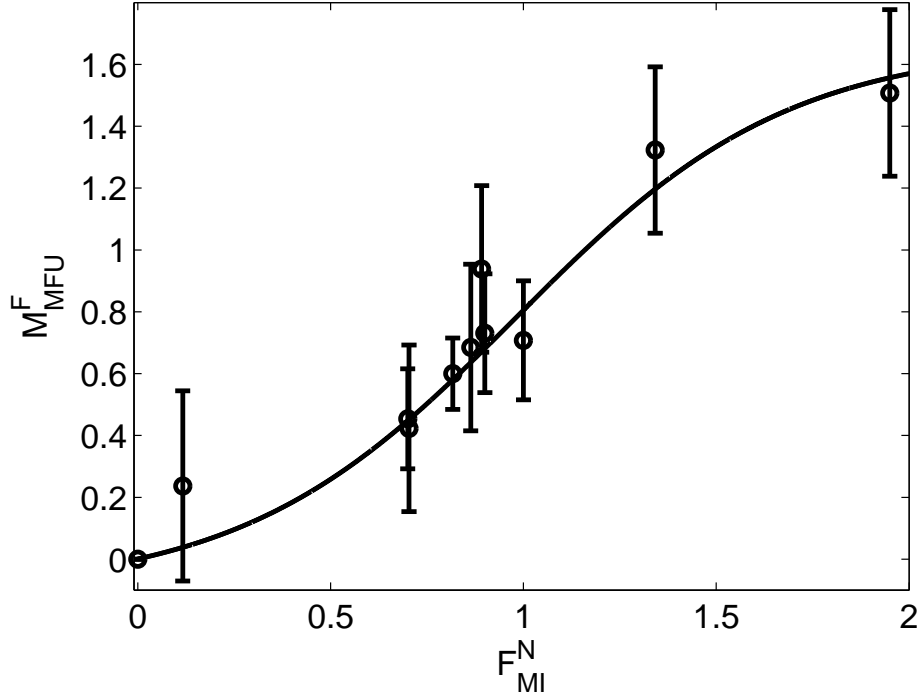


Figure 5.7: Model fit (line) versus published data ($\mu \pm \sigma$) (circle) [30, 31] of FFA uptake rate multiplier function in the muscle compartment, M_{MFU}^F , as a function of normalized muscle interstitial space FFA concentration, F_{MI}^N

5.4.6 AT FFA Production Rate (R_{AFP})

The main function of AT is to store and release energy in the form of fatty acids [182]. During the pre-prandial period, FFA are predominantly generated in the adipocyte by the action of hormone sensitive lipase (HSL), which hydrolyzes stored TG into FFA and glycerol. Once

hydrolyzed, FFA enters into the common intracellular pool from where it might be released into the circulatory system. This process is known as lipolysis. Insulin is reported to have a profound inhibiting effect on lipolysis [173, 182]. Insulin reduces the intracellular levels of cAMP, thus reducing the activation of HSL [182]. This suppression of lipolysis under the influence of insulin lowers the rate of FFA production from AT, thereby reducing the circulating levels of FFA. For modeling purposes, R_{AFP} could be written as:

$$R_{AFP} = M_{AFP}^I \times R_{AFP}^B \quad (5.78)$$

$$\frac{dM_{AFP}^I}{dt} = \frac{1}{T_{AFP}}(M_{AFP}^{I\infty} - M_{AFP}^I) \quad (5.79)$$

$$M_{AFP}^{I\infty} = \left[6.2937 \times \frac{I_{AI}^N(t)}{I_{AI}^N(t) + 12.297} + 0.57879 \right]^{-1} \quad (5.80)$$

The inhibitory effect of insulin on lipolysis is captured by the multiplier function $M_{AFP}^{I\infty}$. The superscript ‘ ∞ ’ indicates that this is the steady state effect of insulin on lipolysis. Parameters in equation (5.80) were estimated from data obtained from Campbell et al. [16], where the lipolytic rate of healthy humans was measured at various hyperinsulinemic levels, as shown in Figure 5.8. I_{AI}^N represents the normalized interstitial space AT insulin concentration. The basal rate of FFA production, R_{AFP}^B , was fixed at $575.35 \frac{\mu\text{mol}}{\text{min}}$ [16]. Due to the nature of the dynamics as observed in the data, an inverse Michaelis-Menten expression (equation (5.80)) was used instead of a hyperbolic tangent function to capture the correlation between AT FFA production and insulin. A hyperbolic tangent function was inadequate to capture the slow decrease in $M_{AFP}^{I\infty}$ after the I_{AI} concentration exceeded 15-fold of its basal value.

In order to capture the time course of insulin inhibition on lipolysis, a first-order filter, equation (5.79) was introduced. The time constant, T_{AFP} , was estimated from a study performed by Howard et al. [4], where euglycemic-hyperinsulinemic clamps were employed. Plasma insulin concentration was elevated to 20, 30, and $100 \frac{\mu\text{U}}{\text{ml}}$ ($10 \frac{\mu\text{U}}{\text{ml}}$ being the basal level), as shown in the top, middle, and bottom plots in Figure 5.9. Due to the elevation of plasma insulin concentration, FFA concentration was suppressed in all the three cases.

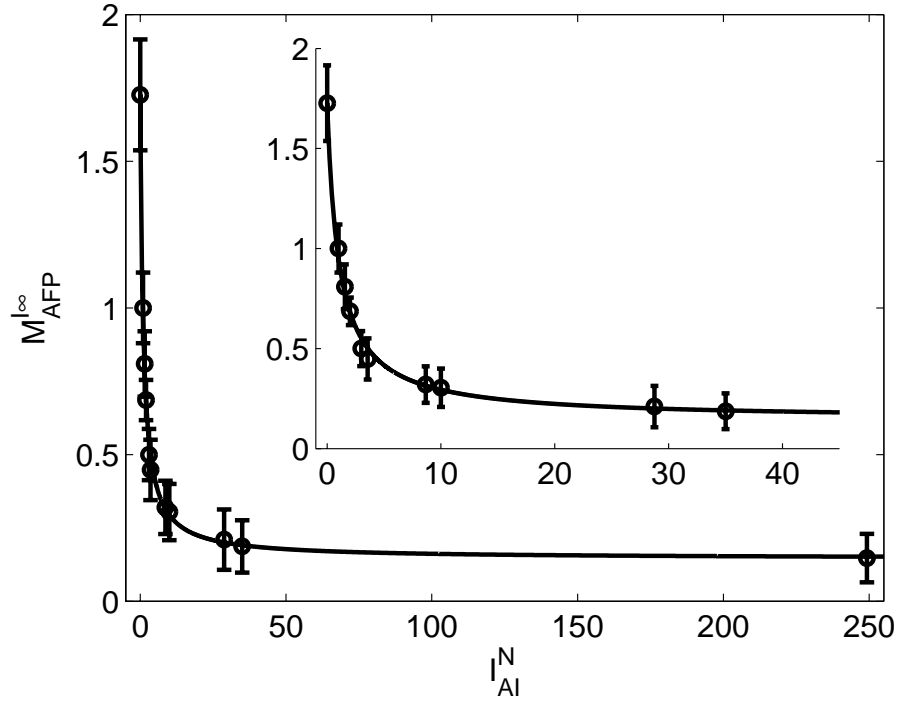


Figure 5.8: Model fit (line) versus published data ($\mu \pm \sigma$) (circle) [16] of normalized FFA production rate in the AT compartment, M_{AFP}^{∞} , as a function of normalized adipocyte insulin concentration I_{AI}^N . The inset includes magnified coordinates, x-axis $\in [0 \text{ to } 45]$ and y-axis $\in [0 \text{ to } 2]$

5.4.7 AT FFA Uptake Rate (R_{AFU})

As discussed earlier, FFA is mainly taken up by the AT for storage purpose in the form of TG [54, 182]. This phenomenon is known as lipogenesis. Lipoprotein lipase (LPL) enzyme present in the adipocyte capillary hydrolyzes circulating chylomicrons, low-density lipoproteins (LDL) and very low-density lipoproteins (VLDL) into FFA and glycerol. The released FFA then enters into the AT where it is esterified into TG. Fatty acids influx into the adipocytes depends mainly upon the existence of an FFA concentration gradient

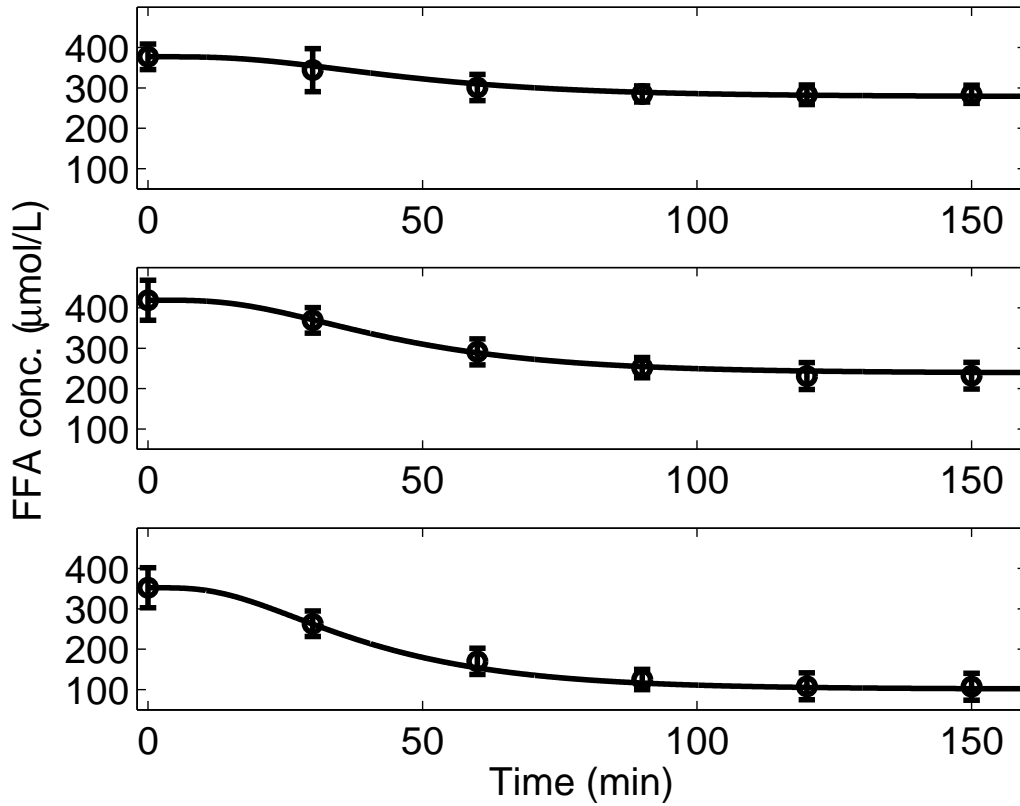


Figure 5.9: Model predicted (line) and published ($\mu \pm \sigma$) (circle) [4] plasma FFA concentration in response to euglycemic hyperinsulinemic clamps. Plasma insulin concentration was maintained at $20 \frac{\mu U}{ml}$ (top), $30 \frac{\mu U}{ml}$ (middle), $100 \frac{\mu U}{ml}$ (bottom)

[54]. Researchers have estimated the rate of lipogenesis by measuring the arterial-venous differences *in vivo* [173, 183]. Data obtained from such studies are quite scattered and hence portray less confidence. In the model, AT FFA uptake rate was used to close the FFA mass balance. Studies performed by Howard *et al.* [4] was used to calculate the correlation between R_{AFU} and FFA concentration, where plasma fatty acid concentrations were measured at various hyperinsulinemic levels. From the steady state FFA values at given hyperinsulinemic levels, the total FFA uptake rates, R_{Tot} (where, $R_{Tot} = R_{HFU} + R_{LFU} + R_{KFU} + R_{GFU} + R_{MFU}$), and the AT FFA production rate, R_{AFP} , were estimated by using

the above FFA metabolic sink/source rate equations. AT FFA uptake rates (R_{AFU}) were calculated by taking the difference between R_{Tot} and R_{AFP} values, as shown in Table 5.7. Mathematically R_{AFU} can be written as:

$$R_{AFU} = M_{AFU}^F \times R_{AFU}^B \quad (5.81)$$

$$M_{AFU}^F = 0.63198 + 2.3088 \times \tanh(0.4434(F_{AI}^N(t) - 0.6339)) \quad (5.82)$$

Here, F_{AI}^N is the normalized AT interstitial space FFA concentration. The basal rate of AT FFA uptake, R_{AFU}^B , was fixed at $218.62 \frac{\mu\text{mol}}{\text{min}}$ [4]. The uptake of FFA in the AT is unaffected by fluctuations in insulin or glucose concentrations [54].

Table 5.7: Closing the FFA mass balance at R_{AFU} . Symbol † indicates mean data obtained from [4]

Basal		Steady State		Total Uptake Rate (R_{Tot})	R_{AFP}	R_{AFU}
FFA† ($\frac{\mu\text{mol}}{L}$)	Insulin† ($\frac{\mu\text{U}}{\text{mL}}$)	FFA† ($\frac{\mu\text{mol}}{L}$)	Insulin† ($\frac{\mu\text{U}}{\text{mL}}$)	$= R_{HFU} + R_{LFU} + R_{KFU}$ $+ R_{GFU} + R_{MFU}$ ($\frac{\mu\text{mol}}{\text{min}}$)	($\frac{\mu\text{mol}}{\text{min}}$)	$= R_{AFP} - R_{Tot}$ ($\frac{\mu\text{mol}}{\text{min}}$)
377	10	377	10	328.22	546.85	218.62
377	10	285	20	227.1	394.28	164.12
419	10	230	30	156.68	317.33	118.28
352	10	110	100	98.27	169.14	66.16

5.5 INTER-CONNECTING POINTS BETWEEN THE FFA AND GLUCOSE MODEL

Randle and colleagues [184] were the first to postulate a glucose-fatty acid cycle in which FFA competes with glucose as an energy providing metabolic substrate. Over the years research has demonstrated that FFA reduces skeletal muscle and hepatic glucose uptake

rate [185, 186], thereby leading to glucose intolerance [8]. Studies performed by Boden *et al.* [21] have revealed that an increase in FFA oxidation in the muscle inhibits pyruvate dehydrogenase, which is a key enzyme for controlling glucose oxidation. The authors also reported that high FFA concentration is associated with an increase in tissue glucose-6-phosphate levels, which decreases glucose transport into cells.

To capture this inhibitory effect of FFA on muscular and hepatic glucose uptake rate, multiplier functions representing FFA effects were added to the equations (5.58) and (5.24), respectively. Therefore, the updated version of equation (5.58) is given by:

$$R_{MGU} = M_{MGU}^G \times M_{MGU}^I \times M_{MGU}^F \times 35 \times f_M \quad (5.83)$$

The only new term, M_{MGU}^F , captures the correlation between the muscular glucose uptake rate and FFA concentration, and can be mathematically written as:

$$M_{MGU}^F = 1.4228 + 0.52007 \times \tanh(-1.86(F_{MI}^N(t) - 0.42743)) \quad (5.84)$$

Here, F_{MI}^N is the normalized FFA concentration at the interstitial space of the muscle. Parameters in equation (5.84) were estimated using data from [8, 21], where euglycemic-hyperinsulinemic clamps were employed to healthy subjects and then peripheral and hepatic glucose uptake rates were measured at various plasma FFA levels. Figure 5.10 clearly indicates the inhibitory effects of FFA on muscle glucose uptake rate. Similarly, the hepatic glucose uptake rate (equation 5.24), was updated by adding M_{HGU}^F , which captured the inhibitory effects of FFA on R_{HGU} . This can be mathematically written as:

$$R_{HGU} = M_{HGU}^G \times M_{HGU}^I \times M_{HGU}^F \times 20 \quad (5.85)$$

$$M_{HGU}^F = 1.0557 + 0.3308 \times \tanh(-1.6429(F_L^N(t) - 0.91148)) \quad (5.86)$$

Here, F_L^N is the normalized liver FFA concentration. Parameters in equation (5.86) were estimated using data from [8, 21], as shown in Figure 5.11. Once again, it could be observed from the figure that increasing FFA downregulates R_{HGU} .

Historically, it is believed that insulin is the primary direct regulator of hepatic glucose production (HGP) [32]. However, recent studies have revealed that some of insulin's HGP regulatory effect is indirect and may be mediated by plasma FFA concentration [32, 187]. Experiments performed by Boden *et al.* [21] have revealed that elevated plasma FFA concentration inhibited insulin-induced suppression of hepatic glucose production by attenuating the insulin suppression of glycogenolysis. In another euglycemic-hyperinsulinemic study performed by Rebrin *et al.* [35], FFA was either allowed to fall or was prevented from falling with liposyn plus heparin infusion. It was observed that preventing the fall in FFA at higher insulin level significantly prevented the fall in HGP rate. The effect of FFA concentration on hepatic glucose production can be captured by the following multiplier function:

$$M_{HGP}^{F\infty} = 0.96123 + 0.34199 \times \tanh(1.8663(F_L^N(t) - 0.85815)) \quad (5.87)$$

Parameters in equation (5.87) were estimated using data obtained from [32, 33], where hepatic glucose production rate was estimated at various FFA concentrations and constant basal insulin level, as shown in Figure 5.12.

In the original Sorensen model [2], the rate of hepatic glucose production is mathematically expressed as shown in equation (5.17). Multiplier functions M_{HGP}^I , M_{HGP}^X , and M_{HGP}^G capture the effects of insulin, glucagon, and glucose concentration on hepatic glucose production, as represented by equations (5.18), (5.20), and (5.23), respectively. The function $M_{HGP}^{I\infty}$ (equation (5.19)) captures the effect of steady state insulin on R_{HGP} . In order to estimate the parameters of $M_{HGP}^{I\infty}$, data were obtained from [19, 20] where FFA concentration was allowed to fluctuate freely along with changing levels of insulin without any restriction. Hence, $M_{HGP}^{I\infty}$ basically represented the combined effect of insulin and FFA on R_{HGP} . Therefore, in order to separate the effects of insulin and FFA on the rate of hepatic glucose production, equation (5.19) was modified as follows:

$$M_{HGP}^{I\infty} = M_{HGP}^{IF\infty} \quad (5.88)$$

$$M_{HGP}^{IF\infty} = M_{HGP}^{Io\infty} \times M_{HGP}^{F\infty} \quad (5.89)$$

$$M_{HGP}^{Io\infty} = 1.019 + 0.3512 \times \tanh(2.095(I_L^N(t) - 0.97867)) \quad (5.90)$$

Here, the multiplier function $M_{HGP}^{IF\infty}$, represents the combined steady state effect of FFA and insulin concentrations on hepatic glucose production rate. I_L^N is the normalized liver insulin concentration. The multiplier function, $M_{HGP}^{Io\infty}$, captures the steady state effect of only insulin concentration on hepatic glucose production rate. The steady state FFA effect on hepatic glucose production represented by the multiplier function $M_{HGP}^{F\infty}$ is given in equation (5.87). Parameters of equation (5.90) were estimated to emulate the dynamics of $M_{HGP}^{I\infty}$ obtained from the Sorensen model [2]. The three dimensional surface plot in Figure 5.13 captures the combined steady state effect of insulin and FFA concentrations on R_{HGP} . The data obtained from several studies, including the one used to estimate the parameters in equation (5.19), [19, 21, 32, 34, 35, 36] coincided with the surface within one standard deviation (Figure 5.13). It is clear from the surface plot that an increasing liver insulin concentration suppresses hepatic glucose production rate. On the other hand, an increasing liver FFA concentration promotes hepatic glucose production rate.

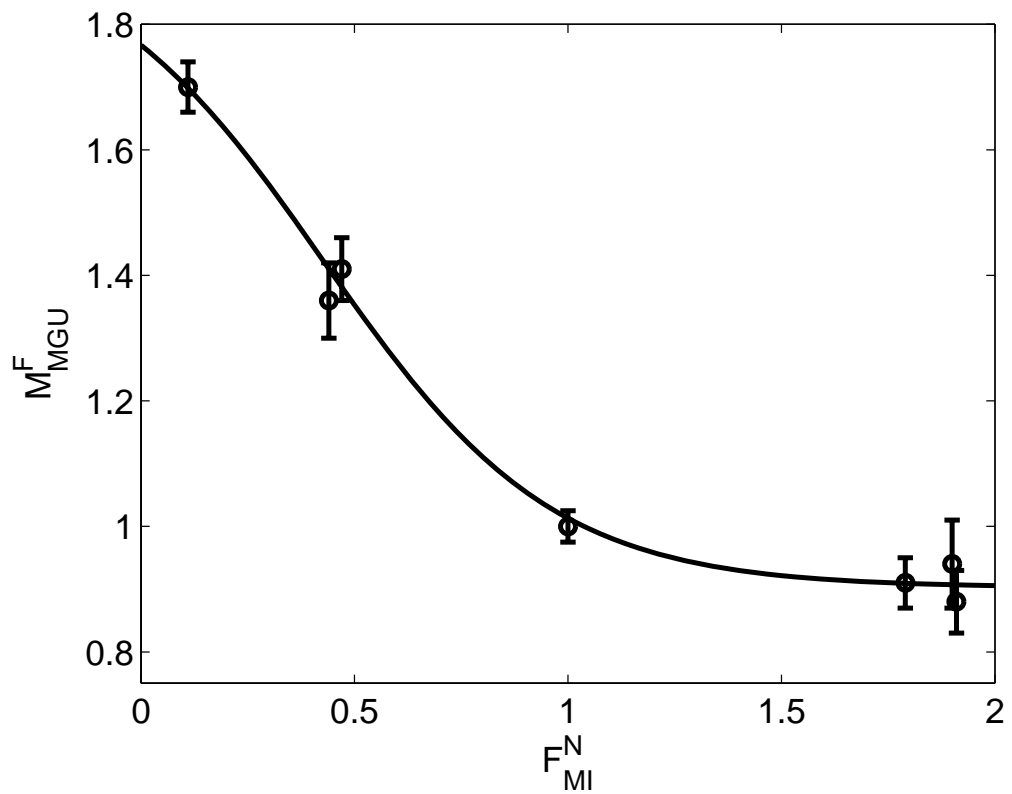


Figure 5.10: Model fit (line) versus published data ($\mu \pm \sigma$) (circle) of glucose uptake rate multiplier function in the muscle compartment, M_{MGU}^F , as a function of normalized muscle interstitial space FFA concentration, F_{MI}^N , data obtained from [8, 21]

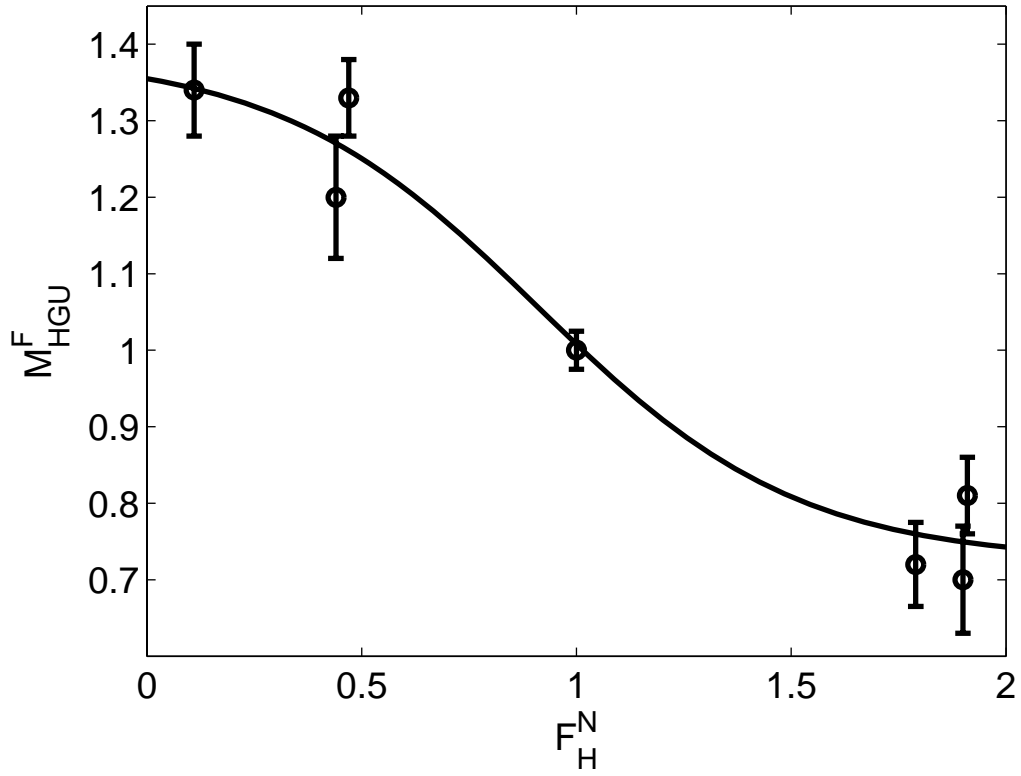


Figure 5.11: Model fit (line) versus published data ($\mu \pm \sigma$) (circle) of glucose uptake rate multiplier function in the liver compartment, M_{HGU}^F , as a function of normalized liver FFA concentration, F_L^N , data obtained from [8, 21]

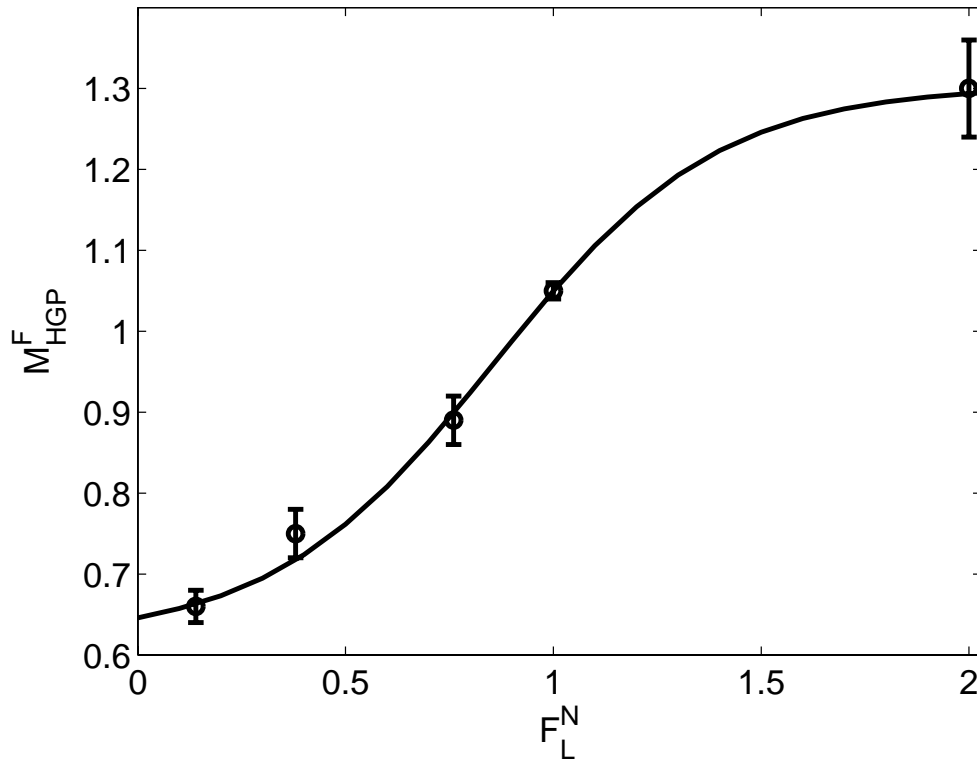


Figure 5.12: Model fit (line) versus published data ($\mu \pm \sigma$) (circle) of glucose production rate multiplier function in the liver compartment, M_{HGP}^F , as a function of normalized liver FFA concentration, F_L^N , data obtained from [32, 33]

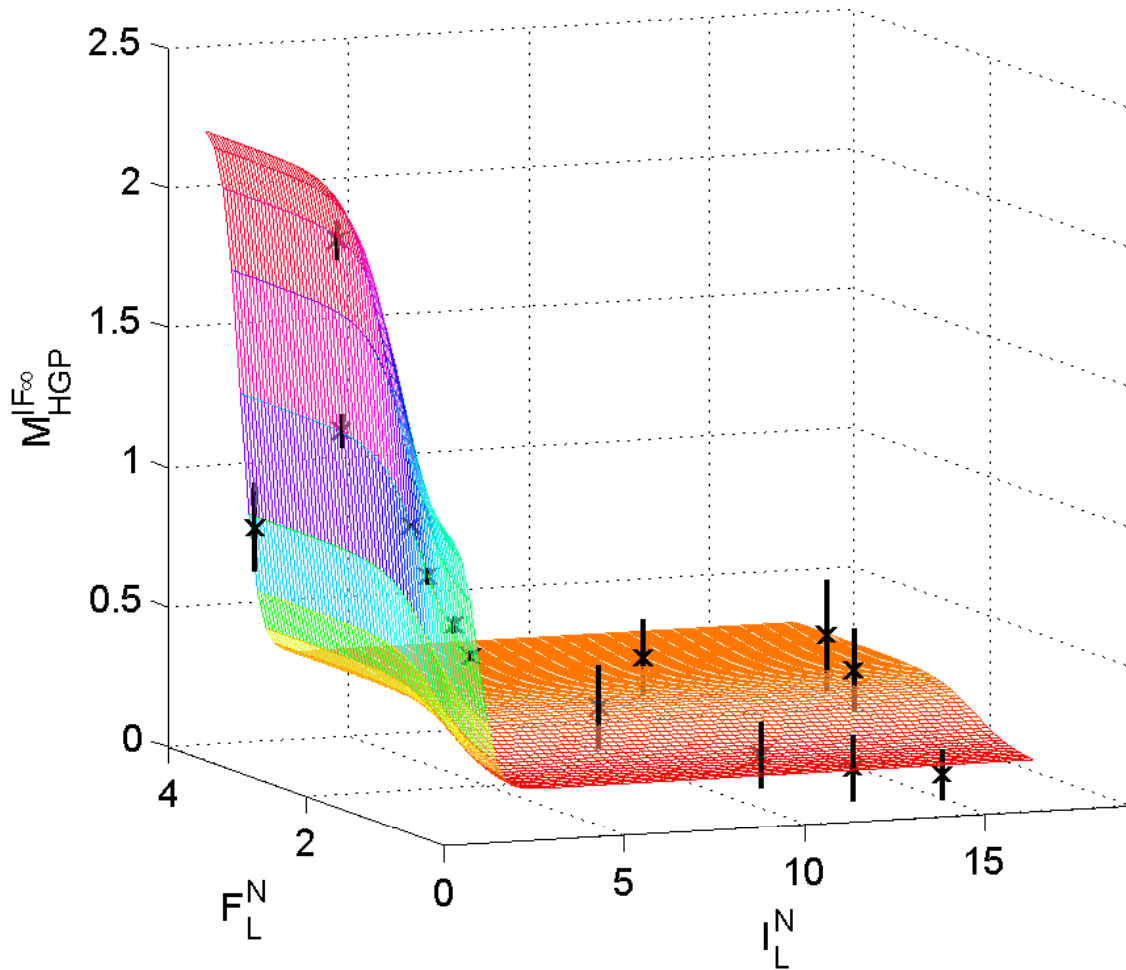


Figure 5.13: Surface plot of the multiplier function, $M_{HGP}^{IF\infty}$, as a function of normalized liver insulin, I_L^N , and FFA concentration, F_L^N , versus published data (cross) ($\mu \pm \sigma$) of normalized hepatic glucose production rate with respect to its basal value [19, 21, 32, 34, 35, 36]

5.6 THE PHYSIOLOGICALLY-BASED FFA, GLUCOSE, AND INSULIN MODEL

5.6.1 Modified-Insulin Frequently Sampled Intravenous Glucose Tolerance Test (MI-FSIGT)

For the MI-FSIGT simulation study, a bolus of glucose was infused at $t = 0 \text{ min}$ and boluses of insulin were infused at $t = 0$ and $t = 20 \text{ min}$, in order to emulate the data obtained from Sumner et al. [17]. Due to the second insulin peak, glucose concentration was suppressed below its original basal level between 50 and 100 *min*. The insulin boluses caused the FFA level to decline and achieve a nadir at around 70 *min*. After the 80 *min* mark, FFA level rose gradually and returned to its original basal state. The model predictions captured the data well, except the last 70 *min* of the FFA dynamics where the fatty acid level of the data reached a pseudo-basal level which is higher than the original basal condition. The authors have suggested that this phenomenon is due to the diurnal variation of the FFA level and has nothing to do with insulin or glucose kinetics [17]. The muscle (T_M^F) and AT (T_A^F) diffusion time constants were estimated to fit the data [17], as shown in Figure 5.14. The parameter values are given in Table 5.4.

5.6.2 Validation of the Physiologically-Based Model

5.6.2.1 MI-FSIGT: For validation purpose all the model parameters were fixed and then a MI-FSIGT simulation study was performed, where a bolus of glucose was infused at $t = 0$ and boluses of insulin were infused at $t = 0$ and $t = 20 \text{ min}$ at a rate similar to the experiment performed by Brehm et al. [37]. Due to the insulin boluses, FFA level was suppressed much below its original basal level. After the 60 *min* mark, FFA level increased gradually in order to return to its basal state. The comparison between model predictions and experimental data are provided in Figure 5.15. The model predictions are within one standard deviation of the experimental data.

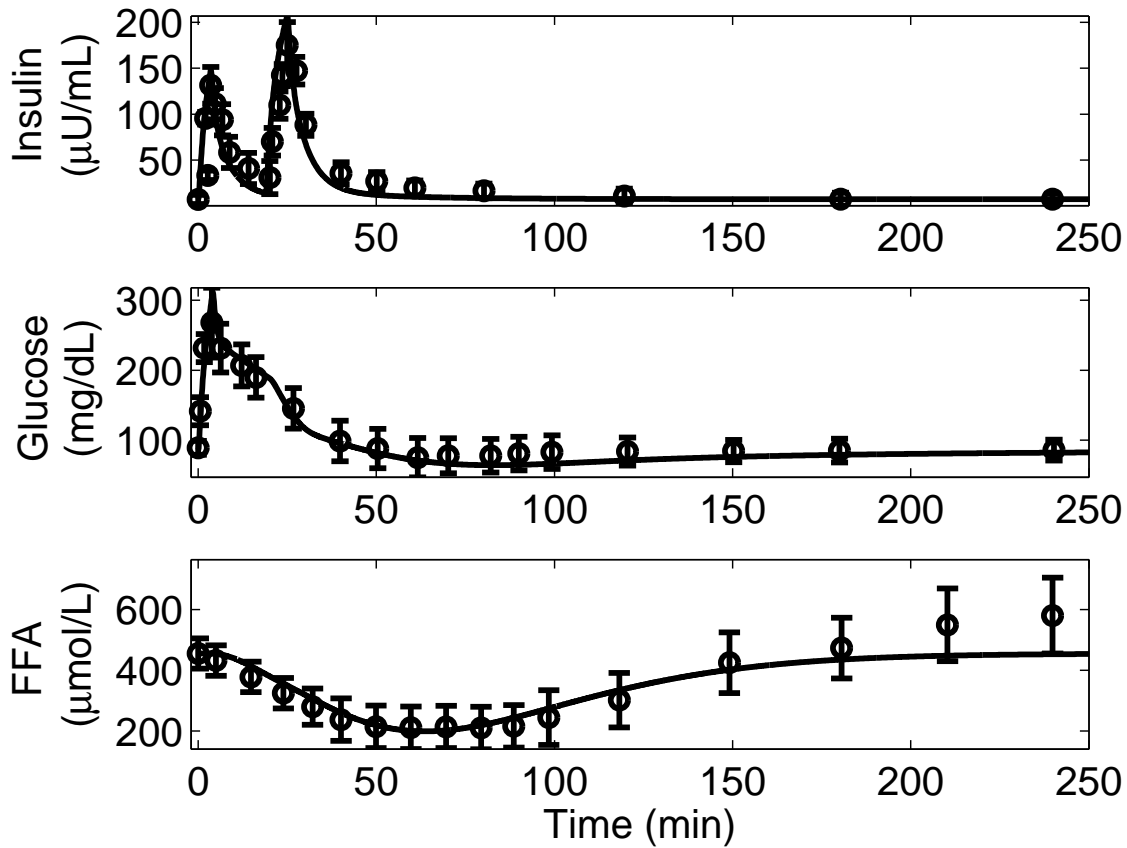


Figure 5.14: Model fit (line) and experimental data ($\mu \pm \sigma$) (circle) [17] of a MI-FSIGT test. Glucose bolus was infused at time (t) = 0 min and insulin boluses were infused at $t = 0 \text{ min}$ and $t = 20 \text{ min}$ to obtain predictions of insulin (top); glucose (middle); and FFA (bottom) concentrations

5.6.2.2 Effect of plasma FFA on plasma glucose levels: In order to validate the inhibitory effect of insulin on glucose uptake and insulin-mediated HGP suppression, a simulation study was performed where plasma FFA concentration was elevated at a rate similar to Staehr *et al.* [33]. Plasma insulin concentration was maintained at the basal level. Due to the elevation of plasma FFA level, plasma glucose concentration reached hyperglycemic levels, as shown in Figure 5.16.

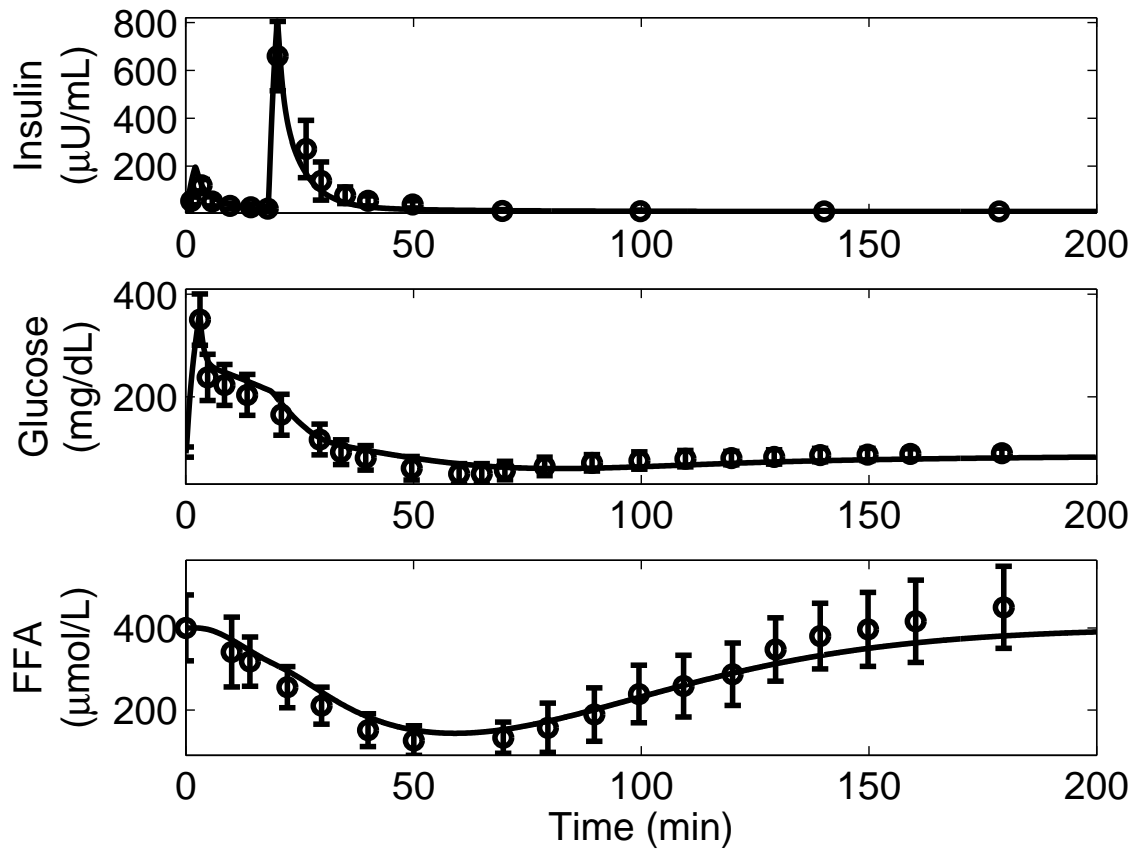


Figure 5.15: Model validation (line) versus experimental data ($\mu \pm \sigma$) (circle) [37] of a MI-FSIGT test. Glucose bolus was infused at time (t) = 0 min and insulin boluses were infused at $t = 0$ min and $t = 20$ min to obtain predictions of insulin (top), glucose (middle), and FFA (bottom) concentrations.

5.7 SUMMARY

In this chapter, a physiological FFA model was developed and incorporated with the existing glucose-insulin model of Sorensen [2]. The FFA model has the same structural formulation as the Sorensen model. Here, the human body was divided into seven physiologic compartments representing the major FFA utilizing organs/tissues. Mass balances were performed across

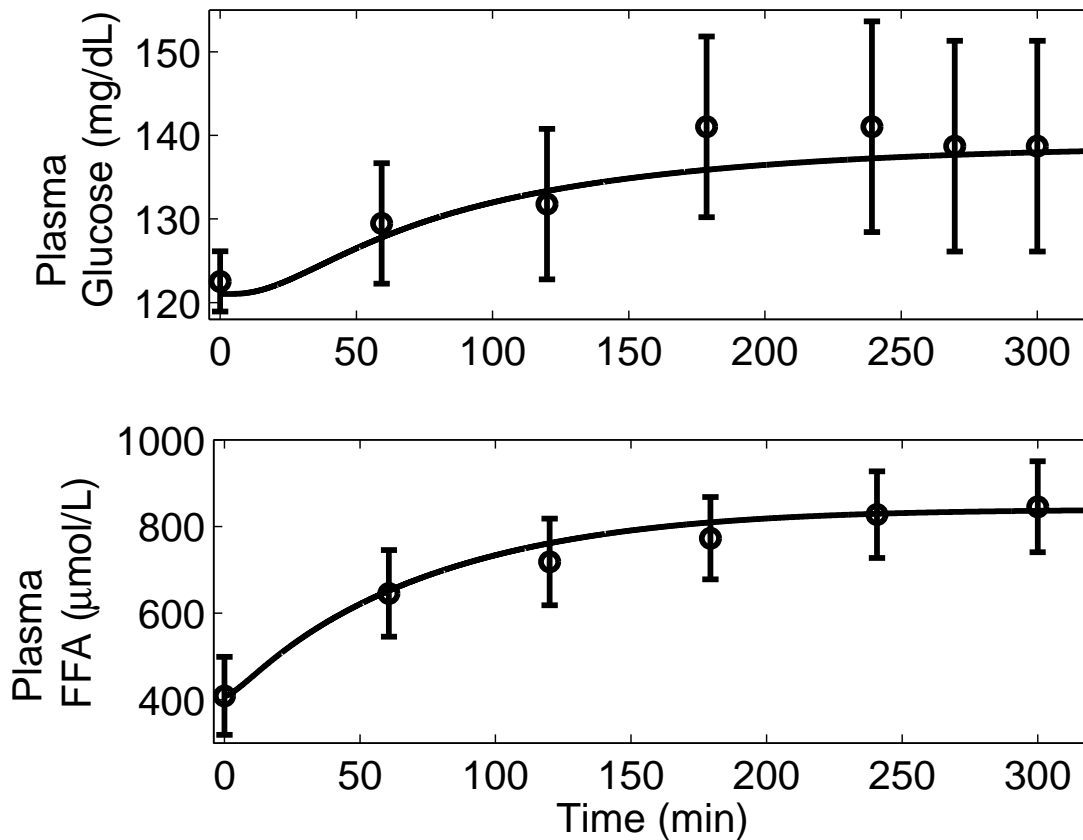


Figure 5.16: Model validation (line) versus experimental data ($\mu \pm \sigma$) (circle) [33] of the effects of high FFA levels on plasma glucose concentration. Plasma glucose concentration reached hyperglycemic levels (top) due to elevation of FFA concentration by lipid infusion (bottom)

each compartment to obtain the FFA distribution at various organ/tissue levels. Metabolic sinks and sources, representing the rate of FFA consumption and addition, respectively, were added to the compartments. The insulin model [2] was linked with the FFA model at the AT compartment to capture the anti-lipolytic effect of insulin. In order to capture the effects of fatty acids on glucose, the FFA model was linked with the glucose model [2] at the muscle and liver compartments. The physiologically-based model successfully emulated

insulin, glucose, and FFA concentrations after a MI-FSIGT test. The model is also capable of predicting the physiological effects of FFA on glucose at the organ/tissue level.

Such a detailed physiological model enables the diabetes research community to visualize the profiles of the major energy-providing substrates at the organ/tissue levels, particularly at the postprandial period. It also helps researchers to better understand the various physiologic interactions taking place between glucose, FFA, and insulin at the various body parts. But, such a level of detailed knowledge comes at the cost of model complexity. The physiologically-based model as proposed, consists of 34 ODEs. Even though the complexity of the model in terms of dynamic order and total number of parameters is high, majority of the physiologic parameters (*i.e.*, volumes and flow rates) can be directly obtained from the literature. The only estimated parameters were the trans-capillary time constants and those belonging to the metabolic sink/source equations.

The model is capable of generating ‘what-if’ scenarios to investigate the effect of fluctuating FFA levels on plasma glucose concentration. With the long-term goal of synthesizing an automatic closed-loop model-based insulin delivery system, this more complete physiologically-based model of the major energy-providing metabolic substrates gives the control community a more detailed model for use in control design. This detailed model could contribute substantially in developing a realistic (true-to-life) artificial pancreas, which would be capable of maintaining normoglycemia by rejecting disturbances such as mixed meal consumption.

6.0 MODEL PREDICTIVE CONTROL OF BLOOD GLUCOSE FOR T1DM PATIENTS¹

As mentioned in Chapter 1, the long-term goal is to develop a closed-loop artificial pancreas system to control blood glucose levels for T1DM patients. The three major components of an artificial pancreas are a continuous insulin pump, a continuous glucose sensor, and a control algorithm to regulate the insulin pump in order to maintain normoglycemia [48, 47, 65]. In a model-based control approach, a diabetic patient model is integrated in the controller, as shown in Figure 6.1. Based on the model output and the current measurement obtained from the sensor, the controller calculates the next manipulated input value. Theoretically, such a device can produce tight glucose control during pre- and post-prandial conditions [48]. Hence, fully automatic glucose control by an artificial pancreatic system can efficiently prevent or delay the chronic complications of hyperglycemia and lower the risk of hypoglycemia.

Various types of control algorithms for blood glucose control have been reported in the literature. Some of these algorithms include: Biostator and related nonlinear PD control [110, 112], PID control [117, 120, 188], optimal control [121, 122], MPC [65, 124, 126], control based on neural networks incorporating MPC [81, 189], advanced model-based control technique using parametric programming algorithms [190], *etc.* Some of these control algorithms were tested on T1DM patients [120, 126], whereas, others were mainly simulation studies. The main purpose of all of the published closed-loop algorithms is to maintain the blood glucose level near its basal value.

The control algorithm used in the first commercially available closed-loop insulin delivery system, Biostator, was adapted from the nonlinear control algorithm synthesized by Albisser *et al.* [110]. Mathematically, the Albisser algorithm can be expressed as follows:

¹Portions of this chapter have been published in [130]

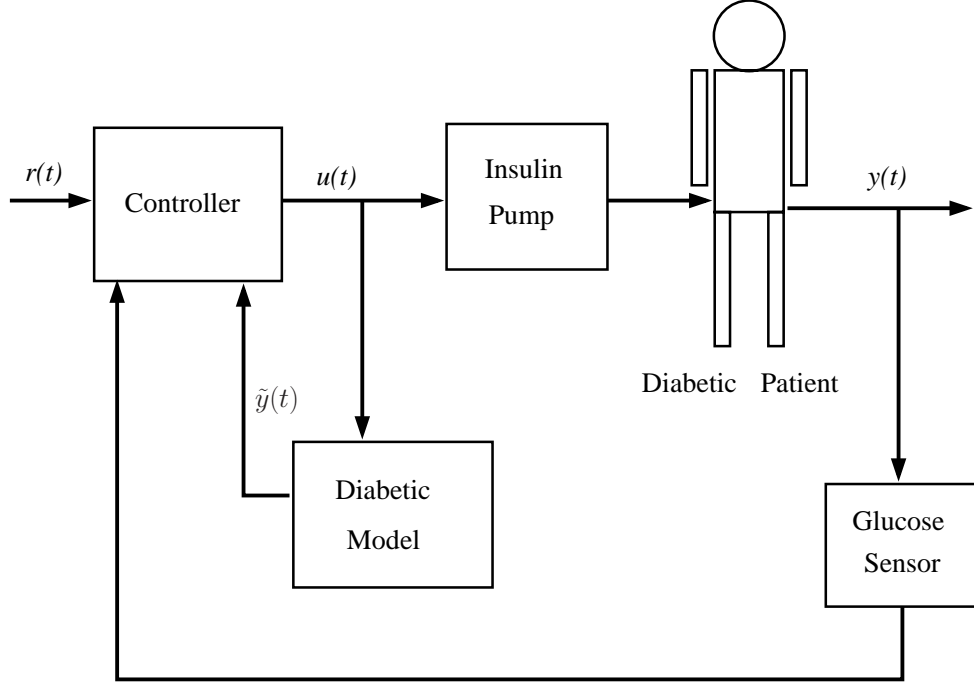


Figure 6.1: A schematic diagram of the closed-loop model-based insulin delivery system. Here, $r(t)$ is the desired glucose setpoint, $u(t)$ is the manipulated variable (exogenous insulin), $y(t)$ is the measured variable, and $\tilde{y}(t)$ is the model predicted output

$$u_i(t) = \frac{1}{2}M_i [1 + \tanh(S_i(G_p(t) - B_i))] \quad (6.1)$$

$$u_d(t) = \frac{1}{2}M_d [1 + \tanh(S_d(G_p(t) - B_d))] \quad (6.2)$$

Here, subscripts i and d represent insulin and glucose (dextrose) infusions, respectively. The insulin infusion was based on projected blood glucose, $G_p(t)$, which included a difference factor, $DF(t)$:

$$G_p(t) = G(t) + DF(t) \quad (6.3)$$

$$DF(t) = K_1 \left[\exp\left(\frac{dG(t)/dt}{K_2}\right) - 1 \right] \quad (6.4)$$

The rate of change of glucose ($dG(t)/dt$) was averaged over the previous 4 *min*. For adjusting insulin infusion rate, five tuning parameters were available (M_i , S_i , B_i , K_1 , and K_2). Later, Clemens *et al.* [112] modified the Albisser algorithm by including a quadratic function of the derivative of glucose with time in order to expedite the insulin infusion dynamics during post-prandial periods. All these Biostator-related algorithms can be classified as nonlinear PD controllers [48].

A closely studied control approach for the automated insulin delivery system is the PID controller [120, 117]. The PID algorithm has the following mathematical representation [191]:

$$u(t) = u_0 + k_c \left[e(t) + \frac{1}{\tau_I} \int e(t) + \tau_D \frac{de(t)}{dt} \right] \quad (6.5)$$

Here, $e(t)$ (error) is the difference between the desired glucose concentration and the measured glucose signal, $u(t)$ is the insulin infusion rate, and u_0 is the basal insulin infusion rate. The PID controller is composed of three functions: (i) a term directly proportional to the error (tuning parameter k_c); (ii) a correction proportional to the integral of the error (tuning parameter τ_I); and (iii) a term proportional to the derivative of the error (tuning parameter τ_D). The PID-based insulin pump currently under development by Medtronic MiniMed is aptly named as the external Physiologic Insulin Delivery (ePID) system [120, 117, 192, 51].

Linear quadratic (LQ) optimal control of blood glucose for diabetic patient, compares the model predicted output obtained from a linear state–space model of the glucose–insulin system with the actual measured output, updates the model, and calculates the next manipulated input value by minimizing a quadratic cost function [121, 122]. The cost function can be mathematically written as follows (adapted from [121]):

$$J(u) = \int_0^{\infty} \{ [x_1(t) - x_d]^2 + \rho u^2(t) \} dt \quad (6.6)$$

Here, x_d denotes a predetermined glucose setpoint value. $x_1(t)$ and $u(t)$ represent the state and input variables obtained from the state–space model. Constant ρ (> 0) is a weighting factor; higher values of ρ will make the control performance sluggish. The main goal here is

to determine the positive, bounded, control $u(t)$ in order to minimize the deviation of blood glucose from the desired setpoint while penalizing usage of large amounts of infused insulin.

One of the most promising control approaches for diabetes is MPC [6, 65, 124, 126]. It was primarily developed by the petrochemical industry in the 1970s to control large-scale constrained processes with many manipulated inputs and measured outputs [193]. Compared to a LQ controller, a model predictive controller is more robust to measurement noise and plant-model mismatch [194], which is primarily a result of the MPC controller being a discrete-time relaxation of the LQ controller in the linear model case. The gained robustness is critical in the diabetes implementation given the prevalence of glucose sensor noise and model inaccuracy (both structural and parametric). Also, nonlinear MPC formulations can be constructed and constraints are handled in a straightforward manner in the optimization problem. A detailed description of the model predictive controller is presented in the following Section (6.1).

6.1 MODEL PREDICTIVE CONTROLLER

The MPC controller solves an optimization problem at each time step by calculating the manipulated variable sequence (in this case, insulin delivery rate) that minimizes a user-specified objective function. The optimization scheme uses the process model (in this case, a diabetic patient model) to generate future output predictions. Based on these future model predictions (in this case, glucose concentration), the user-defined objective function is minimized by computing a manipulated variable sequence. Process measurements obtained at each sampling time are used to update the optimization, thus incorporating feedback in the control scheme. From the calculated manipulated variable sequence, only the first step is implemented, and the algorithm is repeated for the next sampling time [195].

The control algorithm minimizes the following 2-norm squared objective function:

$$\min_{\Delta U(k|k)} \|\Gamma_y(R(k+1|k) - Y(k+1|k))\|_2^2 + \|\Gamma_u \Delta U(k|k)\|_2^2 \quad (6.7)$$

Here, vectors $R(k+1|k)$ and $Y(k+1|k)$ of length p are the desired future glucose trajectory and the future model prediction resulting from the open-loop optimal control sequence vector $\Delta U(k|k)$ of length m (where, $m \leq p$). The goal is to minimize the objective function (equation (6.7)) by manipulating $\Delta U(k|k)$. The first part of equation (6.7) represents the error in setpoint tracking, and the second part represents the penalization factor which restricts the controller from making drastic changes in the manipulated variable sequence. Γ_y and Γ_u are the weighing matrices for setpoint tracking and control move penalization, respectively. Controller tuning involves adjustments to the four parameters p , m , Γ_y , and Γ_u .

Figure 6.2 presents the schematic diagram of implementation of the MPC algorithm. The x-axis represents the time scale. The reference trajectory, representing the desired blood glucose concentration, is indicated by the horizontal dashed line. At current time, k , the diabetes model calculates blood glucose concentration for a predetermined future horizon p , in absence of further control action. The same model is used to calculate a sequence of control moves $(u(k), \dots, u(k+m-1))$, as indicated by the solid line, in order to minimize the objective function (equation (6.7)) subject to prespecified operating constraints so that the desired output behavior for p time steps into the future (dash-dotted line with circles) is obtained. To incorporate the unmodeled errors in the optimization process, glucose measurements from the sensor ($y_m(k)$) are obtained at every sampling time to compare with the model prediction ($y(k)$), and the prediction error, $\epsilon(k) = y_m(k) - y(k)$, thus obtained is used to update future predictions.

As the optimization process of MPC relies on the forecast of process behavior obtained from a model, therefore the process model is regarded as an essential component of the MPC [196, 195]. Based on the type of the model used and the constraints used, model predictive control algorithms can be classified into linear and nonlinear MPC. A linear model predictive controller (LMPC) refers to a particular case when the process model linear. A state-space linear model used in an LMPC has the following form (adapted from [195]):

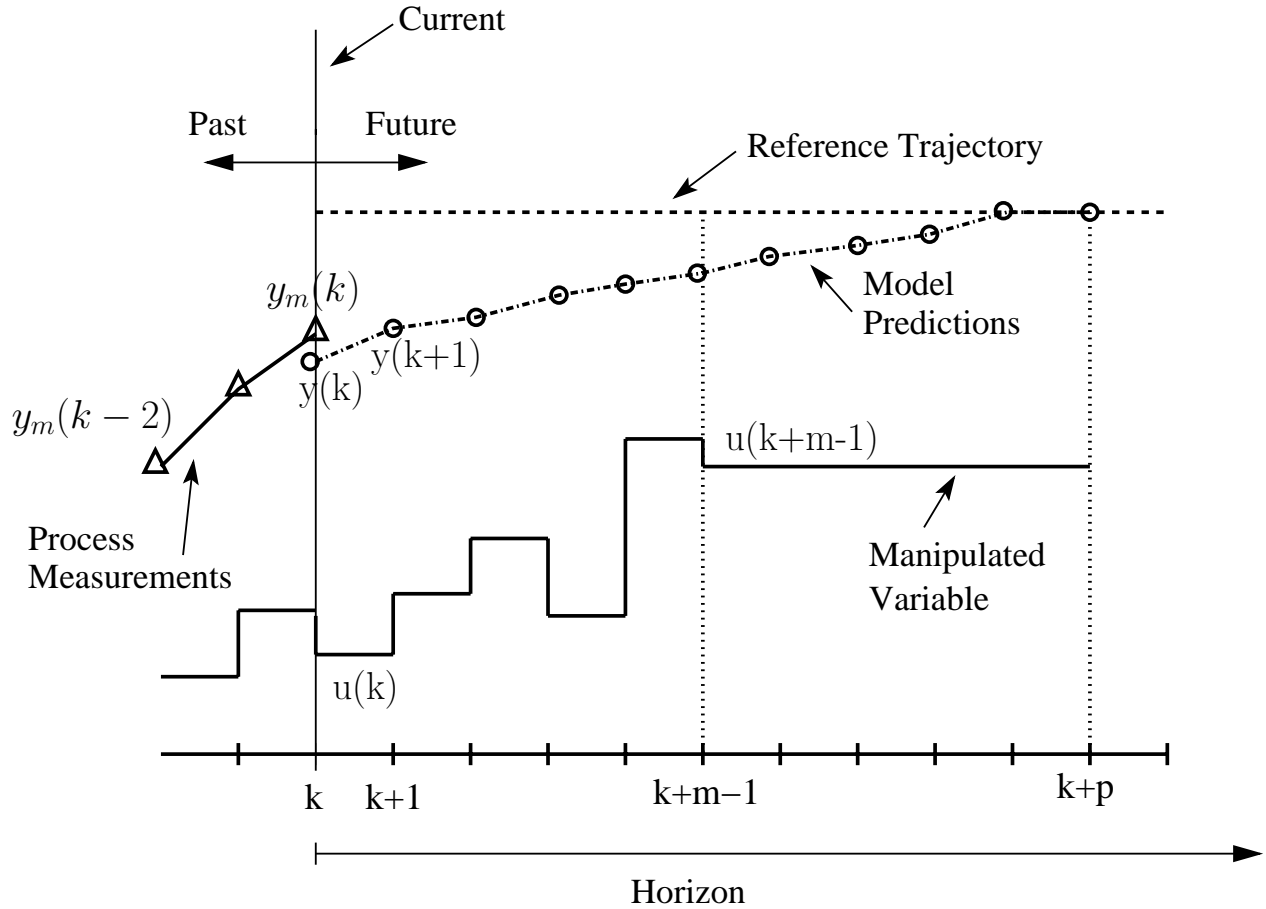


Figure 6.2: A schematic diagram of the MPC algorithm implementation

$$\frac{dx(t)}{dt} = Ax(t) + Bu(t) \quad (6.8)$$

$$y(t) = Cx(t) \quad (6.9)$$

Here, vector $x(t)$, $y(t)$, and $u(t)$ represent state variables, measured output variables, and input variables. A , B , and C are constant coefficient matrices. A quadratic objective function is commonly used for the online optimization subjected to linear input and output constraints (if present).

In case of a nonlinear model predictive controller (NMPC), a nonlinear process model is used. The motivation of using a nonlinear model is the possibility to improve control action by improving the quality of the forecasting, particularly in systems with a high degree of nonlinearity [196, 195]. A state space form of a nonlinear model used in a MPC can be written as follows (adapted from [196]):

$$\frac{dx(t)}{dt} = f(x(t), u(t)) \quad (6.10)$$

$$y(t) = g(x(t)) \quad (6.11)$$

Functions $f(\cdot, \cdot)$ and $g(\cdot)$ are smooth nonlinear mappings for the state and output variables, respectively. The objective function can be non-quadratic. In addition, the optimization problem can be subjected to nonlinear input and output constraints.

The MPC has an edge over the other control algorithms for blood glucose control because of its characteristics. For example, an unconstrained MPC can guarantee optimal insulin dosage when $\Gamma_u = 0$ [127]. Also for safety reasons and mechanical limitations of the pump, input constraints can be intrinsically formulated in the MPC algorithm [127]. Moreover, the MPC can take control actions much before a hyper- or hypo-glycemic event has occurred under certain formulations. Successful implementation of MPC for meal disturbance rejection in simulations and to maintain glucose homeostasis during fasting state in T1DM patients can be found in [65, 124] and [126], respectively.

Previously, closed-loop simulation studies have been performed to evaluate the performance of MPC in the presence of a CHO-containing meal disturbance [65, 124]. Closed-loop performance in response to mixed meal containing fat and protein along with CHO has been ignored, mainly due to lack of lipid-based metabolic models. In this chapter, performance of closed-loop MPC algorithms for maintenance of normoglycemia in presence of mixed meals was evaluated. In Section 6.2.1, both NMPC and LMPC algorithms were synthesized based on the extended minimal model from Chapter 2. In the following Section (6.2.2), a separate closed-loop simulation study was performed where both NMPC and LMPC algorithms were

developed by using the composite model from Chapter 4. Finally, the Chapter ends with a brief Summary 6.3.

6.2 CLOSED-LOOP SIMULATION OF MIXED MEAL DISTURBANCE REJECTION

6.2.1 MPC Formulation Based on the Extended Minimal Model

Both linear and nonlinear MPC algorithms were synthesized based on the extended minimal model for disturbance rejection from mixed meal ingestion. The optimization problem was solved by minimizing the quadratic objective function as presented in Equation (6.7). In a diabetic system, input magnitude constraints are essential, mainly for safety reasons. This makes the MPC an ideal candidate for the glucose-insulin feedback system, as the algorithm can explicitly enforce constraints. It has been observed that the plasma insulin level can reach upto $70 \frac{\mu U}{ml}$ in healthy patients after consumption of 108 g of mixed meal [10]. Hence the upper bound of insulin delivery rate was set at $100 \frac{mU}{min}$ which corresponded to a plasma insulin concentration of $69.5 \frac{\mu U}{ml}$. The insulin input magnitude bounds used for the simulation study can be written as:

$$0 \leq U(k|k) \leq 100 \frac{mU}{min} \quad (6.12)$$

In order to make sure that the maximum change in insulin delivery rate is not higher than the mechanical characteristics of the pump, a maximum rate of change of input constraint was employed as shown below:

$$|\Delta U(k)| \leq 50 \frac{mU}{min \cdot \Delta T_s} \quad (6.13)$$

In case of the NMPC (NMPC_{E-E}), the controller model was represented by the extended minimal model developed in Chapter 2. For simulation purposes, the diabetic patient

measurements were also obtained from the extended minimal model, thus assuming a perfect model scenario (no plant-model mismatch). For the LMPC (LMPC_{E-LE}) case, the extended minimal model was linearized using a first-order Taylor series expansion (see Appendix). Plant-model mismatch was considered by incorporating the unmodeled disturbances at every sampling time (ΔT_s) given by the difference between the plant (patient) measurement, obtained from the original extended minimal model, and the controller model output represented by the linearized extended minimal model. A mixed meal of 108 g (CHO = 70 g, protein = 18 g, and FFA = 20 g) was consumed by the simulated patient, at $t = 20$ min. Gut absorption kinetics of the nutrients from mixed meal into the circulatory system was captured by the meal model presented in Section 2.5.1. The controller tuning parameters were adjusted such that the setpoint sum squared error (SSE) (*i.e.*, the deviation of glucose concentration from the reference trajectory) was minimized. Best controller performance was achieved when the tuning parameters were: $p = 10$, $m = 2$, $\Gamma_y = 1$, and $\Gamma_u = 0.002$; sampling time (ΔT_s) was set at 5 min. Comparison between the NMPC_{E-E} and the LMPC_{E-LE} are provided in Figure 6.3. It can be observed that the performance of LMPC_{E-LE} is closely comparable with the performance of NMPC_{E-E} (Table 6.1).

For comparison purposes, another set of NMPC (NMPC_{E-B}) and LMPC (LMPC_{E-LB}) algorithms were synthesized. For the NMPC_{E-B} formulation, the model was represented by the original Bergman minimal model [1] (from Section 2.1) and the patient (plant) measurements were obtained from the original extended minimal model. In case of the LMPC_{E-LB} formulation, a linearized version of the Bergman minimal model (see Appendix) was used to represent the controller model and, once again, the patient measurements were obtained from the original extended minimal model. A mixed meal of equal mass and composition as above was consumed by the simulated patient. Unlike the extended minimal model, the Bergman model and its linearized version does not consider FFA dynamics. Tuning parameters and input constraints were the same as above. Closed-loop simulation results of LMPC_{E-LE}, NMPC_{E-B}, and LMPC_{E-LB} are shown in Figure 6.4. Based on the simulated performance of the three controllers (see Table 6.1), it can be concluded that LMPC_{E-LE} provides a tighter glucose control than the NMPC_{E-B} or LMPC_{E-LB}. The oscillation in the closed-loop performances of NMPC_{E-B} and LMPC_{E-LB} is due to the

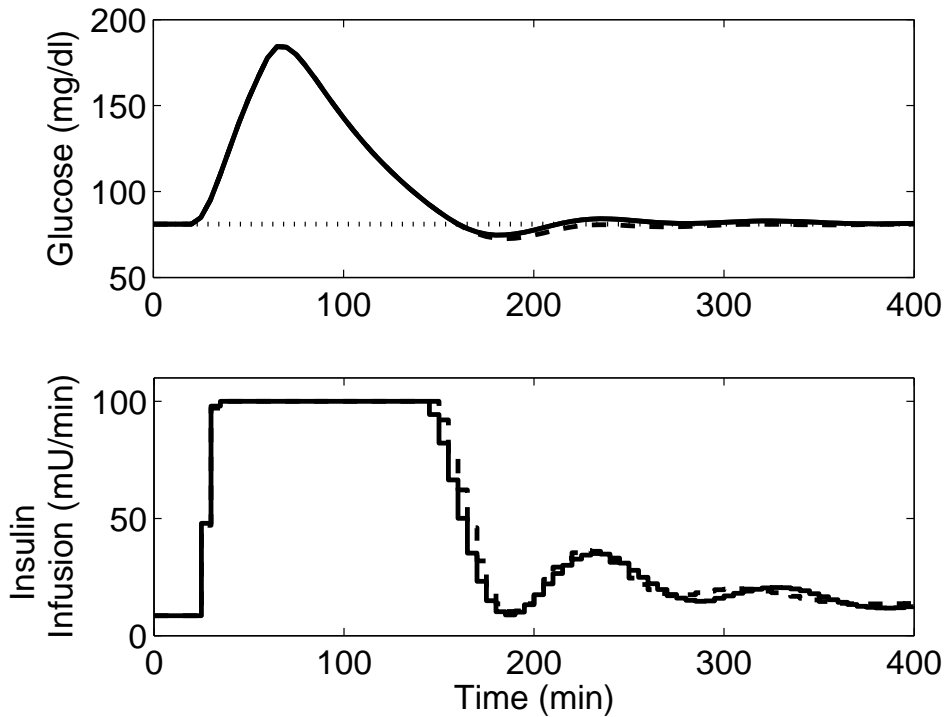


Figure 6.3: Comparison between mixed meal disturbance rejection by LMPC_{E-LE} (solid line) and NMPC_{E-E} (dashed line) with input constraint. Setpoint (dotted line) is set at $81 \frac{\text{mg}}{\text{dl}}$

plant-model mismatch between the extended minimal model (plant) and the original/linear Bergman minimal model (controller model). Presence of FFA dynamics in the extended minimal model caused the plasma glucose to subside slower than the Bergman minimal model (original/linear) after consumption of a mixed meal.

6.2.2 MPC Formulation Based on the Composite Model

In order to evaluate the closed-loop performance of the composite model developed in Chapter 4, both LMPC and NMPC algorithms were developed based on the composite model. Once again, the objective of the closed-loop simulation was to maintain normoglycemia by

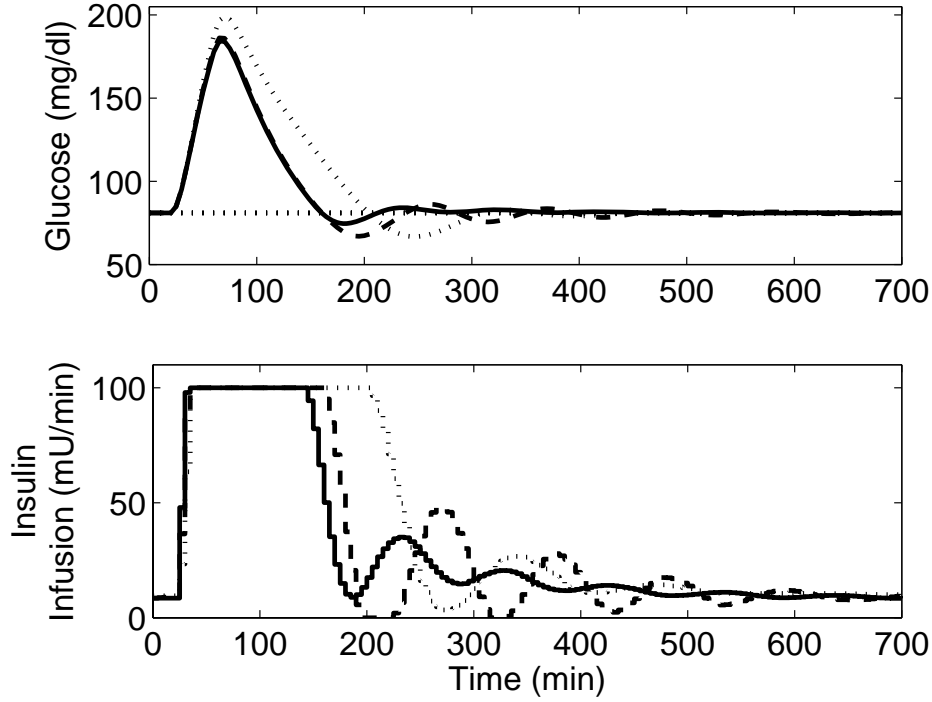


Figure 6.4: Comparison between mixed meal disturbance rejection by LMPC_{E-LE} (solid line), NMPC_{E-B} (dashed line), and LMPC_{E-LB} (dotted line) with input constraint. Setpoint (dotted line) is set at $81 \frac{mg}{dl}$

Table 6.1: Performance of NMPC_{E-E} , LMPC_{E-LE} , NMPC_{E-B} , and LMPC_{E-LB}

	NMPC_{E-E}	LMPC_{E-LE}	NMPC_{E-B}	LMPC_{E-LB}
Maximum glucose (mg/dL)	184.2	184.2	186.2	199
Minimum glucose (mg/dL)	74.61	72.48	66.87	66.74
99% Settling time (min)	355	355	545	435
Setpoint SSE	1.007e5	1.007e5	1.066e5	1.026e6
Infused insulin above basal (mU)	14620	14633	15845	19621

rejecting disturbances from mixed meal ingestion. The insulin infusion magnitude constraint and the maximum rate of change of insulin infusion were same as equations (6.12) and (6.13),

respectively. The quadratic objective function, as presented in equation (6.7), was minimized to achieve the desired control action.

For the NMPC (NMPC_{PB-C}) case, the in-built controller model was represented by the composite model. To simulate the diabetic patient (plant), a physiologically-based metabolic model from Chapter 5 was used. This strategy of using a higher-order model for the plant and a lower-order model for the controller model introduced a plant-model mismatch in the closed-loop system; a phenomenon which is expected if implemented in a clinical setup due to inter- and intra-patient variability. In case of the LMPC (LMPC_{PB-LC}), the composite model was linearized using a first-order Taylor-series expansion, just like the previous section (see Appendix). The linearized composite model represented the controller model and patient data was obtained from the physiologically-based metabolic model for feedback to the controller in order to incorporate the unmodeled errors. A mixed meal of same size and composition as the previous section (108 g of 65% CHO, 17% protein, and 18% fat) was ingested by the simulated patient at $t = 20 \text{ min}$. The controller tuning parameters were adjusted such that sum-squared deviation of glucose concentration from reference trajectory ($81 \frac{\text{mg}}{\text{dl}}$) was minimized. Best closed-loop performance was achieved at $p = 18$, $m = 2$, and $\Gamma_y = 2$ and $\Gamma_u = 0.02$. Once again, measurements were obtained at every 5 min intervals. Comparison between the closed-loop simulations of NMPC_{PB-C} and LMPC_{PB-LC} are provided in Figure 6.5. It is clearly noticeable that NMPC_{PB-C} (solid lines in Figure 6.5 (top)) produced tighter glucose control. In case of the LMPC_{PB-LC}, hypoglycemia was reached after 170 min of meal consumption and blood glucose remained suppressed below the normal level for more than 200 min. The mismatch between the plant data obtained from the physiologically-based model and the model prediction procured from the linearized composite model was significantly high when the insulin infusion rate deviated more than 4-fold of its basal value, thereby causing hypoglycemia.

For comparison purposes, LMPC and NMPC algorithms were developed using the Bergman minimal model [1] (Section 2.1). In case of the NMPC (NMPC_{PB-B}), the controller model was represented by the original Bergman minimal model, whereas the diabetic patient was simulated by the physiologically-based metabolic model. Input constraints and controller tuning parameters were used as above. As pointed out by Quon *et al.* [87] and Cobelli *et al.*

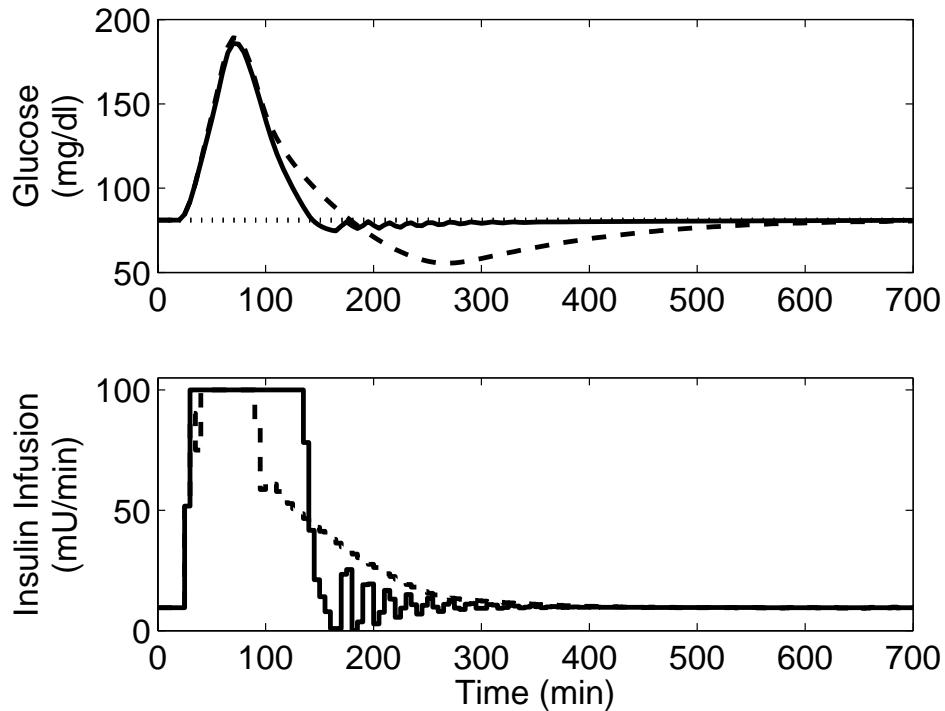


Figure 6.5: Comparison between mixed meal disturbance rejection by NMPC_{PB-C} (solid line) and LMPC_{PB-LC} (dashed line) with input constraints. Setpoint (dotted line) is set at $81 \frac{\text{mg}}{\text{dl}}$

[5], the parameters of the minimal model estimated from unlabeled (cold) IVGTT data [1], as presented in Table 2.1, resulted in underestimation of insulin sensitivity and overestimation of glucose effectiveness. The disparity in insulin sensitivity between the plant and model resulted in a sustained oscillation of the blood glucose during a closed-loop simulation of mixed-meal disturbance rejection, as shown in Figure 6.6.

To overcome this limitation, parameter values of p_1 , p_2 , and p_3 of the minimal model (equations (2.3) and (2.2) in Chapter 2) were obtained from Cobelli *et al.* [5], where parameter estimation was performed by fitting cold and hot (labeled) IVGTT data, simultaneously. Glucose effectiveness and insulin sensitivity values obtained from the revised (hot and cold) minimal model were almost identical to the measured values procured by the hepatic arterial-

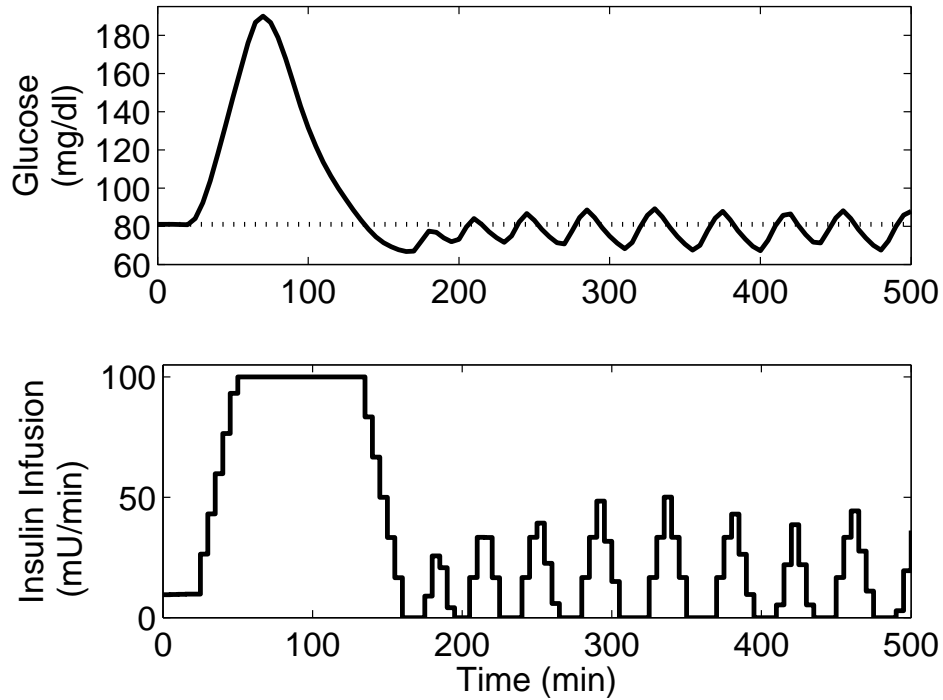


Figure 6.6: Mixed meal disturbance rejection by NMPC_{PB-B} with input constraints. Setpoint (dotted line) is set at $81 \frac{\text{mg}}{\text{dl}}$. Controller model parameters were obtained from Bergman *et al.* [1].

venous difference technique [5], thereby validating the model estimates. The new parameter values of the minimal model are provided in Table 6.2. A more stable closed-loop performance of the NMPC_{PB-B} was obtained by using the minimal model with the new parameter values, as shown by the solid lines in Figure 6.7 (top).

The LMPC (LMPC_{PB-LB}) algorithm was developed based on a linearized version of the Bergman minimal model. Once again, patient data was obtained from the physiologically-based model. Closed-loop performance of the LMPC_{PB-LB} algorithm is presented in Figure 6.7 (dashed-lines). Due to plant-model mismatch, both the NMPC_{PB-B} and LMPC_{PB-LB} algorithms produced hypoglycemic events; especially, in the case of LMPC_{PB-LB} the minimum glucose concentration was dangerously low. The performances of all the four control

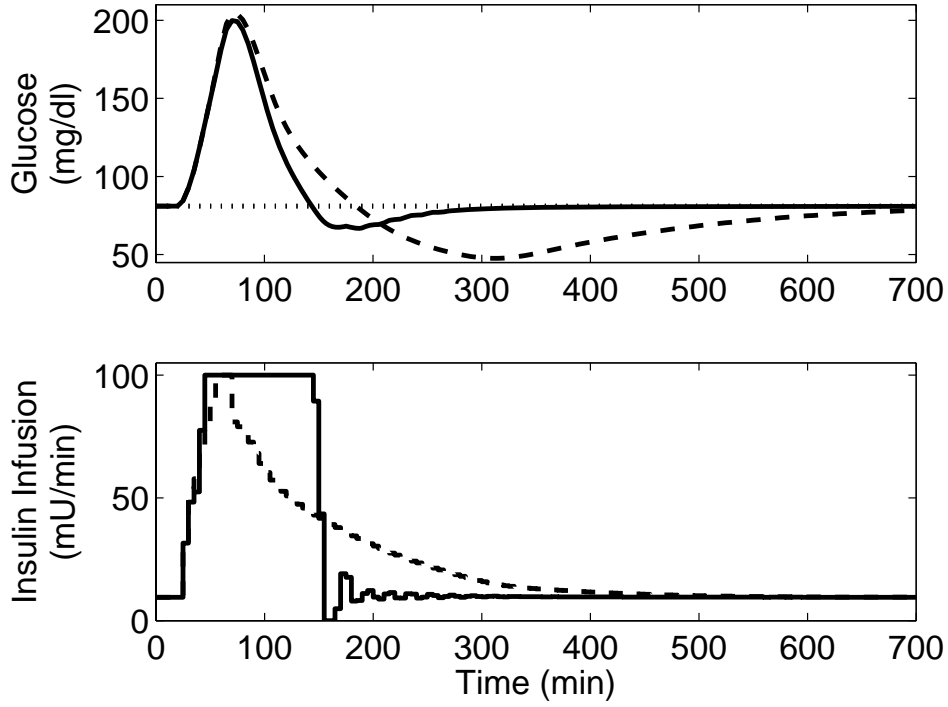


Figure 6.7: Comparison between mixed meal disturbance rejection by NMPC_{PB-B} (solid line) and LMPC_{PB-LB} (dashed line) with input constraints. Setpoint (dotted line) is set at $81 \frac{mg}{dl}$. The Bergman minimal model parameters were obtained from Table 6.2.

Table 6.2: New Parameters of the Bergman minimal model, from [5]

Parameter	Value	Unit
p_1	0.0092	$\frac{1}{min}$
p_2	0.116	$\frac{1}{min}$
p_3	0.00068	$\frac{1}{min}$

algorithms are highlighted in Table 6.3. It is quite evident that NMPC_{PB-C} produced the tightest glucose control. Both the LMPC algorithms caused blood glucose concentration to reach below $60 \frac{mg}{dl}$, which could be a source of major concern as hypoglycemia may lead to

unconsciousness or even death. Once again, the closed-loop simulation results revealed that incorporation of FFA dynamics significantly improved the controller performance.

Table 6.3: Performance of NMPC_{PB-C} , LMPC_{PB-LC} , NMPC_{PB-B} and LMPC_{PB-LB}

	NMPC_{PB-C}	LMPC_{PB-LC}	NMPC_{PB-B}	LMPC_{PB-LB}
Maximum glucose (mg/dL)	186	189.2	199.2	204
Minimum glucose (mg/dL)	74.65	55.47	66.77	47.59
99% Settling time (min)	415	650	345	820
Setpoint SSE	9.228e4	1.119e6	1.538e5	1.119e6
Infused insulin above basal (mU)	10495	10404	10541	10150

For comparison purposes, a closed-loop NMPC formulation (NMPC_{PB-PB}) was designed with no plant-model mismatch. In other words, the model was assumed to be perfect. Hence, both the plant (patient) and the controller model were represented by the physiologically-based model (from Chapter 5). In such an ideal case, best possible glucose control is expected due to the absence of unmodelled errors. A mixed meal of the same size and composition as the above cases was ingested at $t = 20 \text{ min}$. No alterations were made to the controller tuning parameters. The simulation results as shown in Figure 6.8 (and Table 6.4) revealed a much superior control performance than any other previously studied closed-loop formulations in terms of the minimum glucose level, and 99% settling time.

6.3 SUMMARY

For a tighter blood glucose control of T1DM patients, the current focus is on developing automated closed-loop insulin delivery systems. One of the most optimistic approaches for controlling an insulin pump is the MPC algorithm. In this chapter, both nonlinear and linear MPC algorithms were developed to evaluate the effects of FFA on closed-loop glucose control. The simulated controller performances were evaluated by perturbing the system with mixed meal ingestion. MPC algorithms based on the extended minimal model (Chapter 2) and the composite model (Chapter 4) provided a tighter glucose control as compared to MPC

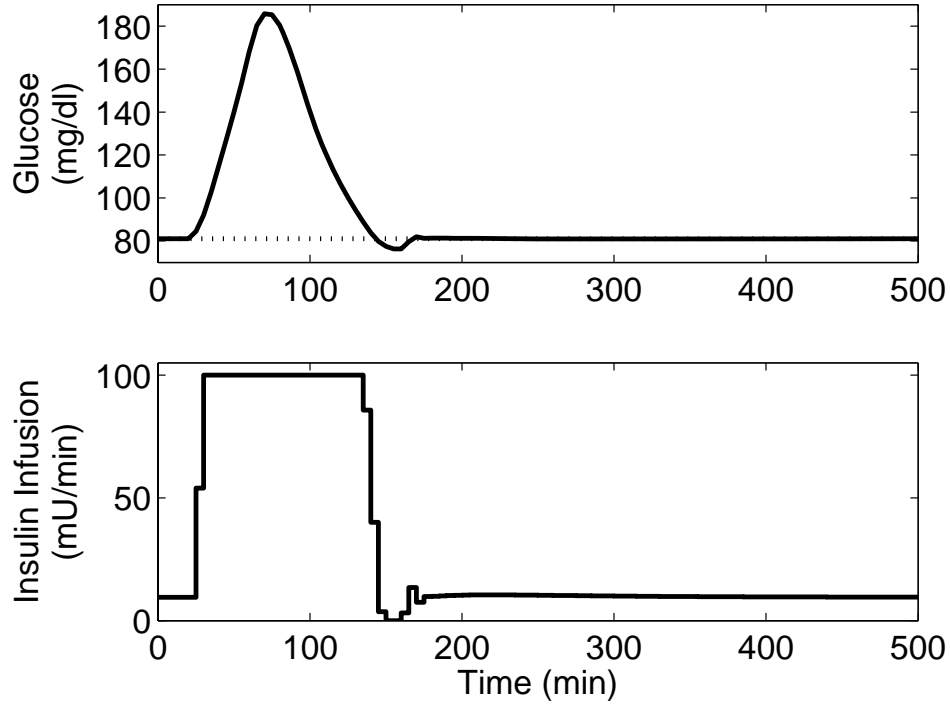


Figure 6.8: Mixed meal disturbance rejection by NMPC_{PB-PB} with input constraints. Setpoint (dotted line) is set at $81 \frac{mg}{dl}$

Table 6.4: Performance of NMPC_{PB-PB}

	NMPC_{PB-PB}
Maximum glucose (mg/dL)	185.8
Minimum glucose (mg/dL)	76.25
99% Settling time (min)	165
Setpoint SSE	9.163e4
Infused insulin above basal (mU)	10250

algorithms based on the Bergman minimal model [1]. Hence, the simulated results indicated that inclusion of FFA absorption from mixed meal and its interactions with glucose improved the quality of the controller performance.

In case of plant-model mismatch simulations, where the plant was represented by the higher-order physiologically-based model (Chapter 5), the NMPC performances were far superior than the LMPC formulations. Prolonged hypoglycemia was observed for LMPC_{PB-LC} and LMPC_{PB-LB}. The deviation in glucose prediction between the linearized models and their original nonlinear forms was significantly high when the insulin infusion rate exceeded 4-fold of its basal value. This is mainly due to the presence of the saturation terms in the physiologically-based model describing the effects of insulin on glucose uptake and hepatic glucose production rates. During higher insulin infusion rates (4-fold above basal), the effects of insulin on tissue glucose uptake and hepatic glucose production rates reach a saturation point for the physiologically-based model. Such a biologically-relevant characteristic is absent in the linearized composite or the Bergman minimal model (both linear and nonlinear forms). The LMPC formulations, especially LMPC_{PB-LC}, performed far better when the mixed meal load was reduced to 67 g with the same composition (which is equivalent to approximately 50 g of glucose).

The simulated results demonstrated the capability of the closed-loop algorithms to produce tight blood glucose control by rejecting disturbances from meals containing all the major nutrients. The inclusion of gut absorption of FFA and protein, along with glucose in the closed-loop simulation might prove to be beneficial for the control community in development of robust automated artificial pancreas equipped to handle disturbances which are confronted in real life. In order to minimize hypoglycemic events after meal consumption without sacrificing controller aggressiveness, the MPC framework can be tailored by altering the objective function [6, 128]. More details of such advanced control strategies are provided in Chapter 7.

Efforts have been made to develop automated insulin delivery systems since the 1960s [109]. Commercial pumps to deliver insulin subcutaneously have been available since the 1980s [197], continuous glucose monitoring sensors have been available since the late 1990s [198], and controller algorithms for delivery of insulin have been in development since the early 1960s [69]. Still, there are many reasons that not a single closed-loop automated insulin delivery pump is available commercially [188]. Starting with the continuous glucose sensors, the accuracy of such a device is in the 15 - 20% error range [199]. Also the

reliability of continuous monitoring systems is questionable mainly because of the time lag due to glucose equilibration between blood and subcutaneous interstitial fluid [200]. Insulin delivery is likely to be either intravenous using an external insulin pump (as shown in Figure 6.1), or intraperitoneal using an implantable pump [188]. Both delivery sites introduce additional dynamics in the insulin kinetics [201]. Closed-loop algorithms have not adequately demonstrated ability to efficiently handle these delays especially during meal intake and exercise [188]. Also, closed-loop controller performance is significantly affected by the intra-patient variability of insulin sensitivity throughout the day [188, 201]. Extensive research and validation is still required before a fully automated insulin delivery system could be used by a T1DM patient at home.

7.0 SUMMARY AND FUTURE RECOMMENDATIONS

The work presented in this dissertation focused on incorporation of the physiological effects of FFA and exercise into existing glucose-insulin metabolic models [1, 2]. Both low-order semi-empirical model structures and higher-order physiologically-based model structures were investigated. A mixed meal model was also developed to emulate the absorption kinetics of major nutrients (CHO, protein, and fat) present in a mixed meal into the circulatory system. The meal model outputs served as disturbance inputs for the metabolic models. One of the major goal of developing metabolic models accounting for all the major energy-providing metabolites was to evaluate the closed-loop performance of a model-based controller in maintaining normoglycemia during the post-prandial period, particularly after ingestion of a mixed meal. Hence, MPC algorithms were synthesized based on the newly developed metabolic models for maintenance of glucose homeostasis. The contribution of each of the investigations have been presented in the summary section of each chapter. The following section once again summarizes the major findings of this dissertation.

7.1 SUMMARY

7.1.1 Semi-Empirical Metabolic Models

The glucose-insulin metabolic model developed by Bergman *et al.* [1] was extended to include FFA dynamics and its interactions with glucose and insulin. Three additional ODEs were added to the original model to capture the dynamics of plasma FFA, the anti-lipolytic action of insulin on FFA, and the inhibitory effect of FFA on glucose uptake rate. Due to inclusion

of FFA dynamics, the extended minimal model in its present form is capable of predicting FFA fluctuations and its effects on plasma glucose dynamics. Also, the extended minimal model coupled with a mixed meal model can be utilized to determine the dynamics of plasma glucose and FFA after mixed meal ingestion of varying sizes and compositions. This more complete minimal model of the major energy-providing metabolic substrates may provide the control community a better tool for the design of model-based controllers.

In a separate study, a semi-empirical model of exercise effects on the glucose-insulin system was developed. Once again, the Bergman minimal model [1] was extended to incorporate mild-to-moderate exercise effects on plasma glucose and insulin. Linear ODEs were added in the model to capture the exercise-induced accelerated clearance rate of plasma insulin, elevated glucose consumption rate, and increased hepatic glucose production rate. During prolonged exercise, the model successfully captured the decline in hepatic glucose production due to depletion of the rate of glycogenolysis leading towards hypoglycemia. With the ultimate goal of developing a closed-loop model-based insulin delivery system, it is essential to synthesize control-relevant metabolic models that are capable of predicting fluctuations in glucose dynamics during exercise. Hence, the exercise minimal model can provide the control community an alternative tool for use in controller design for maintenance of glucose homeostasis especially during exercise. Open-loop simulations from such models can also give prior intimation to T1DM patients regarding the time-span during which exercise could be performed at a given intensity without reaching hypoglycemia.

Although, the extended minimal model developed in Chapter 2 successfully captured FFA, glucose, and insulin dynamics, the effects of exercise on these metabolites and hormones were neglected. Similarly, the exercise minimal model developed in Chapter 3 successfully captured the effects of exercise on plasma glucose and insulin levels; however, the model overlooked the contributions (interactions) of FFA. Hence, in order to obtain a single metabolic model capturing the effects of FFA and exercise, a composite model was developed by integrating the extended minimal model with the exercise minimal model. To make the composite model more biologically relevant, necessary modifications were made to the original model structures. The model consisted of four parts capturing the insulin, glucose, FFA, and exercise dynamics. The dynamical effects of insulin on glucose and FFA were

divided into three sections: the anti-lipolytic action to suppress endogenous FFA release; the gluco-regulatory action to promote glucose uptake in the tissues; and, the suppression of hepatic glucose production. Parameters of the insulin action on glucose were fitted by using labeled-IVGTT data which facilitated separation of insulin action on glucose utilization and production. Exercise effects on insulin, glucose, and FFA were divided into five sections. Mainly, these effects are the exercise-mediated plasma insulin clearance, elevated glucose uptake and production rate during exercise, and elevated FFA uptake and production rate during exercise. The model also captured the decline of plasma glucose concentration during prolonged exercise due to the depletion of glycogen leading to a decrease in the rate of hepatic glycogenolysis. The model can be used in development of model-based controller for blood glucose control particularly in presence of disturbances from mixed meal ingestion, as well as exercise.

7.1.2 Physiologically-Based Metabolic Model

A detailed physiologically-based circulation model of FFA was developed, where the body was divided into compartments representing the major organs/tissues. FFA was distributed to each of these physiologic compartments via the circulatory system. Mass balances were considered at each compartment to obtain the FFA distribution at various organ/tissue levels. Metabolic sinks and sources were added to represent the rate of FFA consumption and addition at various organs and tissues, respectively. The FFA model was integrated with the existing glucose-insulin model developed by Sorensen [2], which has a similar structure. The model successfully captured the glucose, FFA, and insulin dynamics after a modified insulin-frequently sampled intravenous glucose tolerance test. It also captured the effects of FFA on tissue glucose uptake rate and hepatic glucose production rate.

Such a detailed model can prove to be a valuable tool for the diabetes research community for better understanding of the various physiologic interactions taking place between glucose, FFA, and insulin at the organ/tissue levels. The integrated physiologically-based model accounting for all the major energy-providing substrates has a better chance of accurately predicting glucose concentration at the major organs/tissues after consumption of a mixed

meal. The model can also provide more insight regarding the combined effects of insulin and FFA on hepatic glucose production rate. However, such in-depth knowledge comes at the cost of model complexity in terms of number of states and parameters.

7.1.3 Model-Based Control of Blood Glucose for T1DM

Both linear and nonlinear MPC were developed to evaluate the effects of mixed meal ingestion on closed-loop performance of blood glucose control. The MPC algorithms were tested after perturbing the system with mixed meal ingestion. The control algorithms based on the extended minimal model (Chapter 2) and the composite model (Chapter 4) provided superior blood glucose control when compared to controller based on the Bergman minimal model [1]. Hence, the closed-loop results indicated that inclusion of FFA dynamics and its interactions with glucose improved the quality of the controller performance in rejecting disturbances from mixed meal ingestion. In case of the plant-model mismatch, the patient data (plant) was obtained either from the extended minimal model or the physiologically-based model (Chapter 5), and the controller model was represented either by the composite model or the Bergman minimal model. The nonlinear MPC formulations provided a tighter glucose control in terms of maximum glucose level, minimum glucose level, and 99% settling time, than the linear MPC formulations.

7.2 FUTURE RECOMMENDATIONS

7.2.1 Incorporating Exercise Effects in the Physiologically-Based Model

The physiologically-based model developed in Chapter 5 did not include the exercise effects on FFA, glucose, and insulin. As discussed earlier, exercise plays a significant role in altering the dynamics of the major energy-providing metabolites. With the long-term goal of developing model-based controllers for the maintenance of glucose homeostasis by rejecting disturbances from mixed meal ingestion and exercise, it is essential to develop accurate

metabolic models capturing all the major energy-providing metabolites (glucose and FFA) at rest and during exercise.

Lenart and Parker [202] modified the physiologically-based glucose-insulin model developed by Sorensen [2] to incorporate the effects of short-term mild-to-moderate exercise. The model captured the changes in blood flow dynamics associated with exercise. An increase in glucose uptake by the active muscles during exercise was also captured successfully for $t < 90 \text{ min}$. However, the model as proposed considered liver to be an infinite source of glucose in the form of glycogen, which is not physiologically accurate.

A similar strategy can be implemented to incorporate exercise effects in the physiologically-based FFA model developed in Chapter 5. To capture the increased muscle FFA uptake (R_{MFU}) during exercise, multiplier functions representing the exercise effects on R_{MFU} (M_{MFU}^E) can be incorporated in equation (5.76) (Chapter 5). Hence, the modified form of equation (5.76) can be written as follows:

$$R_{MFU} = M_{MFU}^F \times M_{MFU}^E \times R_{MFU}^B \quad (7.1)$$

The correlation between the exercise intensity and muscle FFA uptake (M_{MFU}^E) can be obtained from published literature [162, 203], where stable isotope tracer and indirect calorimetry techniques were used to evaluate regulation of FFA metabolism at various levels and duration of exercise. Data from these studies revealed that the contribution of plasma FFA as a source of muscle fuel declines as the exercise intensity increases from 25% to 65% PVO_2^{max} .

Similarly, exercise effects on the rate of FFA release from the AT into the circulatory system (lipolysis) can be captured by incorporating a multiplier function, M_{AFP}^E , in equation (5.78) (Chapter 5), as shown below:

$$R_{AFP} = M_{AFP}^I \times M_{AFP}^E \times R_{AFP}^B \quad (7.2)$$

Once again, the correlation between the exercise intensity and the lipolytic rate (M_{AFP}^E) can be procured from the same studies as above [162, 203]. The experimental results showed

that, unlike the endogenous glucose production rate, the lipolytic rate was maximum at mild intensity exercise ($PVO_2^{max} = 25\%$), and decreased with increasing exercise intensity.

The hepatic glucose production rate due to exercise can be represented by two separate multiplying functions capturing the gluconeogenesis and glycogenolysis process, as the relative contributions of these processes in total glucose production change according to the exercise duration and intensity [204]. This will enable the model to capture the depletion of glycogenolysis due to exhaustion of hepatic glycogen reservoir during prolonged exercise.

7.2.2 *A Priori* Structural Identifiability of the Metabolic Models

Dynamical models representing biological systems usually contains unknown parameters describing unobservable states. Typically, these parameters cannot be directly measured, and are required to be estimated from data collected experimentally by measuring the observable model variables (inputs and outputs). An important criterion for the parameter estimation to be well posed is global identifiability of the parametric model [205, 206, 207]. In other words, under ideal conditions of noise free measurements and error free model structure, the unknown parameters of the proposed model can be uniquely recovered from the specially designed input-output experimental data [205]. If the proposed model is not *a priori* identifiable, then the estimates of the unknown parameters could be unreliable and erroneous [205, 208].

Identifiability also impacts on the design of the experimental study by providing guidelines on the selection of input and output sites to allow unique identifiability [209]. It has been shown that *a priori* identifiability results can be used to formulate a minimal (necessary and sufficient) input-output configuration for experimental data.

For *a priori* global identifiability of linear and nonlinear models, various approaches have been proposed: power series [210], differential algebra [207], and similarity transformation methods [206]. Audoli *et al.* developed an algorithm to test *a priori* global identifiability of a class of nonlinear models [208]. The algorithm automatically tests *a priori* identifiability of nonlinear models of state space structure with a general input/output experimental configuration, as shown below:

$$\frac{dx(t)}{dt} = f(x(t), p) + \sum_{i=1}^m g_i(x(t), p)u_i(t) \quad (7.3)$$

$$y(t) = h(u(t), x(t), p) \quad (7.4)$$

Here, $x(t)$ is the n -dimensional state variable, $u(t)$ is the m -dimensional input vector, and $y(t)$ is the r -dimensional output vector. The v -dimensional vector of unknown parameters is represented by $p \in \mathcal{P}$. The entries f , $G = [g_1, \dots, g_m]$ and h are assumed to be polynomial functions of their arguments with no fraction or negative order expressions.

The algorithm resorts to tools from differential algebra; in particular, it is based on the characteristic set of a differential ideal generated by the polynomial defining the model [208]. A characteristic set is a special (“minimal”) set of differential polynomials which consists only the input-output relation of the dynamic system. It generates r polynomial differential equations involving only variables $u(t)$ and $y(t)$ [211]. Studies have shown that the characteristic set of a dynamic system in state space form has a special structure which easily allows parameter identifiability testing [205, 208, 209]. The algorithm computes the characteristic set via Ritt’s pseudo-division algorithm [211].

An analysis of *a priori* parameter identifiability of the extended minimal model and the exercise minimal model developed in Chapter 2 and 3, respectively, can be performed by employing the software developed by Audoli *et al.* [208]. *A priori* global identifiability will guarantee uniqueness of the solution for the unknown model parameters from measured input-output data. It can also be helpful to provide guidelines to deal with non-identifiability, either by providing information on how to simplify the model structure or indicating when more information (in terms of measured data) is needed for the specific experiment.

7.2.3 Advanced MPC for Blood Glucose Control of T1DM

Advanced control strategies using the MPC framework can be developed to deliver exogenous insulin to T1DM patients in order to improve the closed-loop control performance by minimizing hypoglycemic events in the post-prandial condition without sacrificing controller

aggressiveness during hyperglycemia [6, 212]. Two types of controller formulations can be studied: (i) asymmetric objective function MPC, and (ii) prioritized objective MPC.

7.2.3.1 Asymmetric objective function: For diabetic patients, the performance requirement of a controller is asymmetric in nature, as hypoglycemic events are much less tolerable than hyperglycemia. To capture this asymmetric performance requirement, an alternative formulation of equation (6.7) (Chapter 6) is required. One way is to use different weights for positive and negative deviation of glucose from the reference trajectory [6].

The objective function equation, (6.7), can be re-written as:

$$\min_{\Delta U(k|k)} [e^T(k+1|k)\Gamma_y^T\Gamma_y e(k+1|k) + \Delta U^T(k|k)\Gamma_u^T\Gamma_u\Delta U(k|k)] \quad (7.5)$$

subject to:

$$R(k+1|k) - Y(k+1|k) \leq e(k+1|k) \quad (7.6)$$

$$-R(k+1|k) + Y(k+1|k) \leq e(k+1|k) \quad (7.7)$$

Here, $e(k+1|k)$ is the reference error across the prediction horizon which is given by:

$$e(k+1|k) = |R(k+1|k) - Y(k+1|k)| \quad (7.8)$$

Equation (7.6) is an active constraint when the error term is positive (glucose concentration is below the desired level) and equation (7.7) becomes active when the error is negative (glucose concentration is above the desired level). For asymmetric objective function weighting, the above two equations (7.6), (7.7) can be written as:

$$R(k+1|k) - Y(k+1|k) \leq \Gamma^- e(k+1|k) \quad (7.9)$$

$$-R(k+1|k) + Y(k+1|k) \leq \Gamma^+ e(k+1|k) \quad (7.10)$$

Here, two different weights, Γ^- and Γ^+ , are used such that positive and negative deviations of glucose have different contributions to the objective function value. The optimization may be performed by using the *fmincon* function from the MATLAB Optimization Toolbox (©2008 The Mathworks Inc., Natick, MA).

7.2.3.2 Prioritized objective function: Another way of formulating MPC to ensure desired objectives are met is by designing a prioritized objective function (PO). Just like the asymmetric objective formulation, PO is a technique to implement soft output constraints [213], avoiding possible numerical infeasibilities associated with hard output constraints in MPC [214, 215]. One major advantage of such a formulation is that control objectives are explicitly stated and prioritized, making it easy to follow for people from non-technical backgrounds. In PO MPC, the objective function equation (6.7) is modified to describe whether the objectives were met in a pre-specified ranking of priority or not. Large objective function penalties are assigned if a specified objective is not met, and even larger penalties are implemented on not meeting in order of their priority. PO MPC incorporates both binary (0 or 1) and continuous variables making it a standard mixed-integer optimization problem (MIP).

In a PO formulation, the following objective function is minimized at each sampling time (adapted from [212]):

$$\min_{\Delta U(k|k), P, O} [-\Gamma_p P - \Gamma_o O + \|\Gamma_y(R(k+1|k) - Y(k+1|k))\|_2^2 + \|\Gamma_u \Delta U(k|k)\|_2^2] \quad (7.11)$$

Here, P and O are the vectors of priority and objective variables which can be mathematically written as (adapted from [212]):

$$P = [p_1, p_2, \dots, p_N] \quad (7.12)$$

$$O = [o_1, o_2, \dots, o_N] \quad (7.13)$$

$$p_j, o_j \in \{0, 1\} \quad \forall j = 1, 2, \dots, N \quad (7.14)$$

The binary variables, p_j and o_j , represent the status of objectives met in order of priority and the satisfied objective for the control problem, respectively. Objectives are implemented by defining ranges ($\pm B_j$) in the output (and/or input) variables as shown below (adapted from [6]):

$$|R(k+i) - Y(k+i)| < B_j(k+i) \quad \forall, i = 1 \dots p; \quad \forall, j = 1 \dots N \quad (7.15)$$

The objective constraints can be written as (adapted from [6]):

$$R(k+i) - Y(k+i) - B_j(k+i) \leq O_w(1 - o_j) \quad (7.16)$$

$$-R(k+i) + Y(k+i) - B_j(k+i) \leq O_w(1 - o_j) \quad (7.17)$$

where, O_w is a large number. When the objective constraint, Eq. (7.15), is satisfied, the left hand side of Eq. (7.16) and (7.17) will always be negative; hence, the value of o_j can be 1. These constraints can be relaxed by setting $B_j(k+i) = \infty, \forall i = 0 \dots \phi$, where ϕ is the number of steps over which objective constraint is relaxed. The binary values of p_j can be used to weight heavily for objectives to be met according to their level of priority. If objective j cannot be met, then the variable for the corresponding priority must be 0. This can be expressed mathematically as:

$$\begin{aligned} p_1 &\leq o_1 \\ &\vdots \\ p_N &\leq o_N \end{aligned}$$

The constraints are imposed such that the priorities are met according to their level of importance (priority). If priority j is not met, then the values of lower priorities, $j + 1$ to $j + N$, are forced to be 0. This can be mathematically expressed as:

$$\begin{aligned} p_2 &\leq p_1 \\ &\vdots \\ p_N &\leq p_{N-1} \end{aligned}$$

Table 7.1, adapted from [6], represents the discretized objectives that could be used in PO MPC. The optimization problem may be formulated in MATLAB. However, as it is an MIP optimization, the *fmincon.m* function might not be able to efficiently handle the problem. In such a case, other optimization tools, like CPLEX, might be considered for solving the problem. By using such tailored objective functions for a MPC-based insulin delivery system, hypoglycemic events could be minimized thereby preventing insulin shock leading towards unconsciousness or even death for T1DM patients, thus enforcing safety without compromising controller performance.

Table 7.1: Discretized objectives that could be used in PO MPC, numbered in order of priority. The glucose measurement is represented as $G(k + \phi) \frac{mg}{dl}$, where ϕ is the number of steps over which the objective is not enforced (adapted from [6]).

No.	Objectives	No.	Objectives
1.	$G > 70, \phi = 2$	6.	$G > 75, \phi = 0$
2.	$G > 70, \phi = 1$	7.	$G < 110, \phi = 2$
3.	$G > 70, \phi = 0$	8.	$G < 110, \phi = 1$
4.	$G > 75, \phi = 2$	9.	$G < 110, \phi = 0$
5.	$G > 75, \phi = 1$		

APPENDIX

LINEARIZATION USING TAYLOR SERIES EXPANSION

A general nonlinear model can be written as follows (adapted from [191]):

$$\frac{dx}{dt} = f(x, u) \quad (.1)$$

$$y = h(x) \quad (.2)$$

Here, $f(\cdot, \cdot)$ is a generalized nonlinear function of process state variables (x) and process input (u). The process output is indicated by y , and the relationship between y and x is captured by another nonlinear function $h(\cdot)$.

The linearization of the nonlinear model can be obtained by employing Taylor series expansion around the point (x_s, u_s) , as follows (adapted from [191]):

$$\begin{aligned} \frac{dx(t)}{dt} = & f(x_s, u_s) + \left(\frac{\partial f}{\partial x} \right)_{(x_s, u_s)} (x - x_s) + \dots + \left(\frac{\partial^n f}{\partial x^n} \right)_{(x_s, u_s)} \frac{(x - x_s)^n}{n!} + \dots \\ & + \left(\frac{\partial f}{\partial u} \right)_{(x_s, u_s)} (u - u_s) + \dots + \left(\frac{\partial^n f}{\partial u^n} \right)_{(x_s, u_s)} \frac{(u - u_s)^n}{n!} \end{aligned} \quad (.3)$$

$$y(t) = h(x_s) + \left(\frac{\partial h}{\partial x} \right)_{(x_s)} (x - x_s) + \dots + \left(\frac{\partial^n h}{\partial x^n} \right)_{(x_s)} \frac{(x - x_s)^n}{n!} \quad (.4)$$

Ignoring the higher order terms, the linear approximation can be written as:

$$\frac{dx}{dt} = f(x_s, u_s) + a(x_s, u_s)(x - x_s) + b(x_s, u_s)(u - u_s) \quad (.5)$$

$$y = h(x_s) + c(x_s)(x - x_s) \quad (.6)$$

where,

$$a(\cdot, \cdot) = \left(\frac{\partial f}{\partial x} \right)_{(x_s, u_s)} \quad (.7)$$

$$b(\cdot, \cdot) = \left(\frac{\partial f}{\partial u} \right)_{(x_s, u_s)} \quad (.8)$$

$$c(\cdot, \cdot) = \left(\frac{\partial h}{\partial x} \right)_{(x_s)} \quad (.9)$$

Usually, equations (.5) and (.6) are written in deviation variables:

$$\tilde{x} = x - x_s \quad (.10)$$

$$\tilde{u} = u - u_s \quad (.11)$$

$$\tilde{y} = y - y_s \quad (.12)$$

In addition to this, linearization point (x_s, u_s) is chosen to be a steady state operating condition. Hence, equations (.5) and (.6) can be written as:

$$\frac{d\tilde{x}}{dt} = a\tilde{x} + b\tilde{u} \quad (.13)$$

$$\tilde{y} = c\tilde{x} \quad (.14)$$

BIBLIOGRAPHY

- [1] R. N. Bergman, L. S. Phillips, and C. Cobelli. Physiological evaluation of factors controlling glucose tolerance in man. *J. Clin. Invest.*, 68:1456–1467, 1981.
- [2] J. T. Sorensen. *A physiologic model of glucose metabolism in man and its use to design and access improved insulin therapies for diabetes*. PhD thesis, Department of Chemical Engineering, MIT, Cambridge, MA, 1985.
- [3] American Diabetes Association. Standards of medical care in diabetes-2008. *Diabetes Care*, 31(Suppl. 1):S12–S54, 2008.
- [4] B. V. Howard, I. Klimes, B. Vasquez, D. Brady, M. Nagulesparan, and R. H. Unger. The antilipolytic action of insulin in obese subjects with resistance to its glucoregulatory action. *J. Clin. Endocrinol. Metab.*, 58:544–548, 1984.
- [5] C. Cobelli, G. Pacini, G. Toffolo, and L. Sacca. Estimation of insulin sensitivity and glucose clearance from minimal model: New insights from labeled IVGTT. *Am. J. Physiol.*, 250:E591–E598, 1986.
- [6] R. S. Parker, E. P. Gatzke, and F. J. Doyle III. Advanced model predictive control (MPC) for type 1 diabetic patient blood glucose control. *In Proc. of American Control Conf.*, 2000. Chicago, IL.
- [7] D. E. DeWitt and I. B. Hirsch. Outpatient insulin therapy in type 1 and type 2 diabetes mellitus. *JAMA*, 289:2254–2264, 2003.
- [8] D. Thiebaud, R. A. DeFronzo, E. Jacot, A. Golay, K. Acheson, E. Maeder, E. Jequier, and J. P. Felber. Effect of long chain triglyceride infusion on glucose metabolism in man. *Metabolism*, 31(11):1128–1136, 1982.
- [9] T. Szkudelski and K. Szkudelska. Glucose as a lipolytic agent: Studies on isolated rat adipocytes. *Physiol. Res.*, 49:213–217, 2000.
- [10] D. R. Owens, S. D. Luzio, and P. A. Coates. Insulin secretion and sensitivity in newly diagnosed NIDDM caucasians in the UK. *Diabet. Med.*, 13:S19–S24, 1996.
- [11] E. D. R. Pruettt. Glucose and insulin during prolonged work stress in men living on different diets. *J. App. Physiol.*, 28:199–208, 1970.

- [12] R. R. Wolfe, E. R. Nadel, J. F. Shaw, L. A. Stephenson, and M. H. Wolfe. Role of changes in insulin and glucagon in glucose homeostasis in exercise. *Am. Soc. Clin. Invest.*, 77:900–907, 1986.
- [13] G. Ahlborg, J. Wahren, and P. Felig. Splanchnic and peripheral glucose and lactate metabolism during and after prolonged arm exercise. *J. Clin. Invest.*, 77:690–699, 1986.
- [14] B. Zinman, F. T. Murray, M. Vranic, A. M. Albisser, B. S. Leibel, P. A. McClean, and E. B. Marliss. Glucoregulation during moderate exercise in insulin treated diabetes. *J. Clin. Endocrinol. Metab.*, 45:641–652, 1977.
- [15] G. Ahlborg and P. Felig. Lactate and glucose exchange across the forearm, legs, and splanchnic bed during and after prolonged exercise in man. *J. Clin. Invest.*, 69:45–54, 1982.
- [16] P. J. Campbell, M. G. Carlson, J. O. Hill, and N. Nurhahan. Regulation of free fatty acid metabolism by insulin in humans: Role of lipolysis and reesterification. *Am. J. Physiol.*, 263:E1063–E1069, 1992.
- [17] A. E. Sumner, R. N. Bergman, G. L. Vega, D. J. Genovese, C. S. Cochran, K. Pacak, R. M. Watanabe, and R. C. Boston. The multiphasic profile of free fatty acids during the intravenous glucose tolerance test is unresponsive to exogenous insulin. *Diabetes*, 52:1202–1207, 2003.
- [18] S. Klein, E. F. Coyle, and R. R. Wolfe. Fat metabolism during low-intensity exercise in endurance-trained and untrained man. *Am. J. Physiol.*, 267:E934–E934, 1994.
- [19] J. M. Miles, R. A. Rizza, M. W. Haymond, and J. E. Gerich. Effects of acute insulin deficiency on glucose and ketone body turnover in man. *Diabetes*, 29:926–930, 1980.
- [20] R. A. DeFronzo, E. Ferrannini, R. Hendler, P. Felig, and J. Wahren. Regulation of splanchnic and peripheral glucose uptake by insulin and hyperglycemia in man. *Diabetes*, 32:35–45, 1983.
- [21] G. Boden, X. Chen, J. Ruiz, J. V. White, and L. Rossetti. Mechanisms of fatty acid-induced inhibition of glucose uptake. *J. Clin. Invest.*, 93:2438–2446, 1994.
- [22] W. Regittnig, Z. Trajanoski, H-J. Leis, M. Ellmerer, A. Wutte, G. Sendlhofer, L. Schaupp, G. A. Brunner, P. Wach, and T. R. Pieber. Plasma and interstitial glucose dynamics after intravenous glucose injection. *Diabetes*, 48:1070–1081, 1999.
- [23] T. Bremer and D. A. Gough. Is blood glucose predictable from previous values? A solicitation for data. *Diabetes*, 48:445–451, 1999.
- [24] S. Nagasaka, K. Tokuyama, I. Kusaka, H. Hayashi, K. Rokkaku, T. Nakamura, A. Kawakami, M. Higashiyama, S. Ishikawa, and T. Saito. Endogenous glucose production and glucose effectiveness in type 2 diabetic subjects derived from stable-labeled minimal model approach. *Diabetes*, 8:1054–1060, 1999.

- [25] F. B. Ballard, W. H. Danforth, S. Naegle, and R. J. Bing. Myocardial metabolism of fatty acids. *J. Clin. Invest.*, 39(5):717–723, 1960.
- [26] M. E. Rothlin and R. J. Bing. Extraction and release of individual free fatty acids by the heart and fat depots. *J. Clin. Invest.*, 40:1380–1386, 1961.
- [27] E. W. Gertz, J. A. Wisneski, W. C. Stanley, and R. A. Neese. Myocardial substrate utilization during exercise in humans. *J. Clin. Invest.*, 82:2017–2025, 1988.
- [28] L. Hagenfeldt, J. Wahren, B. Pernow, and L. Raf. Uptake of individual free fatty acids by skeletal muscle and liver in man. *J. Clin. Invest.*, 51:2324–2330, 1972.
- [29] P. Lozzo, A. K. Turpeinen, T. Takala, V. Oikonen, O. Solin, E. Ferrannini, P. Nuutila, and J. Knuuti. Liver uptake of free fatty acids in vivo in humans as determined with 14(R,S)-[¹⁸F]fluoro-6-thia-heptadecanoic acid and PET. *Eur. J. Nucl. Med. Mol. Imaging*, 30:1160–1164, 2003.
- [30] B. Capaldo, R. Napoli, L. D. Marino, R. Guida, F. Pardo, and L. Sacca. Role of insulin and free fatty acid availability on regional FFA kinetics in the human forearm. *J. Clin. Endocrinol. Metab.*, 79:879–882, 1994.
- [31] D. E. Kelley, M. Mokan, J. Simoneau, and L. J. Mandarino. Interaction between glucose and free fatty acid metabolism. *J. Clin. Invest.*, 92:91–98, 1993.
- [32] S. D. Mittelman and R. N. Bergman. Inhibition of lipolysis causes suppression of endogenous glucose production independent of changes in insulin. *Am. J. Physiol. Endocrinol. Metab.*, 279:E630–E637, 2000.
- [33] P. Staehr, O. Hother-Nielsen, B. R. Landau, V. Chandramouli, J. J. Holst, and H. Beck-Nielsen. Effects of free fatty acids per se on glucose production, gluconeogenesis, and glycogenolysis. *Diabetes*, 52:260–267, 2003.
- [34] E. Ferrannini, E. J. Barrett, S. Bevilacqua, and R. A. DeFronzo. Effect of fatty acids on glucose production and utilization in man. *J. Clin. Invest.*, 72:1737–1747, 1983.
- [35] K. Rebrin, G. M. Steil, S. D. Mittelman, and R. N. Bergman. Causal linkage between insulin suppression of lipolysis and suppression of liver glucose output in dogs. *J. Clin. Invest.*, 98:741–749, 1996.
- [36] G. Boden, P. Cheung, T. P. Stein, K. Kresge, and M. Mozzoli. FFA cause hepatic insulin resistance by inhibiting insulin suppression of glycogenolysis. *Am. J. Physiol. Endocrinol. Metab.*, 283:E12–E19, 2002.
- [37] A. Brehm, K. Thomaseth, E. Bernroider, P. Nowotny, W. Waldhausl, G. Pacini, and M. Roden. The role of endocrine counterregulation for estimating sensitivity from intravenous glucose tolerance tests. *J. Clin. Endocrinol. Metab.*, 91:2272–2278, 2006.

- [38] American Diabetes Association. Diagnosis and classification of diabetes mellitus. *Diabetes Care*, 30(Suppl. 1):S42–S47, 2007.
- [39] P. Dejkhamron, R. K. Menon, and M. A. Sperling. Childhood diabetes mellitus: Recent advances and future prospects. *Indian J. Med. Res.*, 125:231–250, 2007.
- [40] J. D. McGarry. Banting lecture 2001: Dysregulation of fatty acid metabolism in the etiology of type 2 diabetes. *Diabetes*, 51:7–18, 2002.
- [41] American Diabetes Association. Economic costs of diabetes in the US in 2002. *Diabetes Care*, 26(3):917–932, 2003.
- [42] DCCT – The Diabetes Control and Complications Trial Research Group. The effect of intensive treatment of diabetes on the development and progress of long-term complications in insulin-dependent diabetes mellitus. *N. Engl. J. Med.*, 329:977–986, 1993.
- [43] DCCT – The Diabetes Control and Complications Trial Research Group. The absence of a glycemic threshold for the development of long-term complications: The perspective of the diabetes control and complications trial. *Diabetes*, 51:7–18, 1996.
- [44] DCCT/EDIC – The Writing Team for the Diabetes Control, Complications Trial/Epidemiology of Diabetes Interventions, and Complications Research Group. Effect of intensive therapy on the microvascular complications of type 1 diabetes mellitus. *JAMA*, 287:2563–2569, 2002.
- [45] DCCT/EDIC – The Writing Team for the Diabetes Control, Complications Trial/Epidemiology of Diabetes Interventions, and Complications Research Group. Sustained effect of intensive treatment of type 1 diabetes mellitus on development and progression of diabetic nephropathy: The epidemiology of diabetes interventions and complications (EDIC) study. *JAMA*, 290:2159–2167, 2003.
- [46] P. Raskin, A. Riis, R. A. Guthrie, L. Jovanovic, and L. Leiter. Use of insulin aspart, a fast-acting insulin analog, as the mealtime insulin in the management of patients with type 1 diabetes. *Diabetes Care*, 23:583–588, 2000.
- [47] D. C. Klonoff. The artificial pancreas: How sweet engineering will solve bitter problems. *J. Diabetes Sci. Technol.*, 1(1):72–80, 2007.
- [48] W. Bequette. A critical assessment of algorithms and challenges in the development of a closed-loop artificial pancreas. *Diabetes Technol. Ther.*, 7(1):28–47, 2005.
- [49] R. S. Parker, F. J. Doyle III, and N. A. Peppas. The intravenous route to blood glucose control. *IEEE Eng. Med. Biol.*, 20(1):65–73, 2001.
- [50] M. Morari and E. Zafiriou. *Robust Process Control*. Prentice-Hall, Englewood Cliffs, NJ, 1989.

- [51] G. M. Steil, B. Clark, S. Kanderian, and K. Rebrin. Modeling insulin action for development of a closed-loop artificial pancreas. *Diabetes Technol. Ther.*, 7(1):94–108, 2005.
- [52] G. R. Dagenais, R. G. Tancredi, and K. L. Zierler. Free fatty acid oxidation by forearm muscle at rest, and evidence for an intramuscular lipid pool in the human forearm. *J. Clin. Invest.*, 58:421–431, 1976.
- [53] G. A. Brooks and J. Mercier. Balance of carbohydrate and lipid utilization during exercise: The “crossover” concept. *J. Appl. Physiol.*, 76(6):2253–2261, 1994.
- [54] K. N. Frayn. Non-esterified fatty acid metabolism and postprandial lipaemia. *Atherosclerosis*, 141 (Suppl. 1):S41–S46, 1998.
- [55] A. H. Khan and J. E. Pessin. Insulin regulation of glucose uptake: A complex interplay of intracellular signalling pathways. *Diabetologia*, 45:1475–1483, 2002.
- [56] D. A. Hems and P. D. Whitton. Control of hepatic glycogenolysis. *Physiol. Rev.*, 60:1–50, 1980.
- [57] A. Girard. The inhibitory effects of insulin on hepatic glucose production are both direct and indirect. *Diabetes*, 55:1475–1483, 2006.
- [58] P. J. Randle, C. N. Hales, P. B. Garland, and E. A. Newsholme. The glucose-fatty acid cycle. its role in insulin sensitivity and the metabolic disturbances of diabetes mellitus. *Lancet I*, pages 785–789, 1963.
- [59] P. J. Randle, E. A. Newsholme, and P. B. Garland. Regulation of glucose uptake by muscle. Effects of fatty acids, ketone bodies, and pyruvate, and of alloxan-diabetes and starvation, on the uptake and metabolic fate of glucose in rat heart and diaphragm muscles. *Biochem. J.*, 93:652–665, 1964.
- [60] E. Ghanassia, J. F. Brun, J. Mercier, and E. Raynaud. Oxidative mechanisms at rest and during exercise. *Clinica. Chemica. Acta.*, 383:1–20, 2007.
- [61] J. F. Horowitz and S. Klein. Lipid metabolism during endurance exercise. *Am. J. Clin. Nutr.*, 72:558S–563S, 2000.
- [62] D. H. Wasserman, R. J. Geer, D. E. Rice, D. Bracy, P. J. Flakoll, L. L. Brown, J. O. Hill, and N. Abumrad. Interaction of exercise and insulin action in humans. *Am. Physiol. Society.*, 34:E37–E45, 1991.
- [63] G. Ahlborg, P. Felig, L. Hagenfeldt, R. Hendler, and J. Wahren. Substrate turnover during prolonged exercise in man. *J. Clin. Invest.*, 53:1080–1090, 1974.
- [64] J. H. Exton and C. R. Park. Control of gluconeogenesis in liver. I. General features of gluconeogenesis in the perfused liver of rats. *J. Biol. Chem.*, 242(11):2622–2632, 1967.

- [65] R. S. Parker, F. J. Doyle III, and N. A. Peppas. A model-based algorithm for blood glucose control in type I diabetic patients. *IEEE Trans. Biomed. Eng.*, 46:148–157, 1999.
- [66] T. Van Herpe, M. Espinoza, B. Pluymers, P. Wouters, F. De Smet, G. Van Den Berghe, and B. De Moor. Development of a critically ill patient input-output model. *In Proceedings of the 14th IFAC Symposium System Identification*, 2006. Newcastle, Australia.
- [67] D. A. Finan, H. Zisser, L. Jovanovic, W. C. Bevier, and D. E. Seborg. Identification of linear dynamic models for type 1 diabetes: a simulation study. *In Proceedings of the 14th IFAC ADCHEM Symposium*, 2006. Gramado, Brazil.
- [68] S. J. Qin and T. A. Badgwell. *An overview of nonlinear MPC applications*, In, Nonlinear model predictive control: assesment and future directions. Birkhauser, 1999.
- [69] V. W. Bolie. Coefficients of normal blood glucose regulation. *J. Appl. Physiol.*, 16:783–788, 1961.
- [70] E. Ackerman, L. C. Gatewood, J. W. Rosevear, and G. D. Molnar. Model studies of blood glucose regulation. *Bull. Math. Biophys.*, 37:21–37, 1965.
- [71] C. Cobelli, G. Federspil, G. Pacini, A. Salvan, and C. Scandellari. An integrated mathematical model of the dynamics of blood glucose and its hormonal control. *Math. Biosci.*, 58:27–60, 1982.
- [72] C. Cobelli and A. Mari. Validation of mathematical models of complex endocrine metabolic systems. A case study on a model of glucose regulation. *Med. Biol. Eng. Comput.*, 21:390–399, 1983.
- [73] A. Caumo, P. Vicini, and C. Cobelli. Is the minimal model too minimal? *Diabetologia*, 39:997–1000, 1996.
- [74] C. Cobelli, A. Caumo, and M. Omenetto. Minimal model SG overestimation and SI underestimation: Improved accuracy by a Bayesian two compartment model. *Am. J. Physiol. – End. Metab.*, 277:481–488, 1999.
- [75] R. Hovorka, F. Shojaee-Moradie, P. V. Carroll, L. J. Chassin, I. J. Gowrie, N. C. Jackson, R. S. Tudor, A. M. Umpleby, and R. H. Jones. Partitioning glucose distribution/transport, disposal, and endogenous production during IVGTT. *Am. J. Physiol.*, 282:E992–E1007, 2002.
- [76] J. Tiran, L. I. Avruch, and A. M. Albisser. A circulation and organs model for insulin dynamics. *Am. J. Physiol.: Endocrinol. Metab. Gastrointest. Physiol.*, 237:E331–E339, 1979.

- [77] R. Srinivasan, A. H. Kadish, and R. Sridhar. A mathematical model for the control mechanism of free fatty acid-glucose metabolism in normal humans. *Comput. Biomed. Res.*, 3:146–166, 1970.
- [78] C. Cobelli, G. Nucci, and S. D. Prato. A physiological simulation model of the glucose-insulin system. *In Proc. IEEE Eng. Med. Biol. Soc.*, 1999. Atlanta, GA.
- [79] G. D. Mitsis and V. Z. Marmarelis. Nonlinear modeling of glucose metabolism: comparison of parametric vs. nonparametric methods. *In, Proc. IEEE-EMBS Annual Int. Conf., Lyon, France*, 29:5968–5971, 2007.
- [80] J. A. Florian Jr. and R. S. Parker. Empirical modeling for glucose control in critical care and diabetes. *Eur. J. Control*, 11:601–616, 2005.
- [81] Z. Trajanoski, W. Regittnig, and P. Wach. Simulation studies on neural predictive control of glucose using the subcutaneous route. *Comput. Methods Programs Biomed.*, 56:133–139, 1998.
- [82] R. Bellazzi, L. Ironi, R. Guglielmann, and M. Stefanelli. Qualitative models and fuzzy systems: An integrated approach for learning from data. *Artif. Intell. Med.*, 14:5–28, 1998.
- [83] G. Bleckert, U. G. Oppel, and E. Salzsieder. Mixed graphical models for simultaneous model identification and control applied to the glucose-insulin metabolism. *Comput. Methods Programs Biomed.*, 56:141–155, 1998.
- [84] G. Serge, M. Turcogl, and G. Varcellone. Modelling blood glucose and insulin kinetics in normal diabetic and obese subjects. *Diabetes*, 22:94–97, 1973.
- [85] R. N. Bergman, Y. Z. Ider, C. R. Bowden, and C. Cobelli. Quantitative estimation of insulin sensitivity. *Amer. J. Physiol.*, 5:E667–E677, 1979.
- [86] R. N. Bergman and J. C. Lovejoy. *The minimal model: Yesterday, today, and tomorrow*. LSU Press, 1997.
- [87] M. J. Quon, C. Cochran, S. I. Taylor, and R. C. Eastman. Non-insulin-mediated glucose disappearance in subjects with IDDM. discordance between experimental results and minimal model analysis. *Diabetes*, 43:890–896, 1994.
- [88] K. Weber, I. K. Martin, J. D. Best, F. P. Alford, and R. C. Boston. Alternative method for minimal model analysis of intravenous glucose tolerance data. *Am. J. Physiol. Endocrinol. Metab.*, 256:E524–E535, 1989.
- [89] R. N. Bergman. Minimal model: perspective from 2005. *Horm. Res.*, 64:8–15, 2005.
- [90] C. Cobelli and A. Ruggeri. Evaluation of portal/peripheral route and of algorithms for insulin delivery in the closed-loop control of glucose in diabetes – a modeling study. *IEEE Trans. Biomed. Eng.*, 30:93–103, 1983.

- [91] G. Pacini and C. Cobelli. Estimation of β -cell secretion and insulin hepatic extraction by minimal modeling technique. *Comp. Method. Program. Biomed.*, 32:241–248, 1990.
- [92] M. Berger and D. Rodbard. Computer simulation of plasma insulin and glucose dynamics after subcutaneous insulin injection. *Diabetes Care*, 12:725–736, 1989.
- [93] E. Salzsieder, G. Albrecht, U. Fischer, and E. J. Freyse. Kinetic modeling of the glucoregulatory system to improve insulin therapy. *IEEE Trans. Biomed. Eng.*, 32:846–855, 1985.
- [94] U. Fischer, W. Schenk, E. Salzsieder, G. Albrecht, P. Abel, and E. J. Freyse. Does physiological blood glucose control require an adaptive strategy? *IEEE Trans. Biomed. Eng.*, 34:575–582, 1987.
- [95] U. Fischer, E. Salzsieder, E. J. Freyse, and G. Albrecht. Experimental validation of a glucose-insulin control model to simulate patterns in glucose turnover. *Comp. Meth. Prog. Biomed.*, 32:249–258, 1990.
- [96] M. A. Boroujerdi, A. M. Umpleby, R. H. Jones, and P. H. Sonksen. A simulation model for glucose kinetics and estimates of glucose utilization rate in type 1 diabetic patients. *Am. J. Physiol.*, 268:E766–E774, 1995.
- [97] E. D. Lehman and T. Deutsch. *A clinical model of glucose-insulin interaction*. Computer Modelling, North Holland, Amsterdam, 1991.
- [98] E. D. Lehman. Preliminary experience with the internet release of AIDA – an interactive educational diabetes simulator. *Comput. Methods Programs Biomed.*, 32:311–318, 1995.
- [99] I. M. Tolic, E. Mosekilde, and J. Sturis. Modeling the insulin glucose feedback system: The significance of pulsatile insulin secretion. *J. Theor. Biol.*, 207:361–375, 2000.
- [100] P. Vicini and C. Cobelli. The iterative two-stage population approach to IVGTT minimal modeling: Improved precision with reduced sampling. *Am. J. Physiol.*, 280:E179–E186, 2001.
- [101] K. E. Andersen and M. Hojbjerre. A population-based bayesian approach to the minimal model of glucose and insulin homeostasis. *Statistics in Medicine*, 24:2381–2400, 2005.
- [102] K. Engelborghs, V. Lemaire, J. Belair, and D. Roose. Numerical bifurcation analysis of delay differential equations arising from physiological modeling. *J. Math. Biol.*, 42:361–385, 2001.
- [103] E. W. Kraegen and D. J. Chisholm. Insulin responses to varying profiles of subcutaneous insulin infusion: Kinetic modelling studies. *Diabetologia*, 26:208–213, 1984.

- [104] W. R. Puckett and E. N. Lightfoot. A model for multiple subcutaneous insulin injections developed from individual diabetic patient data. *Am. J. Physiol. Endocrinol. Metab.*, 269:E1115–E1124, 1995.
- [105] P. Wach, Z. Trajonoski, P. Kotanko, and F. Skrabal. Numerical approximation of mathematical model for absorption of subcutaneously injected insulin. *Med. Biol. Engrg. Comput.*, 33(1):18–23, 1995.
- [106] J. Tiran, K. R. Gale, and D. Porte Jr. A simulation model of extracellular glucose distribution in the human body. *Ann. Biomed.*, 3:34–46, 1975.
- [107] J. R. Guyton, R. O. Foster, J. S. Soeldner, M. H. Tan, C. B. Kahn, L. Koncz, and R. E. Gleason. A model of glucose-insulin homeostasis in man that incorporates the heterogenous fast pool theory of pancreatic insulin release. *Diabetes*, 27:1027–1042, 1978.
- [108] J. Kim, G. M. Saidel, and M. E. Cabrera. Multi-scale computational model of fuel homeostasis during exercise: effect of hormonal control. *Ann. Biomed. Eng.*, 35:69–90, 2007.
- [109] A. H. Kadish. Automation control of blood sugar. I. A servomechanism for glucose monitoring and control. *Am. J. Med. Electron.*, 39:82–86, 1964.
- [110] A. M. Albisser, B. S. Leibel, T. G. Ewart, Z. Davidovac, C. K. Botz, and W. Zingg. An artificial endocrine pancreas. *Diabetes*, 23:389–396, 1974.
- [111] A. M. Albisser, B. S. Leibel, T. G. Ewart, Z. Davidovac, C. K. Botz, and W. Zingg. Clinical control of diabetes by the artificial pancreas. *Diabetes*, 23:397–404, 1974.
- [112] A. H. Clemens, P. H. Chang, and R. W. Myers. The development of biostator, a glucose-controlled insulin infusion system. *Horm. Metab. Res. Supplement*, 7:23–33, 1977.
- [113] C. K. Botz. An improved control algorithm for an artificial beta-cell. *IEEE Trans. Biomed. Eng.*, 23:252–255, 1974.
- [114] E. B. Marliss, F. T. Murray, E. F. Stokes, B. Zinman, A. F. Nakhoda, and A. Denoga. Normalization of glycemia in diabetes during meals with insulin and glucagon delivery by the artificial pancreas. *Diabetes*, 26:663–672, 1977.
- [115] E. W. Kraegen, L. V. Campbell, Y. O. Chia, H. Meler, and L. Lazarus. Control of blood glucose in diabetes using an artificial pancreas. *Aust. NZ. J. Medical*, 7:280–286, 1977.
- [116] H. M. Broekhuysse, J. D. Nelson, B. Zinman, and A. M. Albisser. Comparison of algorithms for the closed-loop control of blood glucose using the artificial beta cell. *IEEE Trans. Biomed. Eng.*, 28:678–687, 1981.

- [117] G. M. Steil, K. Rebrin, F. Hariri, Y. Chen, C. Darwin, and M. F. Saad. Continuous automated insulin delivery based on subcutaneous glucose sensing and an external insulin pump. *Diabetes*, 53:A2, 2004.
- [118] G. M. Grodsky. A threshold distribution hypothesis for packet storage of insulin and its mathematical modeling. *J. Clin. Invest.*, 51:2047–2059, 1972.
- [119] A. D. Cherrington, D. Sindelar, D. Edgerton, K. Steiner, and O. P. McGuinness. Physiological consequences of phasic insulin release in the normal animal. *Diabetes*, 51:S103–S108, 2002.
- [120] G. M. Steil, K. Rebrin, R. Janowski, C. Darwin, and M. F. Saad. Modeling β -cell insulin secretion—implications for closed-loop glucose homeostasis. *Diabetes Technol. Ther.*, 5:953–964, 2003.
- [121] G. W. Swan. An optimal control model of diabetes mellitus. *Bull. Math. Bio.*, 44:793–808, 1982.
- [122] R. L. Ollerton. Application of optimal control theory to diabetes mellitus. *Int. J. Control*, 50:2503–2522, 1989.
- [123] M. E. Fisher and K. L. Teo. Optimal insulin infusion resulting from a mathematical model of blood glucose dynamics. *IEEE Trans. Biomed. Eng.*, 36:479–486, 1989.
- [124] S. M. Lynch and B. W. Bequette. Model predictive control of blood glucose in type i diabetics using subcutaneous glucose measurements. *In Proc. American Control Conference*, 2002. Anchorage, AK.
- [125] M. E. Fisher. A semi-closed loop algorithm for the control of blood-glucose levels in diabetics. *IEEE Trans. Biomed. Eng.*, 38:57–61, 1991.
- [126] R. Hovorka, V. Canonico, L. J. Chassin, U. Haueter, M. Massi-Benedetti, M. O. Federici, T. R. Pieber, H. C. Schaller, L. Schaupp, T. Vering, and M. E. Wilinska. Nonlinear model predictive control of glucose concentration in subjects with type 1 diabetes. *Physiol. Meas.*, 25(4):905–920, 2004.
- [127] M. Morari and N. L. Ricker. *Model Predictive Control Toolbox*. The MathWorks, Inc., Natick, MA, 1994.
- [128] E. P. Gatzke and F. J. Doyle III. Model predictive control of a granulation system using soft output constraints and prioritized control objectives. *J. Powder Technology*, 121(2):149–158, 2004.
- [129] A. Roy and R. S. Parker. Dynamic modeling of free fatty acid, glucose, and insulin: An extended “minimal model”. *Diabetes Technol. Ther.*, 8(6):617–626, 2006.

- [130] A. Roy and R. S. Parker. Mixed meal modeling and disturbance rejection in type 1 diabetes patients. *In, Proc. IEEE-EMBS Annual Int. Conf., New York, NY*, 28:323–326, 2006.
- [131] R. N. Bergman. Pathogenesis and prediction of diabetes mellitus: Lessons from integrative physiology, in: Irving I. Schwartz lecture. *Mount Sinai J. Medicine*, 60:280–290, 2002.
- [132] M. Ader and R. N. Bergman. Peripheral effects of insulin dominate suppression of fasting hepatic glucose production. *Am. J. Physiol. Endocrinol. Metab.*, 258:E1020–E1032, 1990.
- [133] K. Rebrin, G. M. Steil, L. Getty, and R. N. Bergman. Free fatty acid as a link in regulation of hepatic glucose production by peripheral insulin. *Diabetes*, 44:1038–1045, 1995.
- [134] P. J. Randle, A. L. Kerbey, and J. Esinol. Mechanisms decreasing glucose oxidation in diabetes and starvation: role of lipid fuels and hormones. *Diabetes Metab. Rev.*, 4:623–628, 1988.
- [135] V. Mougios, C. Kotzamanidis, C. Koutsari, and S. Atsopardis. Exercise induced changes in the concentration of individual fatty acids and triglycerols of human plasma. *Metabolism*, 44:681–688, 1995.
- [136] G. M. Cooper. *The cell: A molecular approach. 2nd Edition*. Sinauer Associates Publication, Washington, DC, 2000.
- [137] L. M. Botion and A. Green. Long-term regulation of lipolysis and hormone-sensitive lipase by insulin and glucose. *Diabetes*, 48:1691–1697, 1999.
- [138] E. Carsonc and C. Cobelli. *Modelling methodology for physiology and medicine*. Academic press, San Diego, CA, 2001.
- [139] H. Akaike. A bayesian extension of the minimum AIC procedure of autoregressive model fitting. *Biometrika*, 66(2):237–242, 1979.
- [140] C. M. Hurvich and C. L. Tsai. Regression and time series model selection in small samples. *Biometrika*, 76:297–307, 1989.
- [141] E. Moussalli, R.W. Downs, and J.M. May. Potentiation by glucose of lipolytic responsiveness of human adipocytes. *Diabetes*, 35:759–763, 1986.
- [142] M. Roden, T. B. Price, G. Perseghin, K. Petersen, D. Rothman, and G. Cline. Mechanism of free fatty acid-induced insulin resistance in humans. *J. Clin. Invest.*, 97:2859–2865, 1996.

- [143] P. J. Coon, E. M. Rogus, and A. P. Goldberg. Time course of plasma free fatty acid concentration in response to insulin: Effect of obesity and physical fitness. *Metabolism*, 41:711–716, 1992.
- [144] G. Boden, X. Chen, J. Ruiz, J. V. White, and L. Rossetti. Mechanism of fatty acid induced inhibition of glucose uptake. *J. Clin. Invest.*, 93:2438–2446, 1993.
- [145] E. D. Lehman and T. Deutsch. The physiological model of glucose-insulin interaction in t1dm. *J. Biomed. Eng.*, 14:235–242, 1992.
- [146] C. Dalla Man, R. A. Rizza, and C. Cobelli. Meal simulation model of the glucose-insulin system. *IEEE Trans. Biomed. Eng.*, 54:1740–1749, 2007.
- [147] S. L. Wolman, A. L. Fields, S. Cheema-Dhadli, and M. L. Halperin. Protein conversion to glucose: An evaluation of the quantitative aspects. *J. Parenter. Enteral. Nutr.*, 4(5):487–489, 1980.
- [148] P. J. Collins, M. Horowitz, A. Maddox, J. C. Myers, and B. E. Chatterton. Effects of increasing solid compartment size of a mixed solid/liquid meal on solid and liquid gastric emptying. *Am. Physiol. Soc.*, 39:G549–G554, 1996.
- [149] S. Doran, K. L. Jones, J. M. Andrews, and M. Horowitz. Effects of meal volume and posture of gastric emptying of solids and appetite. *Am. J. Physiol.*, 275:R1712–R1718, 1998.
- [150] A. Roy and R. S. Parker. Dynamic modeling of exercise effects on plasma glucose and insulin levels. *J. Diabetes Sci. Technol.*, 1(3):164–173, 2007.
- [151] R. Felig and J. C. Wahren. Fuel homeostasis in exercise. *N. Engl. J. Med.*, 293:1078–1084, 1975.
- [152] D. R. Seals, J. M. Hagberg, W. K. Allen, B. F. Hurley, G. P. Dalsky, A. A. Ehsani, and J. O. Holloszy. Glucose tolerance in young and older athletes and sedentary men. *J. Appl. Physiol.*, 56(6):1521–1525, 1984.
- [153] J. A. Tuominen, P. Ebeling, and V. A. Koivisto. Exercise increase insulin clearance in healthy man and insulin-dependent diabetes mellitus patients. *Clinical Physiology*, 17:19–30, 1997.
- [154] D. H. Wasserman and A. D. Cherrington. Hepatic fuel metabolism during muscular work: Role and regulation. *Am. J. Physiol.*, 260:E811–E824, 1991.
- [155] J. Wahren and R. Felig. Glucose metabolism during leg exercise in man. *J. Clin. Invest.*, 50:2715–2725, 1971.
- [156] E. B. Marliss and M. Vranic. Intense exercise has unique effects on both insulin release and its roles in glucoregulation. *Diabetes*, 51:S271–S283, 2002.

- [157] E. S. Horton and R. L. Terjung. *Exercise, nutrition and energy metabolism*. Macmillan Publishing Company, New York, NY, 1988.
- [158] D. H. Wasserman, D. B. Lacy, D. R. Green, P. E. Williams, and A. D. Cherrington. Dynamics of hepatic lactate and glucose balances during prolonged exercise and recovery in the dog. *J. Appl. Physiol.*, 63:2411–2417, 1987.
- [159] I. Astrand. Aerobic work capacity in men and women with specific reference to age. *Acta. Physiol. Scan.*, 49:1–92, 1960.
- [160] P. A. Ivey and G. A. Gaesser. Postexercise muscle and liver glycogen metabolism in male and female rats. *J. Appl. Physiol.*, 62:1250–1254, 1987.
- [161] G. I. Shulman, D. L. Rothman, D. Smith, C. M. Johnson, J. B. Blair, R. G. Shulman, and R. A. DeFronzo. Mechanism of liver glycogen repletion in vivo by nuclear magnetic resonance spectroscopy. *J. Clin. Invest.*, 76:1229–1236, 1985.
- [162] R. R. Wolfe, S. Klein, F. Carraro, and J. M. Weber. Role of triglyceride-fatty acid cycle in controlling fat metabolism in humans during and after exercise. *Am. J. Physiol.*, 258:E382–E389, 1990.
- [163] P. Raskin, Y. Fujita, and R. Unger. Effect of insulin-glucose infusions on plasma glucagon levels in fasting diabetics and nondiabetics. *J. Clin. Invest.*, 56:1132–1138, 1975.
- [164] C. Asplin, T. Paquette, and J. Palmer. In vitro inhibition of glucagon secretion by pancreatic beta cell activity in man. *J. Clin. Invest.*, 56:314–318, 1981.
- [165] A. Cherrington. Control of glucose uptake and release by the liver in vivo. *Diabetes*, 48:1198–1214, 1999.
- [166] P. B. Garland and P. J. Randle. Regulation of glucose uptake by muscle. *Biochem. J.*, 93:678–687, 1964.
- [167] P. B. Garland, P. J. Randle, and E. A. Newsholme. Citrate as an intermediary in the inhibition of phosphofructokinase in rat heart by fatty acids, ketone bodies, pyruvate, diabetes, and starvation. *Nature*, 200:678–687, 1963.
- [168] L. M. Odland, G. J. F. Heigenhauser, D. Wong, M. G. Hollidge-Horvat, and L. L. Spriet. Effects of increased fat availability on fat-carbohydrate interaction during prolonged exercise in men. *Am. J. Physiol.*, 274:1198–1214, 1998.
- [169] D. J. Dyck, C. T. Putman, G. J. F. Heigenhauser, E. Hultman, and L. L. Spriet. Regulation of fat-carbohydrate interaction in skeletal muscle during intense aerobic cycling. *Am. J. Physiol.*, 265:E852–E859, 1993.

- [170] H. Yue, M. Brown, J. Knowles, H. Wang, D. S. Broomhead, and D. B. Kell. Insights into the behavior of systems biology models from dynamic sensitivity and identifiability analysis: A case study of an NF- κ B signalling pathway. *Mol. Biosyst.*, 2:640–649, 2006.
- [171] D. E. Zak, G. E. Gonye, J. S. Schwaber, and F. J. Doyle III. Importance of input perturbations and stochastic gene expression in the reverse engineering of genetic regulatory networks: Insights from an identifiability analysis of an in silico network. *Genome Res.*, 13:2396–2405, 2003.
- [172] H. Davson and E. Spaziani. The blood-brain barrier and the extracellular space of the brain. *J. Physiol.*, 149:135–143, 1959.
- [173] S. W. Coppack, M. D. Jensen, and J. M. Miles. In vivo regulation of lipolysis in humans. *J. Lipid Research*, 35:177–193, 1994.
- [174] O. E. Owen, A. P. Morgan, H. G. Kemp, J. M. Sullivan, M. G. Herrera, and Jr. G. F. Cahill. Brain metabolism during fasting. *J. Clin. Invest.*, 46:1589–1595, 1967.
- [175] B. Davies and T. Morris. Physiological parameters in laboratory animals and humans. *Pharmaceutical Research*, 10(7):1093–1095, 1993.
- [176] A. Tsuji, K. Nishide, H. Minami, E. Nakashima, T. Terasaki, and T. Yamana. Physiologically based pharmacokinetic model for cefazolin in rabbits and its preliminary extrapolation to man. *Drug Metab. Dispos.*, 13:729–739, 1985.
- [177] R. Kawai, D. Mathew, C. Tanaka, and M. Rowland. Physiologically based pharmacokinetics of cyclosporine A: Extension to tissue distribution kinetics in rats and scale-up to human. *Pharmaceuticals/biotech*, 287(2):457–468, 1998.
- [178] B. J. Potter, D. Sorrentino, and P. D. Berk. Mechanisms of cellular uptake of free fatty acids. *Annu. Rev. Nutr.*, 9:253–270, 1989.
- [179] L. V. Basso and R. J. Havel. Hepatic metabolism of free fatty acids in normal and diabetic dogs. *J. Clin. Invest.*, 49:537–547, 1970.
- [180] T. K. Lam, A. Carpentier, G. F. Lewis, G. Van de Werve, I. G. Fantus, and A. Giacca. Mechanisms of the free fatty acid-induced increase in hepatic glucose production. *Am. J. Physiol. Endocrinol. Metab.*, 284:E863–E873, 2003.
- [181] C. Meyer, V. Nadkarni, M. Stumvoll, and J. Gerich. Human kidney free fatty acid and glucose uptake: Evidence for a renal glucose-fatty acid cycle. *Am. J. Physiol.*, 273:E650–E654, 1997.
- [182] J. Saleh, A. D. Sniderman, and K. Cianflone. Regulation of plasma fatty acid metabolism. *Clinica. Chimica. Acta*, 286:163–180, 1999.
- [183] R. R. Wolfe and E. J. Peters. Lipolytic response to glucose infusion in human subjects. *Am. J. Physiol.*, 252:E218–E223, 1987.

- [184] P. J. Randle, P. B. Garland, E. A. Newsholme, and C. N. Hales. The glucose fatty acid cycle in obesity and maturity onset diabetes mellitus. *An. NY Acad. Sci.*, 131:324–333, 1965.
- [185] M. Walker, G. R. Fulcher, C. F. Sum, H. Orskov, and K. G. Alberti. Effect of glycemia and nonesterified fatty acids on forearm glucose uptake in normal humans. *Am. J. Physiol.*, 261:E304–E311, 1991.
- [186] P. M. Piatti, L. D. Monti, M. Pacchioni, A. E. Pontiroli, and G. Pozza. Forearm insulin- and noninsulin-mediated glucose uptake and muscle metabolism in man: Role of free fatty acids and blood glucose in man. *Metabolism*, 40:926–933, 1991.
- [187] G. F. Lewis, B. Zinman, Y. Groenewoud, M. Vranic, and A. Giacca. Hepatic glucose production is regulated both by direct hepatic and extrahepatic effects of insulin in humans. *Diabetes*, 45:454–462, 1996.
- [188] G. M. Steil and M. F. Saad. Automated insulin delivery for type 1 diabetes. *Curr. Opin. Endocrinol. Diabetes*, 13:205–211, 2006.
- [189] G. Schlotthauer, L. G. Gamero, M. E. Torres, and G. A. Nicolini. Modeling identification and nonlinear model predictive control of type 1 diabetic patient. *Med. Eng. Phys.*, 28:240–250, 2006.
- [190] P. Dua, III F. J. Doyle, and E. N. Pistikopoulos. Model-based blood glucose control for type 1 diabetes via parametric programming. *IEEE Trans. Biomed. Eng.*, 53:1478–1491, 2006.
- [191] B. A. Ogunnaike and W. H. Ray. *Process dynamics, modeling and control*. Oxford University Press, New York, NY, 1994.
- [192] G. M. Steil, A. E. Panteleon, and K. Rebrin. Close-loop insulin delivery – the path to physiological glucose control. *Adv. Drug Deliv. Rev.*, 56:125–144, 2004.
- [193] B. W. Bequette. *Process Control: Modeling, Design, and Simulation*. Prentice-Hall, Upper Saddle River, NJ, 2003.
- [194] G. Pannocchia, N. Laachi, and J. B. Rawlings. A candidate to replace PID control: SISO-constrained LQ control. *AIChE Journal*, 51:1178–1189, 2005.
- [195] J. B. Rawlings. Tutorial overview of model predictive control. *IEEE Control Systems Magazine*, pages 38–52, 2000.
- [196] J. B. Rawlings. Tutorial: Model predictive control technology. *In Proc. American Control Conf., San Diego, CA*, pages 662–676, 1999.
- [197] H. Wolpert. *Smart pumping: A practical approach to mastering the insulin pump*. American Diabetes Association, 2002.

- [198] K. Rebrin, G. M. Steil, W. P. Van Antwerp, and J. J. Mastrototaro. Subcutaneous glucose predicts plasma glucose independent of insulin: implications for continuous monitoring. *Am. J. Physiol. Endocrinol Metab.*, 277:E561–E571, 1999.
- [199] B. H. Ginsberg. The current environment of CGM technologies. *J. Diabetes Sci. Technol.*, 1:117–121, 2007.
- [200] H. A. Wolpert. Use of continuous glucose monitoring in the detection and prevention of hypoglycemia. *J. Diabetes Sci. Technol.*, 1:146–150, 2007.
- [201] V. R. Kondepati and H. M. Heise. Recent progress in analytical instrumentation for glycemic control in diabetic and critically ill patients. *Anal. Bional. Chem.*, 388:545–563, 2007.
- [202] P. J. Lenart and R. S. Parker. Modeling exercise effects in type 1 diabetic patients. *In, Proc. of the 15th Triennial World Congress, Barcelona, Spain*, 2002.
- [203] J. A. Romijn, E. F. Coyle, L. S. Sidossis, A. Gastaldelli, J. F. Horowitz, E. Endert, and R. R. Wolfe. Regulation of endogenous fat and carbohydrate metabolism in relation to exercise intensity. *Am. J. Physiol.*, 265:E380–E391, 1993.
- [204] J. Radziuk and S. Pie. Hepatic glucose uptake, gluconeogenesis, and regulation of glycogen synthesis. *Diabetes Metab.*, 17:250–272, 2001.
- [205] S. Audoly, L. D. Angio, M. P. Saccomani, and C. Cobelli. Global identifiability of linear compartmental models. *IEEE Trans. Biomed. Eng.*, 45:36–47, 1998.
- [206] M. J. Chappel and K. R. Godfrey. Structural identifiability of the parameters of a nonlinear batch reactor model. *Math. Biosci.*, 108:245–251, 1992.
- [207] L Ljung and S. T. Glad. On global identifiability for arbitrary model parameterization. *Automatica*, 30(2):265–276, 1994.
- [208] S. Audoly, G. Bellu, L. D. Angio, M. P. Saccomani, and C. Cobelli. Global identifiability of nonlinear models of biological systems. *IEEE Trans. Biomed. Eng.*, 48(1):55–65, 2001.
- [209] M. P. Saccomani and C. Cobelli. A minimal input-output configuration for *a priori* identifiability of a compartmental model of leucine metabolism. *IEEE Trans. Biomed. Eng.*, 40:797–803, 1993.
- [210] H. Pohjanpalo. Systems identifiability based on the power series expansion of the solution. *Math. Biosci.*, 41:21–33, 1978.
- [211] J. F. Ritt. *Differential Algebra*. American Mathematical Society, Providence, RI, 1950.

- [212] E. P. Gatzke and F. J. Doyle III. Model predictive control of a granulation system using soft output constraints and prioritized control objectives. *J. Powder Technology*, 121(1):149–158, 2001.
- [213] M. L. Tyler and M. Morari. Propositional logic in control and monitoring problems. *Automatica*, 35:565–582, 1999.
- [214] E. Zafiriou and H. W. Chiou. Output constraint softening for SISO model predictive control. *In Proc. American Control Conf., San Francisco, CA*, pages 372–376, 1993.
- [215] A. Bemporad and M. Morari. Control of systems integrating logic, dynamics, and constraints. *Automatica*, 35:407–427, 1999.